### Polymeric Biomaterials for Tissue Regeneration Applications

#### **Doctoral Thesis**

by

"Deepa"

(2019BMZ0001)



# DEPARTMENT OF BIOMEDICAL ENGINEERING INDIAN INSTITUTE OF TECHNOLOGY ROPAR

October, 2024

## Polymeric Biomaterials for Tissue Regeneration Applications

A Thesis Submitted
In Partial Fulfillment of the Requirements
for the Degree of

#### **DOCTOR OF PHILOSOPHY**

by

"Deepa"

(2019BMZ0001)



## DEPARTMENT OF BIOMEDICAL ENGINEERING INDIAN INSTITUTE OF TECHNOLOGY ROPAR

October, 2024

**Dedicated** 

to

my

Grandparents

and Parents

**Declaration of Originality** 

I hereby declare that the work, which is being presented in the thesis, entitled "Polymeric

Biomaterials for Tissue Regeneration Applications", has been solely authored by me. It presents

the result of my independent investigation/research conducted from July, 2019 to August, 2024

under the supervision of Dr. Yashveer Singh, Associate Faculty, Department of Biomedical

Engineering, IIT Ropar, Rupnagar. To the best of my knowledge, it is an original work, both in

terms of research content and narrative, and has not been submitted or accepted elsewhere, in parts

or in full, for the award of any degree, diploma, fellowship, associateship, or similar title of any

university or institution. Further, due credit has been attributed to the relevant state-of-the-art

collaborations with appropriate citations and acknowledgments, in line with the established ethical

norms and practices. I also declare that any idea/data/fact/source stated in my thesis has not been

fabricated/falsified/misrepresented. All the principles of academic honesty and integrity have been

followed. I fully understand that if the thesis is found to be unoriginal, fabricated, or plagiarized,

the institute reserves the right to withdraw the thesis from its archive and revoke the associated

degree conferred. Additionally, the institute also reserves the right to appraise all concerned sections

of the society of the matter for their information and necessary action. If accepted, I hereby consent

for my thesis to be available online in the Institute's Open Access Repository, inter-library loan,

and the title and abstract to be made available to outside organizations.

Signature

Name: Deepa

Entry Number: 2019BMZ0001

Program: PhD

Department: Biomedical Engineering

Indian Institute of Technology Ropar

Rupnagar, Punjab 140001

Date: 21-10-24

٧

#### Acknowledgments

I am extremely grateful and humbled to have reached this major accomplishment in my academic journey. Without the continuous support, direction, and encouragement of several people this would not have been possible. I'd want to express my sincere gratitude to everyone who have contributed to the completion of this research work. Firstly, I would like to thank God. When I was in doubt, I took comfort in knowing that God's knowledge was directing me in the correct direction. His boundless mercy and blessings gave me the courage to endure challenges and come out stronger.

I owe a great deal of gratitude to my esteemed supervisor **Dr. Yashveer Singh** for his expert guidance and unwavering support throughout my PhD journey. His persistent faith in my potential and willingness to push me outside my comfort zone has greatly impacted how I have developed personally and professionally. Also, his perceptive criticism and patient direction were crucial in helping me refine this thesis and develop my research skills. I want to thank him for his constant motivation and for inspiring me to take new opportunities, helping me find strengths I never knew I had. I also extend my appreciation to my doctoral committee members **Dr. Durba Pal, Prof. Rajendra Srivastava, Dr. Mukesh Kumar,** and chairperson **Dr. Srivatsava Naidu** for their insightful comments and valuable time. Their well-considered recommendations and insightful critiques have greatly improved the quality of my thesis.

I am also extremely grateful to the faculty of IIT Ropar for providing a supportive environment for learning and research. I am deeply indebted to the Department of Biomedical Engineering and the Department of Chemistry for providing me research facilities. I am also thankful to all the staff of the Department of Biomedical Engineering and Department of Chemistry.

I would also like to extend my sincere appreciation to my lab mates for their insightful contributions, encouragement and for creating a friendly environment throughout our time together. I am extremely thankful to **Dr. Nahida Rasool** for being an amazing senior. I express my heartfelt gratitude to **Dr. Moumita Halder**, whose knowledge and direction were extremely helpful to me as I worked through the challenges of my research. Her commitment to encouraging a culture of information sharing has been incredibly motivating. I am also thankful to **Yashika Thakur** for always being there to help whenever I needed it. My gratitude also extends to other members of the lab **Vatan, Pruthviraj, Gurpreet, Ankit, and Soumyajit** for their valuable suggestions and insightful discussions. **Rupali, Meghna, Mukul, Subhajit, Ananya, Sakshi, Srijani, John, Ankur, Gayatri, and Tumpa** for all the beautiful moments we shared.

I am also deeply thankful to my interns **Chetan**, **Himani**, and **Aditi**. I am also indebted to my intern **Manisha Bharti** for her efforts in data collection and analysis. Her efficiency and dedication have notably improved the quality of this thesis.

I would like to take a moment to express my sincere gratitude to my friends **Bhavya Thakur**, **Rahul Shukla**, **Bijit Basumatary**, **Varun Rathi**, **and Adarsha Mallick**, who have been a constant source of solace, joy, and comfort. I am extremely blessed to have pals who knew how to make me smile when the stress was at its highest. I will always appreciate our trips, laughter, and light-hearted moments, as they brought happiness and optimism to my work.

I am incredibly appreciative of my family, who have provided me with love, support, and encouragement throughout my academic career. I am thankful to my grandparents Late **Sh. Sujan Singh Negi** for his blessings and **Sh. Gopal Singh Negi**, **Mrs. Chander Negi**, **Mrs. Shakuntala Negi for** their strong belief in me. I want to thank my parents **Sh. Ashok Negi** and **Mrs. Kamla Negi** for their faith and support. My ideals and work ethic have been moulded by their advice and experience, and I am grateful for their presence in my life.

I extend my heartfelt appreciation to my siblings **Anushtha Negi**, **Anuja Negi**, and **Rohit Negi** for their belief in me, lending a listening ear and genuine enthusiasm for my small achievements that have motivated me to continue learning new things.

Finally, I would like to acknowledge the financial assistance from the Department of Biotechnology India (grant # BT/PR40669/MED/32/761/2020) to my PhD supervisor and IIT Ropar, Rupnagar for the institute fellowship to me.

#### Certificate

This is to certify that the thesis, entitled **Polymeric Biomaterials for Tissue Regeneration Applications**, submitted by **Deepa (Entry # 2019BMZ0001)** for the award of the degree of **Doctor of Philosophy** of the Indian Institute of Technology Ropar, Rupnagar, is a record of original research work carried out under my guidance and supervision at the Department of Biomedical Engineering, IIT Ropar, Rupnagar. All other sources of information, material, and mentorship have been acknowledged at appropriate places in the thesis. To the best of my knowledge and belief, the work presented in this thesis is original and has not been submitted, either in part or full, for the award of any other degree, diploma, fellowship, associateship or similar title of any university or institution.

In my opinion, the thesis meets the requirements of the regulations relating to the award of PhD degree.

Hingh.

Signature of the Supervisor

Dr. Yashveer Singh

Department: Biomedical Engineering

Indian Institute of Technology Ropar

Rupnagar, Punjab 140001

Date: 21-10-2024



#### **Lay Summary**

Biomaterials are materials specifically designed to interact with the body for medical purposes. They can be either natural or synthetic and are used in various medical treatments, like replacing a damaged bone, healing wounds, and repairing damaged tissue. The key feature of biomaterials is that they are safe to use in the body. Out of different biomaterials, polymeric biomaterials are a specific type of biomaterial made from polymers. These materials are particularly useful in medicine because they can be customized in many ways. For example, they can be made to mimic the body's natural tissue structure or to release drugs over time. Common examples of polymeric biomaterials include hydrogels, which are soft and flexible, making them great for wound dressings. Polymeric nanoparticles and polymer-coated nanoparticles are materials with at least one dimension measuring less than 100 nanometers. Their unique shapes, sizes, and flexible surfaces give them distinct biological properties. As a result, polymeric biomaterials have shown significant potential in various biomedical applications, particularly in regenerative medicine. Wound healing is a complex process that affects millions worldwide and is often hindered by bacterial infections, bleeding, and biofilm formation. Current treatments, including antibiotics, can be ineffective and contribute to antibiotic resistance, highlighting the need for advanced wound dressings with antibacterial, antibiofilm, and hemostatic properties. Similarly, bone tissue regeneration, essential for repairing damage from infections, surgeries, or trauma, faces challenges like graft rejection and post-operative complications, necessitating new therapeutic approaches. This thesis explores the development of polymeric biomaterials aimed at improving tissue regeneration, with a focus on wound healing and bone regeneration. It is organized into five chapters. An introduction to tissue regeneration and polymeric biomaterials, a review of previous research, identification of unmet needs, and the objectives of the thesis are discussed in Chapter 1. A metallic nanoparticle-based hydrogel has been reported in Chapter 2. It effectively fights bacteria, prevents biofilm formation, controls bleeding, and speeds up wound healing without using antibiotics. Chapter 3 introduces a new approach to boost bone healing using nanoparticles coated with acemannan and doped with cobalt. These nanoparticles not only promote bone growth but also create a supportive immune environment by reducing inflammation, thus, making them a promising strategy for effective bone regeneration. Chapter 4 reports the development of a phytoestrogen-loaded gel that mimics natural tissue and reduces oxidative stress, effectively supporting bone regeneration in osteoporotic conditions. Chapter 5 provides a summary of the thesis, highlights its contributions to the field, and discusses future research directions.

#### **Abstract**

One of the biggest threats to human health is the loss of tissues and organs. Every year, injuries and trauma result in the suffering and deaths of millions of people. According to the WHO, injuries and trauma claim the lives of 4.4 million people globally each year, accounting for nearly 8% of all deaths. In the process of researching ways to repair injured tissues, scientists have come up with the innovative concept of tissue regeneration, which integrates the principles from biology, engineering, medicine, and materials science to develop in vitro substitutes that can be implanted into the body to restore or enhance biological function. Successful tissue regeneration is hindered by bacterial infections, biofilm formation, and excessive bleeding. Also, conventional methods used for tissue regeneration, such as allografts and autografts, suffer from limitations like donor tissue scarcity, morbidity, immune rejection, and disease transmission risks that pose major public health concerns. Despite advancements, challenges persist in tissue regeneration, which has prompted researchers to explore alternative approaches, and biomaterials have been used to restore damaged tissues. Biomaterials are synthetic or natural materials designed for biomedical applications and exhibit safe interaction with tissue, blood, and biological fluids, without harming the organism. Out of different biomaterials, polymeric biomaterials, such as hydrogels/gels and polymer-coated nanoparticles because of their unique properties and abilities, such as tunability, biocompatibility, degradability, and extracellular matrix (ECM)-mimicking properties, offer tailored solutions to tissue regeneration applications. Wound healing is a complex process, with chronic wounds affecting millions of people globally. Bacterial infection, excessive bleeding, and biofilm formation prolong the inflammatory phase of wound healing and contribute to the delayed healing with increased mortality rates. Bacterial skin infections impact around 150 million people globally, with antibiotic resistance contributing to 700,000 deaths annually. Additionally, blood loss from traumatic injuries accounts for over 30% of trauma-related deaths worldwide, further increasing the risk of infection and mortality. The current treatment approaches lack sufficient efficacy and inclusion of antibiotics elevates the risk of antibiotic resistance. To address these challenges, multifunctional wound dressings with antibacterial, antibiofilm, and rapid hemostatic properties are needed. Also, bone tissue regeneration is the process of restoration of lost or damaged bone caused by infection, surgery, or trauma through natural or engineered means. The Global Burden of Disease (GBD) study done in 2019 reported 178 million new bone fracture cases worldwide. Osteoporosis, which weakens bones by reducing bone mass, contributes to over 8.9 million fractures annually. Autografts and allografts continue to be the most popular therapy options for the treatment of bone defects, with over 2.2 million procedures performed worldwide annually. However, graft rejection, post-operative problems, and other constraints make these approaches less effective clinically. Thus, there is a need for alternative therapeutic interventions to address the unmet challenges in bone regeneration. This thesis deals with the development and evaluation of polymeric biomaterials

for tissue regeneration, in particular, for wound healing and bone regeneration, and is structured into 5 chapters.

Chapter 1: This chapter provides an overview of tissue regeneration, with a focus on wound healing and bone regeneration. It discusses the role of polymeric biomaterials in these applications, highlighting the challenges associated with their use in tissue regeneration. A thorough literature review identifies existing knowledge gaps, leading to the formulation of research hypotheses and the objectives of this thesis. The chapter also outlines the organization of the thesis, detailing its structure and the progression of research topics. Chapter 2: Impaired wound healing poses significant health concerns and also contributes to medical and financial burdens. Currently, available wound dressings, including creams, ointments, and gels suffer from limitations, such as narrow-spectrum activity, cytotoxicity, and ineffectiveness against biofilms. Addressing the limitations of current wound dressings, which often rely on antibiotics and thus, pose an increased risk of antimicrobial resistance, this chapter deals with the development of β-Ga<sub>2</sub>O<sub>3</sub> nanoparticles loaded within an imine crosslinked hydrogel of quaternized chitosan and oxidized sodium alginate. This polymeric hydrogel targets iron-dependent pathways crucial for bacterial growth and biofilm formation. The hydrogels exhibited multifaceted functionality, including broad-spectrum antibacterial properties, antioxidant potential, and antibiofilm activities. Moreover, hydrogels exhibited favorable interactions with platelets by promoting adhesion and thrombus formation, thereby positioning them as a preferred therapeutic option for efficient tissue regeneration in bacteria-infected wounds. Chapter 3: Harnessing the immunomodulatory properties of biomaterials represents a promising strategy for modulating macrophage polarization and creating a conducive environment for bone regeneration. This chapter reports the fabrication and evaluation of cobalt-doped biphasic calcium phosphate nanoparticles coated with acemannan for efficient bone regeneration. The immunomodulatory potential of acemannan and low doses of cobalt along with the osteogenic properties of biphasic calcium phosphate offer a promising solution for bone regeneration. The nanoparticles were cytocompatible and showed enhanced cell proliferation along with osteogenic differentiation as suggested by an increased ALP production and calcium deposition. They reduced the expression of M1 markers with enhanced expression of M2 markers as observed by RT-qPCR, ICC, and flow cytometry studies. The results suggest a strong potential of nanoparticles in modulating immune response and, thereby, facilitating efficient bone regeneration. Chapter 4: Bone regeneration in osteoporotic conditions has emerged as a major public health concern, particularly in elderly patients and postmenopausal women. There is a need of innovative therapeutic interventions for effective bone regeneration in osteoporotic conditions. To address this challenge, this chapter deals with the development of a phytoestrogen, genisteinloaded polymeric gel fabricated using κ-carrageenan/quaternized dextran to target estrogen loss and enhanced reactive oxygen for bone regeneration in osteoporotic conditions. The presence of

genistein endow the gel with excellent antioxidant properties and enhanced mineralization. Also, an upregulation of the expression of osteogenic markers, ALP, OCN, OPN, and RUNX 2 and downregulation in TRAP, an osteoclast differentiation marker, was observed after treatment with the gel. These findings provide evidence of the effectiveness of fabricated gel in suppressing osteoclast differentiation, while concurrently promoting osteoblast differentiation for accelerating bone regeneration in osteoporotic conditions. **Chapter 5:** This chapter provides the conclusions of the thesis, highlights the contributions made to the field of tissue regeneration, and discusses the future perspective of the thesis.

The thesis presents significant research outcomes in the field of tissue regeneration, particularly in wound healing and bone regeneration. In bacteria-infected wounds, the imine crosslinked hydrogel loaded with β-Ga<sub>2</sub>O<sub>3</sub> nanoparticles demonstrated not only broad-spectrum antibacterial and antibiofilm properties but also promoted platelet adhesion and showed strong hemostatic abilities, highlighting its potential for clinical applications. In bone regeneration, cobalt-doped biphasic calcium phosphate nanoparticles coated with acemannan effectively modulated macrophage polarization along with osteogenesis, fostering an immune environment conducive to healing. Additionally, the genistein-loaded polymeric gel effectively addressed the challenges of osteoporotic bone regeneration by exhibiting excellent ROS scavenging capabilities, suppressing osteoclast activity, and promoting osteoblast differentiation.

To summarize, this thesis deals with the development of innovative multifunctional polymeric biomaterials that tackle key challenges in wound healing and bone regeneration through integrated antibacterial, immunomodulatory, and osteogenic properties. This thesis addresses critical challenges such as bacterial infections in wounds and impaired bone healing in osteoporotic conditions by developing innovative biomaterial-based solutions. These findings offer practical advancements for treating difficult clinical conditions while also contributing to the broader field of regenerative medicine. Future research should build on these insights by focusing on the development of multifunctional, smart biomaterials that not only target specific physiological challenges but also respond to environmental triggers such as pH, reactive oxygen species, or infections for controlled therapeutic release. Additionally, integrating bioactive molecules, or growth factors into these systems holds promise for enhancing tissue regeneration and immunomodulation. The incorporation of these strategies with advanced technologies like 3D bioprinting could further enable patient-specific treatments, pushing the boundaries of personalized and regenerative medicine.

#### **List of Publications**

- 1. Negi, D.; Bharti, M.; Singh, Y. Genistein-loaded, quaternized dextran/κ-carrageenan gels for bone regeneration in osteoporotic conditions. (Chapter 4, manuscript under preparation)
- **2. Negi, D.;** Bhavya, K.; Pal, D.; Singh, Y. Acemannan-coated, cobalt doped biphasic calcium phosphate nanoparticles for immunomodulation regulated bone tissue regeneration. *Biomaterials Science*, 2024, 12, 3672-3685. (**Chapter 3**)
- 3. Negi, D.; Singh, Y. Gallium Oxide Nanoparticle-Loaded, Quaternized Chitosan-Oxidized Sodium Alginate Hydrogels for Treatment of Bacteria-Infected Wounds. ACS Appl. Nano Mater. 2023, 6 (14), 13616–13628 (Chapter 2).
- **4.** Bhavya, K.; Agarwal, K.; **Negi, D.**; Niveria, K.; Singh, Y.; Kamra, A.; Dasgupta, S.; Nirmalkar, N.; Pal, D. Delivery of lipid-encapsulated oxygen nanobubbles restricts hypoxia-induced EMT transition in lung and mammary adenocarcinoma. (Submitted)
- Halder, M.; Singh, A.; Negi, D.; Singh, Y. Investigating the Role of Amino Acids in Short Peptides for Hydroxyapatite Binding and Osteogenic Differentiation of Mesenchymal Stem Cells to Aid Bone Regeneration. *Biomacromolecules*, 2024, 25, 2286–2301.
- 6. Rasool, N.; Negi, D.; Singh, Y. Thiol-Functionalized, Antioxidant, and Osteogenic Mesoporous Silica Nanoparticles for Osteoporosis. ACS Biomater. Sci. Eng. 2023, 9, 3535–3545.



#### **Conferences**

- **Negi, D.;** Bhavya, K.; Pal, D.; Singh, Y., Effect of cobalt doping in biphasic calcium phosphate nanoparticles on immunomodulation regulated bone tissue regeneration, *33rd Annual Conference of the European Society for Biomaterials (ESB 2023)*, Davos, Switzerland, 4-8 September, 2023 (**poster**).
- 2. Negi, D.; Singh, Y.; Multifunctional gallium oxide hydrogels for wound repair, International *Conference of Biomaterials, Regenerative Medicine and Devices*, IIT Guwahati, Assam, 14-18 December, 2022 (poster).
- **Negi, D.;** Singh Y. Gallium nanoparticles loaded hydrogels for antibacterial and antibiofilm applications, *International e-conference on nanomaterials and nanoengineering*, 24-26 February, 2022 (**oral presentation**).
- **4.** *Biomaterials Online Conclave*, National center for Nanoscience and Nanotechnology, University of Madras, 7-15, March, 2022.

#### **Table of Contents**

Declaration	v
Acknowledgements	vii
Certificate	ix
	xi
Lay Summary	
Abstract	xiii 
List of Publications	xvii
List of Conferences	xix
List of Figures	XXV
List of Tables	xxvii
Notations and Abbreviations	xxix
Chapter 1: Introduction	1-50
1.1. Biomaterials and polymeric biomaterials	3
1.1.1. Natural polymers	4
1.1.2. Synthetic polymers	8
1.1.3. Different biomaterials forms of polymers	9
1.2. Fabrication of polymeric biomaterials	11
1.2.1. Fabrication of polymeric hydrogels/gels	11
1.2.2. Fabrication of nanoparticles	12
1.2.3. Fabrication of polymer-coated nanoparticles	13
1.3. Characterization of polymeric biomaterials	13
1.3.1. Characterization of hydrogels/gels	13
1.3.2. Characterization of nanoparticles and polymer-coated nanoparticles	14
1.4. Applications of polymeric biomaterials	15
1.4.1. Tissue regeneration	15
1.5. Skin tissue regeneration	15
1.5.1. Anatomy and physiology of skin	16
1.5.2. Different stages of wound healing	16
1.5.3. Role of bacterial infections and biofilm formation in tissue regeneration	17
1.6. Treatment strategies for bacteria-infected wounds (literature review)	18
1.6.1. Polymeric hydrogels/gels for wound healing	19
1.7. Rational design of nanoparticle-based polymeric hydrogels/gels	24

system for skin tissue regeneration (literatur	e review)
1.8. Bone tissue regeneration	26
1.9. Materials based strategies to promote b (literature review)	one tissue regeneration 28
1.10. Rational design of polymer nanopartic gels for bone tissue regeneration (literature)	
1.11. Knowledge gaps in the field	33
1.12. Hypothesis	34
1.13. Research questions	35
1.14. Objectives	36
1.15. Thesis outline	37
References	38-49
Chapter 2: Gallium oxide nanoparticle-loaded sodium alginate hydrogels for treatment of ba	
2.1. Introduction	53
2.1.1. Bacteria-infected wounds	53
2.1.2. Challenges	53
2.1.3. Research gap	54
2.1.4. Nanoparticle-loaded hydrogel	54
2.2. Objectives	54
2.3. Experimental section	55
2.4. Results and discussion	62
2.5. Conclusions	75
References	76-79
Chapter 3: Acemannan coated, cobalt-doped nanoparticles for immunomodulation regulate	1 100
3.1. Introduction	82
3.1.1. Bone abnormalities	82
3.1.2. Challenges	83
3.1.3. Research gap	83
3.1.4. Polymers and nanoparticles	85
3.2. Objectives	86
3.3. Experimental section	87
3.4. Results and discussion	91
3.5. Conclusions	102
References	104-107
Chapter 4: Genistein-loaded, quaternized dex bone regeneration in osteoporotic conditions	tran/ κ-carrageenan gels for 109-129
4.1. Introduction	111
4.1.1. Osteoporosis/postmenopausal ost	eoporosis 111

4.1.2.	Challenges	111
4.1.3.	Research gap	112
4.1.4.	Polymeric gels and phytoestrogens	113
4.2.	Objectives	113
4.3.	Experimental section	114
4.4.	Results and discussion	119
4.5.	Conclusions	131
Referen	References 133	
Chapter 5: Conclusions and perspectives		137-142
5.1.	Summary of the thesis	139
5.1.1.	Contribution to the existing knowledge	140
5.1.2.	Future perspectives	141
Appendix		143-153



#### **List of Figures**

S. No.	Figure caption	Page No.
1.1.	Evolution in biomaterials through generations	2
1.2.	Classification of biomaterials	3
1.3.	Different biomaterials form of polymers	10
1.4.	Different stages of wound healing	15
1.5.	Different stages of biofilm formation	17
1.6.	Properties of an ideal wound dressing	18
1.7.	Nanoparticle-based wound dressing material	20
1.8.	Different stages of bone regeneration	27
1.9.	Timeline of major milestones in biomaterials designed for bone tissue engineering	29
1.10.	Objectives of the thesis	35
2.1.	Fabrication of β-Ga <sub>2</sub> O <sub>3</sub> nanoparticle-loaded hydrogels for bacteria-infected wound healing	52
2.2.	Characterization of polymers	60
2.3.	Characterization of β-Ga <sub>2</sub> O <sub>3</sub> nanoparticles	61
2.4.	Characterization of hydrogels	63
2.5.	Antibacterial activity of nanoparticle-loaded hydrogels	65
2.6.	Mechanism of antibacterial activity using HR-TEM	66
2.7.	Zone of inhibition assay	67
2.8.	Antibiofilm activity of nanoparticle-loaded hydrogels	68
2.9.	Hemostatic potential and blood compatibility of nanoparticle-loaded hydrogels	70
2.10.	In vitro cytotoxicity and wound healing	71
3.1.	Fabrication of CoAceBCP for bone regeneration	81
3.2.	Characterization of nanoparticles	87
3.3.	Characterization of acemannan-coated nanoparticles	88
3.4.	EDX, FESEM, and DLS of nanoparticles	89
3.5.	Cell viability and scratch healing of nanoparticle-treated cells	90
3.6.	Cytoskeletal staining of nanoparticle-treated cells	92
3.7.	Osteogenic potential of cells in the presence of nanoparticles	93
3.8.	Gene expression studies	95
3.9.	Immunocytochemistry assay	96
4.1.	Genistein-loaded gels for bone regeneration in osteoporotic conditions	113
4.2.	Characterization of polymers and gel	114
4.3.	Self-healing and FESEM of gels	115
4.4.	Rheological properties of gels	116
4.5.	Swelling and degradation, antioxidant, and release studies of gels	119

4.6.	Cell viability and scratch healing of gel-treated cells	120
4.7.	DCFDA and cytoskeletal staining of cells treated with gels	122
4.8.	Osteogenic studies and TRAP activity	123
4.9.	Gene expression studies	124

#### **List of Tables**

S. No.	Table caption	Page No
1.1	Various nanoparticle-loaded hydrogel materials used for wound healing	22
A1	List of antibodies used along with their details	144
A2	List of primers and their sequences	145
A3	Primer sequences used in real-time PCR	145



#### **Notations and Abbreviations**

Acronym	Name
2D	Two-dimensional
ABTS	2,2'-Azino-bis(3-ethylbenzothiazoline-6-sulfonic acid)
ALP	Alkaline phosphatase
Arg 1	Arginase 1
β-Ga <sub>2</sub> O <sub>3</sub> NPs	β-Gallium oxide nanoparticles
β-ТСР	β-Tricalcium phosphate
BMP	Bone morphogenetic protein
CS	Chitosan
cDNA	Complementary deoxyribonucleic acid
CD 68	Cluster of differentiation 68
CD 206	Cluster of differentiation 206
CD 163	Cluster of differentiation 163
CFU	Colony-forming unit
CoBCP NPs	Cobalt-doped biphasic calcium phosphate nanoparticles
CoAceBCP	Acemannan coated, cobalt-doped biphasic calcium phosphate
NPs	nanoparticles
DAPI	4',6-Diamidino-2-phenylindole
DCFDA	2',7'-Dichlorodihydrofluorescein diacetate
DI	Deionized water
DLS	Dynamic light scattering
DMEM	Dulbecco's modified eagle medium
DPBS	Dulbecco's phosphate buffered saline
DMSO	Dimethyl sulfoxide
DS	Degree of substitution
ECM	Extracellular matrix
EDTA	Ethylenediaminetetraacetic acid
EDX	Energy dispersive X-ray
EPS	Extracellular polymeric substances
FBS	Fetal bovine serum

FITC	Fluorescein isothiocyanate
FTIR	Fourier transform infrared
GAPDH	Glyceraldehyde-3-phosphate dehydrogenase
GL Hyd	β-Ga <sub>2</sub> O <sub>3</sub> nanoparticle-loaded hydrogels
GelMA	Gelatin methacryloyl
GNPs	β-Ga <sub>2</sub> O <sub>3</sub> nanoparticles
GPC	Gel-permeation chromatography
GTMAC	Glycidyltrimethyl ammonium chloride
TGA	Thermogravimetric analysis
H <sub>2</sub> O <sub>2</sub>	Hydrogen peroxide
HAp	Hydroxyapatite
HR-TEM	High resolution transmission electron microscopy
iNOS	Inducible nitric oxide synthase
kDa	Kilo Dalton
LB	Luria-Bertani
LVR	Linear viscoelastic range
ΜΕΜ α	Minimum essential medium alpha
MPAES	Microwave plasma atomic emission spectroscopy
M-CSF	Macrophage colony-stimulating factor
MRI	Magnetic resonance imaging
MTT	(3-(4,5-Dimethylthiazol-2-yl)-2,5-diphenyltetrazolium bromide
NaOH	Sodium hydroxide
NMR	Nuclear magnetic resonance
NF-κB	Nuclear factor
NP	Nanoparticle
OA	Oxidized alginate
OCN	Osteocalcin
OD	Optical density
OM	Osteogenic media
OPN	Osteopontin
PEG	Poly(ethylene glycol)
PBS	Phosphate Buffer Saline

PLGA	Poly lactic-co-glycolic acid
PDX	Polydioxanone
PHBV	Poly(3-hydroxybutyrate-co-3-hydroxyvalerate)
pNPP	para-Nitrophenyl phosphate
PRP	Platelet rich plasma
QC	Quaternized chitosan
QC-OA Hyd	Quaternized chitosan-oxidized alginate hydrogel
QDex	Quaternized dextran
RANKL	Receptor Activator of Nuclear Factor Kappa-B Ligand
RBC	Red blood cells
ROS	Reactive oxygen species
RPM	Rotation per minute
RPMI	Roswell Park Memorial Institute
RUNX 2	Runt-related transcription factor 2
SD	Standard deviation
SEM	Scanning electron microscopy
SERM	Selective estrogen receptor modulators
TNBS	2,4,6-Trinitrobenzenesulfonic acid
TRAP	Tartrate-resistant acid phosphatase
UV	Ultra violet
XRD	X-ray diffraction

# **CHAPTER - 1**Introduction

## Chapter 1 Introduction

#### 1. Introduction

#### 1.1. Biomaterials and polymeric biomaterials

The term biomaterial emerged between the late 1950s and early 1970s, gaining recognition with the establishment of symposia at Clemson University and the founding of the Society for Biomaterials in 1975<sup>1</sup> and has continued to evolve ever since (**Figure 1.1**). Biomaterials are the materials of synthetic or natural sources designed for biomedical applications to exhibit safe interaction with tissue, blood, and biological fluids<sup>2</sup>. Biomaterials can be broadly categorized into metals, ceramics, polymers, and composites (**Figure 1.2**).

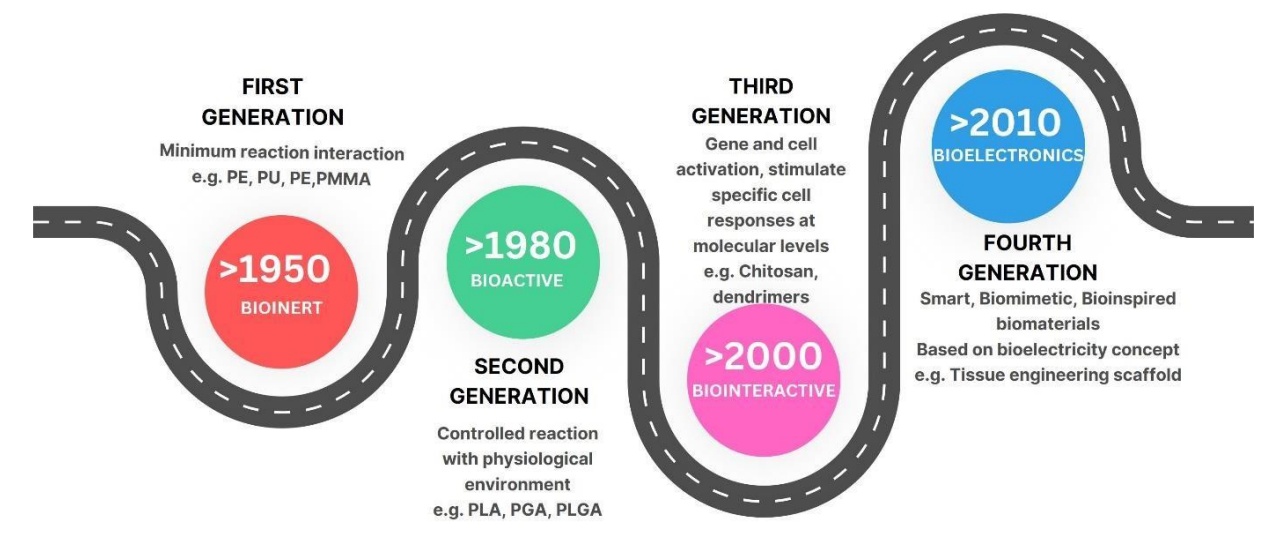


**Figure 1.1.** Evolution in biomaterials through generations.

Among the various types, polymeric biomaterials have gained particular attention since the 1960s, with pioneers like Langer, Folkman, Peppas, and Higuchi leading innovations that revolutionized biomedical applications. A significant breakthrough in the 1990s included the development of hydrogels, crosslinked polymer networks that could absorb large amounts of water, mimicking the extracellular matrix (ECM) and providing a favorable environment for cell growth and tissue regeneration. Researchers like Nicholas Peppas and Wolfgang Ringsdorf contributed to the design

of smart polymers capable of responding to environmental stimuli, further advancing regenerative medicine applications.<sup>2</sup>.

More recently, the focus has shifted toward the use of natural polymers like chitosan, collagen, and alginate, as well as hybrid systems combining synthetic and natural materials. These advancements have improved biocompatibility and tailored degradation rates, making polymeric biomaterials integral to the development of scaffolds, drug delivery systems, and bioactive implants for tissue regeneration. The evolution of polymeric biomaterials continues to shape innovative solutions for challenges in wound healing, bone regeneration, and organ repair.

Polymer-derived biomaterials are classified into two categories: natural and synthetic. Examples of natural biomaterials include chitosan, sodium alginate, collagen, and hyaluronic acid<sup>3</sup>. Synthetic polymers are further divided into non-biodegradable and biodegradable polymers. Examples of synthetic polymers include poly(lactic acid), poly(glycolic acid), poly(lactic-co-glycolic acid), and polycaprolactone<sup>4</sup>.

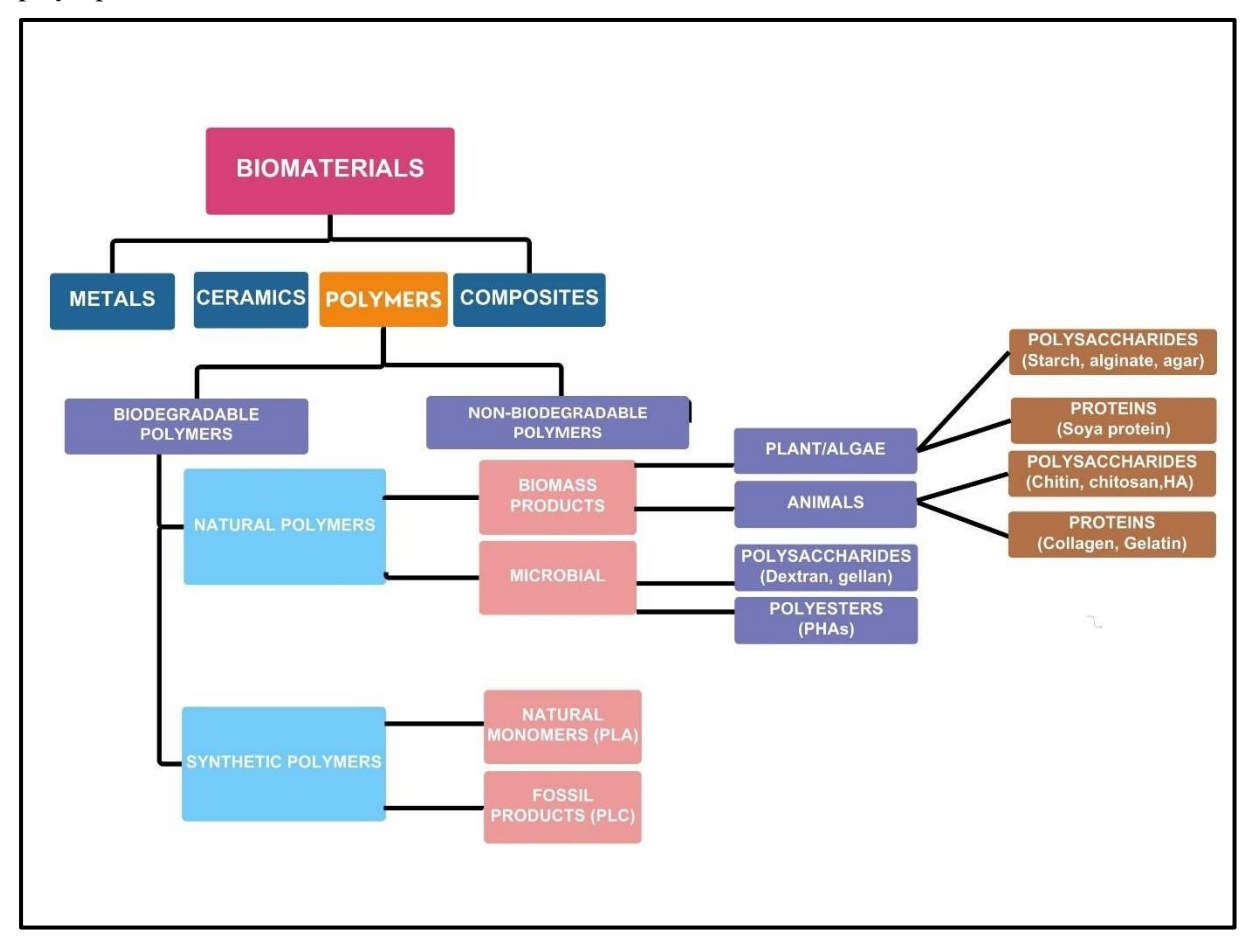


Figure 1.2. Classification of biomaterials.

#### 1.1.1. Natural polymers

#### 1.1.1.1. Chitosan

Chitosan is obtained from the deacetylation of chitin. Glucosamine and N-acetyl glucosamine are the building components of chitosan. The linear polymer chitosan is semi-crystalline in structure and

the crystallinity is influenced by the degree of deacetylation. The cationic properties of chitosan result from the free amino and N-acetyl groups present in the structure. Chitosan can therefore communicate with proteoglycans and glycosaminoglycans (GAGs). Chitosan is widely used in biomedical applications, because of its biocompatibility, low toxicity, structural similarity to natural glycosaminoglycans, and antibacterial activities. However, chitosan readily dissolves in acidic environments but is generally insoluble under neutral conditions and in most organic solvents due to its amino groups and high crystallinity. To improve its solubility and processability, various derivatives have been developed<sup>5</sup>. Chitosan has also found its use in tissue engineering applications. The structure of chitosan is similar to the glycosaminoglycans present in connective tissue. Research has indicated that when it comes to mesenchymal stem cells osteogenic differentiation, chitosan has great potential. Additionally, the chitosan-modified scaffolds showed enhanced osteoblast activity and stem cell osteogenic differentiation<sup>6</sup>. It has also shown the potential to incorporate different growth factors, such as bone morphogenic protein 2 and platelet-derived growth factor<sup>7,8</sup>. The use of chitosan-based scaffolds in bone repair is still in progress.

# **1.1.1.2.** *Alginates*

Alginates are linear polysaccharides that are anionic and obtained from bacteria and algae and bacteria. They are block copolymers composed of 1,4-linked  $\beta$ -D-mannuronic acid (M) and  $\alpha$ -L-guluronic acid (G). Alginates have been studied in many biomedical applications due to their low toxicity, biocompatibility, and cost-effectiveness. Alginates can be made into gels using divalent cations like Sr<sup>2+</sup>, Ba<sup>2+</sup>, Mg<sup>2+</sup>, and Ca<sup>2+</sup>, and used for different biomedical applications<sup>9</sup>. Alginate is used both in solid scaffold form and hydrogel form for tissue regeneration. To enhance the mechanical strength of alginate-based materials different nanoparticles are added<sup>10</sup>.

#### 1.1.1.3. *Dextran*

Dextran is a hydrophilic polymer obtained from bacterial strains and composed of linear  $\alpha$ -1,6-linked D-glucopyranose residues. It consists of various hydroxyl groups, which help in conjugation with proteins and drugs either directly or via a linker. For tissue regeneration applications dextranbased hydrogels were developed using chemical cross-linking, physical cross-linking, and radical polymerization methods<sup>11</sup>. Dextran has several biological functions, including antibacterial, hemostatic, and wound-healing applications<sup>12</sup>. Modified dextran-based hydrogels have been employed for tissue regeneration applications. The hydrogels showed excellent antibacterial properties with good biocompatibility and free radical scavenging activity.

# 1.1.1.4. Carrageenan

 $\kappa$ -Carrageenan is a natural polysaccharide that mimics glycosaminoglycans (GAGs) present in bone, cartilage, and the extracellular matrix. Its biocompatibility, thermo-reversible gelling, ionic crosslinking, and adjustable viscoelastic and mechanical properties make it well-suited for tissue regeneration applications.  $\kappa$ -carrageenan hydrogels have proven effective in regenerative medicine, cartilage regeneration, and as carriers for growth factors, among other biomedical uses. Additionally,  $\kappa$ -carrageenan supports osteogenic potential and chondrogenesis, helps in apatite formation, and promotes osteogenic differentiation thus helping in effective bone regeneration <sup>13</sup>.

## 1.1.1.5. Collagen

Collagen is the predominant tissue-derived natural polymer and it constitutes the primary component of extracellular matrices of mammalian tissues, such as skin, bone, cartilage, tendon, and ligament. Collagen's triple-helix structure is made up of two  $\alpha 1$  and one  $\alpha 2$  polypeptide chains. The chemical composition of the  $\alpha$ 2 chain varies among different types of collagens, with polypeptides rich in glycine (Gly), proline (Pro), and 4-hydroxyproline (Hyp), arranged in a repeating Gly-Pro-Hyp. These three polypeptide chains assemble into a triple helix structure known as procollagen. Mature collagen is produced when metalloproteinase enzymes split the helix's Nand C-terminals. Due to collagen's ability to readily attach to a wide variety of cell types, it has been employed as a scaffold for tissue culture and as an artificial skin substitute. Chemical modifications, such as the addition of fibronectin, chondroitin sulphate, or low concentrations of hyaluronic acid to the collagen matrix, can change the way cells bind to collagen. Collagen gels have been used for the regeneration of the small intestine, liver, skin<sup>14</sup>. It is also prevalent in the extracellular matrix of various tissues like bone, cartilage and dentine<sup>15</sup>. The collagen-based scaffolds are being used widely for bone tissue regeneration applications 16. Studies done by various researchers showed that collagen-based scaffolds enhanced the expression of alkaline phosphatase and increased matrix mineralization. Also, collagen can be combined with different biomaterials like hydroxyapatite, which has proven to enhance the differentiation of MSCs into osteoblasts indicating the potential of collagen in bone regeneration<sup>17</sup>.

#### 1.1.1.5. Gelatin

Gelatin is a natural polymer obtained through the hydrolysis of collagen. Gelatin comes in two varieties: gelatin A and gelatin B. While gelatin B is manufactured by an alkaline method that results in high carboxylic content, gelatin A is prepared by an acidic treatment before thermal denaturation. Additionally, it has arginine-glycine-aspartic acid (RGD) motifs, which are important for cell signalling. It is also rich in functional groups along its backbone, making it suitable for delivering biological materials<sup>18</sup>. Gelatin is well known for its gelation properties. Above 40 °C, it solubilizes in aqueous solutions and as the temperature decreases the random coils convert into a triple helix structure, resulting in the formation of hydrogel<sup>18,19</sup>. Because of the above-mentioned properties, gelatin is used widely in tissue regeneration applications. Researchers have shown the potential of

gelatin-based hydrogels as carriers of growth factors to enhance bone regeneration and repair<sup>20</sup>.

## **1.1.1.6.** *Silk fibroin*

Silk is a biologically active polymer formed by insects like Bombyx mori, spiders, mites, and flies. Its primary constituents are silk fibroin (SF) and sericin. SF is a biocompatible protein, whereas sericin may trigger allergic responses. SF, a fibrous protein, finds extensive application in tissue engineering as it exhibits high biocompatibility, facilitating cell attachment and growth<sup>21,22</sup>. Biomaterials based on SF are FDA-approved and are easily absorbed by the skin, making them ideal for wound dressings. Silk fibroin also possesses excellent mechanical properties with high tensile strength and elastic modulus making it an ideal material to be used for bone regeneration applications. Studies have shown that silk fibroin-based films helped in the growth of osteoblasts<sup>23</sup>. Also, silk fibroin obtained from *B. mori* showed comparable efficacy to commercial collagen scaffolds in regenerating bone defects in rat models after eight weeks<sup>24</sup>.

#### 1.1.1.7. Starch

Starch is produced by various plants, including corn, wheat, and potatoes<sup>25</sup>. D-glucose units, comprising 20%–30% amylose and 70%–80% amylopectin, form the building blocks of starch. Starch is biodegradable, biocompatible, and non-toxic. However, it suffers from limitations, such as low surface area and sensitivity<sup>26</sup>. To address these limitations, natural and synthetic polymers, along with ceramics, have been integrated with starch to enhance its properties.

## 1.1.1.8. *Acemannan*

Acemannan (AC) is a water-soluble mannan polymer with an acetyl group, derived from aloe vera, known for its significant clinical prominence as an antiviral and immune potentiation agent. AC is widely believed to hold promise for treating a range of conditions, including oral diseases, systemic metabolic disorders, cardiovascular diseases, and both benign and malignant tumors. In recent years, clinical cases have increasingly utilized AC as a biomaterial, particularly in tissue regeneration<sup>27</sup>.

#### **1.1.1.9.** *Hyaluronate*

Hyaluronate is an important glycosaminoglycan of the natural extracellular matrix and is used widely in tissue regeneration applications. Hyaluronate has demonstrated great promise in tissue engineering applications, including facial intradermal implants, artificial skin, and wound healing applications<sup>28</sup>.

#### 1.1.1.10. *Cellulose*

Cellulose is one of the most abundant polymers present in nature and is composed of D-glucose unit chains. With the help of hydrogen bonds and van der Waals forces, the cellulose chains connect to form microfibrils<sup>29</sup>. Studies have shown that the presence of cellulose nanocrystals increases the physio-mechanical properties of polymeric materials. Cellulose-based materials have shown strong

potential in tissue regeneration applications. It has been used to reinforce natural and synthetic polymers to enhance their mechanical strength<sup>30</sup>.

#### 1.1.2. Synthetic polymers

# **1.1.2.1.** *Poly* (*vinyl alcohol*)

Poly (vinyl alcohol) (PVA), is a hydrophilic, biocompatible, and biodegradable polymer widely used in various biomedical applications. Recently, hydrogels like PVA have gained attention in tissue engineering and regenerative medicine as matrices for repairing and regenerating multiple tissues and organs. PVA-based scaffolds are being explored as alternatives to existing artificial grafts due to their similarity in appearance and texture to native arterial tissue, making them ideal for vascular implants. With tissue-like elasticity and mechanical strength, PVA is considered a promising biomaterial for tissue simulation<sup>31</sup>.

#### 1.1.2.2. Poly (ethylene oxide)

Poly (ethylene oxide) (PEO) has received FDA approval for various medical applications because of its biocompatibility and low toxicity. PEO is highly hydrophilic and by using cationic and anionic polymerization it can be synthesized. Gels of PEO are formed by UV photopolymerization. There have been reports on the uses of a variety of PEO-based copolymers, particularly in drug delivery applications<sup>32</sup>.

#### 1.1.2.3. PLGA polymers

PLGA comes under the poly(esters) family and this family is characterized by ester bond linkages in their carbon backbone. Aliphatic polyesters, such as PGA, PLA, and PLGA, are among the most thoroughly researched degradable polymers to date. Due to its unique characteristics, PLGA can be customized as per biomedical needs. Additionally, chemical modification with other polymers or bioconjugation with molecules can impart functional properties to PLGA, making it a standout among synthetic polymers in the biomedical field<sup>33</sup>.

#### 1.1.2.4. Polycaprolactones

Poly(caprolactone) (PCL) is another often used degradable aliphatic polyester used in a variety of biomedical applications as it offers unique chemical and physical characteristics like low melting point, excellent biocompatibility, and exceptional blending compatibility. PCL is a promising candidate for tissue engineering as it offers excellent thermal stability and is easy to process. Studies have shown that PCL nanofibers integrated into a carbohydrate matrix enhance cell proliferation, cell viability, and migration<sup>34</sup>.

#### 1.1.2.5. Polyanhydrides

Polyanhydrides are a category of surface-eroding polymers characterized by two carbonyl groups linked by an ether bond. Polyanhydrides were studied for their potential as biomaterials starting in the 1980s, which ultimately resulted in their FDA approval as drug delivery vehicles in 1996. Polyanhydrides have been used widely as delivery vehicles for proteins, antibiotics, vaccines, and chemotherapeutics<sup>35</sup>.

#### 1.1.3. Different biomaterial forms of polymers

Polymeric biomaterials can be fabricated into various biomaterial forms, each tailored for specific medical and biological applications (**Figure 1.3**). Different forms of polymeric biomaterials are discussed below.

#### **1.1.3.1.** *Hydrogels*

Hydrogels consist of a crosslinked polymer network with a high-water content, typically ranging from 70% to 99%. This substantial water composition imparts a physical resemblance to tissues and endows hydrogels with excellent biocompatibility and the ability to encapsulate hydrophilic drugs efficiently. Hydrogels are solid-like due to the crosslinked polymer network, and they can have a variety of mechanical characteristics. Their physical properties can be tailored to meet the soft tissues of different human bodies due to their adjustable stiffness. These systems can be delivered locally through injection, implanted surgically, or administered systemically, releasing drugs over short to long durations in either continuous or pulsatile patterns. Hydrogel-based systems vary in scale, from macroscopic to microgels and nanogels, each tailored for specific applications. Hydrogels find application in diverse fields, such as tissue regeneration and controlled drug delivery<sup>36</sup>.

#### 1.1.3.2. Polymeric films

Polymer-based films because of their ease of preparation and versatility are widely used in tissue engineering applications. Both natural and synthetic polymer-based films are used as wound dressing materials. Polymeric film dressings are classified as either interactive or passive. Natural polymer films are interactive and occlusive, while synthetic polymer films can be either. Passive, non-occlusive dressings merely cover the wound, whereas interactive, occlusive films act as barriers to microorganisms and promote wound healing. Polymer-based films absorb wound exudate and maintain a moist environment, thus, aiding in healing and regeneration. Natural polymers, such as chitosan, collagen, and alginate are widely studied for wound dressings. Synthetic polymers like PCL, PVA, and PEG, also show potential for this application. These polymers, whether used individually or as composites, enhance the film's mechanical properties<sup>37</sup>.

#### 1.1.3.3. Polymeric nanoparticles

Polymeric nanoparticles hold great potential as adaptable nanocarriers for a diverse array of therapeutics in numerous biomedical applications. They are being developed to improve the diagnosis and treatment of a variety of diseases, ranging from viral infections, cancer, pulmonary infections, cardiovascular diseases, and urinary tract infections. Advancements in controlled polymerization have allowed the engineering of advanced multifunctional polymeric nanoparticles with precise control over size, shape, charge, architecture, surface charge, and functionalization. The careful design and control over the targeting properties of these nanoparticles will secure their future development and versatility<sup>38</sup>.

# 1.1.3.4. 3D-printed polymeric biomaterials

Using computer-generated models, additive manufacturing, often known as 3D printing, allows for the automated layer-by-layer creation of complex designs. The 3D printing is currently being utilized to develop organ printing, tissue models for the delivery of drugs, regenerative tissue scaffolds, and craniofacial implants. Materials used for 3D printing should be viscous and biocompatible, and should also possess tunable mechanical properties along with drug delivery abilities. Polymers, such as thermoplastics like PCL, PVA, and PLA, hydrogels, and bio-inks in the form of composite polymers are used widely to develop 3D printed polymeric biomaterials<sup>37</sup>.

# 1.1.3.5. Nanofibers

Nanofiber technology is an emerging area of research with notable potential to address challenges in the biomedical field, including wound care, organ repair, and bone regeneration. Nanofibers offer a variety of properties and their high surface area, which further helps in cell, and drug adhesion. Additionally, they can be crafted into complex macro-scale structures that replicate hierarchical designs found in biological tissues. The versatility of polymers used in nanofiber fabrication further expands their application range. Nanofibers are often produced via electrospinning, a low-cost technique that offers exact control over fiber morphology and scalability for large manufacturing<sup>39</sup>.

#### **1.1.3.6.** *Composites*

Composite materials are combinations of two or more different materials, differing in composition or structure, to achieve specific physical and mechanical properties. Polymer-based composites consist of a polymer matrix and one or more fillers, which enhance physical, chemical, or biological characteristics. Polymer-based composites can be categorized into two main types based on the filler incorporated in the polymer matrix. The first type, bioactive polymer-based composites, includes bioactive fillers or particles. The second type, non-bioactive polymer-based composites, contains fillers, such as reinforcing agents or porogens. The use of polymer-based composites offers different

characteristics including bioactivity, antimicrobial properties, and oxygen supply, thus, making it beneficial for various biomedical applications<sup>40</sup>. Polymer-based composites, such as polymer and nanoparticles combine nanotechnology's benefits with the versatility of polymers. Applications of such combinations are found in controlled drug delivery, enhanced biocompatibility, and cell proliferation, which makes them invaluable in various regenerative medicine applications.

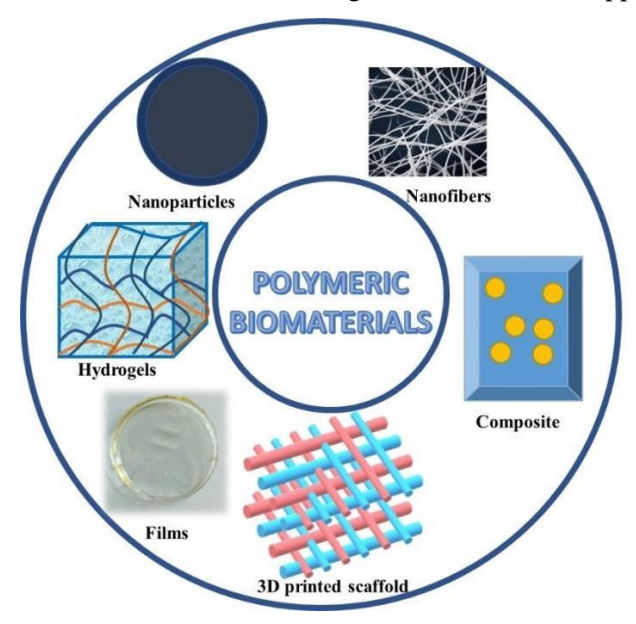


Figure 1.3. Different biomaterial forms of polymers

# 1.2. Fabrication of polymeric biomaterials

# 1.2.1. Fabrication of polymeric hydrogels/gels

Hydrogels are composed of hydrophilic polymers that are crosslinked to form a compact, threedimensional network. The process can occur through either chemical or physical crosslinking mechanisms.

## 1.2.1.1. Physical crosslinking

Physical crosslinking is a widely used method for developing polymeric scaffolds. The resulting materials from this process are known as physical or reversible gels.

# (i) Hydrogen bonding

The formation of hydrogen bonds between polymer chains leads to gelation, providing the crucial intermolecular forces that establishes a stable yet reversible three-dimensional network in gels<sup>41</sup>. The primary drawbacks of these physical crosslinking methods are insufficient mechanical stability and strength.

#### (ii) Ionic interactions

Ionic interactions are also used widely for the development of gels. They include the interaction between the oppositely charged polyelectrolytes or ions resulting in the formation of network

without using any chemical crosslinking<sup>42</sup>.

## (iii) Freeze thawing method

This technique is among the most widely employed physical crosslinking methods, achieved through repeated freeze-thaw cycles<sup>43</sup>. This process leads to the formation of microcrystals within the polymer matrix as a result of repeated freezing and thawing, which reduces the spacing between polymer chains and increases the polymer concentration.

# (iv) Hydrophobic interactions

Gels can also be formed using hydrophobic interactions<sup>44</sup>. The mechanism depends on the aggregation of hydrophobic regions within amphiphilic polymers, resulting in the formation of a stable three-dimensional network that retains water.

# 1.2.1.2. Chemical crosslinking

The chemical cross-linking method of hydrogel formation involves the development of covalent bonds between polymer chains resulting in the formation of a stable gel network with improved durability and mechanical strength.

# (i) Radical polymerization

Free radical polymerization is commonly used to create covalently crosslinked hydrogels using vinyl monomers, a radical initiator, and a crosslinker<sup>45</sup>. The key advantage of this method is the wide availability of various monomers.

#### (ii) Click reactions

Click reactions are also used widely for the development of hydrogels. The major advantage of such reactions is that they can be utilized to develop hydrogels in aqueous solutions without the need for catalysts<sup>46</sup>. Examples of click reactions involve alkyne-azide cycloaddition, Diels-Alder reaction, and thiol-ene reaction, etc.

#### (iii) Schiff base reaction

Hydrogels formed via Schiff base reactions involve the interaction between the amino functional group of polymers with the aldehyde group<sup>47</sup>. Aldehyde-containing natural polymers can be generated through partial oxidation of polysaccharides (sodium alginate, dextran, gum Arabic, hyaluronic acid, chondroitin sulfate), which then reacts with amino group-containing natural or synthetic polymers, resulting in hydrogel formation.

#### (iv) Enzyme-based crosslinking

Enzymatic crosslinking, using polymers like dopamine and tyrosine, enables rapid *in situ* gelation through oxidation with hydrogen peroxide and catalysts<sup>48</sup>. Chemical crosslinkers like formaldehyde and glutaraldehyde are common but pose toxicity risks, which can be reduced by using natural, nontoxic alternatives like genipin, tannic acid, and EDC to improve polymer stability.

# 1.2.2. Fabrication of nanoparticles

# (i) Chemical precipitation method

One of the most widely used method for the development of nanoparticles is the chemical precipitation method<sup>49</sup>. It includes the use of surfactants and non-aqueous solvents to prevent crystallite aggregation and maintain nanoparticle size, with further processing by centrifugation, drying, and optional UV polymerization.

#### (ii) Sol-gel method

The sol-gel process involves the transformation of a liquid solution (sol) into a solid gel phase through controlled processing conditions<sup>50</sup>. This technique enables the preparation of nanoparticles with precise properties. It is versatile and relatively straightforward but can require extended processing times to achieve the desired material characteristics.

#### (iii) Hydrothermal synthesis

Nanoparticle fabrication by hydrothermal synthesis includes heating a precursor solution under high temperature in a sealed container<sup>51</sup>. This method allows a precise control over particle size and shape, making it ideal for a wide variety of applications.

#### (iv) Ball milling method

The ball milling technique involves the fabrication of nanoparticles using a high-energy ball mill<sup>52</sup>. This ball mill grinds bulk materials into small particles. The mechanism involves the collision of balls with the samples, resulting in the mechanical breakdown into nanoscale particles. The major advantages of this technique include simple usage, cost-effectiveness, and ability to fabricate different types of nanoparticles.

# 1.2.3. Fabrication of polymer-coated nanoparticles

#### (i) Physical adsorption

This method involves the development of polymer-coated nanoparticles by adsorption of polymers onto the surface of the nanoparticle with the help of weak interactions, such as hydrogen bonding and Van der Waal forces<sup>53</sup>.

#### (ii) Chemical grafting

Chemical grafting is a method that is widely used for the fabrication of polymer-coated nanoparticles<sup>54</sup>. Polymers are chemically grafted onto the nanoparticle surface with the help of covalent bonds using coupling agents.

#### (iii) Layer-by-layer assembly

Layer by layer method involves the deposition of alternating layers of oppositely charged polymers onto the surface of nanoparticles using electrostatic interactions<sup>55</sup>.

## 1.3. Characterization of polymeric biomaterials

#### 1.3.1. Characterization of hydrogels/gels

# (i) Rheology

The rheological properties of hydrogels are crucial to understand the mechanical and viscoelastic

properties of hydrogels<sup>56</sup>. Different types of tests including amplitude sweep, frequency sweep, and self-healing analysis provide essential insights, which is essential for optimizing their design for specific applications.

# (ii) Swelling and degradation studies

Swelling of the hydrogels is the ability of hydrogel to absorb water and expand, controlled by different factors including the composition of polymer structure and its crosslinking density<sup>36</sup>. The degradation behavior determines the stability of hydrogels, which is important for various biomedical applications including wound healing, drug delivery, and tissue regeneration.

# (iii) Porosity

Porosity and pore size distribution are crucial parameters for vascularization, cell infiltration, and guided tissue regeneration in hydrogels<sup>57</sup>. These properties can be estimated using various techniques, including microcomputed tomography (µCT) for 3D visualization and quantitative analysis, scanning electron microscopy (SEM) for high-resolution imaging of pore structure, and gravimetric methods for indirect estimation based on mass changes. Each method provides valuable insights into the hydrogel's internal architecture, enabling optimization for specific biomedical applications.

## (iv) FTIR

Fourier Transform Infrared (FTIR) spectroscopy is an analytical technique that is used to identify the functional groups and characterize the chemical composition of materials, including hydrogels and other polymers. It can be used to determine the crosslinking composition of hydrogels<sup>58</sup>.

## (iv) FESEM

Field Emission Scanning Electron Microscopy (FESEM) is a technique that is used to determine the surface morphology and microstructure of hydrogels<sup>59</sup>. This technique helps to determine the various properties of hydrogels including porosity and surface morphology.

#### 1.3.2. Characterization of nanoparticles and polymer-coated nanoparticles

## (i) Dynamic light scattering (DLS)

DLS also known as photon correlation spectroscopy helps to investigate the hydrodynamic size of the particles. The principle is based on the analysis of the scattering of light by the particles suspended in the liquid medium<sup>60</sup>. It is widely used to analyze the particle size of different types of materials including nanoparticles.

#### (ii) Zeta analysis

Zeta potential is a crucial property of particles in suspension, macromolecules, and material surfaces. It aids in optimizing formulations of suspensions and emulsions, predicting surface interactions, and assessing the long-term stability of materials. Zeta potential is also widely used in nanoparticle analysis<sup>61</sup>.

# (iii) HRTEM

High-resolution transmission electron microscopy (HRTEM) is a highly effective technique for directly imaging atoms in nanoparticles. Conventional TEMs typically offer image resolutions better than 0.2 nm, which makes them well-suited for resolving atomic-scale structures in nanoparticles<sup>62</sup>.

#### (iv) Ultraviolet-visible spectroscopy

Ultraviolet-visible spectroscopy is a technique used to measure the absorption and scattering of light by a sample. Nanoparticles exhibit optical properties that are sensitive to their size, shape, concentration, agglomeration state, and the refractive index near their surface. This sensitivity makes UV-visible spectroscopy a valuable tool for identifying, characterizing, and studying these materials<sup>63</sup>.

#### (v) Brunauer-Emmett-Teller (BET) analysis

This technique is used to estimate the specific surface area of nanoparticles. Its mechanism is based on the adsorption of gas (usually nitrogen) onto the surface of the particles at different pressures, to calculate the surface area<sup>64</sup>. BET analysis is helps in the characterization of surface properties of nanoparticles, which can influence their properties.

# 1.4. Applications of polymeric biomaterials

# 1.4.1. Tissue regeneration

The loss of tissues and organs poses a significant threat to human health, affecting millions annually due to aging, trauma, or injury. Restoring damaged tissues and failed organs remains a major clinical challenge. In their quest to heal damaged tissues, scientists innovatively developed the concept of "tissue engineering." This interdisciplinary approach integrates principles from materials science, biology, medicine, and engineering to develop *in vitro* substitutes for later *in vivo* implantation. Introduced in the 1980s, "tissue engineering" has seen notable advancements over the past thirty years. The formation of new tissues requires extensive *in vitro* cell isolation, expansion, and maturation. Moreover, the availability of autologous cells is limited, and cells from native tissues are heterogeneous and difficult to standardize. Additionally, tissues engineered *in vitro* lack integrated structures and comprehensive functions. These limitations have driven scientists to seek alternative approaches. With advancements in biomaterials science and a deeper understanding of tissue regeneration, researchers have begun focusing on *in situ* tissue regeneration, aiming to restore damaged tissues directly at the defect sites using biomaterials<sup>65</sup>.

#### 1.5. Skin tissue regeneration

The fundamental function of skin, which makes up around one-sixth of the body, is to shield the internal organs. Skin tissue remodels itself to repair sick or damaged tissue. This process starts with the development of hematomas and continues through a series of phases that eventually lead to the

regeneration of new skin. In some cases, such as burns, trauma, or diseases this complex process is hindered and requires surgery to promote tissue regeneration. In these situations, surgical intervention is the best way to heal the wound. Surgery is considered for wounds that are not deep or have a big surface area. Due to these shortcomings, the idea of tissue engineering to regenerate skin tissue is appealing since it can solve several issues with conventional wound healing techniques<sup>66</sup>.

# 1.5.1. Anatomy and physiology of the skin

The skin tissue consists of three distinct layers: the epidermis, dermis, and hypodermis, which are the outermost, middle, and deepest layers of the skin. Each layer plays a specific role in the overall function of the skin. The epidermis is the outermost layer of the skin and acts as a barrier. It is composed of keratinocytes, melanocytes, and Langerhans cells. The middle layer dermis and the dense connective tissue layer beneath the epidermis contains enzymes, blood vessels, nerves, and glands. The hypodermis, the innermost layer beneath the dermis, is composed of vascularized adipose tissue, providing mechanical strength and thermoregulation. Large collagen fibers are just slightly present in this layer, which is primarily composed of elastin fibers<sup>67</sup>. Skin tissue is a metabolically active tissue that is frequently remodelled. Due to injury or trauma, the process of remodeling is hindered, resulting in wounds. Wound healing is a complex process involving four stages including hemostasis, inflammation, proliferation, and remodeling (**Figure 1.4**).<sup>68</sup>

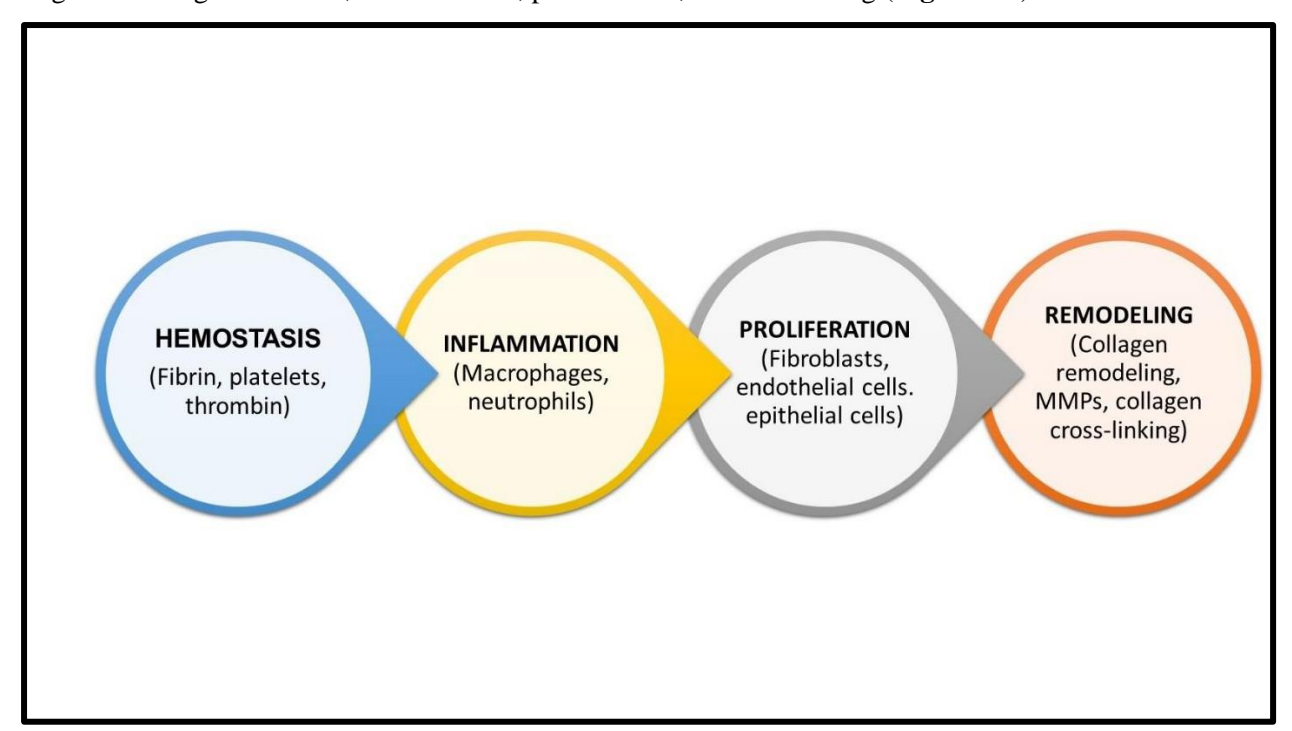


**Figure 1.4.** Different stages of wound healing.

#### 1.5.2. Different stages of wound healing

## (i) Hemostasis

After an injury, thrombin is activated by prothrombin activators, which results in the formation of a fibrin clot. Additionally, platelet-derived growth factor (PDGF) and transforming growth factor- $\beta$  (TGF- $\beta$ ) are released.

#### (ii) Inflammation

The inflammatory phase is marked by the influx of leukocytes into the wound site. Chemokines released during hemostasis, along with mast cells, recruit neutrophils and monocytes, prompting their migration from capillaries to the injured tissue.

#### (iii) Proliferation

In the later stages of inflammation, monocytes get converted into macrophages and remove debris. It releases chemokines like fibronectin, attracting fibroblasts to the wound site to initiate the proliferative phase. This phase typically begins two days after injury. Angiogenesis, collagen deposition, re-epithelialization, and granular tissue formation comprise this phase.

#### (iv) Remodeling

The remodeling phase begins on the 9<sup>th</sup> day of the healing process. This stage includes the synthesis and breakdown of collagen and conversion of type III collagen to type I collagen and depositing in a well-organized and orderly network, thus strengthening the regenerated tissue.

#### 1.5.3. Role of bacterial infections and biofilm formation in tissue regeneration

The presence of bacterial infections and biofilm formation notably hinder the wound healing process, hampering the tissue regeneration process and affecting more than 150 million individuals globally<sup>69</sup>. Also, the prevalence of antibiotic-resistant bacteria, resulting in over 700,000 deaths each year, exacerbates the problem by reducing the effectiveness of conventional antibiotic treatments. The common bacteria involved in wound infections are *Pseudomonas aeruginosa*, *Staphylococcus aureus*, methicillin-resistant *S. aureus*, and *Streptococcus pyrogens*. These bacterial infections at wound sites can delay wound healing and, in certain situations, have major consequences that could be fatal. Bacteria in wounds can further form biofilms, complex aggregations of bacteria enclosed in extracellular polymeric substances (EPSs), which provide a protective barrier against antibiotics and immune responses. This biofilm not only enhances bacterial resistance but also delays wound healing by prolonging chronic inflammation and infection (**Figure 1.5**)<sup>70</sup>.

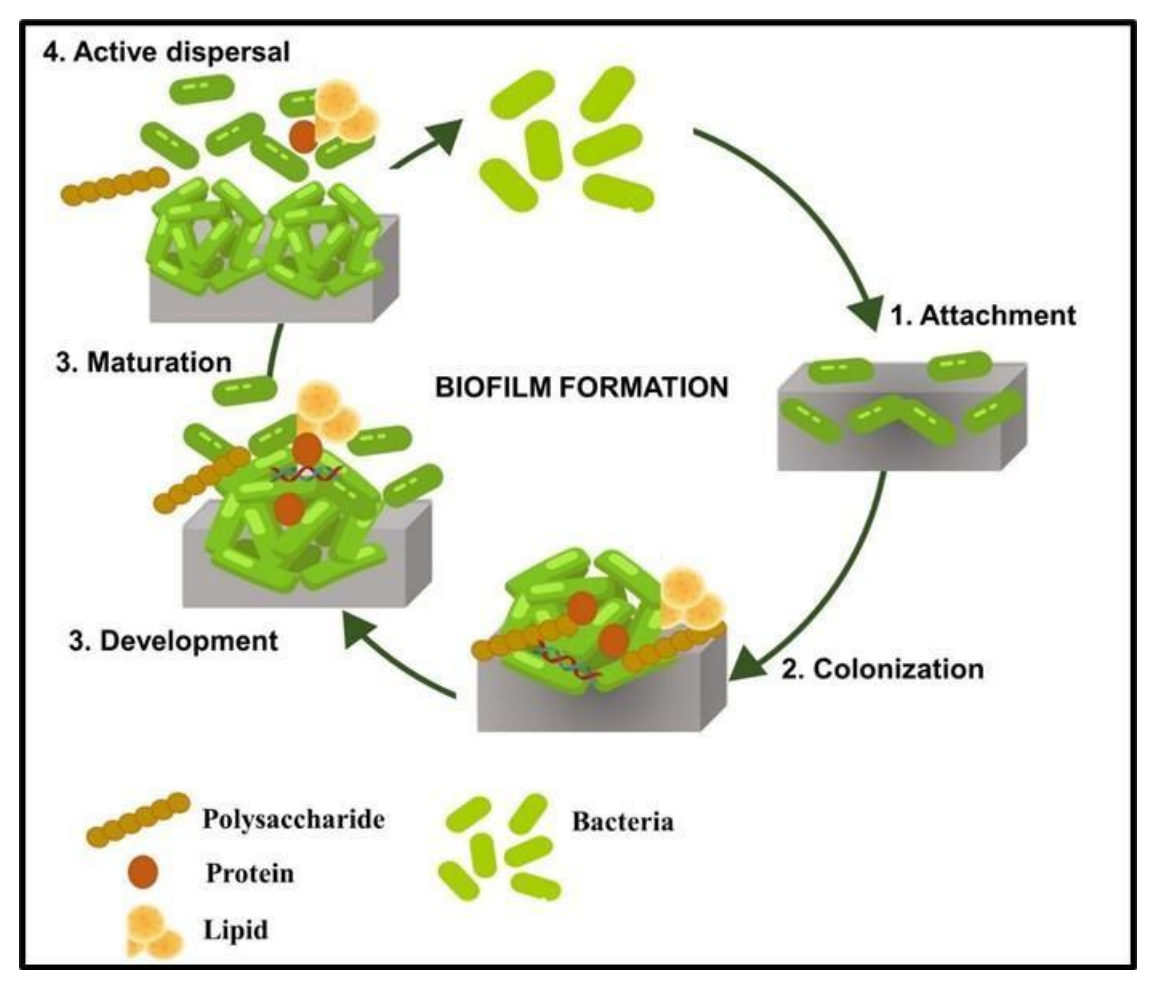


**Figure 1.5.** Different stages of biofilm formation.

# 1.6. Treatment strategies for bacteria-infected wounds (literature review)

Wound healing management in clinical settings varies according to wound classification, the type of tissue involved, innate restorative capacity, and other environmental factors. Current strategies encompass the use of topical medications, growth factors, autografts, allografts, ultrasound, negative pressure therapy, and electrotherapy. Conventional passive wound dressings, such as bandages and cotton wool are often unsuitable for open wounds and do not actively contribute to the healing process. Lately, advanced wound dressings combined with antibiotics, such as cephalosporins, aminoglycosides, and quinolones are used. These dressings act by targeting bacterial cell walls, protein synthesis, nucleic acid synthesis, or metabolic pathways<sup>71</sup>. Also, the use of topical antimicrobials, such as silver-based gels and fusidic-based ointments suffer from restrictions, such as bacterial resistance, ineffectiveness against biofilm, and narrow spectrum antibacterial activity<sup>72</sup>. Consequently, developing new, multifunctional treatment strategies that can effectively combat antibiotic-resistant infections and promote wound healing and skin regeneration is the need of the hour. Recently, the use of different biomaterial-based materials including nanoparticles and hydrogels have been developed. Shoukani *et al.* developed PEG coated ZnO nanoparticles loaded with

ciprofloxacin for enhanced antibacterial and wound healing effects<sup>73</sup>. Li *et al.* worked on novel multifunctional composite nanoparticles with angiogenesis and anti-inflammatory properties for diabetic wound healing applications<sup>74</sup>. Kamalipooya *et al.* developed chitosan/cerium oxide nanoparticle-loaded PCL/ cellulose based scaffold for diabetic wound healing<sup>75</sup>.

An ideal wound dressing must be able to protect against infection and fluid loss, permit gas exchange, maintain high moisture content, offer thermal insulation, and should be easy to handle by clinical practitioners. However, additional expectations for an optimal wound dressing have emerged recently, which includes non-irritant, painless, and easy to remove. The dressings must be able to deliver bioactive agents such as antimicrobials at the site of injury (**Figure 1.6**)<sup>76</sup>.

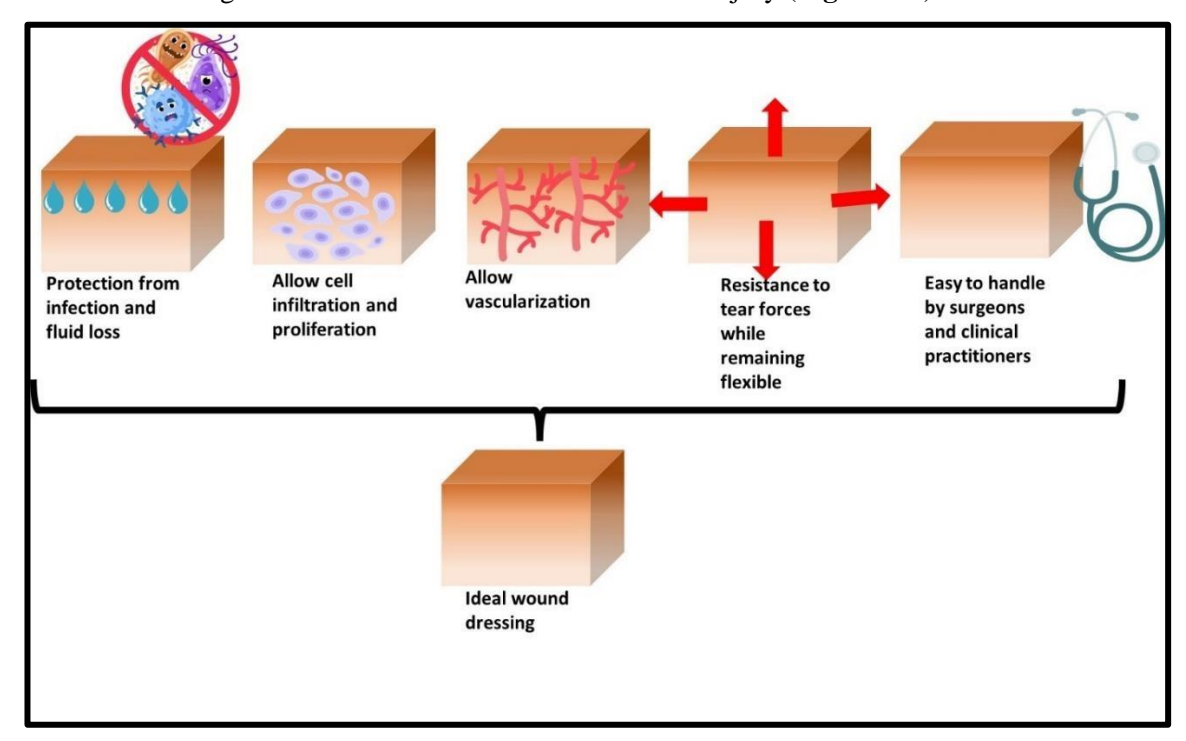


**Figure 1.6.** Properties of an ideal wound dressing.

#### 1.6.1. Polymeric hydrogels/gels for wound healing

Hydrogel-based scaffolds have shown potential as ideal wound dressing material as they offer different properties including moist environment, removal of wound exudates, impermeability to bacteria, and suitable environment for tissue regeneration. A range of commercial hydrogel-based wound dressings have been developed including Coseal®, Evicel®, Algisite M, and Tegaderm™ hydrocolloid dressing<sup>77</sup>. Notably, wound dressings based on hydrogels with polymeric networks mimic extracellular matrix and can be used to deliver different bioactive agents helping in localized and sustained delivery. Natural hydrogels fabricated using natural polymers such as chitosan, gelatin, carboxymethylcellulose, and hyaluronic acid have shown promising results as wound dressing materials. The unique advantages of natural polymers, such as hemostasis, anti-inflammation, and

cell proliferation, have driven the development of natural-based hydrogels as effective wound dressings. These properties accelerate the wound-healing process<sup>76</sup>. Wang *et al.* developed nanodiamond-based hydrogels for infected wound healing<sup>78</sup>. Bhardwaj *et al.* worked on polyacrylamide/gelatin-based self-healing and antimicrobial hydrogel film for wound healing application<sup>79</sup>. Sun *et al.* developed novel natural polymer-based hydrogel patches for hemostasis and wound healing applications<sup>80</sup>. Li *et al.* developed collagen-based injectable hydrogel using self-assembled nanoparticles for wound healing<sup>81</sup>. Liu *et al.* developed a double physical network hydrogel loaded with tannic acid to improve wound healing and prevent scar formation in infected wounds<sup>82</sup>. Ma *et al.* fabricated a composite hydrogel of sodium alginate and gelatin doped with black phosphorus@ZnO for cutaneous wound healing<sup>83</sup>. Deng *et al.* worked on microenvironment-responsive smart hydrogel system with immune regulation and antibacterial activity for chronic wound healing<sup>84</sup>. Qiao *et al.* developed conductive self-healing hydrogel with antibacterial activity with dual dynamic bonds for increased wound healing applications<sup>85</sup>. Wang *et al.* developed multifunctional mussel inspired self-healing, antioxidant, and adhesive hydrogel system for wound healing applications<sup>86</sup>.

Despite the availability of different hydrogel-based products on the market, the development of advanced hydrogel dressings is still ongoing, to improve skin healing for specific therapeutic applications. Notably, there is an increasing trend toward developing hydrogel formulations that incorporate multiple materials.

# 1.6.1.1. Nanoparticle-loaded hydrogels for wound healing

The use of nanoparticles in the treatment of bacteria-infected wounds has shown promising results because of unique optical, biological, and physiochemical characteristics<sup>87</sup>. With the rise in antibiotic resistance, the use of nanoparticles with intrinsic antibacterial properties, such as gold, silver, zinc oxide, and copper has become a viable substitute for managing bacterial infections (**Figure 1.7**). These nanoparticles possess complex antimicrobial mechanisms, significantly reducing the likelihood of bacteria developing drug resistance. Liu *et al.* developed Cu<sub>3</sub>SbS<sub>3</sub>-based nanoparticles for inhibition of bacteria and enhanced wound healing<sup>88</sup>. Yu *et al.* fabricated metal phenolic network nanoparticles with excellent biocompatibility for wound healing applications<sup>89</sup>. The nanoparticles used for the treatment of bacteria-infected wounds are as follows:

## 1.6.1.1.1. Metal and metal oxide nanoparticles

Different metal-based nanoparticles have been developed including gold, silver, copper, gallium, and zinc for antibacterial treatment. The mechanism of action of these antibacterial nanoparticles includes alteration of bacterial cell permeability, generation of reactive oxygen species that damage cellular structures, or absorption of metallic ions by bacterial cells, causing ATP depletion and finally disruption in DNA replication<sup>90</sup>.

# (i) Silver nanoparticles

Silver-based nanoparticles are widely used as antibacterial agents to treat burns and different types of bacteria-infected wounds<sup>91</sup>. These nanoparticles act by disrupting the bacterial cell membrane and inhibiting enzyme activity. These silver nanoparticles attach to the bacterial cell membrane and interact with sulfur and phosphorus groups in DNA and protein, resulting in a strong antibacterial effect. Because of strong antibacterial activity, these nanoparticles have been added to different types of wound dressings like chitosan-based scaffolds and electrospun polycaprolactone scaffolds<sup>92</sup>. These nanoparticle-loaded scaffolds showed enhanced antibacterial activity beneficial for the treatment of bacteria-infected wounds. Zhang *et al.* developed silver nanoparticle-loaded polyasparthydrazide nanofibrous hydrogel for the treatment of full-thickness wound healing<sup>93</sup>. Huang *et al.* fabricated silver nanoparticles/gelatin composite cryogel for the treatment of *P. aeruginosa*-infected wound healing.<sup>94</sup>

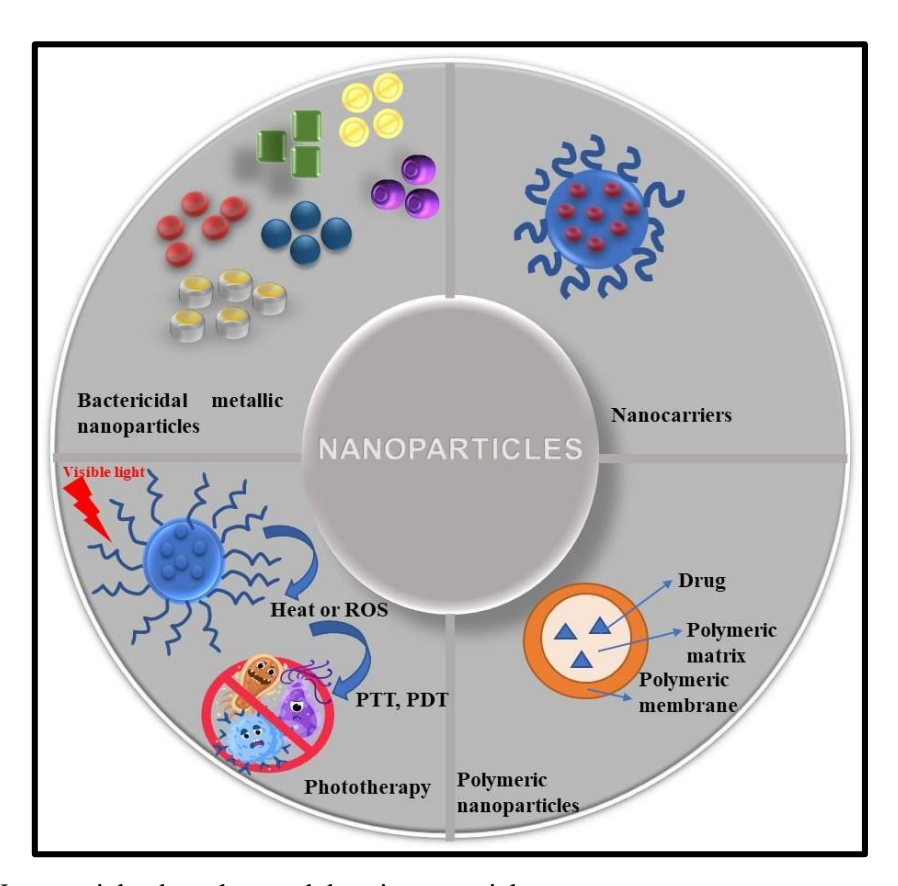


Figure 1.7. Nanoparticles-based wound dressing materials.

## (ii) Copper nanoparticles

Copper nanoparticles because of their antibacterial activities, have been used to inhibit a broad range of bacterial species<sup>95</sup>. They act by releasing copper nanoparticles, which damage bacterial cell walls and membranes by solidifying protein structures. Copper nanoparticles exhibit size and

concentration-dependent activity. They tend to attach to bacteria and possess the ability to penetrate their cell membranes. The released Cu<sup>2+</sup> ions disrupt the bacterial cell wall, resulting in the degradation of cytoplasm, ultimately causing bacterial death. Copper nanoparticles were also incorporated in wound dressings. For example, a copper nanoparticle-coated wound dressing made of cotton using a layer-by-layer electrostatic self-assembly approach showed rapid and effective bacterial eradication of *Acinetobacter baumannii* in skin wounds<sup>96</sup>. Li *et al.* developed copper nanoparticles and deferoxamine-loaded sodium alginate based hydrogels for diabetic wound healing<sup>97</sup>. Zhang *et al.* fabricated copper-based material for controlled release of nitric oxide for enhanced diabetic wound healing<sup>98</sup>.

# (iii) Gallium nanoparticles

Gallium-based nanoparticles have the same ionic radius, charge, and electronic configuration as that of Fe<sup>3+</sup>. <sup>99</sup> However, gallium ions cannot be reduced, unlike iron, rendering redox processes irreversible and disrupting critical bacterial functions, which makes it an efficient antibacterial agent. Studies have shown that gallium possesses broad-spectrum antibacterial activity. Owing to its antimicrobial properties and lack of antibiotic resistance, Ga<sup>3+</sup> has been suggested as a promising candidate for treating wound infections and enhancing biomaterials to prevent implant-associated infections. Gallium-based scaffolds have also been developed. For example, gallium incorporated antibacterial collagen-based dermal scaffold have been reported earlier<sup>100</sup>. Yang *et al.* developed gelatin nanoparticles modified with gallium for wound healing and macrophage polarization<sup>101</sup>. Qin *et al.* worked on gallium (III) mediated dual cross linked alginate-based hydrogels to promote healing in bacterial infected wounds<sup>102</sup>.

# (iv) Gold nanoparticles

Gold nanoparticles also exhibit strong antibacterial activity, which makes them suitable candidates for tissue regeneration applications <sup>103</sup>. These nanoparticles act by getting attached to the bacterial cell membrane and making holes in the cell wall, resulting in intracellular content leakage, which eventually leads to bacterial cell death. Gold nanoparticles have shown effective activity against different bacterial species like *S. aureus*, MRSA, and *P. aeruginosa*<sup>104</sup>. Gold nanoparticles have been loaded in different polymer-based scaffolds. Gold nanoparticles embedded in a poloxamer 407 hydrogel showed strong antibacterial activity against *S. aureus* and *P. aeruginosa*<sup>105</sup>. He *et al.* fabricated gold nanoparticle-based antimicrobial polymer hybrid for the treatment of bacteria-infected wound healing <sup>106</sup>. Chen *et al.* developed gold nanoparticle-loaded self-assembled hydrogel-based wound dressing for the treatment of bacteria infected wounds <sup>107</sup>.

# (v) Zinc oxide nanoparticles

Zinc oxide nanoparticles are also widely used for biomedical applications as fillers in cosmetics and

medical items as they offer different characteristics including cytocompatibility, biosafety, and antibacterial activities <sup>108</sup> Their mechanism of action of antibacterial activity involves the accumulation of zinc ions on the bacterial cell membrane and cytoplasm, resulting in bacterial death. Zinc oxide nanoparticles have been loaded in CS hydrogel and collagen-based wound dressings that showed a decreased risk of infections, thereby, helping in effective wound healing <sup>109</sup>. Hemdan *et al.* developed zinc oxide nanoparticles to combat bacterial skin infections <sup>110</sup>. Batool *et al.* studied the antimicrobial and wound healing properties of biosynthesized zinc oxide nanoparticles <sup>111</sup>.

## 1.6.1.1.2. Polymeric nanoparticles

Polymer-based nanoparticles have garnered a lot of interest in the field of biomedical engineering. They have been used to deliver different therapeutic agents like antibacterial agents, growth factors, and drugs. Different types of polymers including polycaprolactone, PLGA, and chitosan-based nanoparticles have been employed for the development of polymer-based nanoparticles<sup>112</sup>. These nanoparticle scaffold systems hold great promise for revolutionizing wound care, particularly in the treatment of bacterial-infected wounds.

**Table 1.1.** Various nanoparticle-loaded hydrogel materials used for wound healing.

Nanomaterial used	Hydrogel system	Applications	References
Cerium oxide	Polyvinyl	Robust wound	Kalantari et al. <sup>113</sup>
nanoparticles	alcohol/chitosan	dressing material	
	hydrogel		
Titanium	Chitosan hydrogel	Effective	Rahmanpour et al. <sup>114</sup>
dioxide/aluminum		antimicrobial tissue	
oxide nanoparticles		adhesive	
Silver nanoparticles	Guar gum hydrogels	Antibacterial agent	Bhubhanil et al. 115
Chitosan	Calcium alginate	Antibacterial agent	Wang et al.116
nanoparticles	hydrogel	against E.	
		coli and S. aureus	
Silver nanoparticles	Carboxymethylcellulose	Maintains a moist	Das <i>et al</i> . <sup>117</sup>
	hydrogel	wound environment	
		and facilitates early	
		wound healing	
Silk fibroin-sodium	Poly(N-	Induces proliferation	Rezaei et al. <sup>118</sup>
alginate nanoparticles	isopropylacrylamide)	and growth of the	
	(PNIPAM) hydrogel	fibroblast cells	
Cerium oxide	Dextran hydrogel	Prolonged drug	Andrabi et al. <sup>119</sup>
nanoparticles		release, accelerated	

		cell migration, in
		vivo anti-
		inflammatory activity
Eudragit	Polymeric hydrogel	Acts as an efficient Fan et al. 120
nanoparticles		free radical scavenger

# 1.7. Rational design of nanoparticle-based polymeric hydrogels/gels system for skin tissue regeneration (literature review)

Nanoparticles with antibacterial potential have been integrated into different hybrid systems to increase the efficacy of these biomaterials. In this line, adding antibacterial nanoparticles to hydrogel systems has drawn a lot of interest and has shown notable potential in tissue regeneration applications<sup>121</sup>. Encapsulating nanoparticles into a hydrogel system offers various advantages including protection from aggregation and degradation. This combination enhances the bioavailability of therapeutic agents, minimizes side effects, and improves therapeutic effects with patient compliance. Researchers have worked on different nanoparticle-polymer systems for wound-healing applications<sup>122</sup>. Konai et al. fabricated polyacrylamide hydrogel integrated nanoparticle stabilized liposomes have been developed 123. The system resulted in bacterial death via membrane fusion. Tian et al. developed red blood cell membranes coated with polymeric nanoparticles were loaded into hydrogels to treat local bacterial infections<sup>124</sup>. This approach neutralized toxins from Staphylococcus aureus, and notably reduced skin lesions. Khoshmaram et al. developed curcumin-loaded chitosan nanoparticles in gelatin methacrylate hydrogel for wound healing applications<sup>125</sup>. Hu et al. developed novel polyphenol magnesium nanoparticles loaded in multifunctional dual-network to treat MRSA-infected wound healing<sup>127</sup>. Li et al. fabricated phycocyanin loaded chitosan/collagen/genipin hydrogel to accelerate wound healing 126. Zhao et al. developed bioreduced silver nanoparticle-loaded chitosan based multifunctional hydrogel system to accelerate wound healing<sup>127</sup>. Aly et al. developed simvastatin polymeric nanoparticle-loaded hydrogel for wound healing<sup>128</sup>. Abdelkader et al. develop insulin-loaded nanoparticles in poly(vinyl alcohol)-borate hydrogels for cutaneous wound healing 129. Gong et al. developed exudate absorbing antimicrobial dressing to promote burn wound healing 130. Jayabal et al. fabricated chitosan-based wound dressing patch for increased hemostatic, antibacterial, and wound healing applications 131 Overall, these nanoparticle-hydrogel systems combine the properties of two different materials in a single biomaterial with the combined properties of both. With the help of other mechanisms, these nanoparticle-hydrogel systems can facilitate the wound healing process resulting in effective tissue regeneration.

# 1.7.1. Promoting hemostasis

Hemostasis is an important step in the wound-healing process. Certain nanoparticles can interact with blood components to accelerate the coagulation cascade<sup>132</sup>. Also, using cationic polymers, such as chitosan, which can interact with the negatively charged RBC membrane to help in platelet aggregation facilitating the wound healing cascade<sup>133</sup>. Kong *et al.* developed CuS nanoparticles loaded hydrogels with excellent hemostasis, and antibacterial activity<sup>134</sup>. The system promoted the wound-healing process indicating that targeting hemostasis can accelerate the wound healing process.

## 1.7.2. Scavenging reactive oxygen species

Reactive oxygen species (ROS) play a very important role in different stages of wound healing <sup>135</sup>. Low levels of ROS are essential for combating external damage. However, excessive oxidative stress and a decline in antioxidant capacity can lead to a redox imbalance, which is a notable factor in the failure of wounds, especially diabetic wounds. Excessive ROS production can also prolong the inflammatory phase of wound healing, causing chronic inflammation. This chronic inflammation disrupts the normal progression of the healing process. Therefore, targeting oxidative stress could help to improve the wound-healing process <sup>116</sup>. Zhang *et al.* developed polydopamine/puerarin nanoparticle-loaded hydrogel for wound healing applications <sup>136</sup>. The hydrogel exhibited excellent mechanical and swelling properties, caused a reduction in oxidative stress, and accelerated the skin regeneration process.

# 1.7.3. Prevention of microbial infection

Bacterial infection, antibiotic resistance, and biofilm formation are major challenges in efficient tissue regeneration<sup>137</sup>. To tackle this problem, different polymer-based antibacterial techniques have been developed. These polymer-based materials have less chance to cause resistance as they target mainly bacterial cell membranes. Also, some of the polymeric materials have demonstrated excellent antibiofilm properties and have shown excellent activity in case of burn wounds and surgical wounds<sup>123</sup>. Combining polymeric materials with nanoparticles further enhances the antibacterial activity. Zhou *et al.* fabricated a CuS nanoparticle hydrogel system, which provided a sustained release pattern of Cu<sup>2+</sup> ions and fastened the wound healing process *in vivo*<sup>134</sup>.

# 1.7.4. Proliferation and remodeling

This also constitutes one of the major phases of the wound-healing process<sup>138</sup>. Researchers have developed various systems with characteristics resembling those of the ECM. Also, nanoparticles can be loaded with growth factors and hydrogel that can provide the supportive matrix for cell adhesion will ultimately help in the proliferation and migration of fibroblasts and keratinocytes, essential for tissue regeneration. Jing *et al.* developed a titanium-hydroxyapatite nanocomposite for wound healing applications<sup>139</sup>. The system showed excellent biocompatibility against L929 and

HUVECs cells and also exhibited proliferative effects. Thus, the development of an efficient nanoparticle-hydrogel system can help to enhance cell proliferation, collagen deposition, and angiogenesis along with a balanced remodeling process. These combined effects create an optimal environment for tissue regeneration, thereby, accelerating the healing process and improving the quality of the regenerated tissue.

# **1.8.** Bone tissue regeneration

Bone defects because of trauma, infections, and tumors cannot be self-repaired on their own, and it has become a huge clinical and social burden<sup>15</sup>. Currently, bone grafting including autografts and allografts is the gold standard therapeutic option for such cases, but a lack of donor grafts and donor site problems limit its clinical application. Consequently, to address these unmet demands, alternative therapeutic methods are required<sup>140</sup>.

# 1.8.1. Anatomy and physiology of bone

Bone is a tough yet lightweight part of the skeletal system<sup>141</sup>. Bones are attachment points for tendons, ligaments, and muscles, which allows movement. It's a composite material made of a hard, brittle mineral and flexible collagen. This combination gives bone its strength to resist compression and its ability to bend and twist. From a materials perspective, bone is a hierarchical nanomaterial composed of organic collagen nanofibers and inorganic nanocrystalline hydroxyapatite, spanning from the nanoscale to the macroscale<sup>142</sup>. Also, different types of cells are involved in maintaining bone hemostasis. This lineage of cells encompasses osteoblasts, osteoclasts, and chondrocytes. Osteoblasts are the major cells involved in bone regeneration are osteoblasts. These cells produce various proteins osteocalcin, osteopontin, alkaline phosphatase, and collagen type 1. Multiple osteoblasts collaborate to form an osteon, the fundamental unit of bone, and osteoclasts are large, multinucleated cells that are principally in charge of bone resorption. These cells come from the hematopoietic lineage and become mature as a result of the interaction between nuclear factor kappa-B ligand (RANKL) and macrophage colony-stimulating factor (M-CSF)<sup>143</sup>. A balance between osteoblast and osteoclast activity is essential for effective bone repair and maintaining skeletal health. However, bone abnormalities resulting from trauma, surgical procedures, and infections can disrupt this balance, and it leads to local impairments posing a significant public health risk<sup>144</sup>. The whole process of bone regeneration involves different steps (**Figure 1.8**).

#### **1.8.2.** Acute inflammatory phase and hematoma formation

Injury in bone tissue results in acute inflammation, which peaks in 24 h and ends in 7 days<sup>145</sup>. At the site of fracture, blood vessels tear releasing platelets and plasma. Within a day of injury, plasma coagulates to form a fibrin network called hematoma, which serves as a template for the formation

of callus.

## 1.8.3. Inflammatory phase

This phase involves the release of a wide range of factors including vascular endothelial growth factor, and different bone morphogenic proteins, such as BMP-6, BMP-2, interleukin 1, interleukin 6, and interleukin  $11^{146}$ . These factors work together to aid in attracting the inflammatory cells and stimulating the growth of new blood vessels. TNF- $\alpha$  directs the mesenchymal stem cells towards the osteogenic lineage, which also recruits the essential cells for healing. Bone morphogenic factors help in the recruitment of MSCs. IL 6 supports VEGF production and the formation of new blood vessels. This further leads to the development of granulation tissue and bone formation via endochondrogenesis.

#### **1.8.4.** Soft callus formation

Following 7-9 days of injury the development of soft callus begins<sup>147</sup>. Cartilage-like tissue creates a soft callus that gives the fracture a sturdy framework.

#### **1.8.5.** Hard callus formation

The replacement of the soft callus with a firm, bony callus is crucial for bone repair <sup>148</sup>. The Wnt family of molecules regulate the MSC development into the osteoblastic lineage, which is critical for the creation of hard callus. A subperiosteal intramembranous ossification process begins concurrently with the creation of the soft callus, resulting in the hard callus. The development of hard callus peaks on day 14. At this point, the callus hardens and becomes mechanically inflexible. During this period, the presence of ECM markers, such as osteonectin, alkaline phosphatase (ALP), and type I procollagen gene is evident.

# 1.8.6. Remodeling

After an injury, remodeling starts 3-5 weeks later and can take years to fully recover the original shape of the bone <sup>149</sup>. The hard callus finally remodels into the lamellar bone through a resorptive phase. The whole process of bone remodeling is a regulated process and it includes quiescence, activation, resorption, reversal, bone formation, and mineralization. Osteocytes, which control osteoclast and osteoblast differentiation, are principally responsible for this process. The bone returns to its previous shape when osteoblast-mediated bone synthesis and osteoclast-mediated bone resorption are balanced, which is made possible by paracrine factors and signaling <sup>150</sup>.

## 1.8.7. The impact of bone abnormalities on bone regeneration

Bone abnormalities can significantly impede the process of bone regeneration, disrupting the intricate balance required for effective healing<sup>151</sup>. Abnormalities, such as bone infections, genetic disorders, osteoporosis, and other diseases can change the regular physiological process, which

results in inadequate or delayed bone healing. The recruitment and development of mesenchymal stem cells, the synthesis of vital growth factors like VEGF and BMPs, and the equilibrium between osteoblast and osteoclast activity can all be negatively impacted by these anomalies. As a result, the remodeling stage, which is essential for returning the bone to its natural strength and structure is compromised. A weaker, less organized bone tissue may also emerge as a result of bone abnormalities, raising the risk of fractures and other disorders.

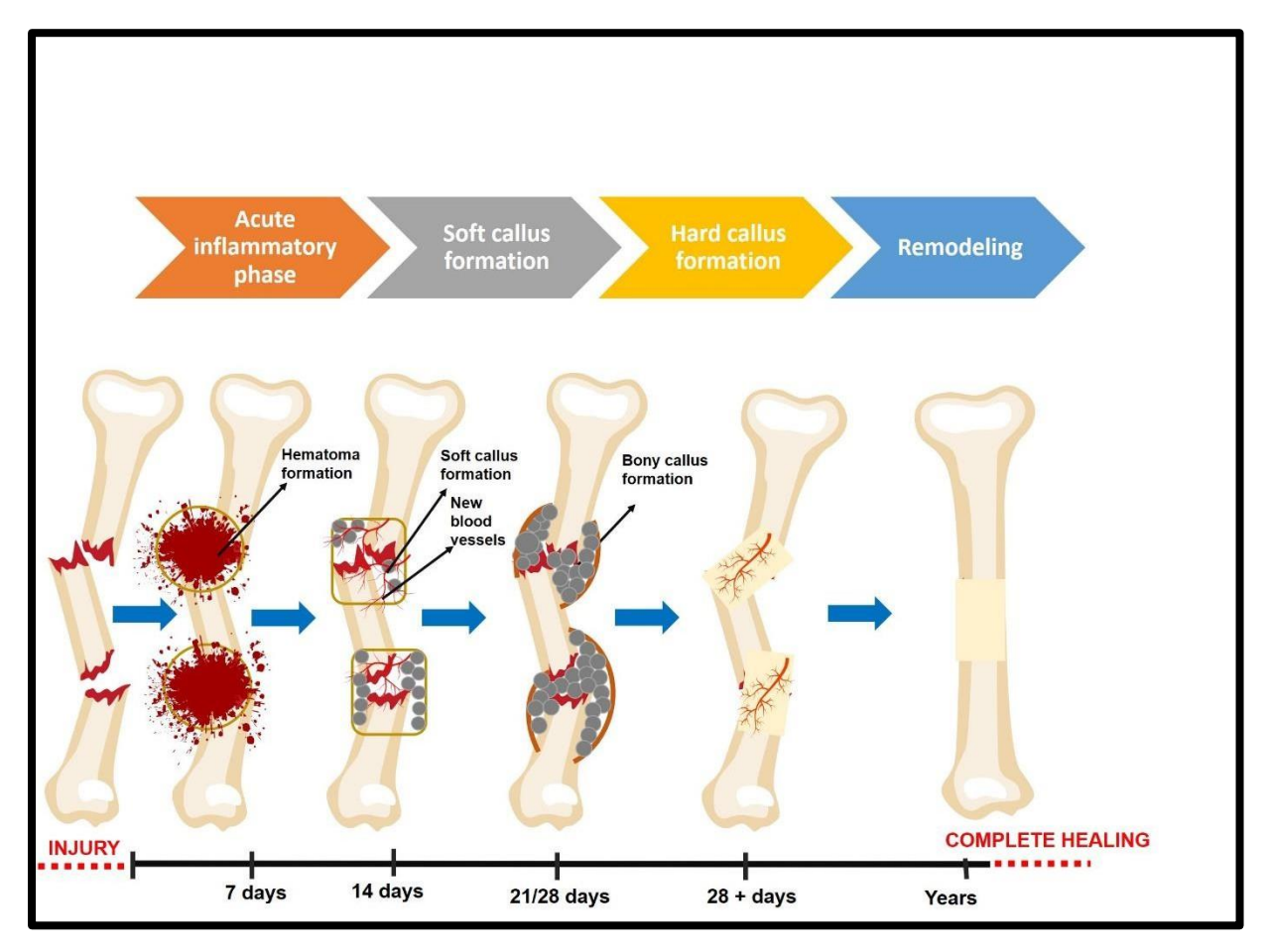


**Figure 1.8.** Different stages of bone regeneration.

# 1.9. Materials-based strategies to promote bone tissue regeneration (literature review)

Comprehending the effects of bone defects is crucial to creating customized treatments and cuttingedge biomaterials that will promote bone growth and boost patient outcomes. Strategies to restore damaged bone with laboratory-made materials began in the early 19th century when surgeons explored calcium phosphates as bone grafts. Initially, implants merely filled bone defects with biologically inert substances. Over time, strategies evolved to use bioactive materials for regenerating functional bone tissue. The field of bone-tissue engineering emerged in the 1990s, and today, advancements in materials synthesis and bone biology offer new opportunities for developing sophisticated materials for bone regeneration (**Figure 1.9**). The goal of bone tissue engineering research is to develop materials that function better than allografts and autografts of bone. The main objective is to develop materials that can help repair bone defects. These substances are frequently designed in the form of scaffolds, which serve as temporary extracellular matrix (ECM) scaffolds by supporting cellular adhesion and mineralized matrix deposition. Yang *et al.* developed GO/Cu nanosheet-loaded scaffold for calvarial bone regeneration <sup>152</sup>. Wang *et al.* fabricated zinc-whitlockite-loaded scaffold for promoting bone differentiation and angiogenesis <sup>153</sup>. Kim *et al.* worked on injectable growth factor-loaded poly(organophosphazene) hydrogel scaffold for bone regeneration applications <sup>154</sup>. Salehi *et al.* developed microporous chitosan and growth factor-coated polylactic acid-baghdadite nanocomposite-based scaffold for bone regeneration <sup>155</sup>. Different structural and functional qualities are needed, depending on the problem site and the patient's health. Various materials used in bone tissue regeneration include:

#### **1.9.1.** Metals

Metals are used widely in bone tissue regeneration as they offer high mechanical strength, biocompatibility, and the ability to integrate into bone tissue <sup>156</sup>. The various metals used in bone tissue regeneration include stainless steel, titanium, and their alloys. The use of titanium suffers from non-biodegradability and surgical removal after supporting bone regeneration at the implantation site is needed. Biodegradable metal-based materials include magnesium, iron, and zinc alloys. Magnesium-based biomaterials are more suited for bone-tissue engineering than titanium-based ones because they can biodegrade through corrosion<sup>157</sup>. Tang *et al.* developed magnesium and zinc nanoparticles in PLGA membrane for guided bone regeneration<sup>158</sup>. Li *et al.* fabricated bisphosphonate gel loaded with magnesium for enhanced bone regeneration<sup>159</sup>. Ali *et al.* worked on BMP-2-loaded 3D printed hydrogel to understand its osteo-immunomodulatory properties for accelerated bone regeneration<sup>160</sup>. Nowadays, emerging metal-based materials like porous tantalum and bismuth alloys are gaining attention as bone implants due to their strong bone affinity and multifunctionality<sup>156</sup>.

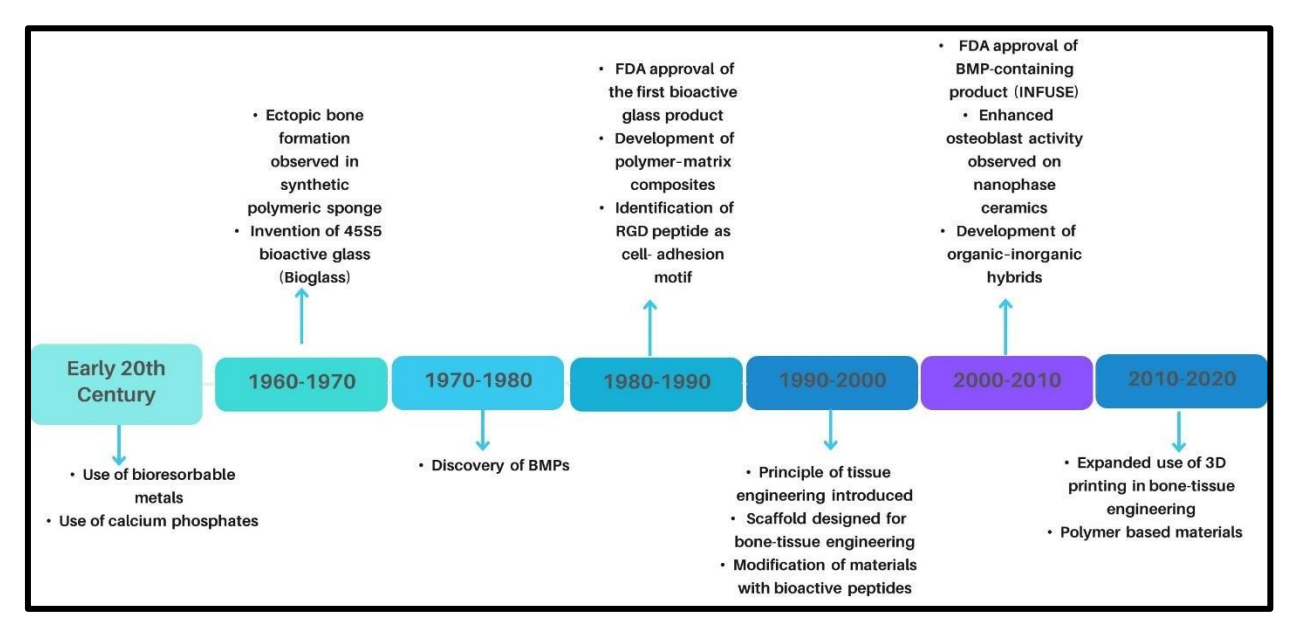


**Figure 1.9**. Timeline of major milestones in biomaterials design for bone-tissue engineering.

#### 1.9.2. Bioceramics

A family of inorganic biomaterials called bioceramics has long been essential to bone tissue engineering<sup>161</sup>. They fall into three categories: amorphous glasses, partially crystalline glass ceramics, and crystalline ceramics. Bioceramics are traditionally considered bioactive if they can bond directly with bone tissue and inert if they cannot. However, there is growing interest in their ability to promote biological effects, such as osteogenesis and angiogenesis, by releasing active ions. This capability has led to the development of bioceramics loaded with different bioactive ions, including magnesium, calcium, magnesium, copper, and silver for bone tissue engineering applications. One of the best examples of bioceramics used in bone tissue engineering is calcium phosphates<sup>162</sup>. They can mimic the inorganic phase of bone. These types of the materials often include hydroxyapatite and β-tricalcium phosphate as injectable bone cements. β-tricalcium phosphate is resorbable and the degradation rate of hydroxyapatite is very slow. Bioceramics combining both have shown the ability to produce mineralized tissue comparable to bone autografts<sup>163</sup>. Feng et al. developed gelatin-amorphous calcium phosphate-coated titanium implants for enhanced bone regeneration<sup>164</sup>. Zhai et al. fabricated akermanite to promote angiogenesis for bone regeneration<sup>165</sup>. Skibinski et al. developed novel β tricalcium phosphate scaffolds co-doped with silicon and silver as multifunctional biomaterials for tissue regeneration <sup>166</sup>.

# 1.9.3. Polymer-based materials for bone regeneration

With the growing prominence of biomaterials and tissue engineering, researchers are striving to develop biomaterials that are easy to manufacture, exhibit desirable properties, and enhance healing rates without causing adverse effects. Also, their degradation rates and mechanical properties can be controlled, which further enhances their suitability for various purposes. Both natural

polymers and synthetic polymers are used for bone tissue regeneration applications. Researchers have worked with different polymers including chitosan, silk, collagen, polycaprolactone, poly (lactic acid), and polyhydroxybutyrate (PHB)<sup>168</sup>. Wang *et al.* developed hyaluronic acid and chitosan-based hydrogel dressing to promote healing of infected bone<sup>169</sup>. Tang *et al.* fabricated icariin-loaded methacrylated carboxymethyl chitosan scaffold for bone regeneration applications<sup>170</sup>.

# 1.9.4. Polymer/nanoparticle composite for bone tissue regeneration

Nanocomposites comprising bioactive or resorbable nanoparticles embedded in a biopolymeric matrix have been extensively studied for bone tissue regeneration. Incorporating nanometer-sized fillers into the polymeric matrix significantly enhances its physical properties, paving the way for the development of advanced biomaterials with superior characteristics. Nanoparticles offer a higher surface area compared to traditional microsized fillers, which enhances their mechanical properties while maintaining their osteoconductive and biocompatible characteristics<sup>171</sup>. Polymers including polysaccharides, such as chitin, and cellulose, and proteins, such as silk, collagen, and elastin mimic the extracellular matrix<sup>172</sup>. They do not cause immunological reactions and are non-toxic. In contrast, bioresorbable fillers, such as calcium phosphates (CaPs, such as hydroxyapatite and βtricalcium phosphate), are highly valued due to their advantageous osteoconductivity, resorbability, and biocompatibility<sup>173</sup>. Various polymer-based composites have been developed for tissue regeneration applications. Different calcium phosphate loaded in collagen-based scaffold material were developed. They showed increased mechanical strength. Different techniques were used including deposition, electrospinning, and direct addition. Kikuchi et al. fabricated a porous HAp/collagen nanocomposite for use as both bone filler and in bone tissue engineering <sup>174</sup>. Barbani et al. developed Gelatin and calcium phosphate-based nanocomposites were developed with enhanced cell attachment and mechanical strength<sup>175</sup>. Wang et al. worked on nanoparticle-loaded methacrylated silk fibroin hydrogel for bone regeneration applications <sup>176</sup>. Derakhshankhah et al. developed silica nanoparticles loaded in alginate hydrogel as biomimetic scaffold for bone regeneration <sup>177</sup>. Taymouri et al. worked on hydroxyapatite and hesperidin-loaded carrageenan based scaffold for bone regeneration<sup>178</sup>. Yao et al. fabricated nano β-TCP/gelatin/collagen-based scaffold for alveolar bone regeneration<sup>179</sup>. Zhan et al. developed mesoporous silica nanoparticle-loaded dual network hydrogel for skull defects<sup>180</sup>.

Bhumiratana *et al.* developed calcium phosphate was also incorporated in silk-based scaffolds. The scaffold showed enhanced osteogenic differentiation with in-vivo bone formation<sup>181</sup>. Tanase *et al.* fabricated CaP/chitosan scaffold was also developed<sup>182</sup>. The scaffold showed compressive strength similar to trabecular bone. Similarly, compared to pure chitosan, human MSCs grown on chitosan/HAP composite scaffolds showed enhanced cell proliferation. Manda *et al.* developed gellan gum blended with hydroxyapatite nanoparticles was developed<sup>183</sup>. The nanocomposite

showed higher mechanical properties with excellent biological properties in comparison to the polymeric hydrogel. All this work done by various researchers indicates the excellent potential of using polymer-based nanocomposites for tissue regeneration applications.

# 1.10. Rational design of polymer nanoparticle composite and polymeric gels for bone tissue regeneration (literature review)

Nanocomposite scaffolds including both nanoparticles and polymers hold a notable potential for tissue regeneration applications<sup>184</sup>. They can mimic the mechanical and structural properties of native tissues. Natural polymers offer varying degradation rates and nanoparticles provide biocompatibility and osteoconductivity. This combination of polymers and nanoparticles leads to the development of scaffolds with structural integrity while promoting cell differentiation and cellular growth. Han *et al.* developed silver nanoparticle-based gelatin hydrogel for bone regeneration<sup>185</sup>. Wei *et al.* developed resveratrol-loaded solid lipid nanoparticle-loaded gelatin methacrylate hydrogel for osteogenic differentiation and effective bone regeneration<sup>186</sup>. Xue *et al.* fabricated CuS nanoparticle-loaded polycaprolactone scaffolds for efficient bone regeneration<sup>187</sup>. Habashy *et al.* developed polycaprolactone/hydroxyapatite nanoparticles in 3D printed core-shell hydrogel scaffolds. Cao *et al.* fabricated rhBMP-2-loaded 2-N, 6-O- sulfated chitosan nanoparticle-loaded photocrosslinked hydrogel for bone regenerations applications<sup>188</sup>. Through various mechanisms, nanoparticle-hydrogel systems can enhance the bone regeneration process.

## **1.10.1.** Mitigation of oxidative stress

One of the factors impeding bone regeneration is oxidative stress damage, mediated by an excess of reactive oxygen species (ROS). Oxidative stress leads to cellular damage through lipid peroxidation, membrane alterations, and oxidation of nucleic acids and proteins, which contributes to various disease conditions. In post-menopausal osteoporosis, decreased estrogen levels are associated with increased NADPH oxidase activity and reduced levels of antioxidant enzymes and glutathione (GSH). Additionally, the prolonged use of steroidal anti-inflammatory drugs for osteoporosis, particularly those caused by inflammatory processes, exacerbates oxidative stress by activating ROS-producing enzymes. Researchers have shown that inhibition of oxidative stress is proven to enhance bone mass<sup>189</sup>. Guo *et al* developed astaxanthin-modified antioxidant aerogel for accelerated bone regeneration<sup>190</sup>. Huang *et al* developed an injectable, adhesive bioactive bone graft to promote bone regeneration by moderating oxidative stress<sup>191</sup>. Singh *et al*. developed nanoceria tailored scaffolds to alleviate oxidative stress and help in diabetic bone regeneration<sup>192</sup>. Wu *et al*. fabricated ROS scavenging hydrogels for the augmentation of mandibular bone regeneration<sup>193</sup>.

## 1.10.2. Immunomodulation

Recent research emphasizes the role of immunomodulation in bone tissue engineering<sup>144</sup>. Immune

cells secrete cytokines that have a direct effect on the recruitment of stem cells and cell differentiation. It is a relatively new field of study to engineer biomaterials to improve tissue regeneration through immunomodulation, and the results look promising for improving the regeneration of soft tissues like muscle and skin tissues. Biomaterials-mediated immunomodulatory strategies can be achieved by adjusting the physical or biochemical properties of the implant, delivering immunomodulators, or scavenging undesirable inflammatory signals. Biochemical cues, such as surface chemistry, ligand density, charge, and hydrophobicity differently modulate the immune system <sup>144</sup>. Qin *et al* developed mussel-inspired osteoinductive and immunomodulatory hydroxyapatite nanoparticles for tissue regeneration applications <sup>194</sup>. Liang *et al*. developed gold nanoparticles loaded mesoporous silica nanoparticles for stimulating bone regeneration by immunomodulation <sup>195</sup>. Zhou *et al*. developed quercitin-loaded solid-lipid nanoparticles in hyaluronic acid hydrogels for bone regeneration applications <sup>196</sup>.

# 1.10.3. Angiogenesis

The prompt emergence of blood vessels in the fracture callus is essential for bone repair<sup>197</sup>. After fracture, the local production of many angiogenic growth factors stimulates angiogenesis, the development of new blood vessels from pre-existing ones. Different types of biomaterials have shown potential in bone regeneration applications. For example Qin *et al.* developed akermanite, a bioceramic composed of silicon, magnesium, and calcium has shown angiogenic properties by promoting the proliferation of human aortic endothelial cells<sup>194</sup>. Wang *et al.* developed silk fibroin combined with graphene oxide for the delivery of salvianolic acid B for efficient osteogenesis and angiogenesis<sup>198</sup>. Liu *et al.* developed deferoxamine-loaded magnesium mediated tantalum oxide nanoplatform for enhanced angiogenesis and immunomodulation<sup>199</sup>.

## 1.10.4. Cell adhesion and proliferation

Using different strategies, biomaterials promote cell proliferation and cell adhesion for effective bone regeneration. The development of nanostructures and microstructures on the surface of scaffolds enhances the surface area promoting cell attachment<sup>200</sup>. Also, biomaterials such as nanofibers and nanotubes augment the adhesion and proliferation of osteoblast, which provides physical cues similar to natural bone tissue. Wang *et al.* developed GelMA cryogel microspheres loaded with hydroxyapatite and calcium silicate nanofibers for bone tissue regeneration<sup>201</sup>. Jaswal *et al.* fabricated polycaprolactone-based nanofibers loaded with PDA-modified gold nanoparticles for robust bone regeneration<sup>202</sup>.

## 1.11. Knowledge gaps in the field

Bacterial infections and biofilms impede the wound-healing process, causing delayed healing and

placing a substantial burden on healthcare systems. Although topical antimicrobial agents are available commercially, their efficacy is limited due to factors, such as narrow-spectrum activity, cytotoxicity, antibiotic resistance development, and ineffectiveness against biofilms. Thus, there is a need to develop new therapeutic strategies to address the various factors contributing to the impaired wound-healing process.

Also, bone abnormalities can lead to localized impairments and significant health risks. While autografts and allografts are commonly used therapeutic options, post-surgery complications, graft rejection, and other limitations often diminish their clinical effectiveness. Recently, the use of biomaterials has proved to be beneficial for tissue regeneration applications but conventional biomaterials also suffer from limitations such as inconsistent correlation between in vitro and in vivo studies. One of the possible reasons behind this is the immune response, which is often overlooked, thus presenting a major challenge. There are very few studies focusing on the immunomodulatory properties of biomaterials. Thus, there is a pressing need to develop immunomodulatory biomaterials for effective bone tissue regeneration applications. Also, bone regeneration in osteoporotic conditions has become a notable public health issue, particularly in post-menopausal women resulting in around 9 million fractures worldwide each year. Current treatment strategies rely on the use of anabolic drugs, hormone replacement therapy, and antiresorptive drugs. These treatment modalities suffer from limitations including elevated risk of cancer, poor bioavailability, and toxicity. Also, there is a lack of strategies focusing on oxidative stress in osteoporotic environments. Hence, there is a need to develop innovative therapeutic approaches for the effective management of this condition. The versatility of polymeric biomaterials has shown potential in advancing tissue regeneration. Herein, we have developed different polymerbased materials and nanomaterials to explore their effectiveness in promoting tissue repair and healing.

#### 1.12. Hypothesis

Tissue regeneration, particularly in wound healing and bone regeneration, faces notable challenges due to bacterial infections, critical immune responses, and oxidative stress. This thesis addresses these challenges through the development of innovative polymeric biomaterials for enhanced tissue regeneration, focusing on bacteria-infected wound healing and bone tissue regeneration.

The first part of the thesis investigates the role of bacterial infections in hindering wound healing, especially in chronic and biofilm-associated infections. Bacteria require iron for growth and biofilm maturation. By leveraging the ionic similarity of gallium to iron, a novel gallium-loaded imine crosslinked hydrogel is designed using biocompatible quaternized chitosan and oxidized alginate. This hydrogel disrupts bacterial iron uptake, exhibiting potent antibacterial effects against biofilm-forming bacteria. The hydrogel is hypothesized to enhance healing in bacteria-infected wounds by promoting antibacterial, antioxidant, and hemostatic properties, thus addressing one of the most pressing

challenges in wound care.

The second part focuses on bone tissue regeneration, particularly through the development of a biphasic calcium phosphate (BCP) nanoparticle system doped with cobalt and coated with acemannan. BCP nanoparticles are well-known for their osteoinductive properties, but the incorporation of acemannan enhances cell proliferation and stimulates alkaline phosphatase activity, key markers of osteogenesis. Meanwhile, cobalt's immunomodulatory properties are explored for the first time in the context of bone healing. This part of the thesis hypothesizes that cobalt-doped BCP nanoparticles, combined with acemannan, will create an immunomodulatory environment conducive to bone repair without the need for exogenous growth factors.

The third part addresses the critical issue of bone degeneration in osteoporotic conditions, where oxidative stress and hormonal imbalances impair bone regeneration. Here, a novel genistein-loaded hydrogel, composed of  $\kappa$ -carrageenan and quaternized dextran, is developed to mimic the extracellular matrix, support cell attachment, and provide controlled release of genistein. Genistein, a phytoestrogen with antioxidant properties, is expected to scavenge reactive oxygen species (ROS), restore estrogen levels, and promote bone regeneration in osteoporotic bone. The hypothesis is that this system will mitigate oxidative stress and support bone tissue repair by enhancing bone mass.

Together, these innovative material systems present a comprehensive approach to tackling the multifaceted challenges of tissue regeneration. The gallium-loaded hydrogel for infected wounds, cobalt-doped nanoparticles for immunomodulatory bone repair, and genistein-loaded hydrogel for osteoporotic bone regeneration represent significant advancements in the field of biomaterials for regenerative medicine, with potential applications in wound healing, bone tissue engineering, and beyond.

#### 1.13. Research questions

This thesis aims to address critical challenges in tissue regeneration, particularly in bacteria-infected wound healing and bone tissue regeneration. The study focuses on the development of novel polymeric biomaterials and nanomaterials that incorporate antibacterial, immunomodulatory, and antioxidant properties. The research questions are as follows:

- Can gallium-loaded, imine-crosslinked hydrogels be developed to effectively treat bacteria-infected wounds by providing antibacterial, antioxidant, and hemostatic benefits while promoting wound healing.
- Can acemannan-coated, cobalt-doped biphasic calcium phosphate nanoparticles be
  engineered to modulate immune responses and enhance bone tissue regeneration,
  addressing the challenges of often neglected immune response in bone healing.

• How can genistein-loaded quaternized dextran/κ-carrageenan hydrogels be optimized to counter oxidative stress, mitigate the effects of estrogen loss, and improve osteoporotic bone regeneration, with a focus on enhancing the osteogenic potential of the ge

## 1.14. Objectives

The overall aim of this thesis is to develop and evaluate polymeric biomaterials and nanomaterials to address the existing challenges/knowledge gaps in the field of wound healing and bone regeneration (**Figure 1.10.**). To address the knowledge gaps/challenges in the field, the thesis has following objectives:

- To fabricate multifunctional β-Ga<sub>2</sub>O<sub>3</sub> nanoparticle-loaded quaternized chitosan and oxidized sodium alginate hydrogel for antibacterial, antioxidant, and hemostatic abilities for efficient tissue regeneration in bacteria-infected wounds
- To develop acemannan-coated, cobalt-doped biphasic calcium phosphate nanoparticles for enhanced osteogenic and immunomodulation to foster a conducive environment for bone regeneration
- To investigate the effectiveness of genistein-loaded quaternized dextran/k-carrageenan gels for targeting oxidative stress and estrogen loss in osteoporotic conditions to facilitate effective bone regeneration.

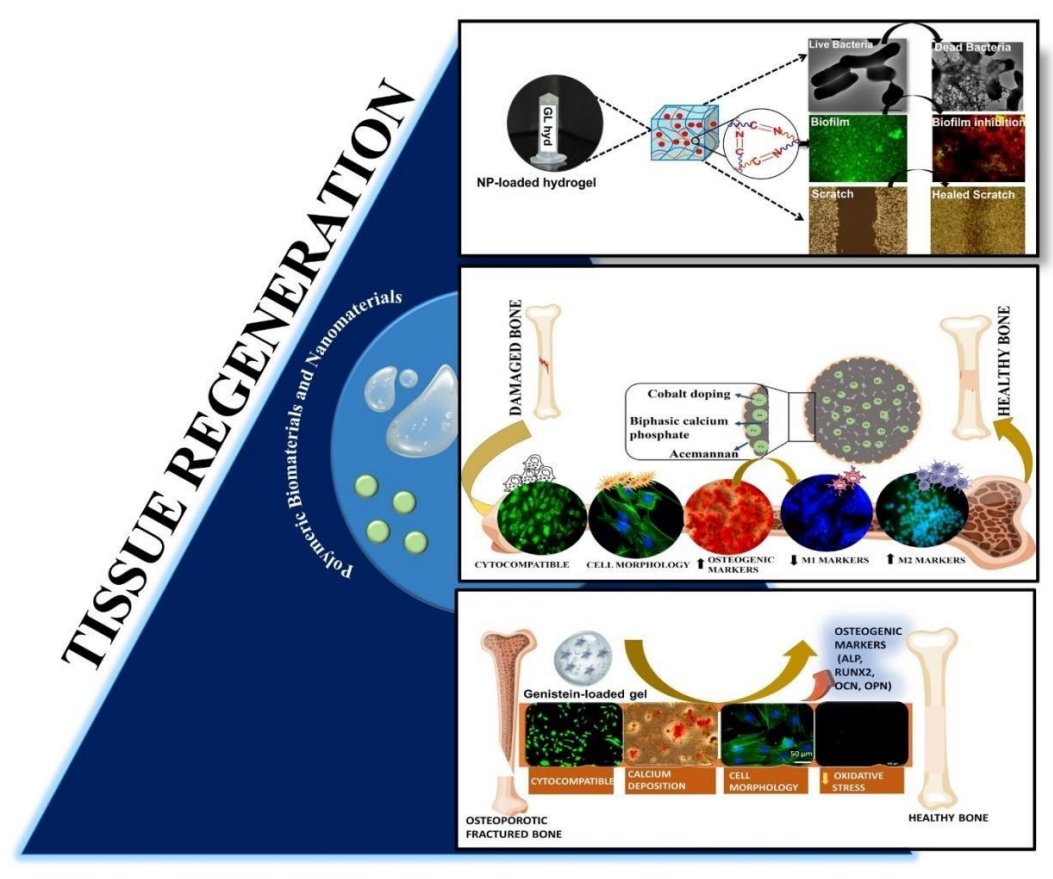


**Figure 1.10.** Objectives of the thesis. Development of polymeric biomaterials and nanomaterials for wound healing and bone tissue regeneration applications.

#### 1.15. Thesis outline

The main focus of this thesis was to develop polymeric biomaterials and nanomaterials for tissue regeneration applications, specifically skin tissue regeneration and bone tissue regeneration. It has been organized into five chapters. The first chapter of the thesis provides an overview of polymeric biomaterials and nanomaterials and their types along with the methods used for their fabrication and characterization. This chapter also presents an overview of wound healing and bone regeneration along with the challenges in their management. The overview is followed by the exhaustive literature survey on the use of polymeric biomaterials and nanomaterials for wound healing and bone regeneration applications, identification of knowledge gaps, and objectives of the thesis to address the challenges in the field. The second chapter presents an exhaustive literature survey related to bacteria-infected wounds, identification of research gaps in the field, and development of a gallium-loaded, imine crosslinked hydrogel fabricated using quaternized chitosan and oxidized sodium alginate for bacteria-infected wounds. The third chapter presents the literature review of bone regeneration, identification of research gaps in the field, and the fabrication and characterization of acemannan-coated, cobalt-doped biphasic calcium phosphate nanoparticles for immunomodulation-based bone regeneration. The fourth chapter, in a similar manner, deals with the development of genistein-loaded, quaternized dextran/κcarrageenan gels to target oxidative stress and loss of estrogen hindering the bone regeneration in osteoporotic environment. Finally, the last chapter presents the conclusions of this work, highlights its impact on addressing the challenges in the field, and outlines its future prospects.

#### References

- (1) Biomaterials Science: An Introduction to Materials in Medicine; Ratner, B. D., Ed.; Academic Press: San Diego, 1996.
- (2) Asadi, N.; Del Bakhshayesh, A. R.; Davaran, S.; Akbarzadeh, A. Common Biocompatible Polymeric Materials for Tissue Engineering and Regenerative Medicine. *Materials Chemistry and Physics* **2020**, 242, 122528.
- (3) Akilbekova, D.; Shaimerdenova, M.; Adilov, S.; Berillo, D. Biocompatible Scaffolds Based on Natural Polymers for Regenerative Medicine. *International Journal of Biological Macromolecules* **2018**, *114*, 324–333.
- (4) Khan, F.; Tanaka, M.; Ahmad, S. R. Fabrication of Polymeric Biomaterials: A Strategy for Tissue Engineering and Medical Devices. *J. Mater. Chem. B* **2015**, *3* (42), 8224–8249.
- (5) Lee, K. Y.; Mooney, D. J. Hydrogels for Tissue Engineering. *Chem. Rev.* **2001**, *101* (7), 1869–1880.
- (6) Machado, C. B.; Ventura, J. M. G.; Lemos, A. F.; Ferreira, J. M. F.; Leite, M. F.; Goes, A. M. 3D Chitosan–Gelatin–Chondroitin Porous Scaffold Improves Osteogenic Differentiation of Mesenchymal Stem Cells. *Biomed. Mater.* **2007**, *2* (2), 124–131.
- (7) Abarrategi, A.; Moreno-Vicente, C.; Ramos, V.; Aranaz, I.; Sanz Casado, J. V.; López-Lacomba, J. L. Improvement of Porous β-TCP Scaffolds with rhBMP-2 Chitosan Carrier Film for Bone Tissue Application. *Tissue Engineering Part A* **2008**, *14* (8), 1305–1319.
- (8) Lee, Y.-M.; Park, Y.-J.; Lee, S.-J.; Ku, Y.; Han, S.-B.; Klokkevold, P. R.; Chung, C.-P. The Bone Regenerative Effect of Platelet-Derived Growth Factor-BB Delivered With a Chitosan/Tricalcium Phosphate Sponge Carrier. *Journal of Periodontology* **2000**, *71* (3), 418–424.
- (9) Reakasame, S.; Boccaccini, A. R. Oxidized Alginate-Based Hydrogels for Tissue Engineering Applications: A Review. *Biomacromolecules* **2018**, *19* (1), 3–21.
- (10) Bhattarai, N.; Li, Z.; Edmondson, D.; Zhang, M. Alginate-Based Nanofibrous Scaffolds: Structural, Mechanical, and Biological Properties. *Advanced Materials* **2006**, *18* (11), 1463–1467.
- (11) Oliveira, C.; Sousa, D.; Teixeira, J. A.; Ferreira-Santos, P.; Botelho, C. M. Polymeric Biomaterials for Wound Healing. *Front. Bioeng. Biotechnol.* **2023**, *11*, 1136077.
- (12) Shen, X.; Zhao, D.; Shi, J.; Li, C.; Bai, Y.; Qiu, L.; Xuan, Y.; Wang, J. Copper Peroxide Loaded Gelatin/Oxide Dextran Hydrogel with Temperature and pH Responsiveness for Antibacterial and Wound Healing Activity. *International Journal of Biological Macromolecules* **2024**, 274, 133258.
- (13) Kumari, S.; Mondal, P.; Tyeb, S.; Chatterjee, K. Visible Light-Based 3D Bioprinted Composite Scaffolds of κ-Carrageenan for Bone Tissue Engineering Applications. *J. Mater. Chem. B* **2024**, *12* (7), 1926–1936.
- (14) Liu, D.; Nikoo, M.; Boran, G.; Zhou, P.; Regenstein, J. M. Collagen and Gelatin. *Annu. Rev. Food Sci. Technol.* **2015**, *6* (1), 527–557.
- (15) Wu, L.; Pei, X.; Dou, Q.; Su, Z.; Qin, Y.; Liu, C.; Zhao, L.; Tan, Y.; Chen, Z.; Fan, Y.; Zhang, X.; Zhou, C. 3D Printed Calcium Phosphate Physiochemically Dual-Regulating Pro-Osteogenesis and Antiosteolysis for Enhancing Bone Tissue Regeneration. *ACS Appl. Mater. Interfaces* **2024**, *16* (28), 37007–37016.
- (16) Mansour, R. N.; Soleimanifar, F.; Abazari, M. F.; Torabinejad, S.; Ardeshirylajimi, A.; Ghoraeian, P.; Mousavi, S. A.; Sharif Rahmani, E.; Hassannia, H.; Enderami, S. E. Collagen Coated Electrospun Polyethersulfon Nanofibers Improved Insulin Producing Cells Differentiation Potential of Human Induced Pluripotent Stem Cells. *Artificial Cells, Nanomedicine, and Biotechnology* **2018**, *46* (sup3), 734–739.
- (17) Aravamudhan, A.; Ramos, D. M.; Nip, J.; Harmon, M. D.; James, R.; Deng, M.; Laurencin, C. T.; Yu, X.; Kumbar, S. G. Cellulose and Collagen Derived Micro-Nano Structured Scaffolds for Bone Tissue Engineering. *Journal of Biomedical Nanotechnology* **2013**, *9* (4), 719–731.
- (18) Mwangi, J. W.; Ofner, C. M. Crosslinked Gelatin Matrices: Release of a Random Coil Macromolecular Solute. *International Journal of Pharmaceutics* **2004**, 278 (2), 319–327.

- (19) Hellio, D.; Djabourov, M. Physically and Chemically Crosslinked Gelatin Gels. *Macromolecular Symposia* **2006**, 241 (1), 23–27.
- (20) Young, S.; Wong, M.; Tabata, Y.; Mikos, A. G. Gelatin as a Delivery Vehicle for the Controlled Release of Bioactive Molecules. *Journal of Controlled Release* **2005**, *109* (1), 256–274.
- (21) Sutherland, T. D.; Young, J. H.; Weisman, S.; Hayashi, C. Y.; Merritt, D. J. Insect Silk: One Name, Many Materials. *Annual Review of Entomology*, 2010, 55, 171–188.
- (22) Padol, A.; Jayakumar, K.; Shridhar, N.; Swamy, NarayanaH. D.; Swamy, N.; Mohan, K. Safety Evaluation of Silk Protein Film (A Novel Wound Healing Agent) in Terms of Acute Dermal Toxicity, Acute Dermal Irritation and Skin Sensitization. *Toxicol Int* **2011**, *18* (1), 17.
- (23) Lai, G.-J.; Shalumon, K. T.; Chen, S.-H.; Chen, J.-P. Composite Chitosan/Silk Fibroin Nanofibers for Modulation of Osteogenic Differentiation and Proliferation of Human Mesenchymal Stem Cells. *Carbohydrate Polymers* **2014**, *111*, 288–297.
- (24) Kim, J.-Y.; Yang, B.-E.; Ahn, J.-H.; Park, S. O.; Shim, H.-W. Comparable Efficacy of Silk Fibroin with the Collagen Membranes for Guided Bone Regeneration in Rat Calvarial Defects. *J Adv Prosthodont* **2014**, *6* (6), 539–546.
- (25) Carvalho, P. P.; Rodrigues, M. T.; Reis, R. L.; Gomes, M. E. Starch-Based Blends in Tissue Engineering. In *Biomaterials from Nature for Advanced Devices and Therapies*; 2016; pp 244–257.
- (26) Malafaya, P. B.; Silva, G. A.; Reis, R. L. Natural–Origin Polymers as Carriers and Scaffolds for Biomolecules and Cell Delivery in Tissue Engineering Applications. *Advanced Drug Delivery Reviews* **2007**, *59* (4), 207–233.
- (27) Bose, S.; Sarkar, N.; Banerjee, D. Natural Medicine Delivery from Biomedical Devices to Treat Bone Disorders: A Review. *Acta Biomaterialia* **2021**, *126*, 63–91.
- (28) Vercruysse, K. P.; Marecak, D. M.; Marecek, J. F.; Prestwich, G. D. Synthesis and *in Vitro* Degradation of New Polyvalent Hydrazide Cross-Linked Hydrogels of Hyaluronic Acid. *Bioconjugate Chem.* **1997**, 8 (5), 686–694.
- (29) Moon, R. J.; Martini, A.; Nairn, J.; Simonsen, J.; Youngblood, J. Cellulose Nanomaterials Review: Structure, Properties and Nanocomposites. *Chem. Soc. Rev.* **2011**, *40* (7), 3941–3994.
- (30) Saska, S.; Teixeira, L. N.; Tambasco de Oliveira, P.; Minarelli Gaspar, A. M.; Lima Ribeiro,
- S. J.; Messaddeq, Y.; Marchetto, R. Bacterial Cellulose-Collagen Nanocomposite for Bone Tissue Engineering. *J. Mater. Chem.* **2012**, 22 (41), 22102–22112.
- (31) Georgieva, N.; Bryaskova, R.; Tzoneva, R. New Polyvinyl Alcohol-Based Hybrid Materials for Biomedical Application. *Materials Letters* **2012**, 88, 19–22.
- (32) Gombotz, W. R.; Pettit, D. K. Biodegradable Polymers for Protein and Peptide Drug Delivery. *Bioconjugate Chem.* **1995**, *6* (4), 332–351.
- (33) Martins, C.; Sousa, F.; Araújo, F.; Sarmento, B. Functionalizing PLGA and PLGA Derivatives for Drug Delivery and Tissue Regeneration Applications. *Adv Healthcare Materials* **2018**, *7* (1), 1701035.
- (34) Suwantong, O. Biomedical Applications of Electrospun Polycaprolactone Fiber Mats. *Polymers for Advanced Techs* **2016**, *27* (10), 1264–1273.
- (35) Ulery, B. D.; Nair, L. S.; Laurencin, C. T. Biomedical Applications of Biodegradable Polymers. *J Polym Sci B Polym Phys* **2011**, *49* (12), 832–864.
- (36) Li, J.; Mooney, D. J. Designing Hydrogels for Controlled Drug Delivery. *Nat Rev Mater* **2016**, *1* (12), 16071.
- (37) Kalirajan, C.; Dukle, A.; Nathanael, A. J.; Oh, T.-H.; Manivasagam, G. A Critical Review on Polymeric Biomaterials for Biomedical Applications. *Polymers* **2021**, *13* (17), 3015.
- (38) Elsabahy, M.; Wooley, K. L. Design of Polymeric Nanoparticles for Biomedical Delivery Applications. *Chem. Soc. Rev.* **2012**, *41* (7), 2545.
- (39) Leung, V.; Ko, F. Biomedical Applications of Nanofibers. *Polymers for Advanced Techs* **2011**, 22 (3), 350–365.
- (40) Guo, Z.; Poot, A. A.; Grijpma, D. W. Advanced Polymer-Based Composites and Structures for Biomedical Applications. *European Polymer Journal* **2021**, *149*, 110388.
- (41) Noro, A.; Matsushita, Y.; Lodge, T. P. Gelation Mechanism of Thermoreversible Supramacromolecular Ion Gels via Hydrogen Bonding. *Macromolecules* **2009**, *42* (15), 5802–5810.

- (42) Tong, Z.; Jin, L.; Oliveira, J. M.; Reis, R. L.; Zhong, Q.; Mao, Z.; Gao, C. Adaptable Hydrogel with Reversible Linkages for Regenerative Medicine: Dynamic Mechanical Microenvironment for Cells. *Bioactive Materials* **2021**, *6* (5), 1375–1387.
- (43) Lau, H. K.; Kiick, K. L. Opportunities for Multicomponent Hybrid Hydrogels in Biomedical Applications. *Biomacromolecules* **2015**, *16* (1), 28–42.
- (44) Tuncaboylu, D. C.; Sari, M.; Oppermann, W.; Okay, O. Tough and Self-Healing Hydrogels Formed via Hydrophobic Interactions. *Macromolecules* **2011**, *44* (12), 4997–5005.
- (45) Dong, M.; Chen, Y. Chapter 7 The Stimuli-Responsive Properties of Hydrogels Based on Natural Polymers. In *Hydrogels Based on Natural Polymers*; Chen, Y., Ed.; Elsevier, 2020; pp 173–222.
- (46) Degirmenci, A.; Sanyal, R.; Sanyal, A. Metal-Free Click-Chemistry: A Powerful Tool for Fabricating Hydrogels for Biomedical Applications. *Bioconjugate Chem.* **2024**, *35* (4), 433–452.
- (47) Amiryaghoubi, N.; Fathi, M.; Safary, A.; Javadzadeh, Y.; Omidi, Y. In Situ Forming Alginate/Gelatin Hydrogel Scaffold through Schiff Base Reaction Embedded with Curcumin-Loaded Chitosan Microspheres for Bone Tissue Regeneration. *International Journal of Biological Macromolecules* **2024**, *256*, 128335.
- (48) Výborný, K.; Vallová, J.; Kočí, Z.; Kekulová, K.; Jiráková, K.; Jendelová, P.; Hodan, J.; Kubinová, Š. Genipin and EDC Crosslinking of Extracellular Matrix Hydrogel Derived from Human Umbilical Cord for Neural Tissue Repair. *Scientific Reports* **2019**, *9* (1), 10674.
- (49) Uddin, J.; Abdur, R.; Hossain, Md. R.; Aziz, S.; Jamal, M. S.; Shaikh, Md. A. A.; Hossain, M. Phase Tunable Nickel Doped Mn <sub>3</sub> O <sub>4</sub> Nanoparticle Synthesis by Chemical Precipitation: Kinetic Study on Dye Degradation. *Nanoscale Adv.* **2024**, *6* (3), 902–909.
- (50) Parashar, M.; Shukla, V. K.; Singh, R. Metal Oxides Nanoparticles via Sol–Gel Method: A Review on Synthesis, Characterization and Applications. *J Mater Sci: Mater Electron* **2020**, *31* (5), 3729–3749.
- (51) Darr, J. A.; Zhang, J.; Makwana, N. M.; Weng, X. Continuous Hydrothermal Synthesis of Inorganic Nanoparticles: Applications and Future Directions. *Chem. Rev.* **2017**, *117* (17), 11125–11238.
- (52) Delogu, F.; Gorrasi, G.; Sorrentino, A. Fabrication of Polymer Nanocomposites via Ball Milling: Present Status and Future Perspectives. *Progress in Materials Science* **2017**. *86*. 75–126.
- (53) ShamsiJazeyi, H.; Miller, C. A.; Wong, M. S.; Tour, J. M.; Verduzco, R. Polymer-Coated Nanoparticles for Enhanced Oil Recovery. *Journal of Applied Polymer Science* **2014**, *131* (15), 40576.
- (54) Hou, Z.; Liu, Y.; Xu, J.; Zhu, J. Surface Engineering of Magnetic Iron Oxide Nanoparticles by Polymer Grafting: Synthesis Progress and Biomedical Applications. *Nanoscale* **2020**, *12* (28), 14957–14975.
- (55) Kim, J.; Sotto, A.; Chang, J.; Nam, D.; Boromand, A.; Van der Bruggen, B. Embedding TiO2 Nanoparticles versus Surface Coating by Layer-by-Layer Deposition on Nanoporous Polymeric Films. *Microporous and Mesoporous Materials* **2013**, *173*, 121–128.
- (56) Baby, D. K. Chapter 9 Rheology of Hydrogels. In *Rheology of Polymer Blends and Nanocomposites*; Thomas, S., Sarathchandran, C., Chandran, N., Eds.; Elsevier, 2020; pp 193–204.
- (57) Behravesh, E.; Timmer, M. D.; Lemoine, J. J.; Liebschner, M. A. K.; Mikos, A. G. Evaluation of the in Vitro Degradation of Macroporous Hydrogels Using Gravimetry, Confined Compression Testing, and Microcomputed Tomography. *Biomacromolecules* **2002**, *3* (6), 1263–1270.
- (58) Sánchez-Cid, P.; Alonso-González, M.; Jiménez-Rosado, M.; Benhnia, M. R.-E.-I.; Ruiz-Mateos, E.; Ostos, F. J.; Romero, A.; Perez-Puyana, V. M. Effect of Different Crosslinking Agents on Hybrid Chitosan/Collagen Hydrogels for Potential Tissue Engineering Applications. *International Journal of Biological Macromolecules* **2024**, *263*, 129858.
- (59) Farshi Azhar, F.; Ahmadinia, A.; Mousazadeh, H.; Kheirkhah, E. A pH-Sensitive Magnetic Hydrogel Nanocomposite Based on Alginate for Controlled Release of Methotrexate. *International Journal of Polymeric Materials and Polymeric Biomaterials* **2024**, *73* (14), 1216–1229.
- (60) Bhattacharjee, S. DLS and Zeta Potential What They Are and What They Are Not?

- Journal of Controlled Release 2016, 235, 337–351.
- (61) Shah, R.; Eldridge, D.; Palombo, E.; Harding, I. Optimisation and Stability Assessment of Solid Lipid Nanoparticles Using Particle Size and Zeta Potential. *Journal of Physical Science* **2014**, 25 (1), 59-75.
- (62) Guo, X.; Waser, R. Electrical Properties of the Grain Boundaries of Oxygen Ion Conductors: Acceptor-Doped Zirconia and Ceria. *Progress in Materials Science* **2006**, *51* (2), 151–210.
- (63) Paramelle, D.; Sadovoy, A.; Gorelik, S.; Free, P.; Hobley, J.; Fernig, D. G. A Rapid Method to Estimate the Concentration of Citrate Capped Silver Nanoparticles from UV-Visible Light Spectra. *Analyst* **2014**, *139* (19), 4855.
- (64) Krishnan, V.; Venkatasubbu, G. D.; Kalaivani, T. Investigation of Hemolysis and Antibacterial Analysis of Curcumin-Loaded Mesoporous SiO2 Nanoparticles. *Applied Nanoscience* **2023**, *13* (1), 811–818.
- (65) Li, Q.; Ma, L.; Gao, C. Biomaterials for in Situ Tissue Regeneration: Development and Perspectives. *J. Mater. Chem. B* **2015**, *3* (46), 8921–8938.
- (66) Kaur, G.; Narayanan, G.; Garg, D.; Sachdev, A.; Matai, I. Biomaterials-Based Regenerative Strategies for Skin Tissue Wound Healing. *ACS Appl. Bio Mater.* **2022**, *5* (5), 2069–2106.
- (67) Menon, G. K. New Insights into Skin Structure: Scratching the Surface. *Advanced Drug Delivery Reviews* **2002**, *54*, S3–S17.
- (68) Liang, Y.; He, J.; Guo, B. Functional Hydrogels as Wound Dressing to Enhance Wound Healing. *ACS Nano* **2021**, *15* (8), 12687–12722.
- (69) Hoque, J.; Haldar, J. Direct Synthesis of Dextran-Based Antibacterial Hydrogels for Extended Release of Biocides and Eradication of Topical Biofilms. *ACS Appl. Mater. Interfaces* **2017**, *9* (19), 15975–15985.
- (70) Xie, Y.; Gan, C.; Li, Z.; Liu, W.; Yang, D.; Qiu, X. Fabrication of a Lignin-Copper Sulfide-Incorporated PVA Hydrogel with Near-Infrared-Activated Photothermal/Photodynamic/Peroxidase-like Performance for Combating Bacteria and Biofilms. *ACS Biomater. Sci. Eng.* **2022**, 8 (2), 560–569.
- (71) Jiang, L.; Loo, S. C. J. Intelligent Nanoparticle-Based Dressings for Bacterial Wound Infections. *ACS Appl. Bio Mater.* **2021**, *4* (5), 3849–3862.
- (72) Yu, R.; Zhang, H.; Guo, B. Conductive Biomaterials as Bioactive Wound Dressing for Wound Healing and Skin Tissue Engineering. *Nano-Micro Lett.* **2022**, *14* (1), 1.
- (73) Ibne Shoukani, H.; Nisa, S.; Bibi, Y.; Zia, M.; Sajjad, A.; Ishfaq, A.; Ali, H. Ciprofloxacin Loaded PEG Coated ZnO Nanoparticles with Enhanced Antibacterial and Wound Healing Effects. *Scientific Reports* **2024**, *14* (1), 4689.
- (74) Li, X.; Qu, S.; Ouyang, Q.; Qin, F.; Guo, J.; Qin, M.; Zhang, J. A Multifunctional Composite Nanoparticle with Antibacterial Activities, Anti-Inflammatory, and Angiogenesis for Diabetic Wound Healing. *International Journal of Biological Macromolecules* **2024**, 260, 129531.
- (75) Kamalipooya, S.; Fahimirad, S.; Abtahi, H.; Golmohammadi, M.; Satari, M.; Dadashpour, M.; Nasrabadi, D. Diabetic Wound Healing Function of PCL/Cellulose Acetate Nanofiber Engineered with Chitosan/Cerium Oxide Nanoparticles. *International Journal of Pharmaceutics* **2024**, *653*, 123880.
- (76) Zhong, Y.; Xiao, H.; Seidi, F.; Jin, Y. Natural Polymer-Based Antimicrobial Hydrogels without Synthetic Antibiotics as Wound Dressings. *Biomacromolecules* **2020**, *21* (8), 2983–3006.
- (77) Pan, Z.; Ye, H.; Wu, D. Recent Advances on Polymeric Hydrogels as Wound Dressings. *APL Bioengineering* **2021**, *5* (1), 011504.
- (78) Wang, P.; Hou, Z.; Wang, Z.; Luo, X. Multifunctional Therapeutic Nanodiamond Hydrogels for Infected-Wound Healing and Cancer Therapy. *ACS Appl. Mater. Interfaces* **2024**, *16* (8), 9656–9668.
- (79) Bhardwaj, D.; Bhaskar, R.; Sharma, A. K.; Garg, M.; Han, S. S.; Agrawal, G. Gelatin/Polyacrylamide-Based Antimicrobial and Self-Healing Hydrogel Film for Wound Healing Application. *ACS Appl. Bio Mater.* **2024**, *7* (2), 879–891.
- (80) Sun, L.; Zhou, J.; Lai, J.; Zheng, X.; Wang, H.; Lu, B.; Huang, R.; Zhang, L.-M. Novel

- Natural Polymer-Based Hydrogel Patches with Janus Asymmetric-Adhesion for Emergency Hemostasis and Wound Healing. *Advanced Functional Materials* **2024**, 2401030.
- (81) Li, S.; Li, X.; Xu, Y.; Fan, C.; Li, Z. A.; Zheng, L.; Luo, B.; Li, Z.-P.; Lin, B.; Zha, Z.-G.; Zhang, H.-T.; Wang, X. Collagen Fibril-like Injectable Hydrogels from Self-Assembled Nanoparticles for Promoting Wound Healing. *Bioactive Materials* **2024**, *32*, 149–163.
- (82) Liu, X.; Sun, Y.; Wang, J.; Kang, Y.; Wang, Z.; Cao, W.; Ye, J.; Gao, C. A Tough, Antibacterial and Antioxidant Hydrogel Dressing Accelerates Wound Healing and Suppresses Hypertrophic Scar Formation in Infected Wounds. *Bioactive Materials* **2024**, *34*, 269–281.
- (83) Ma, S.; Chen, M.; Wang, Y.; Wang, J.; Hao, Y.; Wang, X.; Zhang, H.; Wei, Y.; Liang, Z.; Hu, Y.; Lian, X.; Huang, D. Gelatin-sodium Alginate Composite Hydrogel Doped with Black phosphorus@ZnO Heterojunction for Cutaneous Wound Healing with Antibacterial, Immunomodulatory, and Angiogenic Properties. *International Journal of Biological Macromolecules* **2024**, 274, 133456.
- (84) Deng, X.; Wu, Y.; Tang, Y.; Ge, Z.; Wang, D.; Zheng, C.; Zhao, R.; Lin, W.; Wang, G. Microenvironment-Responsive Smart Hydrogels with Antibacterial Activity and Immune Regulation for Accelerating Chronic Wound Healing. *Journal of Controlled Release* **2024**, *368*, 518–532.
- (85) Qiao, L.; Liang, Y.; Chen, J.; Huang, Y.; Alsareii, S. A.; Alamri, A. M.; Harraz, F. A.; Guo, B. Antibacterial Conductive Self-Healing Hydrogel Wound Dressing with Dual Dynamic Bonds Promotes Infected Wound Healing. *Bioactive Materials* **2023**, *30*, 129–141.
- (86) Wang, L.; Zhao, Z.; Dong, J.; Li, D.; Dong, W.; Li, H.; Zhou, Y.; Liu, Q.; Deng, B. Mussel-Inspired Multifunctional Hydrogels with Adhesive, Self-Healing, Antioxidative, and Antibacterial Activity for Wound Healing. *ACS Appl. Mater. Interfaces* **2023**, *15* (13), 16515–16525.
- (87) Dam, P.; Celik, M.; Ustun, M.; Saha, S.; Saha, C.; Kacar, E. A.; Kugu, S.; Karagulle, E. N.; Tasoglu, S.; Buyukserin, F.; Mondal, R.; Roy, P.; Macedo, M. L. R.; Franco, O. L.; Cardoso, M. H.; Altuntas, S.; Mandal, A. K. Wound Healing Strategies Based on Nanoparticles Incorporated in Hydrogel Wound Patches. *RSC Adv.* **2023**, *13* (31), 21345–21364.
- (88) Liu, H.; Yu, Z.; Liu, L.; Dong, S. Cell Wall Binding Strategies Based on Cu<sub>3</sub>SbS<sub>3</sub> Nanoparticles for Selective Bacterial Elimination and Promotion of Infected Wound Healing. *ACS Appl. Mater. Interfaces* **2024**, *16* (26), 33038–33052.
- (89) Yu, R.; Chen, H.; He, J.; Zhang, Z.; Zhou, J.; Zheng, Q.; Fu, Z.; Lu, C.; Lin, Z.; Caruso, F.; Zhang, X. Engineering Antimicrobial Metal–Phenolic Network Nanoparticles with High Biocompatibility for Wound Healing. *Advanced Materials* **2024**, *36* (6), 2307680.
- (90) Gao, W.; Thamphiwatana, S.; Angsantikul, P.; Zhang, L. Nanoparticle Approaches against Bacterial Infections. *WIREs Nanomed Nanobiotechnol* **2014**, *6* (6), 532–547.
- (91) More, P. R.; Pandit, S.; Filippis, A. D.; Franci, G.; Mijakovic, I.; Galdiero, M. Silver Nanoparticles: Bactericidal and Mechanistic Approach against Drug Resistant Pathogens. *Microorganisms* **2023**, *11* (2), 369.
- (92) Paladini, F.; Pollini, M. Antimicrobial Silver Nanoparticles for Wound Healing Application: Progress and Future Trends. *Materials* **2019**, *12* (16), 2540.
- (93) Zhang, C.; Yang, X.; Yu, L.; Chen, X.; Zhang, J.; Zhang, S.; Wu, S. Electrospun Polyasparthydrazide Nanofibrous Hydrogel Loading with In-Situ Synthesized Silver Nanoparticles for Full-Thickness Skin Wound Healing Application. *Materials & Design* **2024**, *239*, 112818.
- (94) Huang, Y.; Bai, L.; Yang, Y.; Yin, Z.; Guo, B. Biodegradable Gelatin/Silver Nanoparticle Composite Cryogel with Excellent Antibacterial and Antibiofilm Activity and Hemostasis for Pseudomonas Aeruginosa-Infected Burn Wound Healing. *Journal of Colloid and Interface Science* **2022**, 608, 2278–2289.
- (95) Yimeng, S.; Huilun, X.; Ziming, L.; Kejun, L.; Chaima, M.; Xiangyu, Z.; Yinchun, H.; Yan, W.; Di, H. Copper-Based Nanoparticles as Antibacterial Agents. *European Journal of Inorganic Chemistry* **2023**, *26* (4), e202200614.
- (96) Chatterjee, A. K.; Chakraborty, R.; Basu, T. Mechanism of Antibacterial Activity of Copper Nanoparticles. *Nanotechnology* **2014**, *25* (13), 135101.
- (97) Li, S.; Wang, X.; Chen, J.; Guo, J.; Yuan, M.; Wan, G.; Yan, C.; Li, W.; Machens, H.-G.;

- Rinkevich, Y.; Yang, X.; Song, H.; Chen, Z. Calcium Ion Cross-Linked Sodium Alginate Hydrogels Containing Deferoxamine and Copper Nanoparticles for Diabetic Wound Healing. *International Journal of Biological Macromolecules* **2022**, 202, 657–670.
- (98) Zhang, P.; Li, Y.; Tang, Y.; Shen, H.; Li, J.; Yi, Z.; Ke, Q.; Xu, H. Copper-Based Metal-Organic Framework as a Controllable Nitric Oxide-Releasing Vehicle for Enhanced Diabetic Wound Healing. *ACS Appl. Mater. Interfaces* **2020**, *12* (16), 18319–18331.
- (99) Sun, W.; Qi, M.; Cheng, S.; Li, C.; Dong, B.; Wang, L. Gallium and Gallium Compounds: New Insights into the "Trojan Horse" Strategy in Medical Applications. *Materials & Design* **2023**, 227, 111704.
- (100) Xu, Z.; Chen, X.; Tan, R.; She, Z.; Chen, Z.; Xia, Z. Preparation and Characterization of a Gallium-Loaded Antimicrobial Artificial Dermal Scaffold. *Materials Science and Engineering: C* **2019**, *105*, 110063.
- (101) Yang, N.; Shi, N.; Yao, Z.; Liu, H.; Guo, W. Gallium-Modified Gelatin Nanoparticles Loaded with Quercetin Promote Skin Wound Healing via the Regulation of Bacterial Proliferation and Macrophage Polarization. *Front. Bioeng. Biotechnol.* **2023**, *11*, 1124944.
- (102) Qin, J.; Li, M.; Yuan, M.; Shi, X.; Song, J.; He, Y.; Mao, H.; Kong, D.; Gu, Z. Gallium(III)-Mediated Dual-Cross-Linked Alginate Hydrogels with Antibacterial Properties for Promoting Infected Wound Healing. *ACS Appl. Mater. Interfaces* **2022**, *14* (19), 22426–22442.
- (103) Mutalik, C.; Saukani, M.; Khafid, M.; Krisnawati, D. I.; Widodo; Darmayanti, R.; Puspitasari, B.; Cheng, T.-M.; Kuo, T.-R. Gold-Based Nanostructures for Antibacterial Application. *International Journal of Molecular Sciences* **2023**, *24* (12), 10006.
- (104) Sadeghi, S.; Agharazi, F.; Hosseinzadeh, S. A.; Mashayekhi, M.; Saffari, Z.; Shafiei, M.; Nader shahrokhi; Ebrahimi-Rad, M.; Sadeghi, M. Gold Nanoparticle Conjugation Enhances Berberine's Antibacterial Activity against Methicillin-Resistant Staphylococcus Aureus (MRSA). *Talanta* **2024**, 268, 125358.
- (105) Li, Y.; Tian, Y.; Zheng, W.; Feng, Y.; Huang, R.; Shao, J.; Tang, R.; Wang, P.; Jia, Y.; Zhang, J.; Zheng, W.; Yang, G.; Jiang, X. Composites of Bacterial Cellulose and Small Molecule-Decorated Gold Nanoparticles for Treating Gram-Negative Bacteria-Infected Wounds. *Small* **2017**, *13* (27), 1700130.
- (106) He, X.; Dai, L.; Ye, L.; Sun, X.; Enoch, O.; Hu, R.; Zan, X.; Lin, F.; Shen, J. A Vehicle-Free Antimicrobial Polymer Hybrid Gold Nanoparticle as Synergistically Therapeutic Platforms for Staphylococcus Aureus Infected Wound Healing. *Advanced Science* **2022**, *9* (14), 2105223.
- (107) Chen, W.; Chu, R.; Li, H.; Hua, T.; Chen, H.; Li, R.; Zhou, D.; Cao, S.; Ye, S.; Li, H. A Novel Wound Dressing Based on a Gold Nanoparticle Self-Assembled Hydrogel to Promote Wound Healing. *Mater. Adv.* **2023**, *4* (14), 2918–2925.
- (108) Asif, N.; Amir, M.; Fatma, T. Recent Advances in the Synthesis, Characterization and Biomedical Applications of Zinc Oxide Nanoparticles. *Bioprocess and Biosystems Engineering* **2023**, *46* (10), 1377–1398.
- (109) Shahzadi, L.; Chaudhry, A. A.; Aleem, A. R.; Malik, M. H.; Ijaz, K.; Akhtar, H.; Alvi, F.; Khan, A. F.; Rehman, I. U.; Yar, M. Development of K-Doped ZnO Nanoparticles Encapsulated Crosslinked Chitosan Based New Membranes to Stimulate Angiogenesis in Tissue Engineered Skin Grafts. *International Journal of Biological Macromolecules* **2018**, *120*, 721–728.
- (110) Hemdan, B. A.; El-Naggar, M. E.; Abd-Elgawad, Sh. E.; El Zawawy, N. A.; Mahmoud, Y. A.-G. Bacterial Cell-Free Metabolites-Based Zinc Oxide Nanoparticles for Combating Skin-Causing Bacterial Infections. *Biomass Conv. Bioref.* **2023**, *13*, 811-818.
- (111) Batool, M.; Khurshid, S.; Qureshi, Z.; Daoush, W. M. Adsorption, Antimicrobial and Wound Healing Activities of Biosynthesised Zinc Oxide Nanoparticles. *Chemical Papers* **2021**, *75* (3), 893–907.
- (112) Xu, C.; Akakuru, O. U.; Ma, X.; Zheng, J.; Zheng, J.; Wu, A. Nanoparticle-Based Wound Dressing: Recent Progress in the Detection and Therapy of Bacterial Infections. *Bioconjugate Chem.* **2020**, *31* (7), 1708–1723.
- (113) Kalantari, K.; Mostafavi, E.; Saleh, B.; Soltantabar, P.; Webster, T. J. Chitosan/PVA Hydrogels Incorporated with Green Synthesized Cerium Oxide Nanoparticles for Wound Healing

- Applications. European Polymer Journal 2020, 134, 109853.
- (114) Rahmanpour, A.; Farahpour, M. R.; Shapouri, R.; Jafarirad, S.; Rahimi, P. Synthesis and Characterization of Alumina-Based Nanocomposites of TiO<sub>2</sub>/Al<sub>2</sub>O<sub>3</sub>/Chitosan with Antibacterial Properties Accelarate Healing of Infected Excision Wounds. *Colloids and Surfaces A: Physicochemical and Engineering Aspects* **2022**, *644*, 128839.
- (115) Bhubhanil, S.; Talodthaisong, C.; Khongkow, M.; Namdee, K.; Wongchitrat, P.; Yingmema, W.; Hutchison, J. A.; Lapmanee, S.; Kulchat, S. Enhanced Wound Healing Properties of Guar Gum/Curcumin-Stabilized Silver Nanoparticle Hydrogels. *Sci Rep* **2021**, *11* (1), 21836.
- (116) Wang, T.; Zheng, Y.; Shen, Y.; Shi, Y.; Li, F.; Su, C.; Zhao, L. Chitosan Nanoparticles Loaded Hydrogels Promote Skin Wound Healing through the Modulation of Reactive Oxygen Species. *Artificial Cells, Nanomedicine, and Biotechnology* **2018**, *46* (sup1), 138–149.
- (117) Das, A.; Kumar, A.; Patil, N. B.; Viswanathan, C.; Ghosh, D. Preparation and Characterization of Silver Nanoparticle Loaded Amorphous Hydrogel of Carboxymethylcellulose for Infected Wounds. *Carbohydrate Polymers* **2015**, *130*, 254–261.
- (118) Vedadghavami, A.; Minooei, F.; Mohammadi, M. H.; Khetani, S.; Rezaei Kolahchi, A.; Mashayekhan, S.; Sanati-Nezhad, A. Manufacturing of Hydrogel Biomaterials with Controlled Mechanical Properties for Tissue Engineering Applications. *Acta Biomaterialia* **2017**, *62*, 42–63.
- (119) Andrabi, S. M.; Majumder, S.; Gupta, K. C.; Kumar, A. Dextran Based Amphiphilic Nano-Hybrid Hydrogel System Incorporated with Curcumin and Cerium Oxide Nanoparticles for Wound Healing. *Colloids and Surfaces B: Biointerfaces* **2020**, *195*, 111263.
- (120) Fan, Y.; Wu, W.; Lei, Y.; Gaucher, C.; Pei, S.; Zhang, J.; Xia, X. Edaravone-Loaded Alginate-Based Nanocomposite Hydrogel Accelerated Chronic Wound Healing in Diabetic Mice. *Marine Drugs* **2019**, *17* (5), 285.
- (121) Pham, D. T.; Navesit, K.; Wiwatkunupakarn, L.; Chomchalao, P.; Tiyaboonchai, W. Nanoparticles-Hydrogel Composites: A Promising Innovative System for Local Antimicrobial Applications. *Journal of Drug Delivery Science and Technology* **2023**, *89*, 105055.
- (122) Nunes, D.; Andrade, S.; Ramalho, M. J.; Loureiro, J. A.; Pereira, M. C. Polymeric Nanoparticles-Loaded Hydrogels for Biomedical Applications: A Systematic Review on In Vivo Findings. *Polymers* **2022**, *14* (5), 1010.
- (123) Konai, M. M.; Bhattacharjee, B.; Ghosh, S.; Haldar, J. Recent Progress in Polymer Research to Tackle Infections and Antimicrobial Resistance. *Biomacromolecules* **2018**, *19* (6), 1888–1917.
- (124) Tian, R.; Qiu, X.; Yuan, P.; Lei, K.; Wang, L.; Bai, Y.; Liu, S.; Chen, X. Fabrication of Self-Healing Hydrogels with On-Demand Antimicrobial Activity and Sustained Biomolecule Release for Infected Skin Regeneration. *ACS Appl. Mater. Interfaces* **2018**, *10* (20), 17018–17027.
- (125) Khoshmaram, K.; Yazdian, F.; Pazhouhnia, Z.; Lotfibakhshaiesh, N. Preparation and Characterization of 3D Bioprinted Gelatin Methacrylate Hydrogel Incorporated with Curcumin Loaded Chitosan Nanoparticles for in Vivo Wound Healing Application. *Biomaterials Advances* **2024**, *156*, 213677.
- (126) Li, Z.; Qian, C.; Zheng, X.; Qi, X.; Bi, J.; Wang, H.; Cao, J. Collagen/Chitosan/Genipin Hydrogel Loaded with Phycocyanin Nanoparticles and ND-336 for Diabetic Wound Healing. *International Journal of Biological Macromolecules* **2024**, *266*, 131220.
- (127) Zhao, F.; Liu, Y.; Song, T.; Zhang, B.; Li, D.; Xiao, Y.; Zhang, X. A Chitosan-Based Multifunctional Hydrogel Containing *in Situ* Rapidly Bioreduced Silver Nanoparticles for Accelerating Infected Wound Healing. *J. Mater. Chem. B* **2022**, *10* (13), 2135–2147.
- (128) Farghaly Aly, U.; Abou-Taleb, H. A.; Abdellatif, A. A.; Sameh Tolba, N. Formulation and Evaluation of Simvastatin Polymeric Nanoparticles Loaded in Hydrogel for Optimum Wound Healing Purpose. *Drug Design, Development and Therapy* **2019**, *13* (null), 1567–1580.
- (129) Abdelkader, D. H.; Tambuwala, M. M.; Mitchell, C. A.; Osman, M. A.; El-Gizawy, S. A.; Faheem, A. M.; El-Tanani, M.; McCarron, P. A. Enhanced Cutaneous Wound Healing in Rats Following Topical Delivery of Insulin-Loaded Nanoparticles Embedded in Poly(Vinyl Alcohol)-Borate Hydrogels. *Drug Delivery and Translational Research* **2018**, *8* (5), 1053–1065.
- (130) Gong, Y.; Wang, P.; Cao, R.; Wu, J.; Ji, H.; Wang, M.; Hu, C.; Huang, P.; Wang, X. Exudate Absorbing and Antimicrobial Hydrogel Integrated with Multifunctional Curcumin-Loaded

- Magnesium Polyphenol Network for Facilitating Burn Wound Healing. ACS Nano 2023, 17 (22), 22355–22370.
- (131) Jayabal, P.; Kannan Sampathkumar, V.; Vinothkumar, A.; Mathapati, S.; Pannerselvam, B.; Achiraman, S.; Venkatasubbu, G. D. Fabrication of a Chitosan-Based Wound Dressing Patch for Enhanced Antimicrobial, Hemostatic, and Wound Healing Application. *ACS Appl. Bio Mater.* **2023**, *6* (2), 615–627.
- (132) Zhou, M.; An, X.; Liu, Z.; Chen, J. Biosafe Polydopamine-Decorated MnO2 Nanoparticles with Hemostasis and Antioxidative Properties for Postoperative Adhesion Prevention. *ACS Biomater. Sci. Eng.* **2024**, *10* (2), 1031–1039.
- (133) Liu, Z.; Xu, Y.; Su, H.; Jing, X.; Wang, D.; Li, S.; Chen, Y.; Guan, H.; Meng, L. Chitosan-Based Hemostatic Sponges as New Generation Hemostatic Materials for Uncontrolled Bleeding Emergency: Modification, Composition, and Applications. *Carbohydrate Polymers* **2023**, *311*, 120780.
- (134) Kong, Y.; Hou, Z.; Zhou, L.; Zhang, P.; Ouyang, Y.; Wang, P.; Chen, Y.; Luo, X. Injectable Self-Healing Hydrogels Containing CuS Nanoparticles with Abilities of Hemostasis, Antibacterial Activity, and Promoting Wound Healing. *ACS Biomater. Sci. Eng.* **2021**, *7* (1), 335–349.
- (135) He, Y.; Liu, K.; Guo, S.; Chang, R.; Zhang, C.; Guan, F.; Yao, M. Multifunctional Hydrogel with Reactive Oxygen Species Scavenging and Photothermal Antibacterial Activity Accelerates Infected Diabetic Wound Healing. *Acta Biomaterialia* **2023**, *155*, 199–217.
- (136) Zhang, S.; Ou, Q.; Xin, P.; Yuan, Q.; Wang, Y.; Wu, J. Polydopamine/Puerarin Nanoparticle-Incorporated Hybrid Hydrogels for Enhanced Wound Healing. *Biomater. Sci.* **2019**, 7 (10), 4230–4236.
- (137) Garg, S. S.; Dubey, R.; Sharma, S.; Vyas, A.; Gupta, J. Biological Macromolecules-Based Nanoformulation in Improving Wound Healing and Bacterial Biofilm-Associated Infection: A Review. *International Journal of Biological Macromolecules* **2023**, 247, 125636.
- (138) Peña, O. A.; Martin, P. Cellular and Molecular Mechanisms of Skin Wound Healing. *Nature Reviews Molecular Cell Biology* **2024**, *25* (8), 599–616.
- (139) Jing, G.; Suhail, M.; Lu, Y.; Long, B.; Wu, Y.; Lu, J.; Ge, J.; Iqbal, M. Z.; Kong, X. Engineering Titanium—Hydroxyapatite Nanocomposite Hydrogels for Enhanced Antibacterial and Wound Healing Efficacy. *ACS Biomater. Sci. Eng.* **2024**, *10* (8), 5068-5079.
- (140) Deng, H.; Guan, Y.; Dong, Q.; An, R.; Wang, J. Chitosan-Based Biomaterials Promote Bone Regeneration by Regulating Macrophage Fate. *J. Mater. Chem. B* **2024**, *12*, 7480-7496.
- (141) Miculescu, F.; Maidaniuc, A.; Voicu, S. I.; Thakur, V. K.; Stan, G. E.; Ciocan, L. T. Progress in Hydroxyapatite–Starch Based Sustainable Biomaterials for Biomedical Bone Substitution Applications. *ACS Sustainable Chem. Eng.* **2017**, *5* (10), 8491–8512.
- (142) Boskey, A. L.; Robey, P. G. The Composition of Bone. In *Primer on the Metabolic Bone Diseases and Disorders of Mineral Metabolism*; Rosen, C. J., Ed.; Wiley, 2013; pp 49–58.
- (143) Salhotra, A.; Shah, H. N.; Levi, B.; Longaker, M. T. Mechanisms of Bone Development and Repair. *Nat Rev Mol Cell Biol* **2020**, *21* (11), 696–711.
- (144) Su, N.; Villicana, C.; Yang, F. Immunomodulatory Strategies for Bone Regeneration: A Review from the Perspective of Disease Types. *Biomaterials* **2022**, 286, 121604.
- (145) Ullah, I.; Hussain, Z.; Ullah, S.; Zahra, Q. U. A.; Zhang, Y.; Mehmood, S.; Liu, X.; Kamya, E.; Waseem Ghani, M.; Mansoorianfar, M.; Wang, Z.; Wang, Z.; Pei, R. An Osteogenic, Antibacterial, and Anti-Inflammatory Nanocomposite Hydrogel Platform to Accelerate Bone Reconstruction. *J. Mater. Chem. B* **2023**, *11* (25), 5830–5845.
- (146) Yu, Y.; Li, X.; Ying, Q.; Zhang, Z.; Liu, W.; Su, J. Synergistic Effects of Shed-Derived Exosomes, Cu2+, and an Injectable Hyaluronic Acid Hydrogel on Antibacterial, Anti-Inflammatory, and Osteogenic Activity for Periodontal Bone Regeneration. *ACS Appl. Mater. Interfaces* **2024**, *16* (26), 33053–33069.
- (147) Hofbauer, L. C.; Baschant, U.; Hofbauer, C. Targeting Senescent Cells to Boost Bone Fracture Healing. *Journal of Clinical Investigation* **2024**, *134* (12), e181974.
- (148) Dang, Y.; Zhang, Y.; Luo, G.; Li, D.; Ma, Y.; Xiao, Y.; Xiao, L.; Wang, X. The Decisive Early Phase of Biomaterial-Induced Bone Regeneration. *Applied Materials Today* **2024**, *38*,

- 102236.
- (149) Chen, J.; Luo, J.; Feng, J.; Wang, Y.; Lv, H.; Zhou, Y. Spatiotemporal Controlled Released Hydrogels for Multi-System Regulated Bone Regeneration. *Journal of Controlled Release* **2024**, *372*, 846–861.
- (150) Singh, P.; Gupta, A.; Qayoom, I.; Singh, S.; Kumar, A. Orthobiologics with Phytobioactive Cues: A Paradigm in Bone Regeneration. *Biomedicine & Pharmacotherapy* **2020**, *130*, 110754.
- (151) Zhang, M.; Xu, F.; Cao, J.; Dou, Q.; Wang, J.; Wang, J.; Yang, L.; Chen, W. Research Advances of Nanomaterials for the Acceleration of Fracture Healing. *Bioactive Materials* **2024**, *31*, 368–394.
- (152) Yang, Y.; Zhou, B.; Li, M.; Sun, Y.; Jiang, X.; Zhou, X.; Hu, C.; Zhang, D.; Luo, H.; Tan, W.; Yang, X.; Lei, S. GO/Cu Nanosheet-Integrated Hydrogel Platform as a Bioactive and Biocompatible Scaffold for Enhanced Calvarial Bone Regeneration. *International Journal of Nanomedicine* **2024**, *19* (null), 8309–8336.
- (153) Wang, M.; Yao, J.; Shen, S.; Heng, C.; Zhang, Y.; Yang, T.; Zheng, X. A Scaffold with Zinc-Whitlockite Nanoparticles Accelerates Bone Reconstruction by Promoting Bone Differentiation and Angiogenesis. *Nano Res.* **2023**, *16* (1), 757–770.
- (154) Kim, J.; Kim, Y.-M.; Song, S.-C. One-Step Preparation of an Injectable Hydrogel Scaffold System Capable of Sequential Dual-Growth Factor Release to Maximize Bone Regeneration. *Advanced Healthcare Materials* **2023**, *12* (4), 2202401.
- (155) Salehi, S.; Tavakoli, M.; Mirhaj, M.; Varshosaz, J.; Labbaf, S.; Karbasi, S.; Jafarpour, F.; Kazemi, N.; Salehi, S.; Mehrjoo, M.; Emami, E. A 3D Printed Polylactic Acid-Baghdadite Nanocomposite Scaffold Coated with Microporous Chitosan-VEGF for Bone Regeneration Applications. *Carbohydrate Polymers* **2023**, *312*, 120787.
- (156) Fan, L.; Chen, S.; Yang, M.; Liu, Y.; Liu, J. Metallic Materials for Bone Repair. *Advanced Healthcare Materials* **2024**, *13* (3), 2302132.
- (157) Li, J.; Wen, J.; Li, B.; Li, W.; Qiao, W.; Shen, J.; Jin, W.; Jiang, X.; Yeung, K. W. K.; Chu, P. K. Valence State Manipulation of Cerium Oxide Nanoparticles on a Titanium Surface for Modulating Cell Fate and Bone Formation. *Advanced Science* **2018**, *5* (2), 1700678.
- (158) Tang, H.; Qi, C.; Bai, Y.; Niu, X.; Gu, X.; Fan, Y. Incorporation of Magnesium and Zinc Metallic Particles in PLGA Bi-Layered Membranes with Sequential Ion Release for Guided Bone Regeneration. *ACS Biomater. Sci. Eng.* **2023**, *9* (6), 3239–3252.
- (159) Li, J.; Wu, J.; Liu, F.; Li, X.; Yu, P.; Pan, H.; Yeung, K. W. K.; Wong, T. M. Magnesium-Organic Framework-Loaded Bisphosphonate-Functionalized Gel Scaffolds for Enhanced Bone Regeneration. *ACS Biomater. Sci. Eng.* **2023**, *9* (12), 6849–6859.
- (160) Ali, M.; He, Y.; Chang, A. S. N.; Wu, A.; Liu, J.; Cao, Y.; Mohammad, Y.; Popat, A.; Walsh, L.; Ye, Q.; Xu, C.; Kumeria, T. Osteoimmune-Modulating and BMP-2-Eluting Anodised 3D Printed Titanium for Accelerated Bone Regeneration. *J. Mater. Chem. B* **2024**, *12* (1), 97–111.
- (161) Aoki, K.; Ideta, H.; Komatsu, Y.; Tanaka, A.; Kito, M.; Okamoto, M.; Takahashi, J.; Suzuki, S.; Saito, N. Bone-Regeneration Therapy Using Biodegradable Scaffolds: Calcium Phosphate Bioceramics and Biodegradable Polymers. *Bioengineering* **2024**, *11* (2), 180.
- (162) Félix Lanao, R. P.; Leeuwenburgh, S. C. G.; Wolke, J. G. C.; Jansen, J. A. Bone Response to Fast-Degrading, Injectable Calcium Phosphate Cements Containing PLGA Microparticles. *Biomaterials* **2011**, *32* (34), 8839–8847.
- (163) Humbert, P.; Kampleitner, C.; De Lima, J.; Brennan, M. Á.; Lodoso-Torrecilla, I.; Sadowska, J. M.; Blanchard, F.; Canal, C.; Ginebra, M.-P.; Hoffmann, O.; Layrolle, P. Phase Composition of Calcium Phosphate Materials Affects Bone Formation by Modulating Osteoclastogenesis. *Acta Biomaterialia* **2024**, *176*, 417–431.
- (164) Feng, Y.; Wu, D.; Knaus, J.; Keßler, S.; Ni, B.; Chen, Z.; Avaro, J.; Xiong, R.; Cölfen, H.; Wang, Z. A Bioinspired Gelatin–Amorphous Calcium Phosphate Coating on Titanium Implant for Bone Regeneration. *Advanced Healthcare Materials* **2023**, *12* (20), 2203411.
- (165) Zhai, W.; Lu, H.; Chen, L.; Lin, X.; Huang, Y.; Dai, K.; Naoki, K.; Chen, G.; Chang, J. Silicate Bioceramics Induce Angiogenesis during Bone Regeneration. *Acta Biomaterialia* **2012**, 8 (1), 341–349.

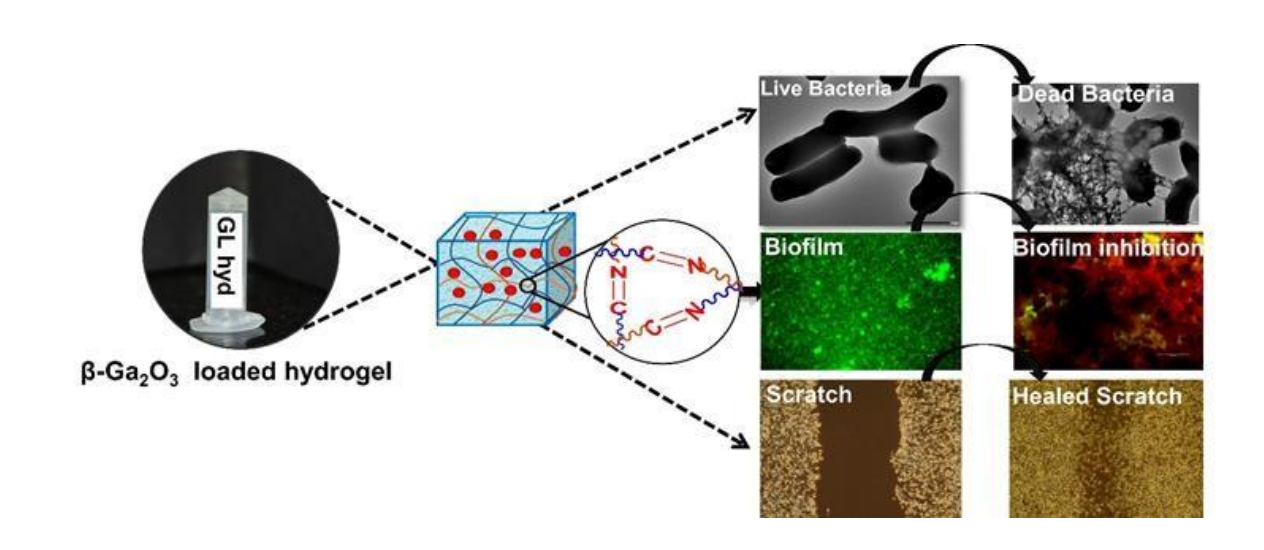
- (166) Skibiński, S.; Czechowska, J. P.; Milivojevic, D.; Nikodinovic-Runic, J.; Guzik, M.; Zima, A. Silver and Silicon Doped βTCP Scaffolds with Gentamicin or Ceftazidime Loaded P(3HB) Coatings as Multifunctional Biomaterials for Bone Regeneration. *Ceramics International* **2024**, *50* (16), 28682–28695.
- (167) Banoriya, D.; Purohit, R.; Dwivedi, R. K. Advanced Application of Polymer Based Biomaterials. *Materials Today: Proceedings* **2017**, *4* (2, Part A), 3534–3541.
- (168) Ozdil, D.; Aydin, H. M. Polymers for Medical and Tissue Engineering Applications: Polymers for Medical and Tissue Engineering Applications. *J. Chem. Technol. Biotechnol.* **2014**, 89 (12), 1793–1810.
- (169) Wang, S.; Lei, H.; Mi, Y.; Ma, P.; Fan, D. Chitosan and Hyaluronic Acid Based Injectable Dual Network Hydrogels Mediating Antimicrobial and Inflammatory Modulation to Promote Healing of Infected Bone Defects. *International Journal of Biological Macromolecules* **2024**, 274, 133124.
- (170) Tang, X.; Wang, Y.; Liu, N.; Deng, X.; Zhou, Z.; Yu, C.; Wang, Y.; Fang, K.; Wu, T. Methacrylated Carboxymethyl Chitosan Scaffold Containing Icariin-Loaded Short Fibers for Antibacterial, Hemostasis, and Bone Regeneration. *ACS Biomater. Sci. Eng.* **2024**, *10* (8), 5181–5193.
- (171) Bonfield, W.; Grynpas, M. D.; Tully, A. E.; Bowman, J.; Abram, J. Hydroxyapatite Reinforced Polyethylene a Mechanically Compatible Implant Material for Bone Replacement. *Biomaterials* **1981**, 2 (3), 185–186.
- (172) Nahar, Q.; Quach, D. M. L.; Darvish, B.; Goldberg, H. A.; Grohe, B.; Mittler, S. Orientation Distribution of Highly Oriented Type I Collagen Deposited on Flat Samples with Different Geometries. *Langmuir* **2013**, *29* (22), 6680–6686.
- (173) Kijeńska, E.; Prabhakaran, M. P.; Swieszkowski, W.; Kurzydlowski, K. J.; Ramakrishna, S. Electrospun Bio-Composite P(LLA-CL)/Collagen I/Collagen III Scaffolds for Nerve Tissue Engineering. *Journal of Biomedical Materials Research Part B: Applied Biomaterials* **2012**, *100B* (4), 1093–1102.
- (174) Kikuchi, M. Hydroxyapatite/Collagen Bone-Like Nanocomposite. *Biological & Pharmaceutical Bulletin* **2013**, *36* (11), 1666–1669.
- (175) Barbani, N.; Guerra, G. D.; Cristallini, C.; Urciuoli, P.; Avvisati, R.; Sala, A.; Rosellini, E. Hydroxyapatite/Gelatin/Gellan Sponges as Nanocomposite Scaffolds for Bone Reconstruction. *J Mater Sci: Mater Med* **2012**, *23* (1), 51–61.
- (176) Wang, R.; He, X.; Su, S.; Bai, J.; Liu, H.; Zhou, F. Multifunctional Tannic Acid-Based Nanocomposite Methacrylated Silk Fibroin Hydrogel with the Ability to Scavenge Reactive Oxygen Species and Reduce Inflammation for Bone Regeneration. *International Journal of Biological Macromolecules* **2024**, 266, 131357.
- (177) Derakhshankhah, H.; Eskandani, M.; Akbari Nakhjavani, S.; Tasoglu, S.; Vandghanooni, S.; Jaymand, M. Electro-Conductive Silica Nanoparticles-Incorporated Hydrogel Based on Alginate as a Biomimetic Scaffold for Bone Tissue Engineering Application. *International Journal of Polymeric Materials and Polymeric Biomaterials* **2024**, *73* (4), 266–278.
- (178) Taymouri, S.; Hasani, F.; Mirian, M.; Farhang, A.; Varshosaz, J. Biocompatible Nanocomposite Scaffolds Based on Carrageenan Incorporating Hydroxyapatite and Hesperidin Loaded Nanoparticles for Bone Tissue Regeneration. *Polymers for Advanced Technologies* **2024**, *35* (1), e6284.
- (179) Yao, C.; Pripatnanont, P.; Zhang, J.; Suttapreyasri, S. Fabrication and Characterization of a Bioactive Composite Scaffold Based on Polymeric Collagen/Gelatin/Nano β-TCP for Alveolar Bone Regeneration. *Journal of the Mechanical Behavior of Biomedical Materials* **2024**, *153*, 106500.
- (180) Zhan, Y.; Yang, K.; Zhao, J.; Wang, K.; Li, Z.; Liu, J.; Liu, H.; Liu, Y.; Li, W.; Su, X. Injectable and In Situ Formed Dual-Network Hydrogel Reinforced by Mesoporous Silica Nanoparticles and Loaded with BMP-4 for the Closure and Repair of Skull Defects. *ACS Biomater*. *Sci. Eng.* **2024**, *10* (4), 2414–2425.
- (181) Bhumiratana, S.; Grayson, W. L.; Castaneda, A.; Rockwood, D. N.; Gil, E. S.; Kaplan, D.

- L.; Vunjak-Novakovic, G. Nucleation and Growth of Mineralized Bone Matrix on Silk-Hydroxyapatite Composite Scaffolds. *Biomaterials* **2011**, *32* (11), 2812–2820.
- (182) Tanase, C. E.; Sartoris, A.; Popa, M. I.; Verestiuc, L.; Unger, R. E.; Kirkpatrick, C. J. *In Vitro* Evaluation of Biomimetic Chitosan–Calcium Phosphate Scaffolds with Potential Application in Bone Tissue Engineering. *Biomed. Mater.* **2013**, *8* (2), 025002.
- (183) Manda, M. G.; da Silva, L. P.; Cerqueira, M. T.; Pereira, D. R.; Oliveira, M. B.; Mano, J. F.; Marques, A. P.; Oliveira, J. M.; Correlo, V. M.; Reis, R. L. Gellan Gum-Hydroxyapatite Composite Spongy-like Hydrogels for Bone Tissue Engineering. *Journal of Biomedical Materials Research Part A* **2018**, *106* (2), 479–490.
- (184) Bharadwaz, A.; Jayasuriya, A. C. Recent Trends in the Application of Widely Used Natural and Synthetic Polymer Nanocomposites in Bone Tissue Regeneration. *Materials Science and Engineering: C* **2020**, *110*, 110698.
- (185) Han, X.; He, J.; Wang, Z.; Bai, Z.; Qu, P.; Song, Z.; Wang, W. Fabrication of Silver Nanoparticles/Gelatin Hydrogel System for Bone Regeneration and Fracture Treatment. *Drug Delivery* **2021**, 28 (1), 319–324.
- (186) Wei, B.; Wang, W.; Liu, X.; Xu, C.; Wang, Y.; Wang, Z.; Xu, J.; Guan, J.; Zhou, P.; Mao, Y. Gelatin Methacrylate Hydrogel Scaffold Carrying Resveratrol-Loaded Solid Lipid Nanoparticles for Enhancement of Osteogenic Differentiation of BMSCs and Effective Bone Regeneration. *Regenerative Biomaterials* **2021**, *8* (5), rbab044.
- (187) Xue, X.; Zhang, H.; Liu, H.; Wang, S.; Li, J.; Zhou, Q.; Chen, X.; Ren, X.; Jing, Y.; Deng, Y.; Geng, Z.; Wang, X.; Su, J. Rational Design of Multifunctional CuS Nanoparticle-PEG Composite Soft Hydrogel-Coated 3D Hard Polycaprolactone Scaffolds for Efficient Bone Regeneration. *Advanced Functional Materials* **2022**, *32* (33), 2202470.
- (188) Cao, L.; Werkmeister, J. A.; Wang, J.; Glattauer, V.; McLean, K. M.; Liu, C. Bone Regeneration Using Photocrosslinked Hydrogel Incorporating rhBMP-2 Loaded 2-N, 6-O-Sulfated Chitosan Nanoparticles. *Biomaterials* **2014**, *35* (9), 2730–2742.
- (189) Domazetovic, V. Oxidative Stress in Bone Remodeling: Role of Antioxidants. *ccmbm* **2017**, *14* (2), 209.
- (190) Guo, J.; Yang, X.; Chen, J.; Wang, C.; Kang, Y.; Jiang, T.; Chen, M.; Li, W.; Zhou, C.; Chen, Z. Accelerated Bone Regeneration by an Astaxanthin-Modified Antioxidant Aerogel through Relieving Oxidative Stress via the NRF2 Signaling Pathway. *ACS Biomater. Sci. Eng.* **2022**, 8 (10), 4524–4534.
- (191) Huang, L.; Zhang, S.; Bian, M.; Xiang, X.; Xiao, L.; Wang, J.; Lu, S.; Chen, W.; Zhang, C.; Mo, G.; Jiang, L.; Li, Y.; Zhang, J. Injectable, Anti-Collapse, Adhesive, Plastic and Bioactive Bone Graft Substitute Promotes Bone Regeneration by Moderating Oxidative Stress in Osteoporotic Bone Defect. *Acta Biomaterialia* **2024**, *180*, 82–103.
- (192) Singh, R. K.; Yoon, D. S.; Mandakhbayar, N.; Li, C.; Kurian, A. G.; Lee, N.-H.; Lee, J.-H.; Kim, H.-W. Diabetic Bone Regeneration with Nanoceria-Tailored Scaffolds by Recapitulating Cellular Microenvironment: Activating Integrin/TGF-β Co-Signaling of MSCs While Relieving Oxidative Stress. *Biomaterials* **2022**, 288, 121732.
- (193) Wu, Y.; Li, X.; Sun, Y.; Tan, X.; Wang, C.; Wang, Z.; Ye, L. Multiscale Design of Stiffening and ROS Scavenging Hydrogels for the Augmentation of Mandibular Bone Regeneration. *Bioactive Materials* **2023**, *20*, 111–125.
- (194) Qin, D.; Zhao, Y.; Cheng, R.; Liu, Y.; Guo, S.; Sun, L.; Guo, Y.; Hao, F.; Zhao, B. Mussel-Inspired Immunomodulatory and Osteoinductive Dual-Functional Hydroxyapatite Nanoplatform for Promoting Bone Regeneration. *J Nanobiotechnol* **2024**, *22* (1), 320.
- (195) Liang, H.; Jin, C.; Ma, L.; Feng, X.; Deng, X.; Wu, S.; Liu, X.; Yang, C. Accelerated Bone Regeneration by Gold-Nanoparticle-Loaded Mesoporous Silica through Stimulating Immunomodulation. *ACS Appl. Mater. Interfaces* **2019**, *11* (44), 41758–41769.
- (196) Zhou, P.; Yan, B.; Wei, B.; Fu, L.; Wang, Y.; Wang, W.; Zhang, L.; Mao, Y. Quercetin-Solid Lipid Nanoparticle-Embedded Hyaluronic Acid Functionalized Hydrogel for Immunomodulation to Promote Bone Reconstruction. *Regenerative Biomaterials* **2023**, *10*, rbad025.

- (197) Cheng, D.; Ding, R.; Jin, X.; Lu, Y.; Bao, W.; Zhao, Y.; Chen, S.; Shen, C.; Yang, Q.; Wang, Y. Strontium Ion-Functionalized Nano-Hydroxyapatite/Chitosan Composite Microspheres Promote Osteogenesis and Angiogenesis for Bone Regeneration. *ACS Appl. Mater. Interfaces* **2023**, *15* (16), 19951–19965.
- (198) Wang, W.; Liu, Y.; Yang, C.; Jia, W.; Qi, X.; Liu, C.; Li, X. Delivery of Salvianolic Acid B for Efficient Osteogenesis and Angiogenesis from Silk Fibroin Combined with Graphene Oxide. *ACS Biomater. Sci. Eng.* **2020**, *6* (6), 3539–3549.
- (199) Liu, Z.; Huang, L.; Qi, L.; Wang, J.; Xu, H.; Yang, H.; Liu, L.; Feng, G.; Zhang, L. Activating Angiogenesis and Immunoregulation to Propel Bone Regeneration via Deferoxamine-Laden Mg-Mediated Tantalum Oxide Nanoplatform. *ACS Appl. Mater. Interfaces* **2024**, *16* (19), 24384–24397.
- (200) Heo, D. N.; Castro, N. J.; Lee, S.-J.; Noh, H.; Zhu, W.; Zhang, L. G. Enhanced Bone Tissue Regeneration Using a 3D Printed Microstructure Incorporated with a Hybrid Nano Hydrogel. *Nanoscale* **2017**, *9* (16), 5055–5062.
- (201) Wang, Y.; Yuan, Z.; Pang, Y.; Zhang, D.; Li, G.; Zhang, X.; Yu, Y.; Yang, X.; Cai, Q. Injectable, High Specific Surface Area Cryogel Microscaffolds Integrated with Osteoinductive Bioceramic Fibers for Enhanced Bone Regeneration. *ACS Appl. Mater. Interfaces* **2023**, *15* (17), 20661–20676.
- (202) Jaswal, R.; Kumar, D.; Kaliannagounder, V. K.; Rezk, A. I.; Kandel, R.; Park, C. H.; Min, K. H. Osteopromotive PDA-Modified Gold Nanoparticles-Incorporated Bioinspired Polycaprolactone-Based Nanofibers for Bone Cancer Therapy and Robust Bone Regeneration. *Materials Today Nano* **2024**, *25*, 100453.

## CHAPTER - 2

Gallium oxide nanoparticles-loaded quaternized chitosan-oxidized sodium alginate hydrogels for treatment of bacteria infected wounds



## 2.1. Introduction

#### 2.1.1. Bacteria infected wounds

The skin is crucial for human health and safety, serving as the primary barrier against bacterial and viral invasion. It is composed of the outer epidermis, dermis, and a fatty subcutaneous layer, all of which contribute to its protective function<sup>1</sup>. However, it is highly susceptible to invasion, and severe injuries or burns can compromise this protective barrier. When the skin is compromised, the denaturation of proteins and lipids, coupled with the loss of the outer epidermal layer, creates an ideal environment for bacterial growth. Bacterial infections and biofilm formation can impede wound healing, resulting in chronic, non-healing wounds<sup>2</sup>. Severe inflammatory reactions increase the incidence of diseases from infected wounds and reduce the quality of wound healing. They aggravate the inflammatory stage of the healing process and generate excessive ROS<sup>3</sup>, which delays wound healing and affects around 6.5 million individuals worldwide, imposing an immense burden on the healthcare system<sup>4</sup>. Moreover, the rise in antibiotic resistance has further intensified the problem, resulting in the loss of 700,000 lives every year<sup>5</sup>. Severe blood loss following traumatic injury can also increase the risk of infection from external sources, further elevating the likelihood of death. Globally, blood loss alone accounts for around 30% of traumatic deaths<sup>6</sup>. Although most wound infections heal without intervention, major untreated or inadequately treated wounds can become fatal. Therefore, the primary objectives in wound management are to control hemorrhage, eradicate or control pathogenic bacteria, and facilitate the healing process.

#### 2.1.2. Challenges

Traditionally, wound dressings have functioned as passive barriers to protect wounds from external contamination and they are available in the form of creams, ointments, and gels. However, most of the time, these products are ineffective because of their limitations, which include cytotoxicity, narrow-spectrum activity, and ineffectiveness against biofilms<sup>7</sup>. Over time, more advanced dressings incorporating antibiotics have been developed. Common antibiotics that are used in dressings include cephalosporins, quinolones, tetracyclines, and aminoglycosides<sup>8,9,10</sup>. These antibiotics act by disrupting bacterial protein and nucleic acid synthesis, leading to metabolic imbalances, or by compromising bacterial cell wall integrity. However, improper use and overuse of antibiotics can lead to the emergence of antibiotic-resistant strains. Also, commercially available hemostatic agents have demonstrated efficacy but also suffer from limitations. Due to exothermic interactions, hemostatic agents such as QuikClot and Sponge Plus can injure tissue<sup>6</sup>.

Thus, effective treatment interventions that can control bleeding to lower the risk of secondary infection and treat bacterial infections without increasing the likelihood of developing resistance have recently attracted attention.

### 2.1.3. Research gap

Different types of biomaterials have been investigated to treat bacteria infected wounds<sup>11</sup>. Researchers have fabricated different formulations including polymeric hydrogels, gels, films, sponges, nanoparticles, nanocomposites, and electrospun nanofibers. Jing *et al.*, developed sodium alginate and silk fibroin-loaded curcumin, which showed good antibacterial activity with enhanced adhesion<sup>12</sup>. Liang *et al.* fabricated hydrogels using dual-dynamic bonds between Fe<sup>3+</sup>, protocatechualdehyde, and quaternized chitosan to treat infected wounds<sup>13</sup>. Feng *et al.* reported the eradication of bacterial infection by fabricating a 2D reduced graphene oxide and Au nanocomposite. Due to the presence of sharp edges on the nanostructure, it showed increased antibacterial activity<sup>14</sup>. Liu *et al.*, fabricated GelMA and cationic quaternary ammonium salt to develop hydrogel coating for implant. The coating demonstrated strong cytocompatibility and good mechanical qualities with a broad spectrum antibacterial activity<sup>15</sup>. Despite extensive research efforts aimed at developing an optimal material for bacteria-infected wounds, a multifunctional material that possesses antioxidant, antibacterial, and antibiofilm qualities in addition to hemostatic potential remains lacking for the effective management of bacteria-infected wounds.

#### 2.1.4. Nanoparticle-loaded hydrogel

An optimal dressing for a wound should have good biocompatibility, maintain moisture in the wound and absorb exudates, offer protection against infection, actively stimulate wound healing and regeneration of injured tissue, and act as a depot for the delivery of medications or other therapies along with hemostatic abilities<sup>12</sup>. The distinctive properties of nanoparticles and biocompatibility of hydrogels combined with their resemblance to the extracellular matrix, capacity to absorb excessive exudates, delivery of bioactive agents, and porous structure facilitates cell migration, adhesion, and the exchange of nutrients, water, and oxygen. It has led to a great deal of interest in research on the use of biomaterials for healthcare<sup>16</sup> and prompted the development of novel strategies to address bacterial infections and wound repair. Tao *et al.*,<sup>17</sup> Alvarez *et al.*,<sup>18</sup> Liu *et al.*,<sup>19</sup> Augustine *et al.*,<sup>20</sup> have fabricated nanoparticle-loaded hydrogels that either have antibacterial, free radical scavenging activity, or the ability to efficiently deliver antibiotics for efficient treatment of bacteria infected wounds. There is still a lack of multifunctional biomaterials with diverse properties needed for the effective treatment of bacteria-infected wounds.

#### 2.2. Objectives

To address the existing challenges in the wound healing process, we have fabricated a multifunctional hydrogel system comprising of  $\beta$ -Ga<sub>2</sub>O<sub>3</sub> nanoparticles loaded in quaternized

chitosan-oxidized sodium alginate hydrogels with excellent antibacterial, antibiofilm, antioxidant, and hemostatic abilities (**Figure 2.1**). The hydrogel will utilize the ability of  $Ga^{3+}$  to kill bacteria due to its similarity to ferric iron ( $Fe^{3+}$ ) in electronic configuration and atomic radius as bacteria require  $Fe^{3+}$  for vital redox-dependent processes such as DNA synthesis and respiration<sup>21</sup>. Additionally, studies have shown that gallium nitrate in aqueous solution promotes platelet activation, coagulation, and clot formation, suggesting its potential as a hemostatic agent. Also, quaternized chitosan due to its characteristics like enhanced solubility, antibacterial, hemostatic, electropositivity<sup>16</sup>, and sodium alginate because of biocompatibility and biodegradability<sup>22</sup> were used to fabricate imine crosslinked hydrogels. The  $\beta$ -Ga<sub>2</sub>O<sub>3</sub> nanoparticle-loaded quaternized chitosan and oxidized sodium alginate hydrogels were fabricated and thoroughly characterized for their antibacterial, antioxidant, antibiofilm, and hemostatic abilities. The proposed nanoparticle-hydrogel system was able to target multiple aspects of wound development and thus holds a notable potential for the treatment of bacteria-infected wounds.

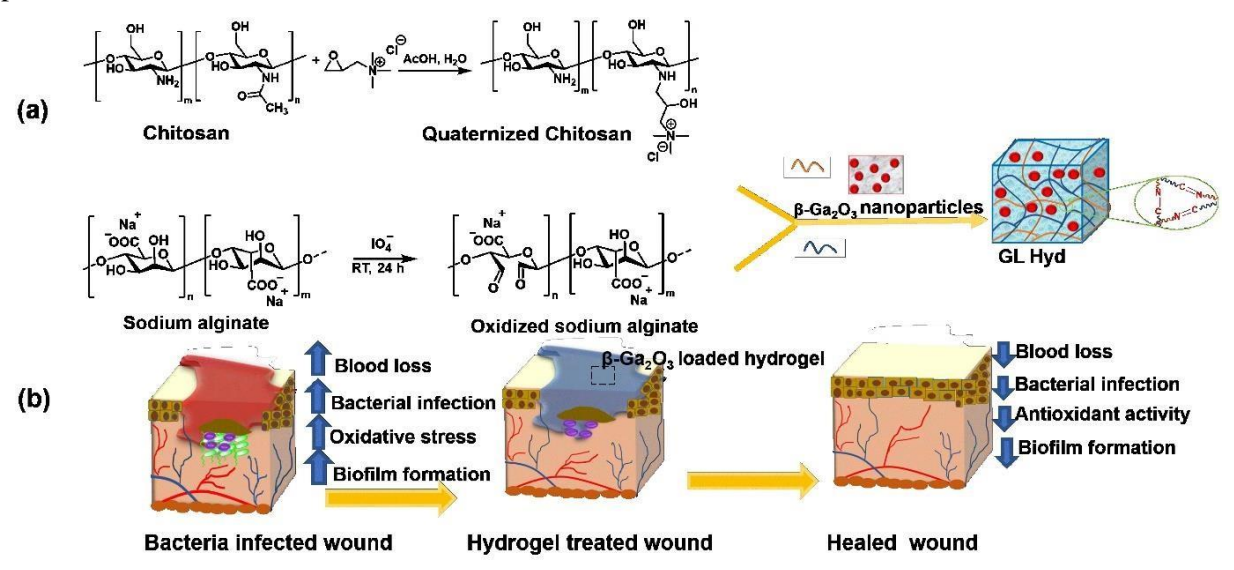


**Figure 2.1.** (a) Fabrication of  $\beta$ -Ga<sub>2</sub>O<sub>3</sub> nanoparticle-loaded quaternized chitosan-oxidized sodium alginate hydrogels (GL Hyd), using biodegradable imine linkages. (b) Antibacterial, antibiofilm, hemostatic, and wound healing activities of hydrogel.

#### 2.3. Experimental section

#### 2.3.1. Materials

Chitosan, Luria broth, bacteriological agar powder, gentamicin, ascorbic acid, and phosphate-buffered saline were obtained from HiMedia. Sodium alginate was obtained from SRL Innovations. The 2,2'- azino-bis (3-ethylbenzothiazoline-6-sulfonic acid (ABTS) and glycidyltrimethyl ammonium chloride (GTMAC) were obtained from TCI. Sodium citrate and sodium metaperiodate were obtained from Fisher Scientific. Glacial acetic acid was purchased from Merck. Ammonia (30%) was obtained from Avra. Gallium nitrate was procured from GLR Innovations. *E. coli* 

(MTCC 1687) and *S. aureus* (MTCC 7443) were obtained from CSIR- IMTECH, Chandigarh. RPMI 1640, trypsin, fetal bovine serum (FBS), Penstrep, and MTT reagent were sourced from Thermo Fisher and Sigma. The bacterial live-dead kit was procured from Thermo Fisher. L929 cells were kindly provided by Dr. Durba Pal, Assistant Professor, DBME, IIT Ropar. Fresh human blood was obtained from healthy female volunteers with informed consent, following protocol no. 07/2021-II/IIT/IEC, approved by the Institutional Biosafety Committee (IBSC).

## 2.3.2. Preparation of gallium oxide nanoparticle-loaded hydrogels (GL Hyd)

The degree of deacetylation of chitosan was estimated using acid-base titration<sup>23</sup>. The degree of deacetylation was calculated using the formula:

DD% = 
$$\frac{(V_1 - V_2) \times 16}{V_1 \times 9.94 \times x} \times 100$$
 Equation 2.1

where, x is the chitosan's weight,  $V_1$  is the volume of chitosan solution prepared in 0.1 N HCl solution in mL and  $V_2$  is the volume of 0.1 N NaOH in mL.

## 2.3.2.1. Preparation of quaternized chitosan (QC)

To fabricate QC, a modified version of the previously reported procedure was employed<sup>24</sup>. A solution of 1.25% chitosan using 0.5% v/v glacial acetic acid in 50 mL distilled water was prepared. The reaction mixture was stirred at 55 °C and glycidyl trimethylammonium chloride (GTMAC) was added. The product was precipitated in pre-cooled acetone and filtered. The QC was vacuum-dried for two days in a desiccator at room temperature, followed by characterization using FTIR, <sup>1</sup>H NMR, and GPC. GPC was carried out using an Agilent gel permeation chromatography (GPC) system that has a 1220 refractive index detector and a GPC/SEC column. The molecular weights were determined using a 1 mg/mL solution of quaternized chitosan and chitosan. The percentage degree of substitution (DS) of quaternized chitosan was determined by conductometric titration and it was calculated using the following equation:

$$DS (\%) = C_{AgNO_3} \times V_{AgNO_3} (m_{HTCC} \times DS)$$
  
/  $[(DS \times M3) + \{(1 - DS - DA) \times M1\} + (DA \times M2)]$ 

#### **Equation 2.2**

where,  $C_{AgNO3}$  = concentration of AgNO<sub>3</sub>,  $V_{AgNO3}$  = AgNO<sub>3</sub> volume, m = QC mass used for titration, DA is acetylation degree of chitosan, M1 = molecular weight of glucosamine, M2 = molecular weight of N-acetyl glucosamine, M3 = GTMAC unit molecular weight.

## 2.3.2.2. Preparation of oxidized alginate (OA)

Sodium alginate solution (2%) was made in 150 mL distilled water. Further, 3 g of sodium periodate solution was made in 10 mL of distilled water. The solution was added dropwise to the sodium alginate solution and stirred in dark at room temperature. Further, the solution was dialyzed using a dialysis bag (MWCO 3500 Da) for 72 h<sup>25</sup>. The solution was finally lyophilized, and the product was further characterized using <sup>1</sup>H NMR, FTIR, and GPC. A published procedure was employed to

determine the M/G ratio of oxidized sodium alginate and sodium alginate using <sup>1</sup>H NMR<sup>26</sup>. The molecular weight of sodium alginate and oxidized sodium alginate was determined using GPC. Percentage oxidation was calculated using hydroxylamine hydrochloride assay. Following equation was used:

Degree of oxidation =  $198 \Delta V \times C \times 10^{-3} / 2w$ 

Equation 2.3

where, 198 is the sodium alginate repeating units (g/ mol) molecular weight, w is weight in g of SA-CHO,  $\Delta V$  is the volume of sodium hydroxide (NaOH) in mL, and C is the concentration of sodium hydroxide solution in mol/L.

#### 2.3.2.3. Preparation of gallium nanoparticles (GNPs)

Sol-gel method was used to prepare  $\beta$ -Ga<sub>2</sub>O<sub>3</sub> nanoparticles and gallium (III) nitrate hydrate was used as the precursor. A 0.1 M solution of gallium salt was prepared in 5 mL of deionized water. Ammonia solution was added to the solution till the pH was 7.5. The mixture was stirred for 24 h and centrifuged at 9000 rpm for 25 min. The resulting precipitate was collected and washed with distilled water to remove excess ammonia. The purified precipitate was dried in oven to yield GaO(OH) powder<sup>27</sup>. This powder was then calcined for around 5 h at 750 °C to produce  $\beta$ -Ga<sub>2</sub>O<sub>3</sub> nanoparticles<sup>28</sup>.

## 2.3.2.4. Fabrication of $\beta$ -Ga<sub>2</sub>O<sub>3</sub> nanoparticle-loaded hydrogels (GL Hyd)

Separately, 2 mL of OA (5%) and QC (3%) solutions were made by dissolving the two polymers in 2 mL of phosphate buffer (7.4). An equal volume of both solutions (100  $\mu$ L) was mixed and allowed to form a gel at room temperature.  $\beta$ -Ga<sub>2</sub>O<sub>3</sub> nanoparticle-loaded hydrogels (GL Hyd) were made by dispersing 100  $\mu$ g of nanoparticles in OA solution to form a 1 mg/mL solution and 100  $\mu$ L of this solution was blended with 100  $\mu$ L of QC solution to create nanoparticle-loaded hydrogels with 1.5% QC and 2.5% sodium alginate as the working concentrations.

# 2.3.3. Characterization of $\beta\text{-}Ga_2O_3$ nanoparticles and $\beta\text{-}Ga_2O_3$ nanoparticle-loaded hydrogels (GL Hyd)

Characterization of nanoparticles was done using SEM, zeta, EDS, DLS, and XRD. XRD was performed with a Rigaku Mini Flex diffractometer to examine the phase structure of nanoparticles. After dispersing nanoparticles in phosphate buffer (7.4), DLS Microtrac/Nanotrac Flex and a particle-matrix zeta sizer were used to quantify the nanoparticles size and zeta potential. Using an EDX Bruker Splash 6130, elemental analysis of nanoparticles was carried out, and the drop-cast method was used to analyze the surface morphology. Hydrogel formation was verified by the vial inversion method, and subsequent characterizations included FTIR, TNBS, SEM, swelling, and degradation. FTIR was performed using Bruker Tensor 27 in ATR mode. SEM was performed to understand the surface morphology of hydrogels loaded with nanoparticles. Rheology was performed using MCR-102 modular rheometer (Anton Paar, Austria) equipped with a parallel plate.

#### 2.3.3.1. TNBS assay

The 2,4,6-trinitrobenzenesulfonic acid (TNBS) assay was used to determine the degree of crosslinking in hydrogels. A 1 mL solution of 0.5% TNBS solution and 1 mL of 4% sodium bicarbonate mixture was treated with 5 mg of lyophilized hydrogel at 60 °C for 4 h followed by treatment of 1 mL of this solution with 3 mL of 6 N HCl for 1.5 h at 40 °C. The absorbance at 334 nm was determined. Following treatment with TNBS at several QC concentrations, a standard curve for non-crosslinked chitosan was plotted<sup>29</sup>. The following formula was used to estimate the crosslinking %:

Crosslinking degree (%) = 
$$\{1 - \frac{\text{Absorbance of crosslinked gel}}{\text{Absorbance of non-crosslinked gel}}\} \times 100$$
 **Equation 2.4**

#### 2.3.3.2. Rheological studies

Anton Par Rheometer MCR 102, was used to determine the viscoelastic characteristics of hydrogels. QC-OA and  $\beta$ -Ga<sub>2</sub>O<sub>3</sub>-loaded hydrogels (GL Hyd) were developed. Hydrogels were subjected to varying amplitude strain from 1% to 1000% in order to investigate their linear viscoelastic range (LVR). The storage modulus data was analyzed to determine hydrogels mechanical toughness. Further, hydrogels were subjected to frequency sweep measurement where the angular frequency was varied from 0.01 to 100 rad/s while keeping the amplitude constant at 1%. The self-healing properties of hydrogels were tested by applying alternating cycles of mild stain of 0.1% and high stain of 100% at constant angular frequency of 10 rad s<sup>-1 30</sup>.

#### 2.3.3.2. Swelling and degradation

QC-OA hydrogel and GL Hyd were fabricated (200  $\mu$ L) and suspended in buffer solution (1 mL) of pH 7.4 and 5.5 followed by incubation at 37 °C with constant shaking at 100 rpm. After regular intervals, the buffer solution was withdrawn, and hydrogels were removed, blotted, and dried<sup>31</sup>. The percentage of swelling and degradation (%) was calculated using the equation below:

Swelling ratio (%) = 
$$\left(\frac{W_S - W_0}{W_0}\right) \times 100$$
 Equation 2.5

where, Ws = weight of swollen hydrogel at time t and Wo = initial weight of hydrogel.

#### 2.3.4. Antioxidant assay

The antioxidant potential of hydrogels was determined by ABTS assay. A 1 mL of ABTS (7 mM) and potassium persulfate (2.45 mM) solution were made in distilled water and mixed in equal volumes. The solution was further left in dark for 12 h for the generation of ABTS radical. The OD of the solution was adjusted to 0.8 AU at 734 nm by diluting it with PBS (pH 7.4). Hydrogels (100 μL) were treated with ABTS solution (200 μL) for 1 h in dark conditions at room temperature followed by the measurement of absorbance at 734 nm. Phosphate-buffered saline (PBS) without a sample and ABTS radical solution without a sample were used as control and blank. Ascorbic acid (1 mg/mL) served as the standard<sup>32</sup>. The ABTS radical scavenging activity of materials was determined using the following equation:

% Radical scavenging effect = 
$$\frac{(A_C - A_S)}{A_S} \times 100$$
 Equation 2.6

#### 2.3.5. Release of gallium in vitro

Agilent Technologies 4200 MPAES was used to analyze the release of gallium ions from nanoparticle hydrogel system. Hydrogels containing approximately 100  $\mu$ g of nanoparticles were suspended for 48 h at 100 rpm in 5 mL of pH 7.4 phosphate buffer. At regular intervals, 5 mL of media was withdrawn and replaced with fresh phosphate buffer. The release media was filtered with 0.22  $\mu$ m pore size filter and analyzed<sup>33</sup>.

## 2.3.6. *In vitro* thrombus formation

In vitro thrombus formation was investigated using human blood. Fresh blood samples from healthy individuals were collected and mixed with 3.2% sodium citrate solution. The whole blood and 3.2% sodium citrate ratio were kept at 9:1. The hydrogels were freeze-dried and weighed. A 1 mL of citrated blood was gradually added to start the thrombus-forming process. Samples were incubated for different time intervals of 15, 30, and 60 min. The reaction was stopped by adding 10 mL of DI water at the appropriate intervals. Formaldehyde (37%) was used to stabilize the thrombus for 10 min. The samples were kept for drying overnight at 50 °C. The weights were recorded as  $W_0$  for the initial weight and  $W_t$  for the end weight. The following equation was used to determine the % degree of thrombogenicity (DT)<sup>34</sup>.

DT (%) = 
$$[(W_t - W_0)/W_0] \times 100\%$$
 Equation 2.7

#### 2.3.7. Whole blood clotting test

To determine the blood-clotting capacity of freeze-dried hydrogels, a whole blood clotting test was performed. After treating the hydrogels with 100  $\mu$ L of citrated human blood, 10  $\mu$ L of a 0.2 M CaCl<sub>2</sub> solution was added to initiate the coagulation process. After 10 minutes of incubation at 37 °C, 12.5 mL of water was added to dissolve the blood clots, which are not stable. Using a microplate reader, the hemoglobin solution's absorbance at 544 nm was calculated<sup>34</sup>.

#### 2.3.8. *In vitro* platelet adhesion

SEM analysis was used to perform *in vitro* platelet adhesion. Briefly, platelet-rich plasma (PRP) was separated from blood by centrifuging it for 20 min at 3000 rpm. The PRP was added to the sample dropwise, and further incubated at 37 °C for 1 h. The samples were fixed using 2.5% glutaraldehyde for 2 h at room temperature. The samples were then subjected to dehydration using 50, 60, 70, 80, 90, and 100% ethanol solutions for ten minutes each. Finally, the samples were washed with PBS, allowed to air dry at room temperature, and observed using SEM<sup>35</sup>.

#### 2.3.9. Hemolysis assay

Human blood was used to check the hemocompatibility of hydrogels. The RBCs were first separated by centrifuging the blood at 2000 rpm for 20 min. The RBCs were washed with PBS  $(1\times)$  two times.

For the formation of a working solution, I mL of the above solution was diluted with 9 mL of PBS. The samples were incubated with 1 mL of working solution at 37 °C for 5 h. A plate reader was used to measure supernatant absorbance at 394 nm. PBS and Triton X (1%) are used as the positive and negative controls. The following equation was used to estimate the % hemolysis<sup>36</sup>:

% Hemolysis = 
$$\frac{OD_{sample - OD_{negative}}}{OD_{positive - OD_{negative}}} \times 100$$
 Equation 2.8

## 2.3.10. Antibacterial activity

The antibacterial activity of hydrogels was investigated using OD method, disc diffusion, live-dead assay, and HRTEM

#### 2.3.10.1. OD method

Gallium NPs and nanoparticle-loaded hydrogels (GL Hyd) were investigated for their antibacterial effectiveness against Gram-positive bacteria *S. aureus* and Gram-negative *E. coli*. Firstly, bacteria were cultured to the mid-log phase in Luria broth at 37 °C for 24 h. The optical density (OD) of bacteria was adjusted to 0.1 AU ( $1 \times 10^7$  CFU/mL). The hydrogel samples were incubated with bacteria for different time intervals in a shaking incubator. After 12, 24, and 48 h, optical density was observed at 600 nm. Bacterial sample without any treatment was taken as a negative control and gentamicin ( $50 \mu g/mL$ ) was taken as a positive control. Luria broth was taken as a blank<sup>37</sup>. The percentage of antibacterial activity was estimated by the following equation:

% Antibacterial activity = 
$$\frac{(OD_{negative} - OD_{sample})}{OD_{negative}} \times 100$$
 Equation 2.9

#### 2.3.10.2. Disc diffusion

Petri plates were made using Luria broth agar solution. For making agar solution, 5 g of Luria broth and 3.75g of agar were dissolved in 250 mL of distilled water. The mix of Luria broth and agar was autoclaved at 121 °C for 15 min. Around 10–15 mL of agar solution was added to petri dishes, which were then left to stand at room temperature. A 100  $\mu$ L of (0.1 OD) bacterial suspension was added to plates with the spreader. The plates were further dried at room temperature. After removing around 10 mm of agar, NPs and GL Hyd were placed in that area and incubated for 24 h at 37 °C<sup>38</sup>.

#### 2.3.10.3. Live/Dead assay

The working dye solution was prepared by mixing SYTO 9 and propidium iodide (PI) in a 1:1 ratio (150  $\mu$ L) in autoclaved water. The solution was then incubated with bacteria for 30 minutes at room temperature in the dark, both with and without samples. The same staining procedure was followed for biofilm staining. After 30 minutes, the dye solution was discarded and the bacterial cells were imaged using fluorescence microscopy (Leica DMi8) using glass slides<sup>39</sup>.

## 2.3.10.4. HR-TEM analysis

HR-TEM imaging (JEM-2100 Plus, 200 kV) was used to investigate the impact of GL Hyd on the bacterial structure. *E. coli* and *S. aureus* were grown as discussed earlier followed by treatment of samples for 24 h. After 24 h, the bacteria treated with samples and untreated bacteria were subjected to centrifugation at 4 °C resulting in the formation of a pellet. The formed pellet was washed with PBS 7.4 three times followed by fixation with 2.5% glutaraldehyde and staining with 1% osmium tetroxide. The pellet was completely dried using ethanol concentrations of 30, 50, 70, and 90% <sup>40</sup>. Ultimately, the pellet was re-dissolved using pure ethanol. Using the drop-cast method, 5 μL of this suspension was placed on a copper grid and imaged using HR-TEM.

#### 2.3.11. Biofilm formation inhibition

The ability of hydrogels to inhibit the formation of biofilm was estimated using crystal violet assay<sup>2</sup>. *S. aureus* was grown as discussed above and OD was set to 0.1 AU. The bacterial suspension (500 μL) in 48 well plate was incubated with GNP, QC-OA Hyd, and GL Hyd for 48 h. After 48 h, the bacterial solution was discarded and planktonic cells were removed by washing the plate two times with PBS. This was followed by bacteria fixation using absolute ethanol for 15 min. Crystal violet (0.1%) was used to stain the bacteria for 10 min. The excess dye was removed by washing the wells with distilled water. Finally, 10% glacial acetic acid was used to dissolve the dye, and the absorbance was measured at 590 nm, and the following equation was used to determine the percentage of antibiofilm activity:

% Antibiofilm activity = 
$$\frac{(OD_{negative} - OD_{sample})}{OD_{negative}} \times 100$$
 Equation 2.10

#### 2.3.12. Inhibition of established biofilm

To investigate the impact of NPs and GL Hyd on biofilm formation, *S. aureus* ( $1 \times 10^7$  CFU/mL) was grown in a 48-well plate. The plate was then incubated for 48 h at 37 °C to allow for the development of biofilm. Samples were incubated with bacterial biofilms for 24 h. After 24 h, the non-adhered bacterial cells were removed followed by washing with PBS. Finally, as previously mentioned, the crystal violet dye was used to quantify the biofilm<sup>41</sup>.

#### 2.3.13. Cytotoxicity analysis

The percentage vitality of cells was estimated using a mouse fibroblast cell line (L929). In a T-25 flask, cells were grown in RPMI supplemented with 10% FBS and 1% antibiotic. Cells were trypsinized once they were about 80 percent confluent, and they were seeded in a 48-well plate at a density of 2 x  $10^4$  cells/mL. Subsequently, the cells were kept in a CO<sub>2</sub> incubator for 24 h. After being incubated with the media at 37 °C for 24 h, the samples were run through a 0.2  $\mu$ M syringe filter. The 48-well plate media was replaced with hydrogel releasates. After cells were incubated for a full day, the vitality of cells was assessed using the techniques discussed below.

2.3.13.1. MTT assay

A modified procedure of an already published protocol was used to determine the percentage of cell viability in the presence of hydrogel samples  $^{42}$ . After 24 h, 20  $\mu$ L, 5 mg/mL solution of MTT was added to each well and incubated for 3.5 h. The MTT solutions were discarded and 100  $\mu$ L dimethyl sulfoxide (DMSO) was added to each well to dissolve formazan crystals and absorbance was measured at 570 nm. The percentage cell viability was estimated by comparing the treated cells absorbance with that of control.

#### 2.3.13.2. Live/Dead assay

Live/dead staining was performed according to the manufacturer's protocol. L929 cells were seeded in 48 well plates and incubated for 24 h at 37 °C. The media was then aspirated, and 200  $\mu$ L of samples were added to each well, followed by an additional 24 h incubation. Subsequently, the samples were removed, and 150  $\mu$ L of a dye solution containing a mixture of calcein AM and ethidium bromide in PBS was added to each well. The cells were incubated with the dye solution for 30 min in dark conditions. Cell imaging was performed using a fluorescence microscope.

#### 2.3.16 Scratch assay

L929 cells were seeded in a six-well plate at a concentration of 10<sup>4</sup> cells per well and were allowed to grow until 100% confluency. A sterile tip was used to create a scratch on the cell monolayer. Cells were further washed with DPBS two times to remove any debris<sup>43</sup>. Cells were further incubated with samples and after regular intervals (0, 12,24 h) healing was observed using a microscope (EVOS XL, Core, Invitrogen).

## **2.3.17.** Statistical analysis

The student's t-test was used to analyze the data and data was presented as mean with standard deviations. P-values of 0.05 or less were considered as significant (\*), and n.s. denotes non-significant difference.

#### 2.4. Results and discussions

## 2.4.1. Fabrication and characterization of QC, OA, and β-Ga<sub>2</sub>O<sub>3</sub> nanoparticles

Acid-base titration was performed to estimate the degree of deacetylation of chitosan. The value was found to be 69.75%, which corresponds with the 75% deacetylation specified by the supplier. GTMAC was grafted onto QC and the grafting was confirmed by FTIR (**Figure 2.2b**), <sup>1</sup>H NMR, and <sup>13</sup>C NMR (**Figure A1, A2 Appendix**). The methyl group of ammonium salt showed a peak at 1482.4 cm<sup>-1</sup>, a 3.06 ppm peak in <sup>1</sup>H NMR, which was attributed to the methyl group proton, and 54.17 ppm peak in <sup>13</sup>C NMR, which was assigned to carbon (C<sub>10</sub>) of triammonium salt, thus, confirming the successful quaternization of chitosan<sup>44</sup>. As per the GPC studies, molecular weights of chitosan and quaternized chitosan were found to be 12 kDa and 15 KDa, with a polydispersity index of 1.06 and 1.22. The increase in molecular weight of quaternized chitosan is due to the presence of quaternary ammonium groups<sup>45</sup>. Conductometric titration was used to calculate the

percentage of quaternization, which came out to be 28% 46.

Oxidation of sodium alginate was performed using sodium periodate. The oxidized sodium alginate was characterized using FTIR and <sup>1</sup>H NMR. An FTIR spectra with a distinctive peak at 1724 cm<sup>-1</sup> confirmed the presence of aldehyde groups (**Figure 2.2a**). <sup>25</sup> The existence of aldehyde groups was also confirmed by a signal at 8.31 in <sup>1</sup>H NMR spectrum of oxidized alginate. The M/G ratio for sodium alginate and oxidized sodium alginate was determined using <sup>1</sup>H NMR and the results showed that the stereochemistry of these polymers is unaffected by oxidation<sup>47</sup> (**Figure A3, A4 Appendix**).

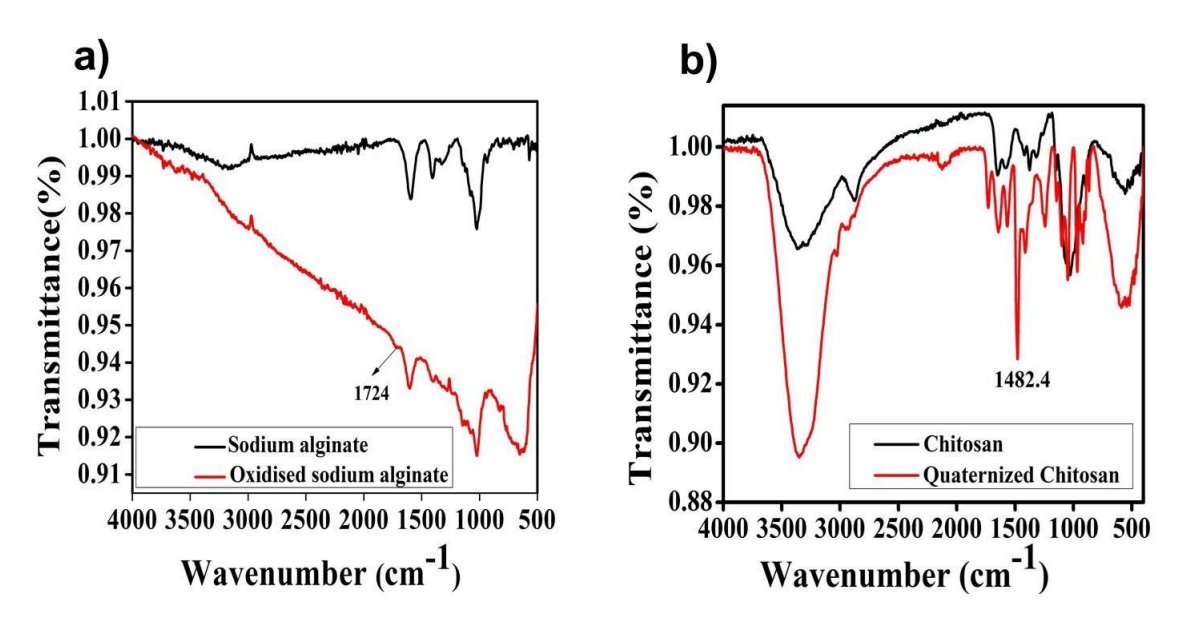


**Figure 2.2.** Characterization of polymers. a) FT-1R spectra of sodium alginate and oxidized sodium alginate. b) FT-IR of chitosan and quaternized chitosan.

GPC was used to measure the  $M_W$  of sodium alginate and oxidized sodium alginate and it was found to be  $1.22 \times 10^5$  g/mol and  $1.9 \times 10^4$  g/mol with a polydispersity index of 1.03 and 1.07. The reduction in molecular weight is because of the cleavage of polysaccharide rings<sup>48</sup>.

Using hydroxylamine hydrochloride assay, the percentage oxidation was calculated and found to be 59.4%. Sol-gel method was used to develop hydrogels, which were further characterized. The particle size of nanoparticles was found to be  $159 \pm 5.196$  nm (**Figure 2.3a, Figure A7 Appendix**) and the polydispersity index was found to be  $0.040 \pm 0.051$ with a surface charge of  $-26 \pm 2.64$  mV. To determine the stability of nanoparticles, changes in particle size after 10 and 15 days were studied. After 10 days the particle size was found to be  $218 \pm 5.17$  nm with a surface charge of  $-25.56 \pm 3.3$  mV and after 15 days a slight increase in particle size was noted where the average particle size was found to be  $261 \pm 7.82$  nm with surface charge of  $-25.43 \pm 2.2$  mV. The SEM analysis indicated a nanorod-like morphology of nanoparticles (**Figure 2.3b**). XRD analysis confirmed the formation of  $\beta$ -Ga<sub>2</sub>O<sub>3</sub> nanoparticles with a monoclinic phase according to JCPDS

data (JCPDS 41-1103)<sup>28</sup> (**Figure 2.3c**). The elemental analysis was done using EDX, which verified the presence of Ga and O (**Figure 2.3d**).

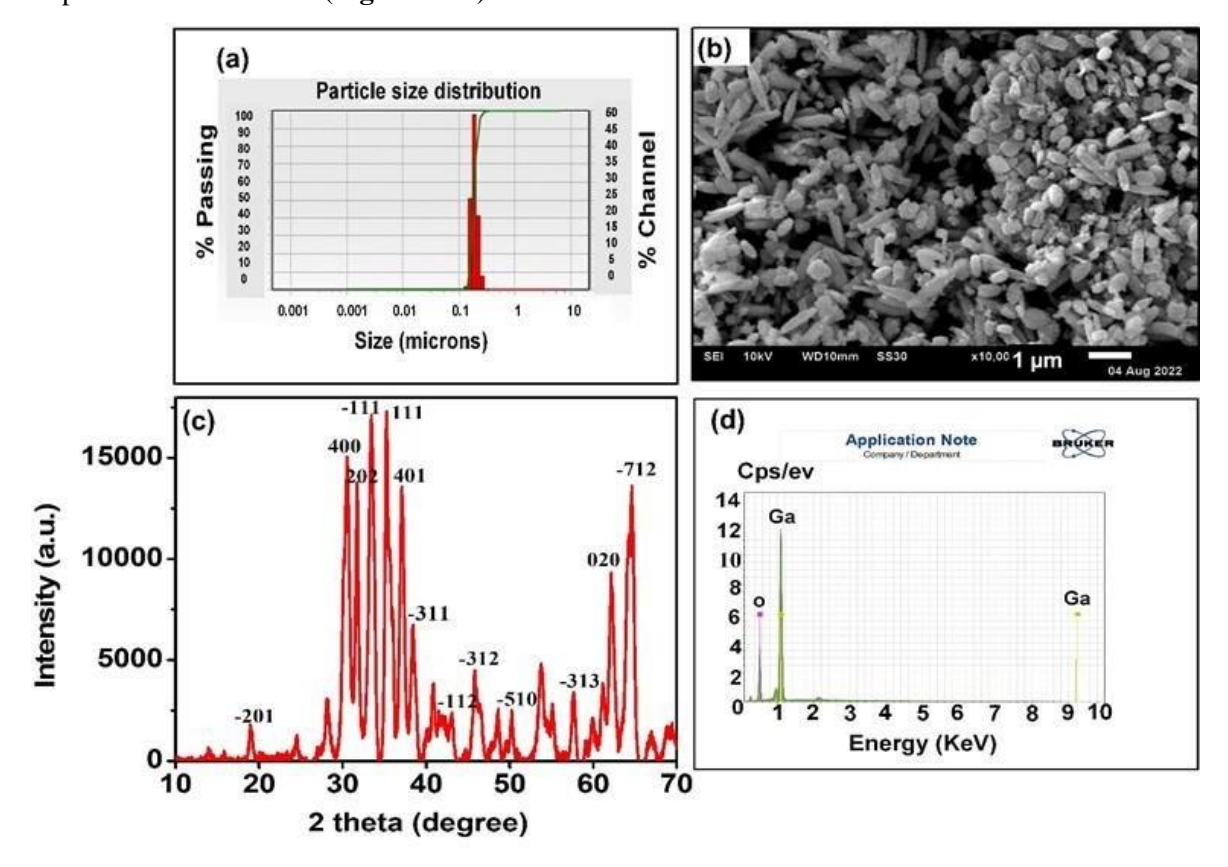


**Figure 2.3.** Characterization of gallium nanoparticles. (a) Particle size distribution; (b) SEM images; scale bar: 1 µm; (c) XRD spectra; and (d) EDS spectra.

## 2.4.2. Fabrication and characterization of nanoparticle-loaded hydrogels (GL Hyd)

For the development of GL Hyd, 100 µg of  $\beta$ -Ga<sub>2</sub>O<sub>3</sub> nanoparticles were dispersed in an oxidized sodium alginate solution (5%). This solution was further mixed with quaternized chitosan solution (3%) at RT, resulting in the formation of imine linked hydrogels loaded with nanoparticles, which were further characterized (**Figure 2.4e**). The hydrogel was freeze-dried and characterized using FTIR analysis. FTIR spectra indicated the presence of a peak at 1670 cm<sup>-1</sup> confirming the presence of C=N linkage<sup>49</sup>. TNBS assay was used to determine the percentage cross-linking and was found to be 92.14  $\pm$  6.48% (**Figure A5, Appendix**). One of the important characteristics of scaffolds is porosity, which is essential for proper cell nutrition and proliferation. The SEM analysis supported the porous morphology of hydrogels (**Figure 2.4a, b**).

#### 2.4.3. Swelling and degradation of hydrogels

Phosphate and acetate buffers of pH 7.4 and pH 5.5 were used to determine hydrogel swelling and degradation behavior (**Figure 2.4c, d**). In buffer solutions, the QC-OA and  $\beta$ -Ga<sub>2</sub>O<sub>3</sub> hydrogels began to swell, within the first eight hours, and higher swelling was observed in pH 5.5 acetate

buffer. This may be due to reduced crosslinking resulting from increased protonated amino groups in an acidic environment. With further incubation, hydrogels exhibited minor degradation. Higher degradation was observed at acidic pH due to the increased hydrolysis rate of the Schiff base in acidic conditions<sup>50</sup>. Also, the inclusion of nanoparticles had no significant impact on the swelling and degradation behavior of hydrogels.

## 2.4.4. Rheological studies

Anton Paar rheometer was used to determine hydrogel's rheological properties (**Figure 2.4g, h, i, j, k, l**). To perform amplitude sweep, varying strains of 0.01 to 1000% were applied<sup>51</sup>. The crossover points for QC-OA Hyd and GL Hyd were 542.7 and 589.28, indicating the outstanding viscoelastic characteristics when compared with hydrogels reported in literature<sup>52</sup>. A frequency sweep ranging from 0.1 to 100 rad/s was conducted, revealing that hydrogels consistently exhibited mechanically robust, solid-like behavior throughout the entire frequency range. As hydrogels can be applied to irregular shaped wounds to absorb excess wound exudate while preserving a moist environment, self-healing hydrogels are considered excellent materials for wound dressings. Alternate six cycles of 100% high and 1% low cycles were applied to investigate the self-healing abilities of hydrogels. The hydrogels showed structure breakdown when the strain was increased to 100% but the value of storage modulus recovered its initial levels when the strain was reduced to 1%, indicating that hydrogels were able to recover quickly because of the re-formation of reversible imine linkages in hydrogels. To further confirm the self-healing potential of hydrogels, we performed the dye diffusion assay and the results indicated that the dye diffused throughout hydrogels, demonstrating its ability to heal itself (**Figure A6, Appendix**).

#### 2.4.5. Antioxidant properties

One of the main causes of microorganism's transition from planktonic to sessile biofilm form is oxidative stress. Furthermore, the host's ability to scavenge free radicals decreases in case of wounds. Therefore, to prevent damage to cells and tissues from free radicals, wound dressings must have significant antioxidant properties<sup>53</sup>. The ABTS assay was used to estimate free-radical scavenging activity of hydrogels (**Figure 2.4f**). The QC-OA hydrogel showed  $85.46 \pm 2.24\%$  antioxidant activity and GL Hyd showed  $86.22 \pm 1.94\%$  antioxidant activity. The hydrogels antioxidant activity was more than 67% antioxidant activity reported for GelMA hydrogels<sup>20</sup>. The positive charge on quaternized chitosan might be the reason of enhanced antioxidant activity.

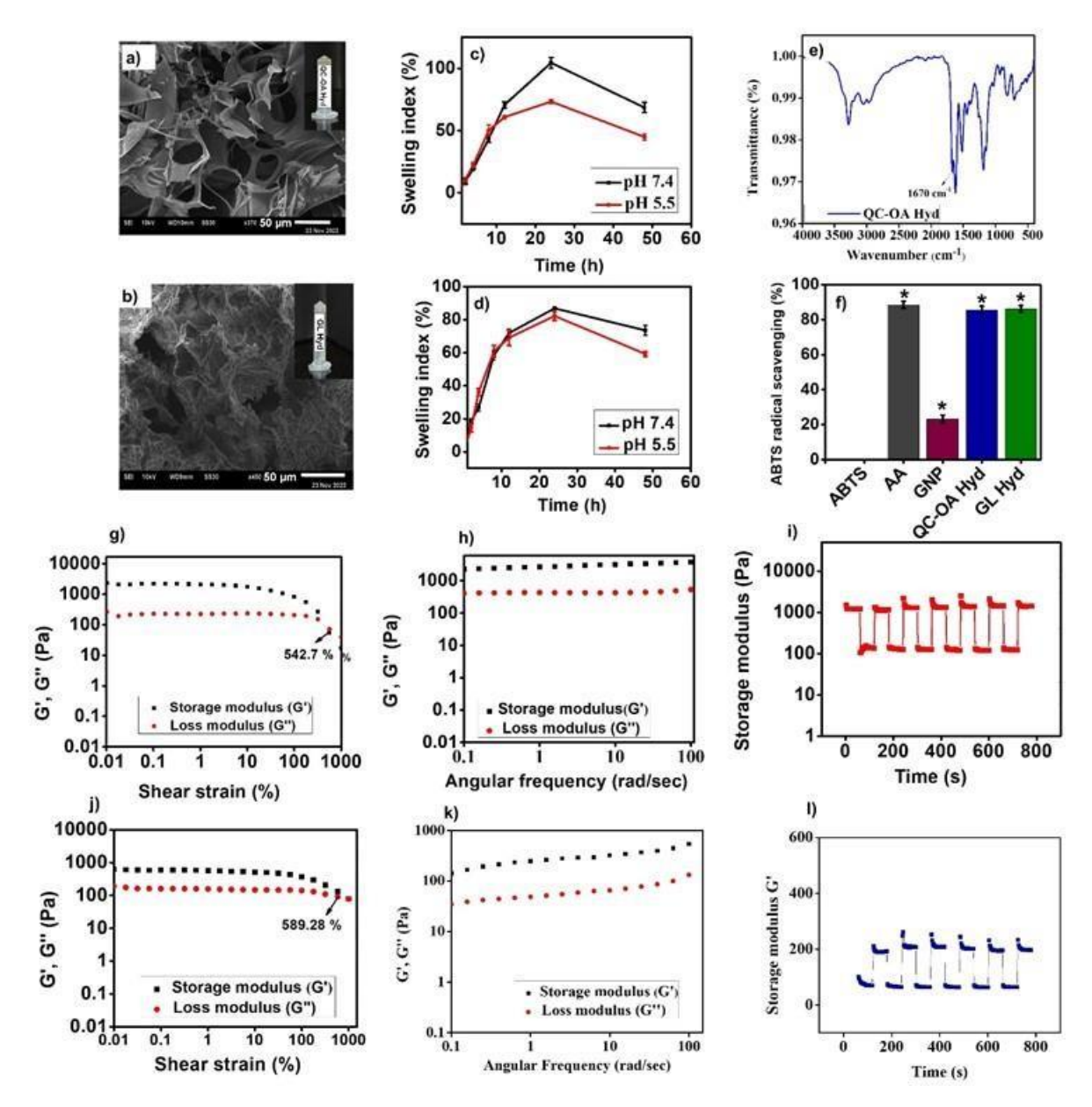


**Figure 2.4.** Characterization of quaternized chitosan-oxidized alginate (QC-OA) hydrogels and gallium NP-loaded hydrogels (GL Hyd). (a, b) SEM analysis of QC-OA and GL Hyd hydrogels; scale bar: 50 μm; (c, d) Swelling and degradation studies of QC-OA and GL Hyd hydrogels at pH 7.4 and pH 5.5; (e) FTIR spectrum of freeze-dried QC-OA hydrogels; and (f) ABTS radical scavenging activity of gallium NPs, and QC-OA and GL Hyd hydrogels. \*p < 0.05 represents statistical significance. Viscoelastic properties of: (g-i) QC-OA hydrogels: (g) amplitude sweep. (h) frequency sweep, and (i) self-healing. (j-l) GL Hyd hydrogels: (j) amplitude sweep, (k) frequency sweep, and (l) self-healing.

#### 2.4.6. Release of gallium in vitro

A pH 7.4 phosphate buffer was used to study the in vitro release of gallium ions from quaternized

chitosan-oxidized sodium alginate hydrogel (**Figure A8, Appendix**). For 48 h, hydrogel was suspended in phosphate buffer and incubated at 37 °C. The samples were withdrawn, filtered, and analyzed using microwave plasma atomic emission spectrometry (MP-AES). The release followed the Weibull model, with R<sup>2</sup> value of 0.9969, which indicated Fickian diffusion.

## 2.4.7. Antibacterial activity

Antibacterial dressings can promote wound healing by reducing the spread of harmful bacteria. Bacteria were treated with different samples including GNP, QC-OA, and GL Hyd to assess their antibacterial properties (**Figure 2.5a, b**). Both Gram-positive and Gram-negative strains, S. aureus and E. coli, showed a significant reduction in optical density (OD) following varying durations of bacterial exposure. The nanoparticle-loaded hydrogels showed a broad-spectrum antibacterial activity with 90  $\pm$  2% bacterial inhibition in case of E. coli and 91  $\pm$  1% in case of S. aureus. One of the possible reasons behind antibacterial activity is the presence of gallium ions. The combined action of gallium NPs and quaternized chitosan polymer resulted in enhanced antibacterial activity. The ability of gallium ions to hinder bacteria's metabolism and strong interaction between quaternized chitosan and negatively charged membrane of bacteria resulted in enhanced disruption of bacterial membrane<sup>13</sup>. The percentage of antibacterial activity was better than 80-85% antibacterial activity of electrospun nanofibrous gelatin/chitosan scaffolds reported earlier<sup>54</sup>. The live-dead fluorescence assay was also conducted to study the antibacterial effect of nanoparticleloaded hydrogels. Propidium iodide (PI) and SYTO 9 were used to stain dead and live bacteria and were imaged using Leica microscope. The images indicated more red emission further indicating the antibacterial potential of GL Hyd (**Figure 2.5c**).

To further understand hydrogels interaction with *S. aureus* and *E. Coli*, the HR-TEM study was also performed (**Figure 2.6**). The images of untreated *E. coli* and *S. aureus* exhibited their characteristic rod-like and round morphologies with intact membranes. In contrast, bacteria treated with NP-loaded hydrogels showed significant membrane distortion. This effect is likely due to the interaction between the positively charged quaternized ammonium groups on QCs and the negatively charged components of bacterial cell membrane, such as lipopolysaccharides and teichoic acids. These electrostatic interactions disrupt the cell membrane, resulting in a damaged cell wall and compromised cell integrity. Consequently, this leads to the leakage of cellular contents and ultimately bacterial cell death.

The zone of inhibition assay was also conducted to further confirm the antibacterial activity of  $\beta$ -Ga<sub>2</sub>O<sub>3</sub> nanoparticles and nanoparticle-loaded hydrogel (**Figure 2.7**).

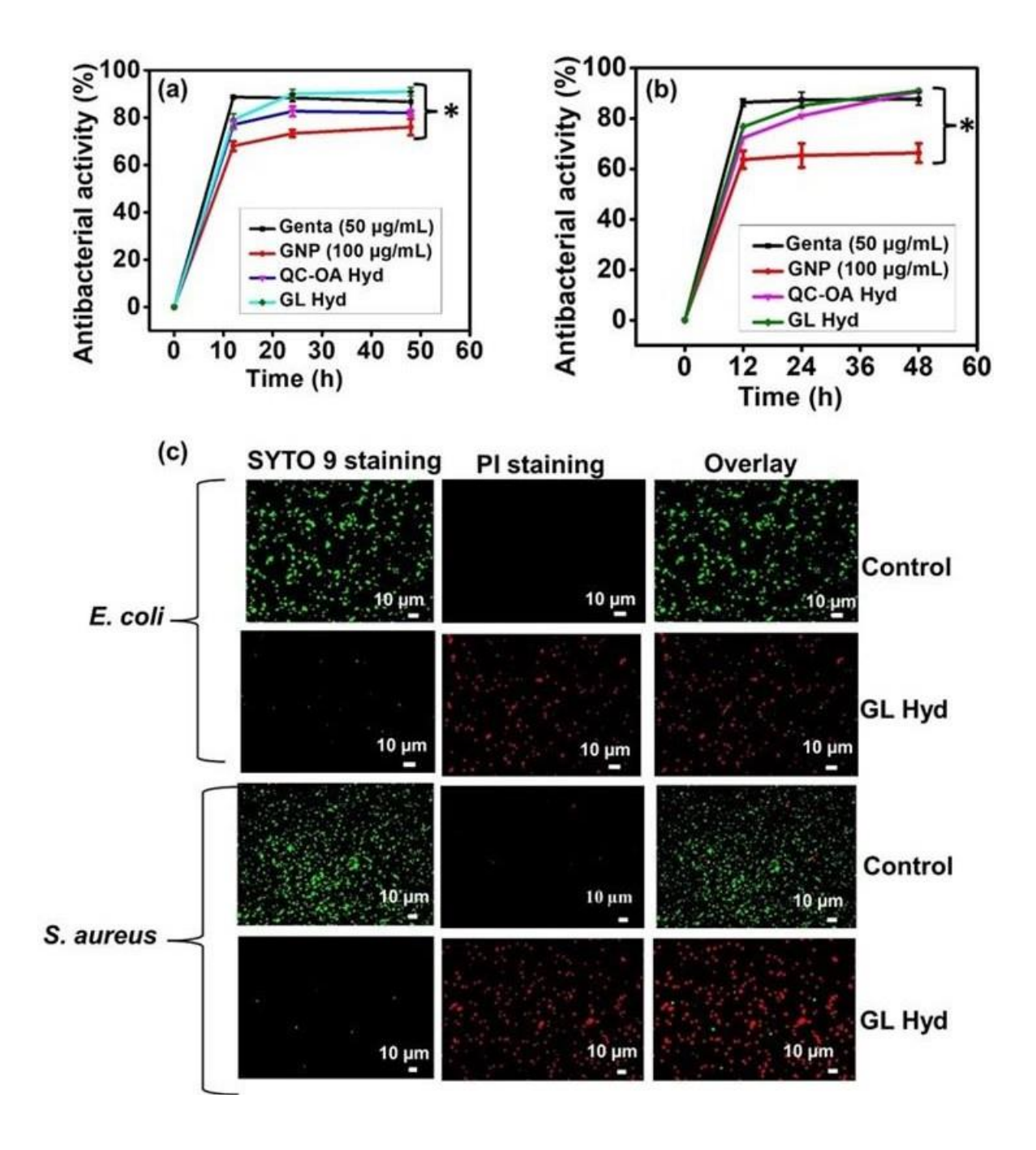


**Figure 2.5.** Antibacterial activity of gallium nanoparticles (GNPs), quaternized chitosan-oxidized alginate hydrogels (QC–OA), and NP-loaded hydrogels (GL Hyd). (a) Percentage antibacterial activity against *E. coli*; (b) Percentage antibacterial activity against *S. aureus*; and (c) Live/dead assay of bacteria after treatment with GL Hyd hydrogels. Untreated samples were taken as a negative control, and gentamicin (50  $\mu$ g/mL) was taken as a positive control; scale bar: 10  $\mu$ m. \*p < 0.05 corresponds to a statistically significant difference, and n.s. corresponds to non-significant data (n = 3).

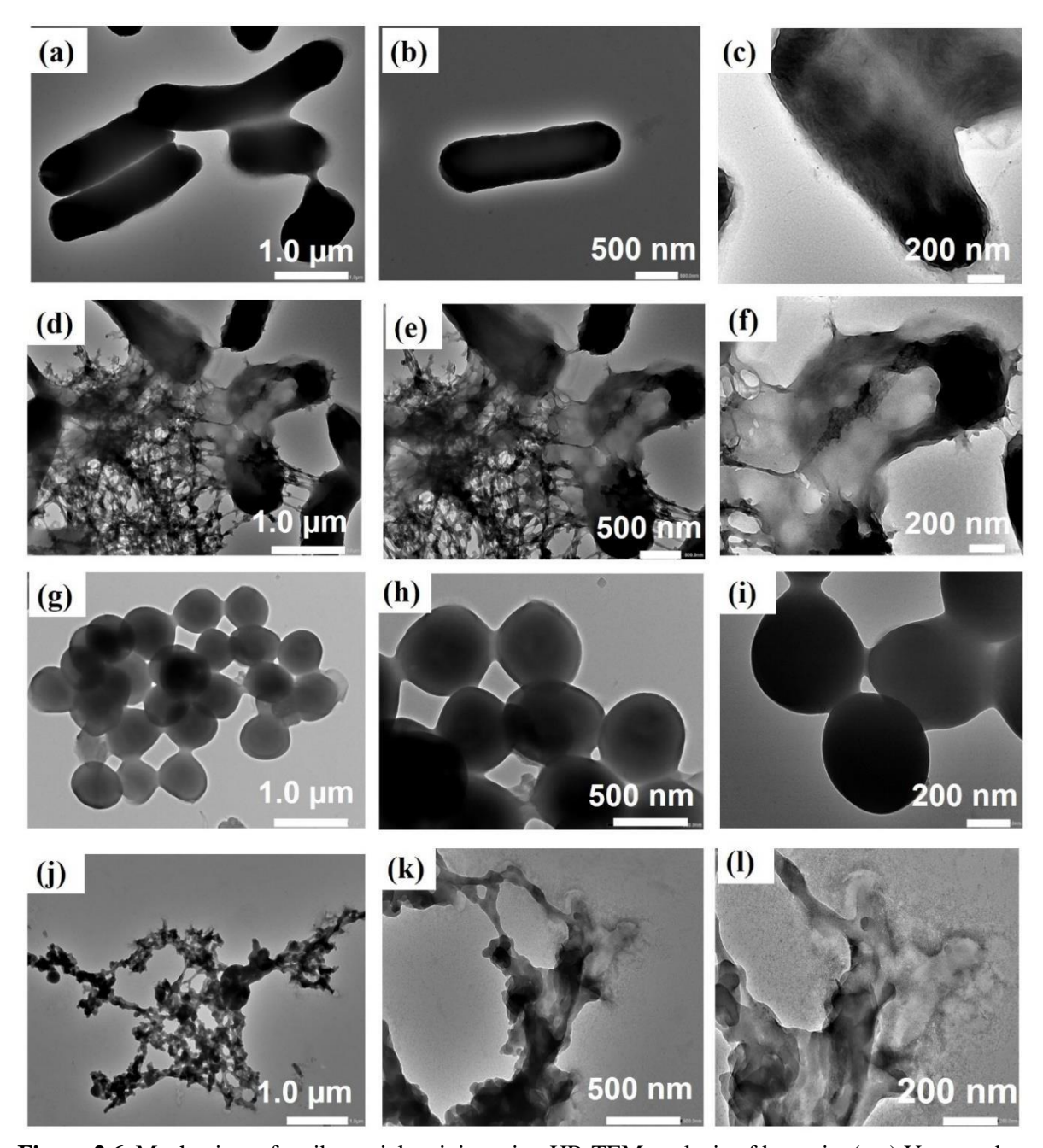


**Figure 2.6.** Mechanism of antibacterial activity using HR-TEM analysis of bacteria. (a-c) Untreated *E. coli* (control); (d-f) *E. coli* treated with GL Hyd hydrogels; (g-i) Untreated *S. aureus* (control); and (i-k) *S. aureus* treated with GL Hyd hydrogels. Scale bar: (a, d, g, j) 1 μm. (b, e, h, k) 500 nm and (c, f, i, l) 200 nm.

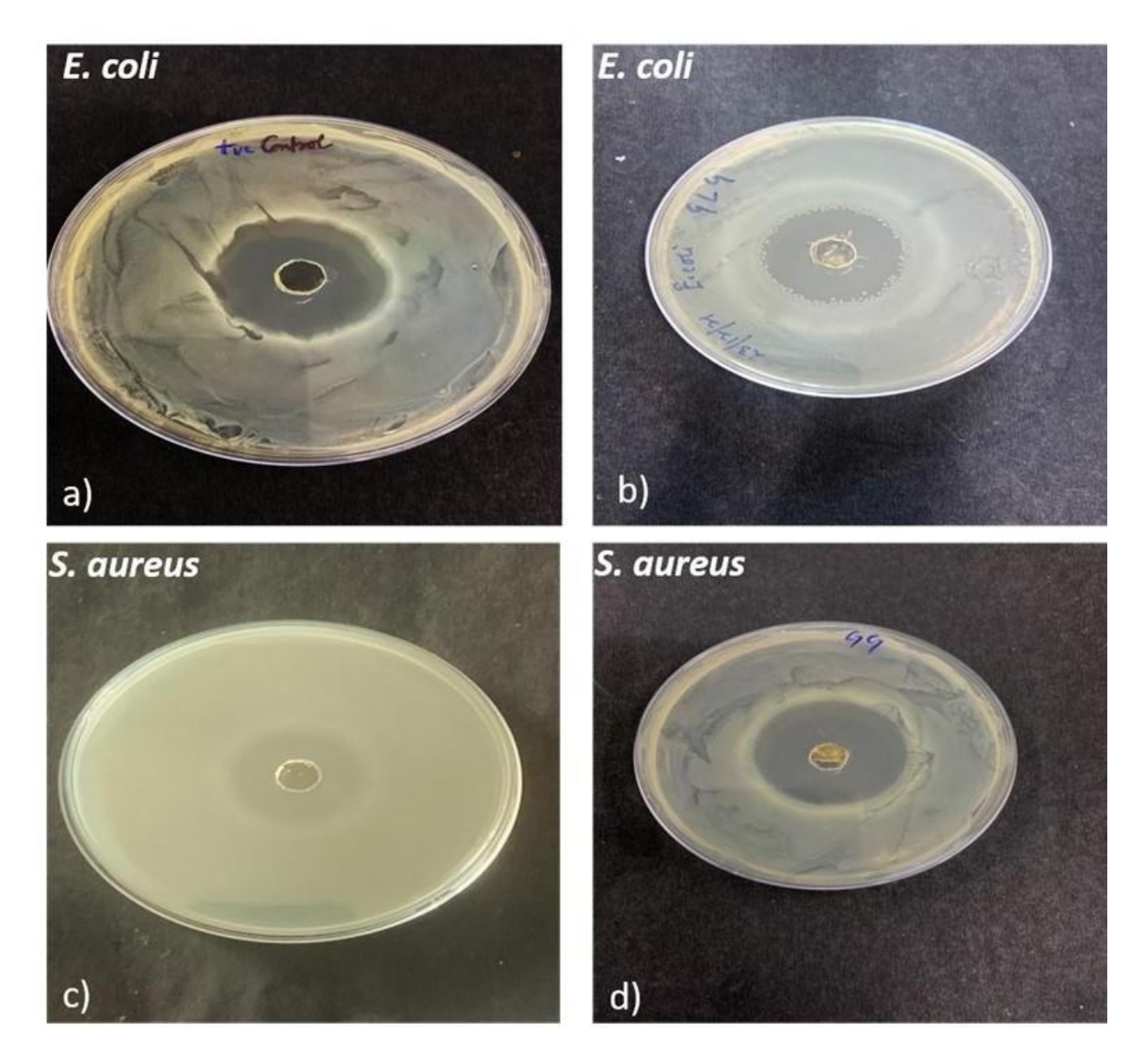


**Figure 2.7.** Zone of inhibition assay. (a) positive control, gentamicin; (b) GL Hyd hydrogels; (c) positive control, gentamicin; and (d) GL Hyd hydrogels.

## 2.4.8. Antibiofilm study

Bacteria within biofilms exhibit increased resistance to antibiotics and other antimicrobial treatments, often leading to chronic infections. The majority of current methods for treating biofilms focus on disrupting the biofilm structure and enhancing the efficacy of antimicrobial agents. There is a need to develop new treatment strategies to eliminate biofilms without causing resistance. Herein, we have studied the antibiofilm abilities of QC-OA Hyd and GL Hyd (**Figure 2.8a, b**). More disruption was seen in GL Hyd-treated biofilms indicating that the presence of GNP enhances antibiofilm activity- 80.33% antibiofilm activity and 75% inhibition of biofilm formation. The results were better than nanosilver-loaded gelatin hydrogel where antibiofilm activity was 55%<sup>55</sup>.

Additionally, we also performed SYTO9 and PI live/dead staining of biofilms to validate the hydrogels antibiofilm properties (**Figure 2.8c**). The higher antibiofilm activity of GL Hyd is because of the presence of gallium, which mimics iron causing iron shortage and its activity as a dispersal agent for mature *S. aureus* biofilms.

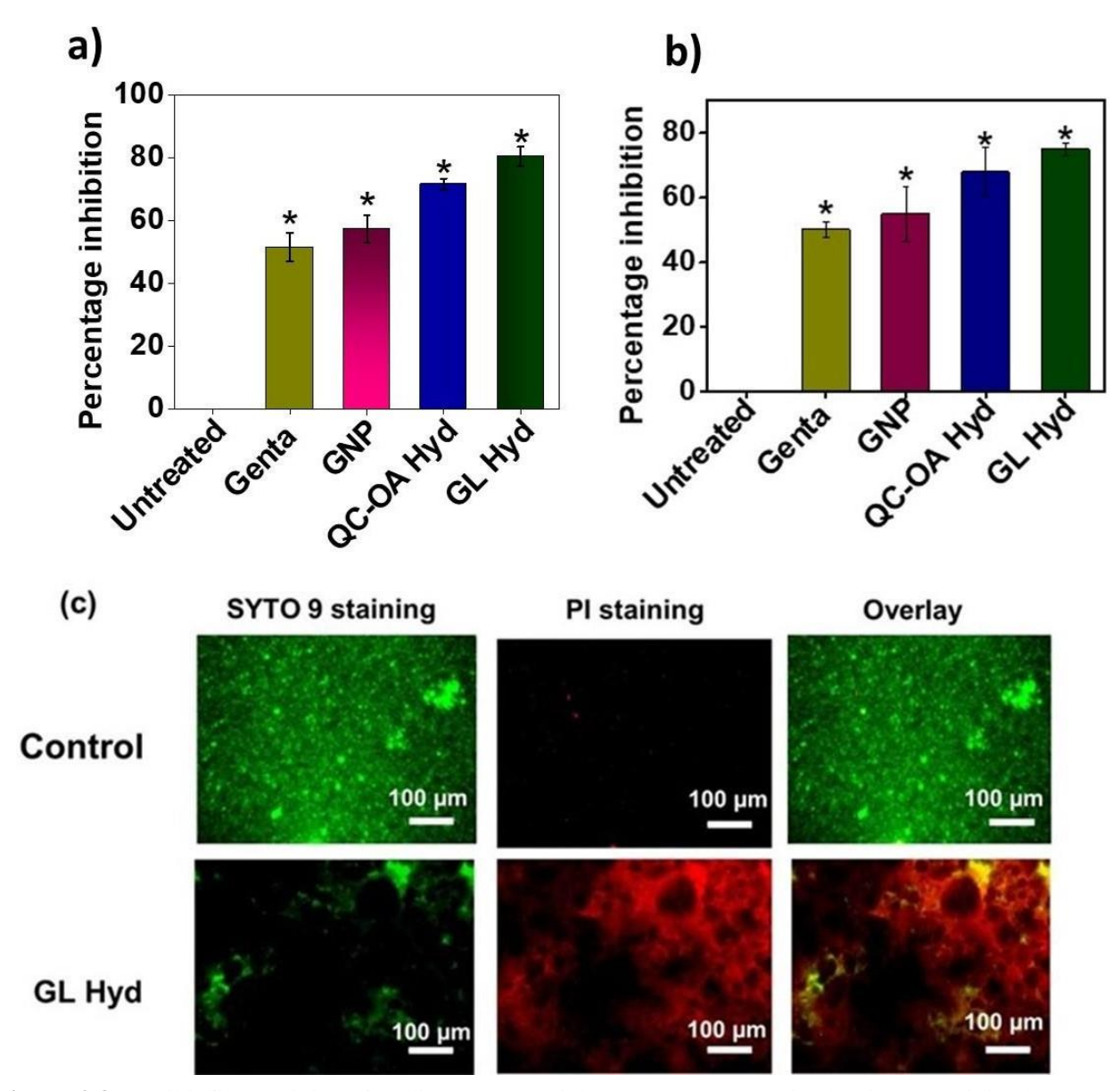


**Figure 2.8.** Antibiofilm activity of gallium nanoparticles (GNPs), quaternized chitosan-oxidized alginate hydrogels (QC-OA), and NP-loaded hydrogels (GL Hyd). (a) Disruptive effect on established biofilm; and (b) Inhibition of biofilm formation. Untreated samples were taken as negative control, and gentamicin (50  $\mu$ g) was taken as a positive control. (c) Live/dead images of untreated and GL Hyd treated biofilm. Scale bar: 100  $\mu$ m. \*p < 0.05 corresponds to statistically significance difference, and n.s. corresponds to non-significant data (n = 3).

#### 2.4.9. In vitro thrombus formation

The thrombogenicity of QC-OA and nanoparticle-loaded hydrogels was assessed to evaluate their

potential to induce thrombus formation. Thrombus formation, suggestive of fibrin clot development, is essential for hemostasis. When citrated blood was added to hydrogels, thrombus formation was initiated. The results demonstrated that gallium-loaded hydrogels exhibited greater thrombus formation on their surface compared to QC-OA hydrogels (**Figure 2.9a**). The results further emphasized that the thrombogenicity percentage increases with longer incubation times. The enhanced thrombus formation observed in GL Hyd is attributed to the presence of gallium ions, which immediately impact the early phases of hemostasis, thereby increasing thrombogenicity<sup>56</sup>. Studies have shown that an aqueous solution of gallium nitrate effectively treats wounds by enhancing the early activation of the clotting pathway<sup>57</sup>. These results were similar to previous studies where gallium nitrate was used as a hemostatic agent<sup>58</sup> and thrombus formation activity of hemostatic graphene and chitosan nanocomposite developed for wound healing applications<sup>59</sup>.

#### 2.4.10. Whole blood clotting time

The whole blood clotting test, which measures the hemoglobin absorbance in uncoagulated blood, was used to further quantify the hemostatic potentials of QC-OA and GL hydrogels (**Figure 2.9b**). More reduced hemoglobin absorbance was found in GL Hyd, which suggests that the material was able to trap more red blood cells, which in turn causes more clots to develop. The reason might be the presence of gallium ions, which is the source of accelerated clot formation since they cause fibrinogen to polymerize into strong fibrin clots, which starts the blood coagulation process. The findings are similar to observations reported by Pourshahrestani *et al.*<sup>34</sup>.

## 2.4.11. Platelet adhesion assay

Platelet adhesion is a crucial indicator of thrombosis. SEM analysis was used to investigate the platelet adhesion potential of materials (**Figure 2.9c**). SEM analysis showed that GL Hyd had a high level of platelet adherence. The electrostatic interaction between the negative charge of platelet and the positive charge of quaternized chitosan in hydrogel might be the possible reason behind the enhanced platelet adhesion. The outcomes are comparable to the outstanding hemostatic hydrogel<sup>60</sup> and mesoporous bioactive glass inspired by mussels that were previously described for hemorrhage management<sup>61</sup>.

## 2.4.12. Hemolysis assay

One of the most important characteristics of hydrogels that can be employed as wound dressings is hemocompatibility. It is imperative that hydrogels have good blood compatibility and do not adversely affect any biological function. The hemolysis assay was used to determine the blood compatibility (**Figure 2.9d, e, f**). The QC-OA and GL Hyd were treated with blood and a UV-Vis spectrometer was used to estimate the hemoglobin release from ruptured RBCs<sup>62</sup>. Triton X (1%) was taken as a positive control and PBS was taken as a negative control. Less than <5% hemolysis was observed indicating good hemocompatibility of nanoparticles-loaded hydrogel<sup>63</sup>.

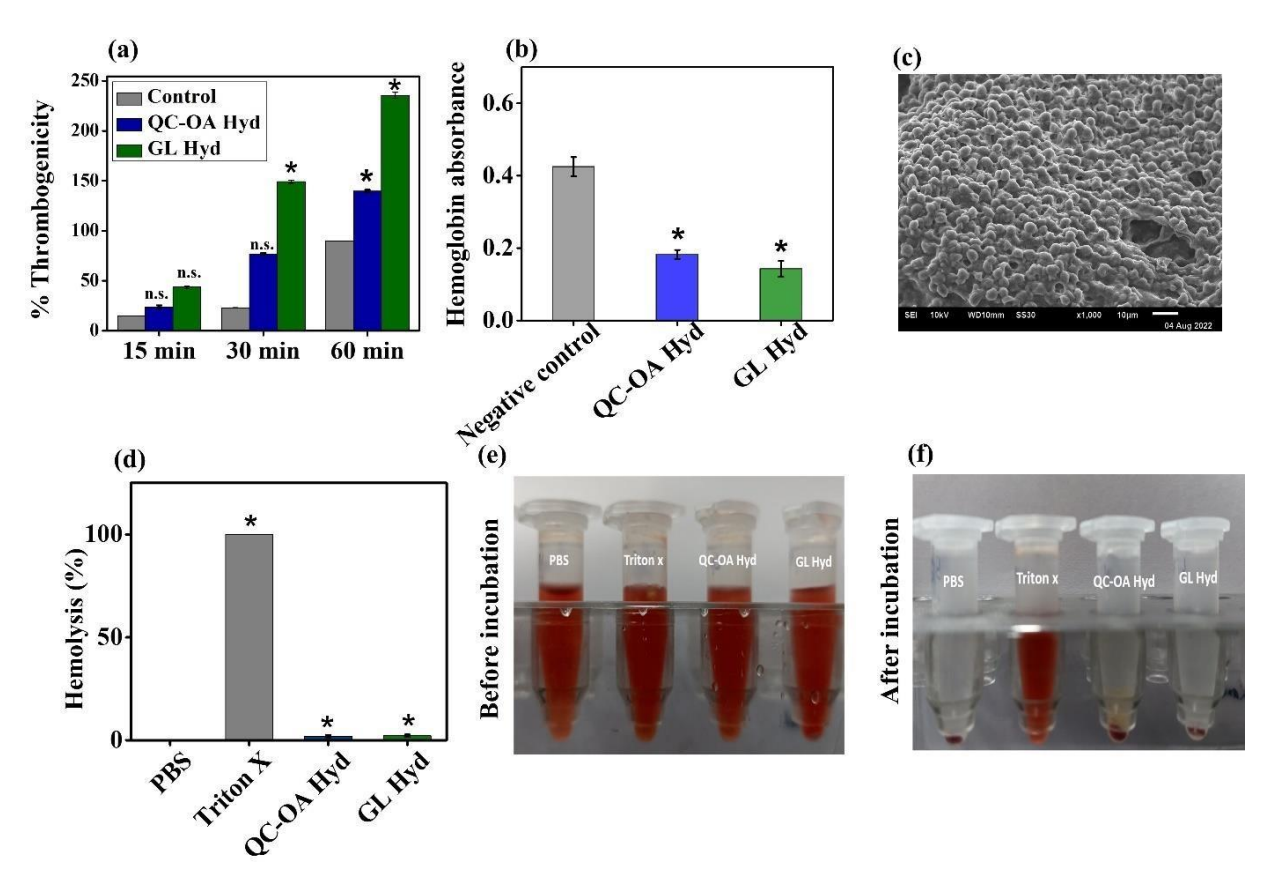


**Figure 2.9.** Hemostatic potential and blood compatibility of quaternized chitosan-oxidized alginate (QC-OA) and gallium NP-loaded (GL Hyd) hydrogels. (a) *In vitro* thrombus formation at different time intervals after treatment with GL Hyd; (b) Whole blood clotting after treatment with QC-OA and GL Hyd hydrogels; (c) *In vitro* platelet adhesion assay; and (d-f) Percentage hemolysis assay. Scale bar:  $10 \ \mu m$ . \*p < 0.05 corresponds to statistical significance and n.s. to non-significant data (n = 3).

#### 2.4.13. Cell viability assay

For biological applications, biomaterials must be compatible with cells. Since fibroblasts are crucial for healing tissue defects, the cytocompatibility of hydrogels was evaluated by testing their impact on L929 cell viability (**Figure 2.10b**). After incubating L929 cells with QC-OA and GL Hyd for 24 h, more than 95% cell viability was observed. Additionally, the cytocompatibility of gallium nanoparticles (NPs) was assessed and found to be 85.49%. Live/dead staining of L929 cells also revealed predominantly green emission, indicating the presence of live cells (**Figure 2.10a**). Moreover, cells treated with hydrogels maintained their typical morphology. These results underscore the cytocompatibility of hydrogels.

#### 2.4.14. In vitro scratch assay

Fibroblasts are needed for wound healing, as they migrate to injury site and produce collagen, which

is closely linked to ECM's remodeling. An *in vitro* scratch assay was used to examine the migration and proliferation of cells<sup>64</sup> (**Figure 2.10c, d**). Almost 100% confluent cells were cultured in GL Hyd-treated medium and monitored at various intervals. When GL Hyd-treated scratch was compared to control, discernible healing occurred after 12 h. About 100% wound closure was seen within 24 h. Using ImageJ, the percentage of healing was calculated. The reason might be presence of quaternized chitosan in hydrogel, which might cause an increased proliferation as it is proven to promote collagen deposition and fibroblast proliferation.<sup>65</sup>

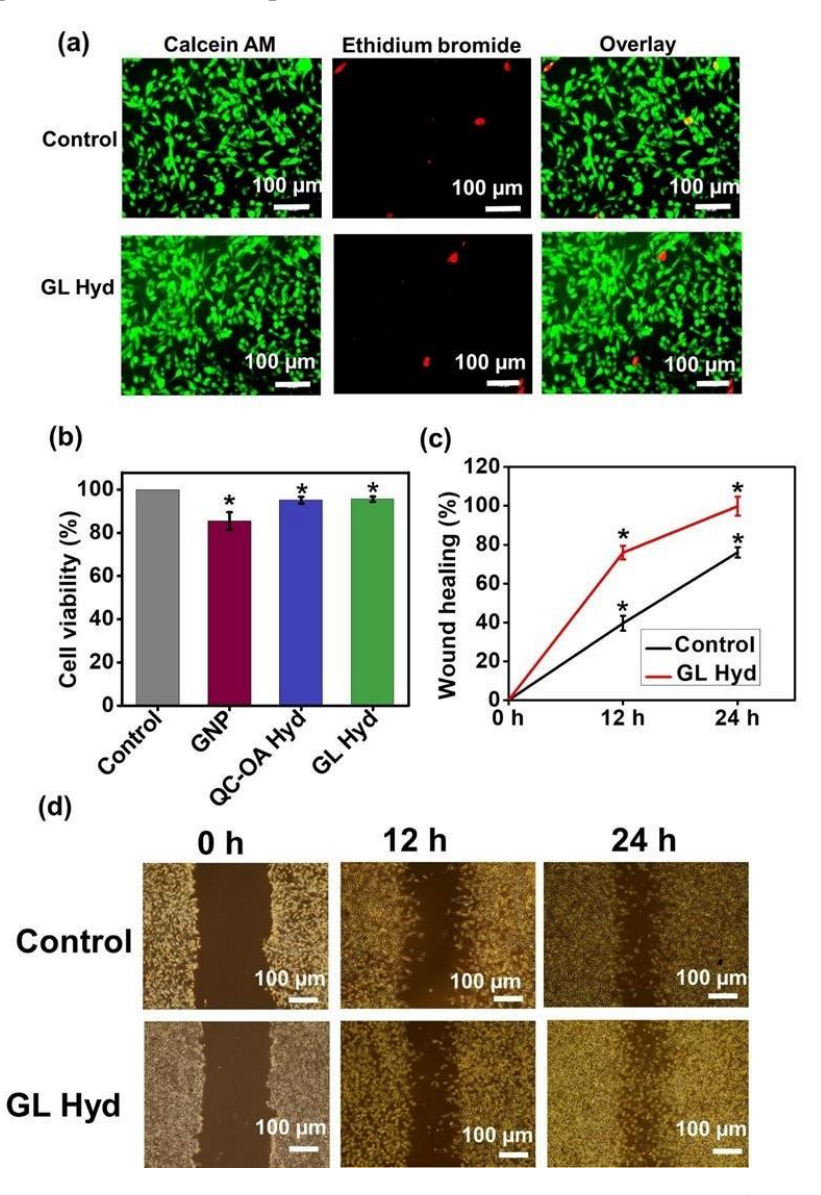


**Figure 2.10.** *In vitro* cytotoxicity and wound healing of GL Hyd using mouse fibroblast cells (L929). (a, b) Images of live/dead stained cells and percentage cell viability; and (c, d) Percentage wound healing and scratch assay at 0, 12, and 24 h. Scale bar:  $100 \, \mu m$ . \*p <  $0.05 \, corresponds$  to statistically significant difference (n = 3).

#### 2.5. Conclusions

In conclusion, our goal was to explore the potential of biomaterials as an antibiotic-free strategy for treating bacteria-infected wounds, addressing challenges, such as blood loss, oxidative stress, biofilm formation, and their impact on wound healing. To achieve these objectives, we have developed gallium oxide nanoparticle-loaded imine cross-linked quaternized chitosan and oxidized sodium alginate hydrogels (GL Hyd) by utilizing the multitargeted approach integrating nanotechnology and smart hydrogel system. The GL Hyd was investigated for its viscoelastic characteristics, antioxidant, antibacterial, antibiofilm, hemostatic, and wound healing abilities. The imine cross-linking imparted excellent viscoelasticity and self-healing properties to hydrogel, enhancing its applicability in wound care. The GL Hyd also exhibited potent broad-spectrum antibacterial activity against both S. aureus and E. coli due to the combined intrinsic antibacterial effects of quaternized chitosan (QC) and gallium nanoparticles (GNP) underscoring the efficacy of this approach in combating bacterial infections. Furthermore, the nanoparticle-hydrogel system demonstrated a robust capability to inhibit biofilm formation and disrupt established biofilms. Its ability to scavenge reactive oxygen species, coupled with excellent thrombus formation, platelet adhesion properties, and cell proliferation abilities positions this system as a promising treatment option for chronic bacterial-infected wounds. Overall, the outcomes of this research underscore the potential of this study to revolutionize wound care practices, offering new avenues for managing bacterial infections while promoting accelerated and effective wound healing.

#### 2.6. Author Contributions

D.N. designed the study, did the experimental work, analyzed the data, and prepared the manuscript draft. Y.S. managed the funding, mentored the work, and edited the manuscript.

#### References

- (1) Hoque, J.; Haldar, J. Direct Synthesis of Dextran-Based Antibacterial Hydrogels for Extended Release of Biocides and Eradication of Topical Biofilms. *ACS Appl. Mater. Interfaces* **2017**, *9* (19), 15975–15985.
- (2) Wang, J.; Chen, X.-Y.; Zhao, Y.; Yang, Y.; Wang, W.; Wu, C.; Yang, B.; Zhang, Z.; Zhang, L.; Liu, Y.; Du, X.; Li, W.; Qiu, L.; Jiang, P.; Mou, X.-Z.; Li, Y.-Q. pH-Switchable Antimicrobial Nanofiber Networks of Hydrogel Eradicate Biofilm and Rescue Stalled Healing in Chronic Wounds. *ACS Nano* **2019**, *13* (10), 11686–11697.
- (3) Zhou, J.; Yao, D.; Qian, Z.; Hou, S.; Li, L.; Jenkins, A. T. A.; Fan, Y. Bacteria-Responsive Intelligent Wound Dressing: Simultaneous In Situ Detection and Inhibition of Bacterial Infection for Accelerated Wound Healing. *Biomaterials* **2018**, *161*, 11–23.
- (4) Parani, M.; Lokhande, G.; Singh, A.; Gaharwar, A. K. Engineered Nanomaterials for Infection Control and Healing Acute and Chronic Wounds. *ACS Appl. Mater. Interfaces* **2016**, 8 (16), 10049–10069.
- (5) Xie, Y.; Gan, C.; Li, Z.; Liu, W.; Yang, D.; Qiu, X. Fabrication of a Lignin-Copper Sulfide-Incorporated PVA Hydrogel with Near-Infrared-Activated Photothermal/Photodynamic/Peroxidase-like Performance for Combating Bacteria and Biofilms. *ACS Biomater. Sci. Eng.* **2022**, 8 (2), 560–569.
- (6) Pourshahrestani, S.; Zeimaran, E.; Djordjevic, I.; Kadri, N. A.; Towler, M. R. Inorganic Hemostats: The State-of-the-Art and Recent Advances. *Materials Science and Engineering: C* **2016.** *58*, 1255–1268.
- (7) Li, C.; Cornel, E. J.; Du, J. Advances and Prospects of Polymeric Particles for the Treatment of Bacterial Biofilms. *ACS Appl. Polym. Mater.* **2021**, *3* (5), 2218–2232.
- (8) Gholipour Choubar, E.; Nasirtabrizi, M. H.; Salimi, F.; Sadeghianmaryan, A. Improving Bone Regeneration with Electrospun Antibacterial Polycaprolactone/Collagen/Polyvinyl Pyrrolidone Scaffolds Coated with Hydroxyapatite and Cephalexin Delivery Capability. *Journal of Biomaterials Science, Polymer Edition* **2024**, *35* (2), 127–145.
- (9) Cesur, S. Combination Techniques towards Novel Drug Delivery Systems Manufacturing: 3D PCL Scaffolds Enriched with Tetracycline-Loaded PVP Nanoparticles. *European Journal of Pharmaceutics and Biopharmaceutics* **2024**, *194*, 36–48.
- (10) Hu, J.; Yang, L.; Cheng, X.; Li, Y.; Cheng, Y. Aminoglycoside-Based Biomaterials: From Material Design to Antibacterial and Gene Delivery Applications. *Advanced Functional Materials* **2021**, *31* (36), 2103718.
- (11) Li, J.; Mooney, D. J. Designing Hydrogels for Controlled Drug Delivery. *Nat Rev Mater* **2016**, *1* (12), 16071.
- (12) Jing, Y.; Ruan, L.; Jiang, G.; Nie, L.; Shavandi, A.; Sun, Y.; Xu, J.; Shao, X.; Zhu, J. Regenerated Silk Fibroin and Alginate Composite Hydrogel Dressings Loaded with Curcumin Nanoparticles for Bacterial-Infected Wound Closure. *Biomaterials Advances* **2023**, *149*, 213405.
- (13) Liang, Y.; Li, Z.; Huang, Y.; Yu, R.; Guo, B. Dual-Dynamic-Bond Cross-Linked Antibacterial Adhesive Hydrogel Sealants with On-Demand Removability for Post-Wound-Closure and Infected Wound Healing. *ACS Nano* **2021**, *15* (4), 7078–7093.
- (14) Feng, Y.; Chen, Q.; Yin, Q.; Pan, G.; Tu, Z.; Liu, L. Reduced Graphene Oxide Functionalized with Gold Nanostar Nanocomposites for Synergistically Killing Bacteria through Intrinsic Antimicrobial Activity and Photothermal Ablation. *ACS Appl. Bio Mater.* **2019**, *2* (2), 747–756.
- (15) Liu, Y.; Dong, T.; Chen, Y.; Sun, N.; Liu, Q.; Huang, Z.; Yang, Y.; Cheng, H.; Yue, K. Biodegradable and Cytocompatible Hydrogel Coating with Antibacterial Activity for the Prevention of Implant-Associated Infection. *ACS Appl. Mater. Interfaces* **2023**, *15* (9), 11507–11519.
- (16) Li, M.; Zhang, Z.; Liang, Y.; He, J.; Guo, B. Multifunctional Tissue-Adhesive Cryogel Wound Dressing for Rapid Nonpressing Surface Hemorrhage and Wound Repair. *ACS Appl. Mater. Interfaces* **2020**, *12* (32), 35856–35872.
- (17) Tao, B.; Lin, C.; Deng, Y.; Yuan, Z.; Shen, X.; Chen, M.; He, Y.; Peng, Z.; Hu, Y.; Cai, K. Copper-Nanoparticle-Embedded Hydrogel for Killing Bacteria and Promoting Wound Healing with

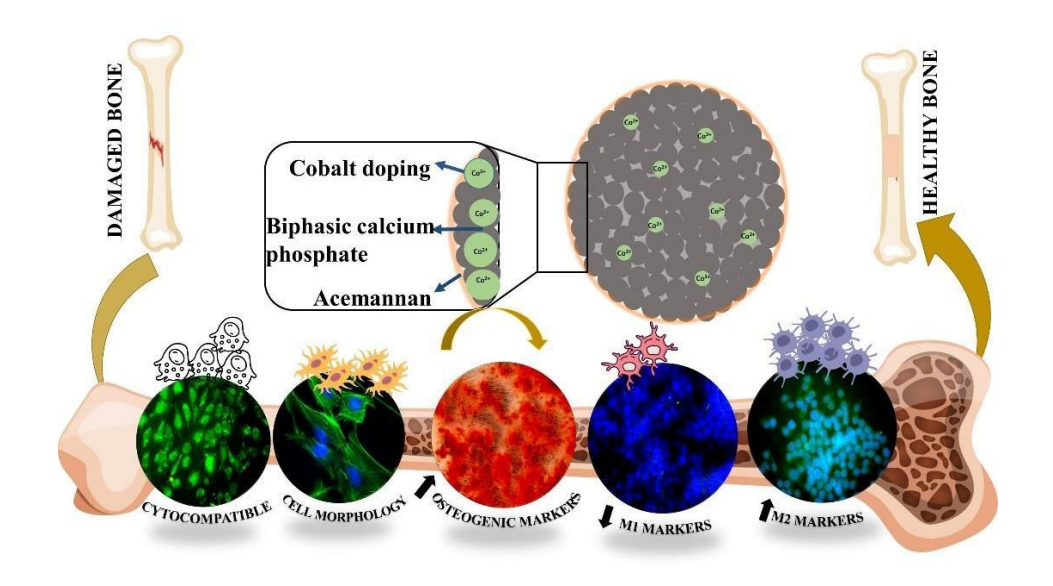
- Photothermal Therapy. J. Mater. Chem. B 2019, 7 (15), 2534–2548.
- (18) Alvarez, G. S.; Hélary, C.; Mebert, A. M.; Wang, X.; Coradin, T.; Desimone, M. F. Antibiotic-Loaded Silica Nanoparticle–Collagen Composite Hydrogels with Prolonged Antimicrobial Activity for Wound Infection Prevention. *J. Mater. Chem. B* **2014**, *2* (29), 4660.
- (19) Liu, J.; Chen, Z.; Wang, J.; Li, R.; Li, T.; Chang, M.; Yan, F.; Wang, Y. Encapsulation of Curcumin Nanoparticles with MMP9-Responsive and Thermos-Sensitive Hydrogel Improves Diabetic Wound Healing. *ACS Appl. Mater. Interfaces* **2018**, *10* (19), 16315–16326.
- (20) Augustine, R.; Zahid, A. A.; Hasan, A.; Dalvi, Y. B.; Jacob, J. Cerium Oxide Nanoparticle-Loaded Gelatin Methacryloyl Hydrogel Wound-Healing Patch with Free Radical Scavenging Activity. *ACS Biomater. Sci. Eng.* **2021**, *7* (1), 279–290.
- (21) Cochis, A.; Azzimonti, B.; Chiesa, R.; Rimondini, L.; Gasik, M. Metallurgical Gallium Additions to Titanium Alloys Demonstrate a Strong Time-Increasing Antibacterial Activity without Any Cellular Toxicity. *ACS Biomater. Sci. Eng.* **2019**, *5* (6), 2815–2820.
- (22) Chen, T.; Chen, Y.; Rehman, H. U.; Chen, Z.; Yang, Z.; Wang, M.; Li, H.; Liu, H. Ultratough, Self-Healing, and Tissue-Adhesive Hydrogel for Wound Dressing. *ACS Appl. Mater. Interfaces* **2018**, *10* (39), 33523–33531.
- (23) Dutta, J.; Priyanka. A Facile Approach for the Determination of Degree of Deacetylation of Chitosan Using Acid-Base Titration. *Heliyon* **2022**, 8 (7), e09924.
- (24) Cho, J.; Grant, J.; Piquette-Miller, M.; Allen, C. Synthesis and Physicochemical and Dynamic Mechanical Properties of a Water-Soluble Chitosan Derivative as a Biomaterial. *Biomacromolecules* **2006**, *7* (10), 2845–2855.
- (25) Chen, H.; Xing, X.; Tan, H.; Jia, Y.; Zhou, T.; Chen, Y.; Ling, Z.; Hu, X. Covalently Antibacterial Alginate-Chitosan Hydrogel Dressing Integrated Gelatin Microspheres Containing Tetracycline Hydrochloride for Wound Healing. *Materials Science and Engineering: C* **2017**, *70*, 287–295.
- (26) Emami, Z.; Ehsani, M.; Zandi, M.; Foudazi, R. Controlling Alginate Oxidation Conditions for Making Alginate-Gelatin Hydrogels. *Carbohydrate Polymers* **2018**, *198*, 509–517.
- (27) Ganguly, B. N.; Verma, V.; Chatterjee, D.; Satpati, B.; Debnath, S.; Saha, P. Study of Gallium Oxide Nanoparticles Conjugated with β-Cyclodextrin: An Application To Combat Cancer. *ACS Appl. Mater. Interfaces* **2016**, 8 (27), 17127–17137.
- (28) Liu, X.; Qiu, G.; Zhao, Y.; Zhang, N.; Yi, R. Gallium Oxide Nanorods by the Conversion of Gallium Oxide Hydroxide Nanorods. *Journal of Alloys and Compounds* **2007**, *439* (1–2), 275–278.
- (29) Balakrishnan, B.; Jayakrishnan, A. Self-Cross-Linking Biopolymers as Injectable in Situ Forming Biodegradable Scaffolds. *Biomaterials* **2005**, *26* (18), 3941–3951.
- (30) Lei, K.; Li, Z.; Zhu, D.; Sun, C.; Sun, Y.; Yang, C.; Zheng, Z.; Wang, X. Polysaccharide-Based Recoverable Double-Network Hydrogel with High Strength and Self-Healing Properties. *J. Mater. Chem. B* **2020**, *8* (4), 794–802.
- (31) McBath, R. A.; Shipp, D. A. Swelling and Degradation of Hydrogels Synthesized with Degradable Poly(β-Amino Ester) Crosslinkers. *Polym. Chem.* **2010**, *1* (6), 860.
- (32) Zheng, L.; Zhao, M.; Xiao, C.; Zhao, Q.; Su, G. Practical Problems When Using ABTS Assay to Assess the Radical-Scavenging Activity of Peptides: Importance of Controlling Reaction pH and Time. *Food Chemistry* **2016**, *192*, 288–294.
- (33) Xu, Z.; Chen, X.; Tan, R.; She, Z.; Chen, Z.; Xia, Z. Preparation and Characterization of a Gallium-Loaded Antimicrobial Artificial Dermal Scaffold. *Materials Science and Engineering: C* **2019**, *105*, 110063.
- (34) Pourshahrestani, S.; Zeimaran, E.; Kadri, N. A.; Gargiulo, N.; Jindal, H. M.; Naveen, S. V.; Sekaran, S. D.; Kamarul, T.; Towler, M. R. Potency and Cytotoxicity of a Novel Gallium-Containing Mesoporous Bioactive Glass/Chitosan Composite Scaffold as Hemostatic Agents. *ACS Appl. Mater. Interfaces* **2017**, *9* (37), 31381–31392.
- (35) Roy, A.; Dadhich, P.; Dhara, S.; De, S. In Vitro Cytocompatibility and Blood Compatibility of Polysulfone Blend, Surface-Modified Polysulfone and Polyacrylonitrile Membranes for Hemodialysis. *RSC Adv.* **2015**, *5* (10), 7023–7034.

- (36) Yin, M.; Wan, S.; Ren, X.; Chu, C.-C. Development of Inherently Antibacterial, Biodegradable, and Biologically Active Chitosan/Pseudo-Protein Hybrid Hydrogels as Biofunctional Wound Dressings. *ACS Appl. Mater. Interfaces* **2021**, *13* (12), 14688–14699.
- (37) Li, X.; Cai, Z.; Ahn, D. U.; Huang, X. Development of an Antibacterial Nanobiomaterial for Wound-Care Based on the Absorption of AgNPs on the Eggshell Membrane. *Colloids and Surfaces B: Biointerfaces* **2019**, *183*, 110449.
- (38) Lee, D.; Cohen, R. E.; Rubner, M. F. Antibacterial Properties of Ag Nanoparticle Loaded Multilayers and Formation of Magnetically Directed Antibacterial Microparticles. *Langmuir* **2005**, *21* (21), 9651–9659.
- (39) Ming, Z.; Han, L.; Bao, M.; Zhu, H.; Qiang, S.; Xue, S.; Liu, W. Living Bacterial Hydrogels for Accelerated Infected Wound Healing. *Advanced Science* **2021**, *8* (24), 2102545.
- (40) Feng, Q. L.; Wu, J.; Chen, G. Q.; Cui, F. Z.; Kim, T. N.; Kim, J. O. A Mechanistic Study of the Antibacterial Effect of Silver Ions on Escherichia Coli and Staphylococcus Aureus. *J. Biomed. Mater. Res.* **2000**, *52* (4), 662–668.
- (41) Zhang, P.; Li, S.; Chen, H.; Wang, X.; Liu, L.; Lv, F.; Wang, S. Biofilm Inhibition and Elimination Regulated by Cationic Conjugated Polymers. *ACS Appl. Mater. Interfaces* **2017**, *9* (20), 16933–16938.
- (42) Wu, M.; Chen, J.; Huang, W.; Yan, B.; Peng, Q.; Liu, J.; Chen, L.; Zeng, H. Injectable and Self-Healing Nanocomposite Hydrogels with Ultrasensitive pH-Responsiveness and Tunable Mechanical Properties: Implications for Controlled Drug Delivery. *Biomacromolecules* **2020**, *21* (6), 2409–2420.
- (43) Khorasani, M. T.; Joorabloo, A.; Adeli, H.; Milan, P. B.; Amoupour, M. Enhanced Antimicrobial and Full-Thickness Wound Healing Efficiency of Hydrogels Loaded with Heparinized ZnO Nanoparticles: In Vitro and in Vivo Evaluation. *International Journal of Biological Macromolecules* **2021**, *166*, 200–212.
- (44) Zhao, X.; Li, P.; Guo, B.; Ma, P. X. Antibacterial and Conductive Injectable Hydrogels Based on Quaternized Chitosan-Graft-Polyaniline/Oxidized Dextran for Tissue Engineering. *Acta Biomaterialia* **2015**, *26*, 236–248.
- (45) Gonil, P.; Sajomsang, W.; Ruktanonchai, U. R.; Pimpha, N.; Sramala, I.; Nuchuchua, O.; Saesoo, S.; Chaleawlert-umpon, S.; Puttipipatkhachorn, S. Novel Quaternized Chitosan Containing β-Cyclodextrin Moiety: Synthesis, Characterization and Antimicrobial Activity. *Carbohydrate Polymers* **2011**, 83 (2), 905–913.
- (46) Hoque, J.; Adhikary, U.; Yadav, V.; Samaddar, S.; Konai, M. M.; Prakash, R. G.; Paramanandham, K.; Shome, B. R.; Sanyal, K.; Haldar, J. Chitosan Derivatives Active against Multidrug-Resistant Bacteria and Pathogenic Fungi: *In Vivo* Evaluation as Topical Antimicrobials. *Mol. Pharmaceutics* **2016**, *13* (10), 3578–3589.
- (47) Liang, L.; Liu, T.; Ouyang, Q.; Li, S.; Li, C. Solid Phase Synthesis of Oxidized Sodium Alginate-Tobramycin Conjugate and Its Application for Infected Wound Healing. *Carbohydrate Polymers* **2022**, 295, 119843.
- (48) Ding, W.; Zhou, J.; Zeng, Y.; Wang, Y.; Shi, B. Preparation of Oxidized Sodium Alginate with Different Molecular Weights and Its Application for Crosslinking Collagen Fiber. *Carbohydrate Polymers* **2017**, *157*, 1650–1656.
- (49) Yuan, Y.; Shen, S.; Fan, D. A Physicochemical Double Cross-Linked Multifunctional Hydrogel for Dynamic Burn Wound Healing: Shape Adaptability, Injectable Self-Healing Property and Enhanced Adhesion. *Biomaterials* **2021**, *276*, 120838.
- (50) Su, H.; Zheng, R.; Jiang, L.; Zeng, N.; Yu, K.; Zhi, Y.; Shan, S. Dextran Hydrogels via Disulfide-Containing Schiff Base Formation: Synthesis, Stimuli-Sensitive Degradation and Release Behaviors. *Carbohydrate Polymers* **2021**, *265*, 118085.
- (51) Li, L.; Yan, B.; Yang, J.; Chen, L.; Zeng, H. Novel Mussel-Inspired Injectable Self-Healing Hydrogel with Anti-Biofouling Property. *Adv. Mater.* **2015**, *27* (7), 1294–1299.
- (52) Yang, L.; Zeng, Y.; Wu, H.; Zhou, C.; Tao, L. An Antioxidant Self-Healing Hydrogel for 3D Cell Cultures. *J. Mater. Chem. B* **2020**, *8* (7), 1383–1388.
- (53) Xu, J.; Xu, J. J.; Lin, Q.; Jiang, L.; Zhang, D.; Li, Z.; Ma, B.; Zhang, C.; Li, L.; Kai, D.;

- Yu, H.-D.; Loh, X. J. Lignin-Incorporated Nanogel Serving As an Antioxidant Biomaterial for Wound Healing. *ACS Appl. Bio Mater.* **2021**, *4* (1), 3–13.
- (54) Ali, I. H.; Ouf, A.; Elshishiny, F.; Taskin, M. B.; Song, J.; Dong, M.; Chen, M.; Siam, R.; Mamdouh, W. Antimicrobial and Wound-Healing Activities of Graphene-Reinforced Electrospun Chitosan/Gelatin Nanofibrous Nanocomposite Scaffolds. *ACS Omega* **2022**, *7* (2), 1838–1850.
- (55) Suleman Ismail Abdalla, S.; Katas, H.; Chan, J. Y.; Ganasan, P.; Azmi, F.; Fauzi, M. B. Gelatin Hydrogels Loaded with Lactoferrin-Functionalized Bio-Nanosilver as a Potential Antibacterial and Anti-Biofilm Dressing for Infected Wounds: Synthesis, Characterization, and Deciphering of Cytotoxicity. *Mol. Pharmaceutics* **2021**, *18* (5), 1956–1969.
- (56) Pourshahrestani, S.; Zeimaran, E.; Adib Kadri, N.; Gargiulo, N.; Samuel, S.; Naveen, S. V.; Kamarul, T.; Towler, M. R. Gallium-Containing Mesoporous Bioactive Glass with Potent Hemostatic Activity and Antibacterial Efficacy. *J. Mater. Chem. B* **2016**, *4* (1), 71–86.
- (57) Keast, D. H.; Janmohammad, A. The Hemostatic and Wound Healing Effect of Chitosan Following Debridement of Chronic Ulcers. *Wounds* **2021**, *33* (10), 263–270.
- (58) Goodley, P. H.; Rogosnitzky, M. The Effect of Gallium Nitrate on Arresting Blood Flow from a Wound. *Case Reports in Medicine* **2011**, 2011, 1–3.
- (59) Choudhary, P.; Ramalingam, B.; Das, S. K. Fabrication of Chitosan-Reinforced Multifunctional Graphene Nanocomposite as Antibacterial Scaffolds for Hemorrhage Control and Wound-Healing Application. *ACS Biomater. Sci. Eng.* **2020**, *6* (10), 5911–5929.
- (60) Suneetha, M.; Rao, K. M.; Han, S. S. Mussel-Inspired Cell/Tissue-Adhesive, Hemostatic Hydrogels for Tissue Engineering Applications. *ACS Omega* **2019**, *4* (7), 12647–12656.
- (61) Gu, B. K.; Park, S. J.; Kim, M. S.; Kang, C. M.; Kim, J.-I.; Kim, C.-H. Fabrication of Sonicated Chitosan Nanofiber Mat with Enlarged Porosity for Use as Hemostatic Materials. *Carbohydrate Polymers* **2013**, *97* (1), 65–73.
- (62) Zhao, X.; Zhang, H.; Gao, Y.; Lin, Y.; Hu, J. A Simple Injectable Moldable Hydrogel Assembled from Natural Glycyrrhizic Acid with Inherent Antibacterial Activity. *ACS Appl. Bio Mater.* **2020**, *3* (1), 648–653.
- (63) Muthiah Pillai, N. S.; Eswar, K.; Amirthalingam, S.; Mony, U.; Kerala Varma, P.; Jayakumar, R. Injectable Nano Whitlockite Incorporated Chitosan Hydrogel for Effective Hemostasis. *ACS Appl. Bio Mater.* **2019**, *2* (2), 865–873.
- (64) Zhu, J.; Jiang, G.; Song, G.; Liu, T.; Cao, C.; Yang, Y.; Zhang, Y.; Hong, W. Incorporation of ZnO/Bioactive Glass Nanoparticles into Alginate/Chitosan Composite Hydrogels for Wound Closure. *ACS Appl. Bio Mater.* **2019**, *2* (11), 5042–5052.
- (65) Xue, H.; Hu, L.; Xiong, Y.; Zhu, X.; Wei, C.; Cao, F.; Zhou, W.; Sun, Y.; Endo, Y.; Liu, M.; Liu, Y.; Liu, J.; Abududilibaier, A.; Chen, L.; Yan, C.; Mi, B.; Liu, G. Quaternized Chitosan-Matrigel-Polyacrylamide Hydrogels as Wound Dressing for Wound Repair and Regeneration. *Carbohydrate Polymers* **2019**, 226, 115302.

# CHAPTER – 3

Acemannan coated, cobalt-doped biphasic calcium phosphate nanoparticles for immunomodulation regulated bone regeneration



# 3.1. Introduction

### 3.1.1. Bone abnormalities

Bone is an intricate tissue with multiple physiological properties, such as safeguarding internal organs, offering mechanical strength for movement, providing support for soft tissues, and accommodating bone marrow, which is primarily because of its hierarchical structure composed of hydroxyapatite nanocrystals, collagen proteins, cells, and various other biomolecules<sup>1</sup>. The mechanical properties of bone are determined by its structure, extracellular matrix (ECM), and minerals. The ECM is primarily composed of type I collagen, which makes up 85–90% of total bone protein and provides structural support. Inorganic minerals like carbonated apatite and hydroxyapatite, account for about 65% of bone mass. Other ECM components, including noncollagenous proteins and polysaccharides, constitute a smaller portion. The main cell types in bone are osteoprogenitors, osteoclasts, osteoblasts, and osteocytes<sup>2</sup>. Osteoblasts are the primary cells responsible for bone formation and produce extracellular matrix proteins like collagen, alkaline phosphatase, osteopontin, and osteocalcin. Multiple osteoblasts collaborate to form a bone unit known as an osteon<sup>3</sup>. Osteoclasts are multinucleated cells primarily responsible for bone resorption. They originate from the hematopoietic lineage and mature into functional osteoclasts through the interaction of RANKL and macrophage colony-stimulating factor (M-CSF)<sup>4</sup>. Research has demonstrated that a balance of activity between the two primary cellular components of bone, osteoblasts and osteoclasts, is required for proper bone development<sup>5</sup>. The remarkable capacity of the human body to regenerate bone and return it to its pre-injury state underscores the critical role that bone plays in mammalian physiology. However, bone abnormalities caused by pathological diseases and traumatic injuries pose significant challenges to society. Successful bone healing faces limitations such as bone loss, insufficient mechanical stability, insufficient vascularization, and damaged soft tissue<sup>6</sup>.

#### 3.1.2. Challenges

About 6.2 million bone fracture cases are recorded in the United States alone each year, of which 5–10% end in non-union or delayed union<sup>7</sup>. In 2004, the annual medical costs due to musculoskeletal diseases amounted to \$849 billion. Autografts and allografts remain the most widely used treatments for appropriately managing bone abnormalities. Each year, more than 2.2

million bone graft procedures are performed globally, establishing it as one of the most prevalent tissue transplant surgeries<sup>8</sup>. The bone substitute market, valued at over \$2.3 billion in 2015, was projected to surpass \$3.6 billion between 2016 and 2022. However, the use of bone grafts is associated with limitations, such as restricted availability, inconsistent resorption, increased morbidity, chances of immunological rejection, and disease transmission<sup>9</sup>. Thus, alternative therapeutic approaches are required to address the unresolved issues with bone repair.

# 3.1.3. Research gap

Different types of biomaterials have been studied for bone regeneration applications, like metals, polymeric scaffolds, composite scaffolds, injectable biomaterials, silk-based materials, and porous bioceramics 10. Oiao et al., developed a GelMA and polypeptide-based hydrogel, that helped in cell adhesion, offered good biocompatibility, and increased gene expression associated with osteogenesis<sup>11</sup>. Shuai et al., fabricated a graphene oxide and hydroxyapatite nanocomposite-based scaffold with better modulus, compressive strength, cytocompatibility, and bioactivity for efficient bone regeneration<sup>12</sup>. Chen et al., developed chitosan hydrogel loaded with MgO nanoparticles, which showed increased in vitro calcium deposition and upregulation of osteogenic genes 10. Feng et al., fabricated scaffolds of β-tricalcium phosphate (β-TCP)/ polyether ether ketone (PEEK), and in just eight weeks, they were able to completely fuse new bone to the host to heal bone deformities<sup>13</sup>. Qiu et al., developed mesoporous hydroxyapatite nanoparticles to effectively release BMP-2, and these materials demonstrated an increase in the osteogenic abilities<sup>14</sup>. Zhang et al., developed porous AuPd alloy for bone regeneration by photothermal therapy. The results showed enhanced cell proliferation and bone regeneration<sup>15</sup>. Yang et al., developed cobalt-doped plasma electrolytic PEO coatings on titanium implants, which were tested for their ability to modulate immunity and showed increased expression and secretion of anti-inflammatory genes 16. Ignjatović et al., developed cobalt-substituted hydroxyapatite nanoparticles to expedite mandibular bone regeneration. The material encouraged osteogenesis, improved bone density, and alkaline phosphatase activity<sup>17</sup>. Sharma et al., developed electrospun polydioxanone (PDX) mats containing hydroxyapatite, acemannan/glucomannan, and PHBV for skeletal tissue regeneration, and these mats demonstrated enhanced blood vessel development and superior in vivo biocompatibility<sup>18</sup>. Sun et al., developed cobalt-loaded GelMA@eIm/ZIF-67 hydrogel, and it showed improved bone formation and neovascularization in vivo<sup>19</sup>. Yu et al., developed hydroxyapatite nanorods with different aspect ratios to investigate the influence of nano-form on osteogenic characteristics, and their findings demonstrated effective control of osteogenesis through T cell and IL-22 modulation<sup>20</sup>. Zhang et al., developed triple-layered scaffolds containing platelet-rich fibrin, which demonstrated improved bone healing<sup>21</sup>. Frasnelli et al., developed hydroxyapatite nanoparticles substituted strontium nanoparticles for bone regeneration applications. The results showed that nanoparticles

containing more Sr content increased osteoblast viability and proliferation<sup>22</sup>.

Thus, biomaterials are being successfully employed for bone regeneration because of the variety of required properties that they offer but the results of *in vitro* and *in vivo* research have produced conflicting results, which has limited the usage of biomaterials in bone regeneration. Low vascularity in damaged bones and the often-ignored innate immune response brought on by biomaterial-mediated osteogenesis are potential causes of their poor translation into the clinic<sup>23</sup>. Therefore, there is a pressing need to develop a material that targets immunomodulation while promoting osteogenesis, for effective bone regeneration.

# 3.1.4. Polymers and nanoparticles

At the molecular level, the extracellular matrix (ECM) of the native tissue, like bone, is made up of a hybrid polymer nanostructure arranged with various types of biopolymers and nanocrystallites<sup>24</sup>. Both hard and soft tissues present inside the body exhibit remarkable physicochemical qualities, such as strength and viscoelasticity, due their hybrid and well-organized structure. They also exhibit outstanding biological activity, as evidenced by their tissue-inductive ability and cellular biocompatibility. Therefore, the interest in the development of novel biodegradable biomaterials that imitate biological activity and physicochemical characteristics of native tissues has increased<sup>25</sup>. The use of different natural polymers, such as chitosan, acemannan, sodium alginate, silk fibroin, collagen, and hyaluronic acid, is highly advantageous as they offer various characteristics, like low toxicity, reduced manufacturing costs, biodegradability, cell adhesion, and ECM mimicking properties<sup>26,27</sup>. Earlier studies have demonstrated the efficacy of the natural polymer acemannan, a mucopolysaccharide, in promoting stromal cell proliferation, alkaline phosphatase activity, and bone repair with immunomodulatory properties<sup>28</sup>, <sup>29</sup>. Also, synthetic polymers like poly (lactic acid), poly (glycolic acid), poly (lactic-co-glycolide), and polycaprolactone have been extensively studied. Pure synthetic polymers, with their simple and well-characterized structures, pose lower risks of toxicity, immunogenicity, and infections. However, they often lack the biological signals found in natural materials that can encourage favorable cellular responses<sup>30</sup>. These polymers can further be combined and adapted into various structures, including three-dimensional scaffolds, hydrogels, microspheres, and composite materials.

Nanoparticles have been gaining attention recently due to the physiochemical properties that can be customized for specialized applications by altering shape, size, and surface chemistry. The use of nanomaterials in regenerative medicine has made strides in recent years<sup>31</sup>. Numerous evaluations of research showing the applications of nanomaterials in medicine, particularly in bone regeneration, have been published<sup>32</sup>. Nanoparticles play a crucial role in promoting tissue regeneration and enhancing implant osseointegration in bone tissue engineering<sup>33</sup>. They also serve as efficient carriers for bioactive agents, overcoming the limitations of poor stability, non-specific

targeting, and low cell membrane permeability often associated with direct delivery. Nanomaterial carriers mitigate these issues by stabilizing bioactive molecules through encapsulation or surface attachment, facilitating cellular entry, and providing controlled drug release<sup>34</sup>. Additionally, nanoparticles enable cell labeling and targeting, and contribute to the development and modification of nano-based scaffolds. These scaffolds enhance physicochemical interactions, biocompatibility, mechanical stability, cellular attachment, and survival, further improving the efficacy of therapeutic agents in bone tissue engineering<sup>8</sup>.

Nanoparticles, such as biphasic calcium phosphate nanoparticles combine the properties of both hydroxyapatite and beta-tricalcium phosphate (β-TCP) and offer excellent bioactivity, biocompatibility, and osteoinductive properties. They have shown promising *in vitro* and *in vivo* results for bone regeneration applications<sup>35</sup>. These nanoparticles can further be substituted with magnesium, strontium, and cobalt ions. Cobalt has been proven to promote angiogenesis in bone tissue and enhance the expression of osteocalcin along with immunomodulatory properties<sup>36,37</sup>. Lately, polymer-coated nanoparticles have been widely used for different biomedical applications. They combine the benefits of nanotechnology with the versatility of polymers and can be engineered to improve biocompatibility, control drug release, and enhance cell adhesion, proliferation, and differentiation for effective bone regeneration.

#### 3.2. Objectives

Despite extensive research to develop materials for bone regeneration, effective strategies for targeting immunomodulation remain lacking. Herein, we have developed cobalt-doped biphasic calcium phosphate nanoparticles using different concentrations of cobalt (0.02, 0.5, and 2%) for immunomodulation-regulated bone regeneration. Our objective was to develop efficient material for tissue regeneration applications by combining the excellent bioactivity, osteoconductivity, and osteoinductivity of biphasic calcium phosphate nanoparticles with osteogenic and immunomodulatory potential of low doses of cobalt and acemannan. The ability of materials to promote osteogenesis was evaluated by ALP production and calcium deposition assay. Also, the ability of the material to promote M2 polarization was analyzed by RT-qPCR, flow cytometry, and immunofluorescence staining techniques.



Figure 3.1. Fabrication of acemannan coated, cobalt-doped biphasic calcium phosphate

# 3.3 Experimental section

#### 3.3.1. Materials

The β-glycerophosphate disodium salt hydrate, calcium nitrate tetrahydrate, and cobalt (II) nitrate hexahydrate were obtained from Sigma. Capsules of aloe vera were purchased from Aloevin Corporation. Ascorbic acid and ammonium phosphate dibasic were purchased from HiMedia, and 4-nitrophenylphosphate (pNPP) and dexamethasone were obtained from TCI. Dimethyl sulfoxide (DMSO) was obtained from Merck. RAW264.7 (mouse macrophage cell line) was procured from NCCS, Pune, and MC3T3-E1 was obtained from ATCC. Dulbecco's Modified Eagle Medium (DMEM), Minimum Essential Medium alpha (MEM-α), trizol, penstrep, SYBR<sup>TM</sup> Green Master Mix, and trypsin were procured from Thermo Fisher Scientific. Fetal Bovine Serum (FBS), MTT reagent, and DAPI (4',6-diamidino-2-phenylindole dihydrochloride) were procured from HiMedia. Alexa Fluor<sup>TM</sup> 488 and phalloidin and LIVE/DEAD kit were procured from Invitrogen. cDNA synthesis kit was obtained from Bio-Rad.

# 3.3.2. Isolation of acemannan, preparation of cobalt-doped, biphasic calcium phosphate nanoparticles (0.02%, 0.5%, 2% CoBCP), and acemannan-coated, cobalt doped biphasic calcium phosphate nanoparticles (0.02%, 0.5%, 2% CoAceBCP)

Acemannan was isolated from the Aloevin capsules. The components of aloevin capsules were dissolved in distilled water and dialyzed for 48 h. The obtained solution was washed 2-3 times with water and dried using a lyophilizer. For the development of cobalt-doped, biphasic calcium phosphate nanoparticles 50 mL of 0.5 M ammonium phosphate dibasic solution was prepared, and about 75 mL of 0.5 M calcium nitrate tetrahydrate solution was slowly added to it<sup>38</sup>. The reaction was kept at 55 °C with stirring at 1000 rpm for 1 h while maintaining a pH of 9.5. Mole percentage of 0.02, 0.5, and 2% cobalt was added to the above solution and further stirred for 2 h. Acemannan coated, cobalt-doped biphasic calcium phosphate nanoparticles were fabricated by adding 1% of acemannan to the above solution<sup>39</sup>. After aging the slurry for roughly 36 h at room temperature, the nanoparticles were washed 3 times using distilled water and dried.

# 3.3.3. Characterization of cobalt doped, biphasic calcium phosphate nanoparticles (CoBCP) and acemannan coated, cobalt-doped biphasic calcium phosphate nanoparticles (CoAceBCP) nanoparticles

The fabricated nanoparticles were analyzed using spectroscopic and microscopic methods to assess their chemical and physical characteristics. Fourier-transform infrared spectroscopy (FT-IR) of nanoparticles was conducted with a Bruker instrument (400-4000 cm<sup>-1</sup>). Thermogravimetric

analysis (TGA) was done under nitrogen flow, and the procedure involved the heating of samples at a rate of 5 °C min<sup>-1</sup>, starting from room temperature and increasing to 800 °C using TA Instruments (SDT-650), USA. Particle size analysis was done using DLS Microtrac/Nanotrac Flex. The elemental analysis was performed using the Bruker Splash 6130 EDX. The morphology of nanoparticles was studied using FESEM (JEOL, JSM-7610F plus). Samples were drop cast on a silicon wafer, followed by air drying and imaging. To examine the phase structure of nanoparticles, Rigaku Mini flex diffractometer was utilized.

#### **3.3.4.** Cell culture studies

For cell culture studies, murine leukemic monocyte macrophage cell (RAW 264.7) and mouse osteoblast precursor (MC3T3-E1) cell lines were employed. Complete media, including MEM- $\alpha$  and DMEM with FBS (10%) and antibiotic (1%) was used to grow cells at 37 °C and 5% CO<sub>2</sub>. Cells were grown to 80% confluency in the T-25 flask and were used further for different studies. For osteogenic studies, osteogenic media was used as a positive control, which is composed of MEM- $\alpha$  with ascorbic acid (50  $\mu$ g/mL),  $\beta$ - glycerophosphate disodium hydrate salt (10 mM), and dexamethasone (100 nM).

#### *3.3.4.1. MTT assay*

MTT assay was used to determine the cytocompatibility of nanoparticles, following a previously reported protocol with slight modifications  $^{40}$ . A 96-well plate was used to grow MC3T3-E1 cells at a concentration of  $1\times10^5$  cells per mL. After 24 h, cells were treated with 100 µg/mL of nanoparticles and were further incubated for another 24 h. Subsequently, 20 µL of 5 mg/mL MTT solution was added to each well, and the plates were incubated for 3.5 h. The purple-colored formazan crystals were dissolved with DMSO (100 µL) and the absorbance was recorded at 570 nm. The same procedure was used to assess the percentage cell viability of RAW 264.7 cells. Untreated cells were taken as a control. Cell viability percentage was calculated using the following equation.

% Cell viability = 
$$\frac{Absorbance\ of\ sample}{Absorbance\ of\ control} \times 100$$
 Equation 3.1

### 3.3.4.2. Live dead assay

To further confirm the cytocompatibility of nanoparticles, live-dead assay was conducted using the previously published method<sup>41</sup>. Initially, cells were seeded onto 48 well plates at a density of  $2 \times 10^4$  cells/well for a duration of 24 h. Following the treatment with a 100 µg/mL nanoparticle suspension, cells were incubated for another 24 h. A live/dead assay kit was used to stain MC3T3-E1 cells. A 20 µL of ethidium bromide and 5 µL of calcein AM solutions were mixed with 10 mL DPBS solution to make a dye solution, and 150 µL of this dye solution per well was added and incubated for 20 min. A Leica fluorescence microscope was used to image cells.

#### 3.3.4.3. In vitro scratch assay

In a 6-well plate, MC3T3-E1 cells were seeded at a concentration of  $1 \times 10^4$  cells/mL. Cells were allowed to grow until they reached 100% confluency. A scratch was created in the cell monolayer using a sterile tip, followed by washing with phosphate-buffered saline to get rid of any cell debris. Cells were treated with different nanoparticle samples and incubated at 37 °C for 48 h. Cell migration was studied at different time points using an Evos microscope, and the healing of scratch percentage was estimated using Image J software<sup>42</sup>.

# 3.3.4.4. In vitro osteogenic activity

The osteogenic properties of nanoparticles were studied using calcium deposition assay and alkaline phosphatase activity assay. MC3T3-E1 cells at a density of  $1 \times 10^5$  cells/mL were seeded in a 48-well plate and allowed to grow for 24 h. After 24 hours, the media was replaced with a 100  $\mu$ g/mL nanoparticle suspension and further incubated at different intervals. The media was replaced every 72 h. Cells treated with osteogenic media were taken as a positive control. Cells without any treatment were taken as a negative control.

# 3.3.4.4.1. Alkaline phosphatase activity (ALP)

ALP activity was performed using a previously published protocol<sup>30</sup>. Cells were grown and treated with nanoparticle samples and incubated for different time intervals of 7 days and 14 days. After day 7 and day 14, media was removed and cells were washed with phosphate buffer, followed by cell lysis using 200  $\mu$ L triton X (0.2%). Cell lysate in each well was treated with p-nitrophenyl phosphate (pNPP) solution (200  $\mu$ L), and incubated under dark conditions at 37 °C for another 90 min. The absorbance was measured at 405 nm.

#### 3.3.4.4.2. Alizarin red assay

Alizarin red S staining was used to assess the calcium deposition potential of nanoparticles according to a previously reported protocol<sup>43</sup>. Alizarin red S (40 mM) was solubilized in distilled water, and the pH was adjusted to 4.2 using NH<sub>4</sub>OH (10%). After 7 and 14 days, cells were incubated followed by media removal. The wells were washed using 200  $\mu$ L of 1x phosphate-buffered saline. Cells were then fixed with 200  $\mu$ L of paraformaldehyde solution (4%) for 10 min. They were subsequently rinsed with distilled water. The solution of alizarin red dye (500  $\mu$ L) was added per well and kept in dark conditions at 37 °C. To remove the extra dye, cells were rinsed with water and analyzed using an Evos microscope. Calcium deposits were quantified using cetyl pyridinium solution (10 %). A 500  $\mu$ L solution of alizarin red S was added to the well plates and incubated for 1 h in the dark at 37 °C. The cells were washed with water two to three times to

remove any excess dye. Mineralized nodules were observed under a microscope. For calcium quantification, 200  $\mu$ L of 10% cetylpyridinium chloride was added and kept for incubation for around 30 min. Absorbance was recorded at 562 nm<sup>44</sup>.

#### 3.3.4.5. Cell morphology analysis

Alexa Fluor 588 phalloidin was used to stain F-actin, and DAPI solution was used to stain nuclei to understand the effect of nanoparticles on cell morphology. Firstly, cells were seeded in 6 well plate at 37 °C for 24 h in a humidified environment. After 24 h, the media was replaced by nanoparticle suspension and further incubated for another day. The cells were rinsed with phosphate-buffered saline and fixed with paraformaldehyde solution (4%) for 30 min. With the help of triton X-100, cells were penetrated for 15 min. Finally, the penetrated cells were treated with a mixture of dye solution for half an hour under dark conditions and imaged using a Leica fluorescence microscope.

#### 3.3.5. Effect of nanoparticles on macrophage polarization

# 3.3.5.1. Real-time RT-qPCR assay

Total RNA was extracted from RAW264.7 cells using Trizol reagent, in accordance with the manufacturer's instructions. A NanoDrop UV-Vis spectrophotometer (Thermo Fisher Scientific, USA) was used to measure the purity of RNA. Using gene-specific primers, RT-qPCR tests were carried out by employing SYBR® Green Master Mix to assess the relative mRNA expression in a Quant-Studio 5 Real-Time PCR machine. The primer sequences are provided in **Table A1**, **Appendix**. The thermal cycling protocol began with an initial 2-minute cycle at 95 °C, followed by 35 cycles consisting of 10 sec of denaturation at 95 °C and 1 min of combined annealing and extension at 60 °C. To confirm the specificity of products, a melt curve analysis was performed by gradually increasing the temperature from 70 °C to 95 °C at a rate of 0.5 °C per sec, with continuous fluorescence monitoring after the final extension. All data were normalized to the expression of the reference gene, β-actin.

# 3.3.5.2. Flow cytometry

After being exposed to nanoparticles, RAW264.7 macrophages were harvested, centrifuged for five min at 350 g, and then washed with PBS. Using TruStain FcX (a Fcg blocker, mouse anti-CD16/32 antibody; BioLegend), cell pellets were blocked at 4 °C for 15 min after being resuspended in cell staining buffer (PBS mixed with 0.2% FBS and 0.09% NaNO<sub>3</sub>). Subsequently, cells were stained with fluorochrome-labeled primary antibodies against anti-mouse CD206 and anti-mouse CD86 for 60 min in a shaker on ice. After being resuspended in a cell-staining buffer, the cells were chilled, washed twice with PBS, and analyzed in a flow cytometer. A list of antibodies is listed in (**Table A2, Appendix**).

### 3.3.5.3. Immunofluorescence staining

Immunostaining was conducted on RAW264.7 murine cell lines by using selective antibodies<sup>44</sup>. Cells were seeded at a density of 100,000 cells per well in a 35-mm dish containing a sterile coverslip. After 24 h, cells were treated with AceBCP, 0.02% AceCoBCP, 0.5% AceCoBCP, and 2% AceCoBCP. The cells underwent a PBS rinse, a 5 min fixation in cold methanol, and a 1 min repeat washing in 1x PBS. Subsequently, cells were permeabilized for 5 min using 0.25% triton. Next, they were blocked for 2 h at room temperature using 1% BSA in PBST, and then they were incubated for an additional night with primary antibodies against iNOS (1:400 dilution) and Arginase 1 (1:100 dilution) from Cell Signalling Technology. The cells were then counter-stained with DAPI for three minutes, rinsed with 1x PBS three times, and treated with appropriate secondary antibodies containing fluorescent tags (1:1,000 dilution, Alexa 495-tagged anti-rabbit). The coverslips were placed on tagged slides, photographed, and analyzed using a Leica fluorescence microscope and LASX software.

# 3.3.6. Statistical analysis

The data was statistically analyzed using a student's t-test. The experiment was performed three times. The acquired data were presented as the average value together, with standard deviations from the mean. A significant difference between the control and sample is indicated by \*\*p < 0.005 and \*p < 0.05, while n.s. represents a non-significant difference.

#### 3.4. Results and discussion

The major goal of this study was to investigate the potential of acemannan-coated, cobalt-doped biphasic calcium phosphate nanoparticles (CoAceBCP) in facilitating osteogenesis and regulating the inflammatory response during bone regeneration. In this study, we have developed nanoparticles and examined their chemical and physical properties, *in vitro* osteogenic activity, cell migration, and immunomodulation characteristics for bone regeneration (**Figure 3.1**).

# 3.4.1. Preparation and characterization of nanoparticles

The varying concentrations of cobalt (0.02%, 0.5% & 2%) were added to biphasic calcium phosphate nanoparticles, which were further coated with acemannan to develop cobalt-doped, biphasic calcium phosphate nanoparticles. Characterization of nanoparticles was done using FT-IR, XRD, EDX, Zeta, and DLS. Biphasic calcium phosphate nanoparticles (BCP) showed peaks at 1105, 1136, and 940 cm<sup>-1</sup>, which correspond to PO<sub>4</sub><sup>3-</sup>, P–O stretching vibration modes. A broadening of peaks was recorded for cobalt-doped biphasic calcium phosphate, suggesting the

presence of cobalt ions (**Figure 3.2a**). The FT-IR spectra of acemannan revealed characteristic peaks at 782 cm<sup>-1</sup> (N-H wagging), 1026 cm<sup>-1</sup> (O-H bending) and 1720 cm<sup>-1</sup> (C=O). The FT-IR spectra of CoAceBCP nanoparticles confirmed the presence of cobalt and acemannan (**Figure 3.3a**). The JCPDS data (9-0169) and the XRD spectrum of BCP matched, thus, revealing the presence of distinctive peaks at 22.9° (3 3 -2), 25.9° (1 0 10), 28° (2 1 4), and 31.4° (2 1 10) confirming the formation of BCP (**Figure 3.2b**). AceBCP, 0.02% CoAceBCP, 0.5% CoAceBCP, and 2% CoAceBCP nanoparticles XRD spectra revealed a widening of peaks, indicating cobalt's entry into the biphasic calcium phosphate nanoparticles crystal structure. Additionally, a decrease in crystallinity was noted as cobalt doping increased. This might be attributed to either the amorphous character of the polymer or the replacement of PO<sub>4</sub><sup>3-</sup> by cobalt ions, confirming the successful polymer coating on CoBCP nanoparticles (**Figure 3.3c**). When CoAceBCP nanoparticles were subjected to thermogravimetric analysis (TGA), a significant weight decrease was seen in the 250–350 °C range, which validates the coating of acemannan on the nanoparticles and the successful doping of cobalt (**Figure 3.3b**).

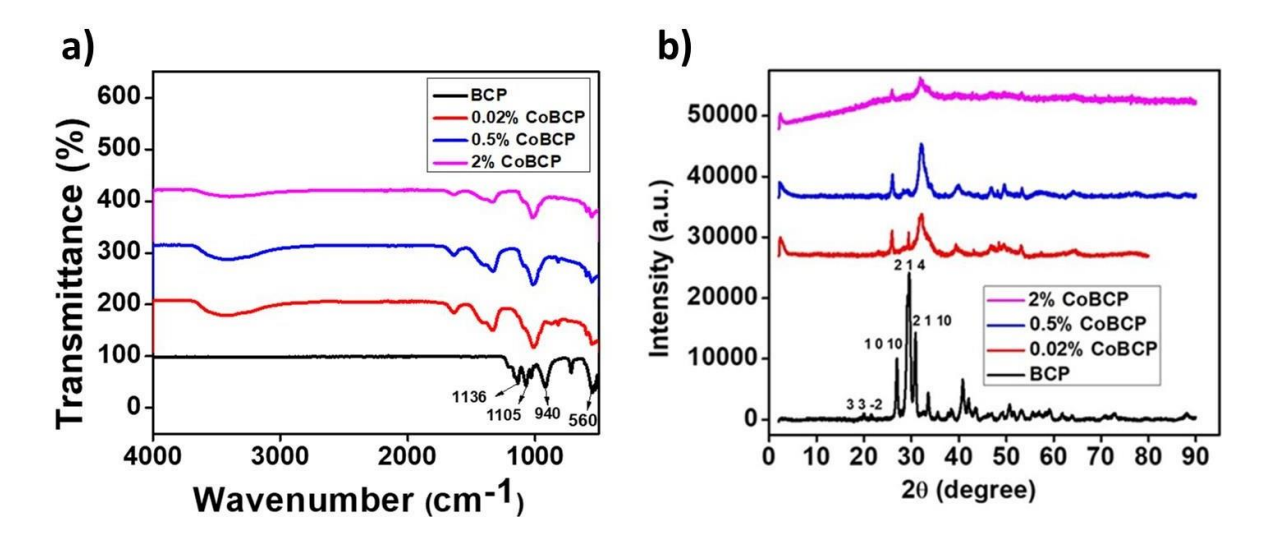


**Figure 3.2.** Characterization of nanoparticles without acemannan coating. a) FTIR spectra of BCP, 0.02% CoBCP, 0.5% CoBCP, and 2% CoBCP. b) XRD spectra of BCP, 0.02% CoBCP, 0.5% CoBCP, and 2% CoBCP.

To ascertain the elemental distribution of components, EDX analysis was performed. Cobalt's presence in the EDX graph demonstrated that cobalt had been successfully doped into BCP nanoparticles (**Figure 3.4a-d**). FESEM investigation revealed that the nanoparticles had a spherical shape (**Figure 3.4e-h**). Dynamic light scattering (DLS) revealed that the particle size of AceBCP was  $128 \pm 31.56$  nm, 0.02% CoAceBCP was  $208 \pm 28.09$  nm, 0.5% CoAceBCP was  $267 \pm 1.73$  nm, and 2% CoAceBCP was  $276 \pm 14.73$  (**Figure 3.4i-l**).

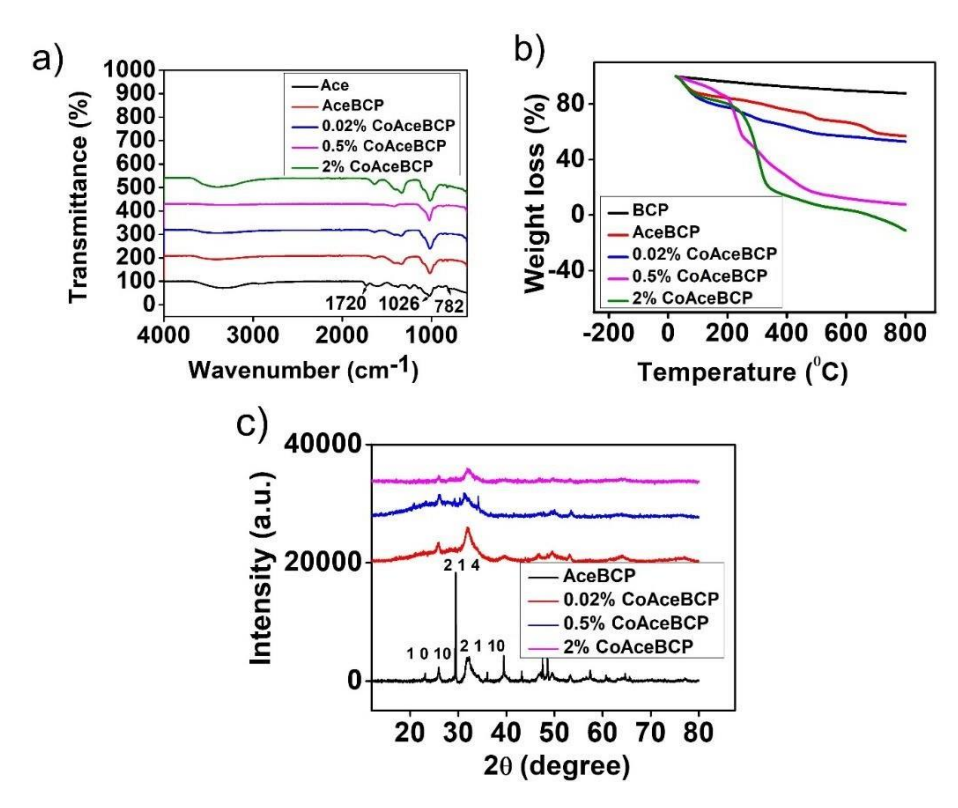


**Figure 3.3.** Characterization of acemannan coated, cobalt-doped biphasic calcium phosphate (CoAceBCP) nanoparticles. (a) FT-IR spectra; (b) TGA; and (c) XRD spectra.

The uniformity of particles was confirmed by polydispersity index (PDI) analysis. The PDI of AceBCP was found to be  $0.101 \pm 0.02$ , 0.02% CoAceBCP was  $0.04 \pm 0.043$ , 0.5% was,  $0.125 \pm 0.07$  and 2% was  $0.10259 \pm 0.08$ . The zeta potential of AceBCP, 0.02% CoAceBCP, 0.5% CoAceBCP, and 2% CoAceBCP were -18, -20, -21, and -24 mV respectively.

### 3.4.2. Cell viability analysis

Biomaterials for bone regeneration must be cytocompatible and must promote cell adhesion, proliferation, and differentiation of cells, all of which lead to successful tissue integration and regeneration. The cell viability analysis was performed on MC3T3-E1 and RAW264.7 cells. Cells were allowed to grow for 24 h. Following 24 h, percentage cell viability was assessed using the MTT assay by comparing the samples treated cells with that of the control. The cells treated with AceBCP showed 96.82% cell viability. A little reduction in cell viability was observed with an increased concentration of cobalt, and it was found to be 92% for 0.02% CoAceBCP, 90.53% for 0.5% CoAceBCP, and 90.51% for 2% CoAceBCP. This could be attributed to higher concentrations of cobalt (**Figure 3.5b**). Nanoparticle treatment of RAW264.7 cells resulted in >90% cell viability, demonstrating the material's cytocompatibility (**Figure A9, Appendix**). The findings were similar to research involving bioactive and biodegradable silica based biomaterial for bone repair<sup>45</sup>. When the concentration of cobalt was increased (3%, 5%, and 7%), the vitality of MC3T3-E1 cells decreased, which further suggested that high concentration of cobalt is associated with decreased

cell viability<sup>46,47</sup>.

Additionally, a live/dead assay was also performed to further verify the nanoparticles cytocompatibility. The MC3T3-E1 cells were grown in 48-well plate for 24 h, and treated with AceBCP, 0.02% CoAceBCP, 0.5% CoAceBCP and 2% CoAceBCP. Following 24 h, cells were stained with live/dead dye and examined under a fluorescence microscope. The prevalence of the green signal demonstrated the presence of living cells, thus, proving the nanoparticles cytocompatibility (**Figure 3.5a**). The migration of cells is also an important factor, contributing significantly to the bone regeneration process. Mesenchymal stem cells along with other cells depend on effective migration to reach the area of injury. MC3T3-E1 cells were used for an *in vitro* scratch test to determine how nanoparticles affect cell migration. After 48 h, a notable decrease in scratch area was observed. In the case of cells treated with 2% CoAceBCP, maximum scratch closure was seen, and the initial scratch area decreased from 40% to 2.47% (**Figure 3.5c-d**). The enhanced cell migration might be because of the synergistic/additive effect of acemannan and cobalt, resulting in efficient cell migration<sup>42</sup>.

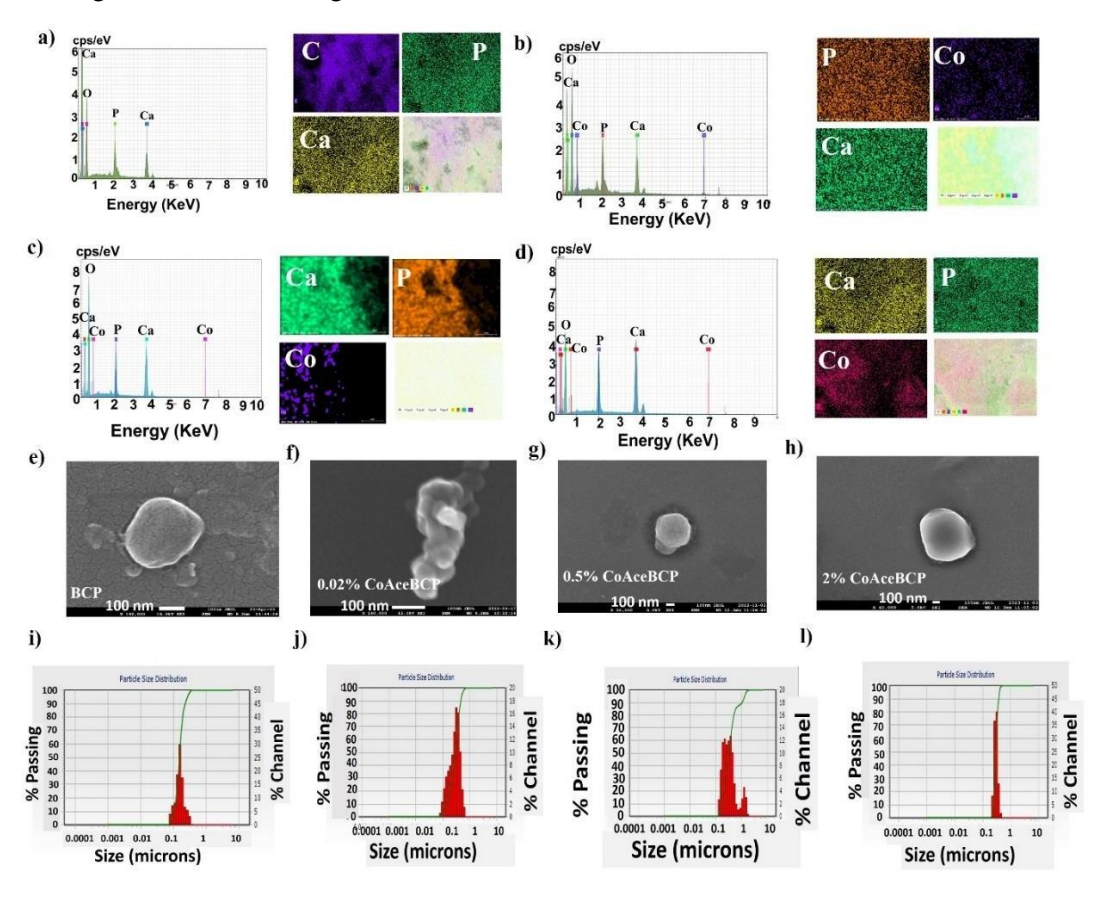


**Figure 3.4.** EDX (a-d), FESEM (e-h), and DLS (i-l) analysis of acemannan coated, cobalt-doped biphasic calcium phosphate nanoparticles: (a, e, i) AceBCP; (b, f, j) 0.02% CoAceBCP; (c, g, k) 0.5% CoAceBCP; and (d, h, l) 2% CoAceBCP.

# 3.4.3. The cell morphology

Staining cells with Alexa Fluor phalloidin and DAPI, we studied the impact of different nanoparticles on the morphology of cells. When compared with the morphology of cells treated with only MEM- $\alpha$ , cells treated with nanoparticles maintained their mononucleated, fibroblast-like shape with extended cytoplasmic projection, confirming the cytocompatibility of nanoparticles (**Figure 3.6**).

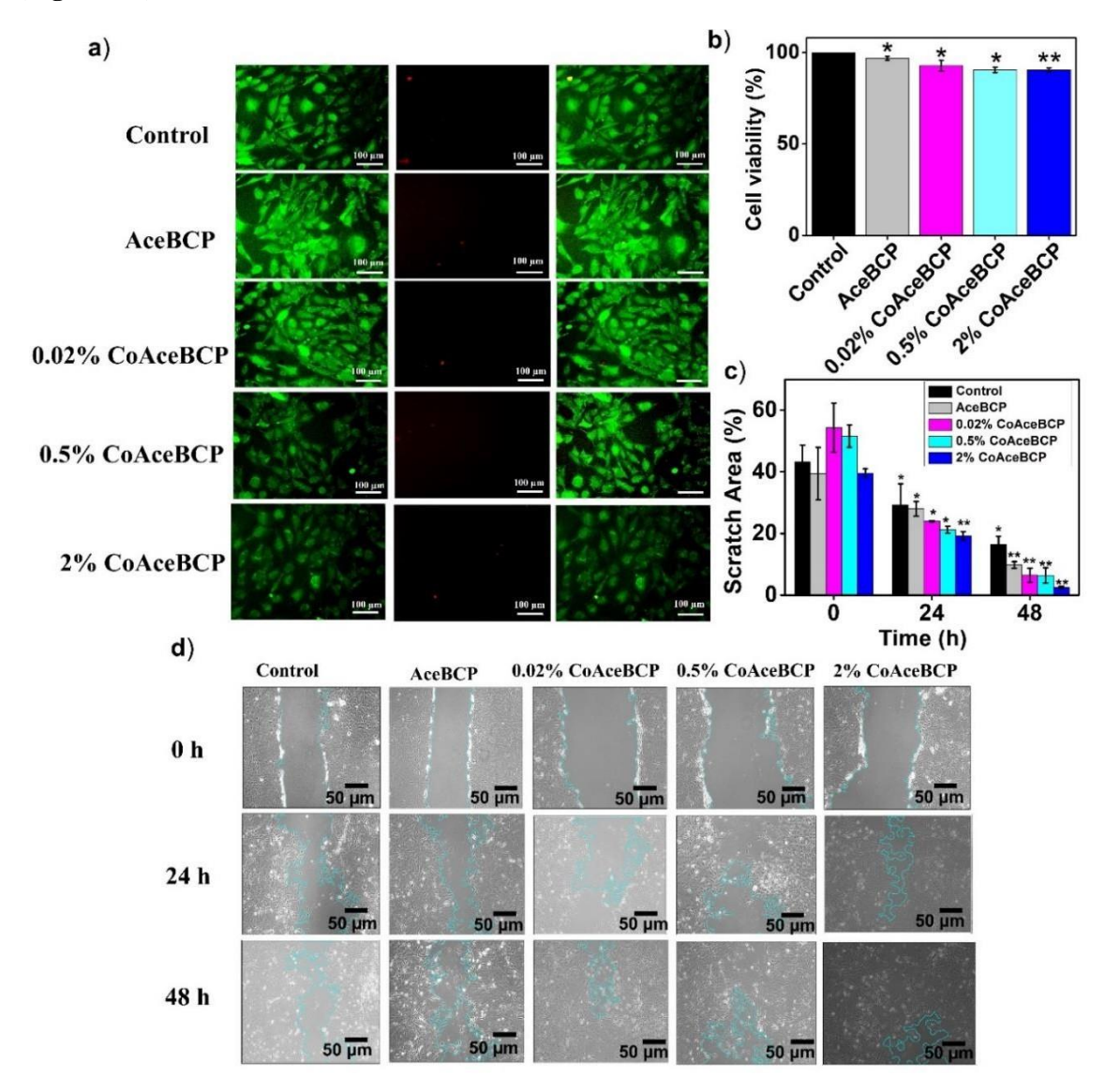


**Figure 3.5.** Cell viability and scratch healing of MC3T3-EI cells in the presence of acemannan coated, cobalt-doped biphasic calcium phosphate nanoparticles. (a) Live/Dead assay, scale bar: 100  $\mu$ m; (b) MTT assay; (c) Scratch area; and (d) Cell migration and scratch healing; scale bar: 50  $\mu$ m. \*\*p < 0.005 and \*p < 0.05 denotes significant difference and n.s. corresponds to non-significant difference (n = 3).

# 3.4.4. Osteogenic studies

Applications for bone regeneration can benefit from the use of biomaterials that support osteogenic indicators, such as ALP activity and calcium deposition, to replicate the natural bone microenvironment, and aid in the growth, adhesion, and differentiation of osteogenic cells. These characteristics enable the biomaterials to be effectively integrated into host tissues and also aid in the restoration of the functional and structural integrity of bone that has been injured. Alkaline phosphatase and calcium deposition were measured, and the osteogenic properties were estimated (**Figure 3.7**). MC3T3-E1 cells were seeded in 48-well plate and treated with nanoparticle suspension for 7 and 14 days. After different time intervals, ALP and calcium deposition were measured.

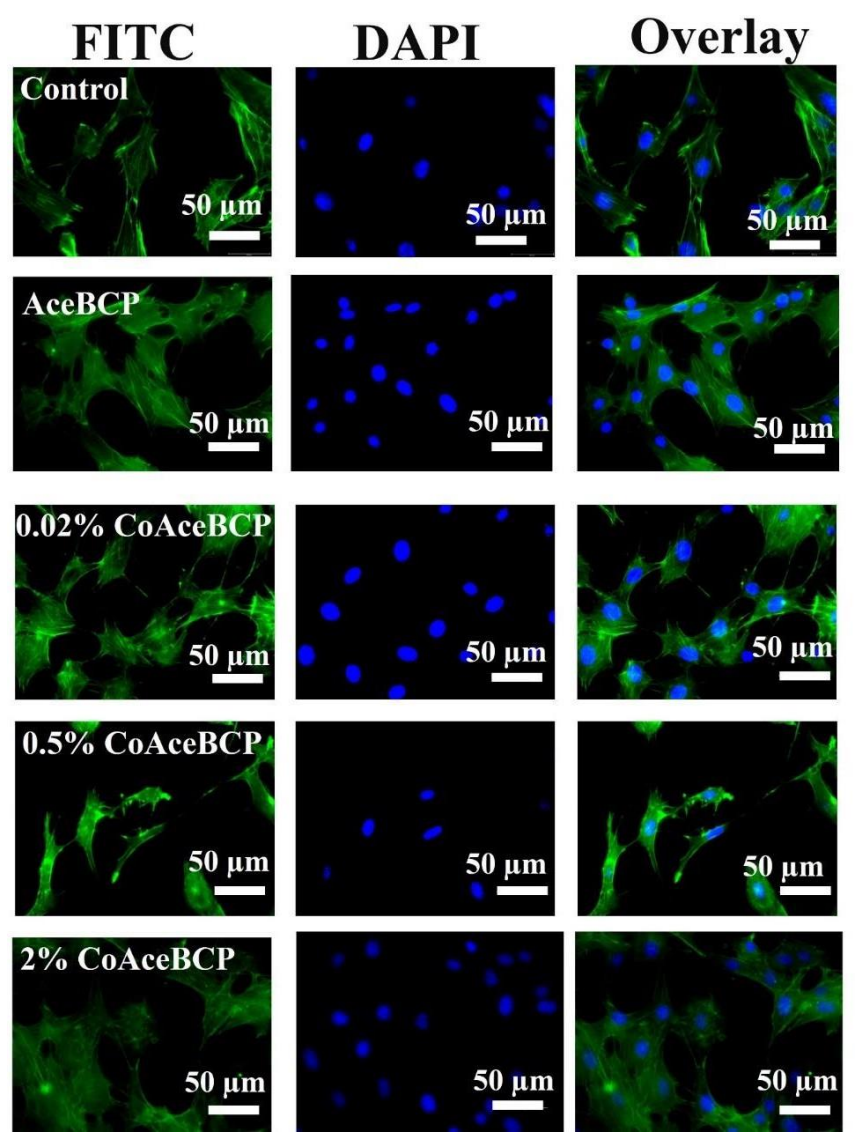
#### 3.4.4.1 ALP assay

A crucial step in bone formation is osteogenic differentiation at the tissue-material intersection. Among other osteogenic markers, alkaline phosphatase, a glycoprotein present on the cellular surface, is a well-known marker of osteoblast development and regulates the calcification of the bone matrix<sup>48,35</sup>. Consequently, ALP is a crucial factor, and after 7 and 14 days, ALP activity was assessed (**Figure 3.7a**). The ALP activity was observed to increase in cells treated with nanoparticles. This rise in ALP activity in the presence of nanoparticles signifies the onset of osteoblast differentiation<sup>31</sup>. The maximum ALP activity was seen in the case of 2% CoAceBCP when compared with AceBCP, 0.02% CoAceBCP, and 0.5% CoAceBCP. Studies have shown that cobalt promotes osteogenesis, and the increased concentration of cobalt ions might be the reason behind the increased activity<sup>49</sup>. Also, research done by various researchers indicates that acemannan increases the expression of markers of osteoblast development, such as ALP, which may also account for the rise in the ALP activity<sup>50</sup>. The outcomes are consistent with a study that examined the impact of bioactive glasses containing strontium and cobalt substitutes on bone regeneration<sup>51</sup>.

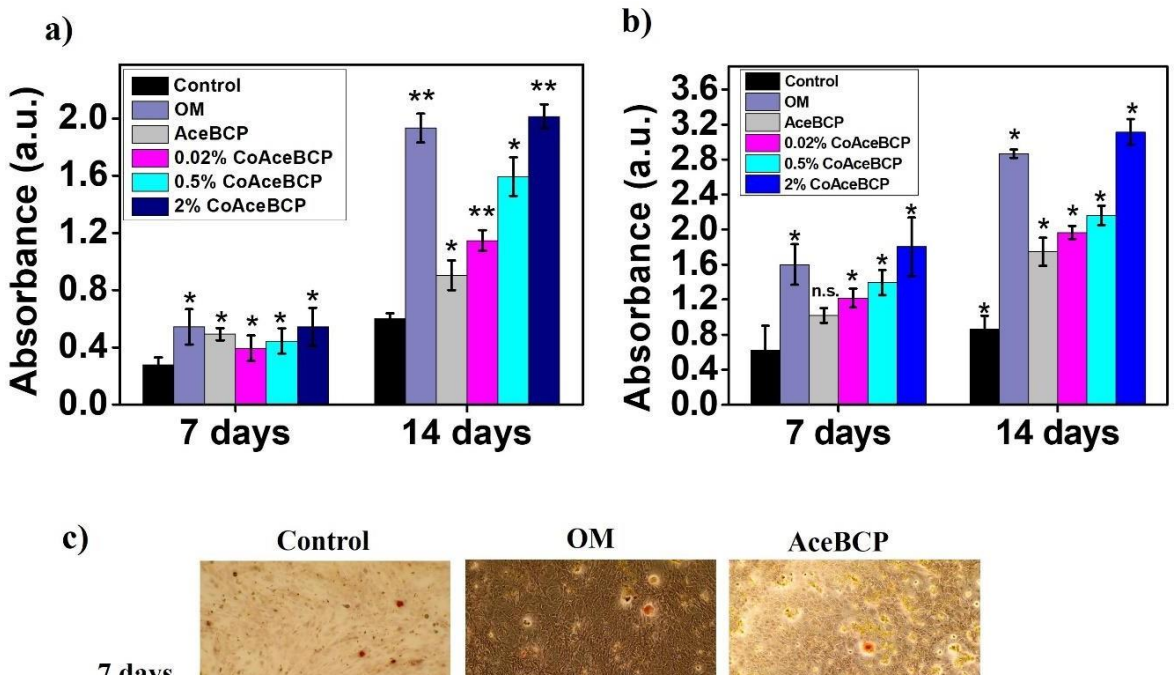
#### 3.4.4.2. Calcium deposition

Calcium deposition is one of the prime indicators of cell differentiation<sup>52</sup>. Alizarin red assay was performed to analyze the calcium deposition. Alizarin Red S selectively reacts with calcium ions to form an Alizarin Red S-calcium complex, producing a red stain that can be observed under the microscope. MC3T3 cells were seeded in a 48-well plate, followed by nanoparticle treatment for different time intervals. After 7 and 14 days, the cells were stained with alizarin red, and the resulting images showed that there were abundant calcium deposits. Calcium quantification was performed by dissolving it in a 10% cetylpyridinium chloride solution and measuring the absorbance at 405 nm (**Figure 3.7b, c**). The calcium deposition assay showed a similar pattern with an increase in cobalt doping, an enhancement in calcium deposition was observed. The highest calcium deposition was recorded in the case of 2% CoAceBCP. The calcium deposition with 2% CoAceBCP was similar to that of osteogenic media (OM), suggesting that nanoparticles possess

significant potential for enhancing osteogenesis. This might be resulting from the presence of cobalt and acemannan. Earlier reports have indicated that cobalt increases VEGF secretion, stimulates proliferation, and boosts the expression of genes related to bone formation<sup>36</sup>. Furthermore, it has been demonstrated that acemannan also promotes osteoblast development by upregulating VEGF, which aids in the formation of extracellular matrix and increases calcium deposition.<sup>28</sup>



**Figure 3.6.** Cytoskeletal staining of MC3T3-E1 cells with Alexa fluor phalloidin (green) and DAPI (blue) after treatment with nanoparticle extracts. Cells without any treatment were taken as a control. Scale bar:  $50 \, \mu m$ .



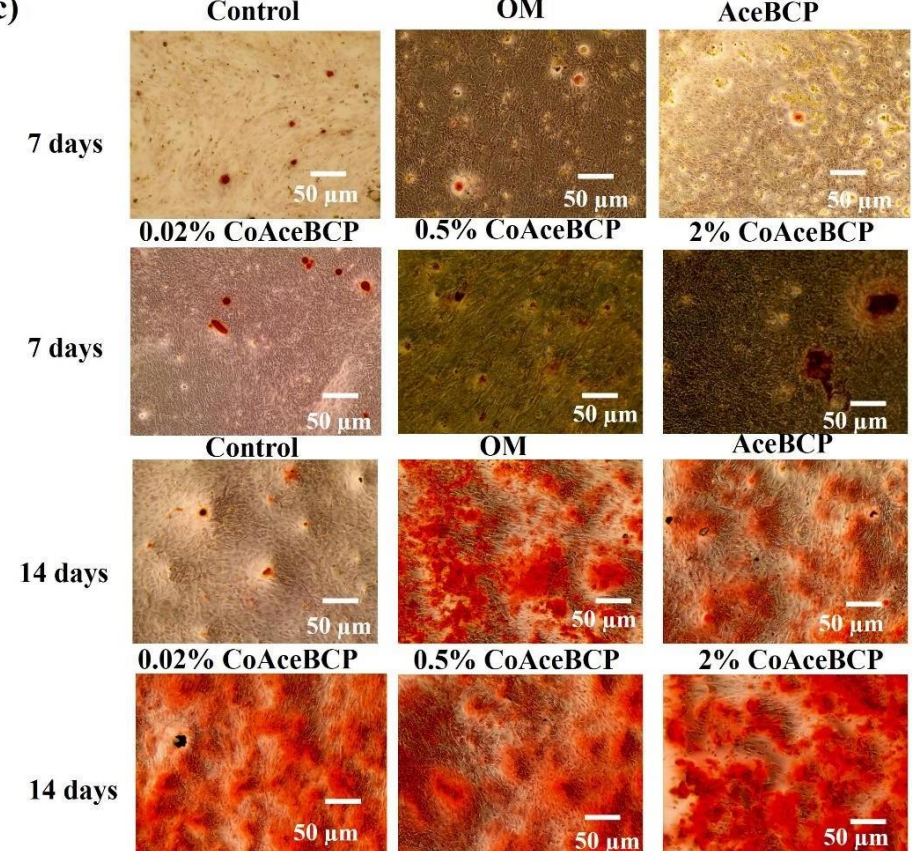
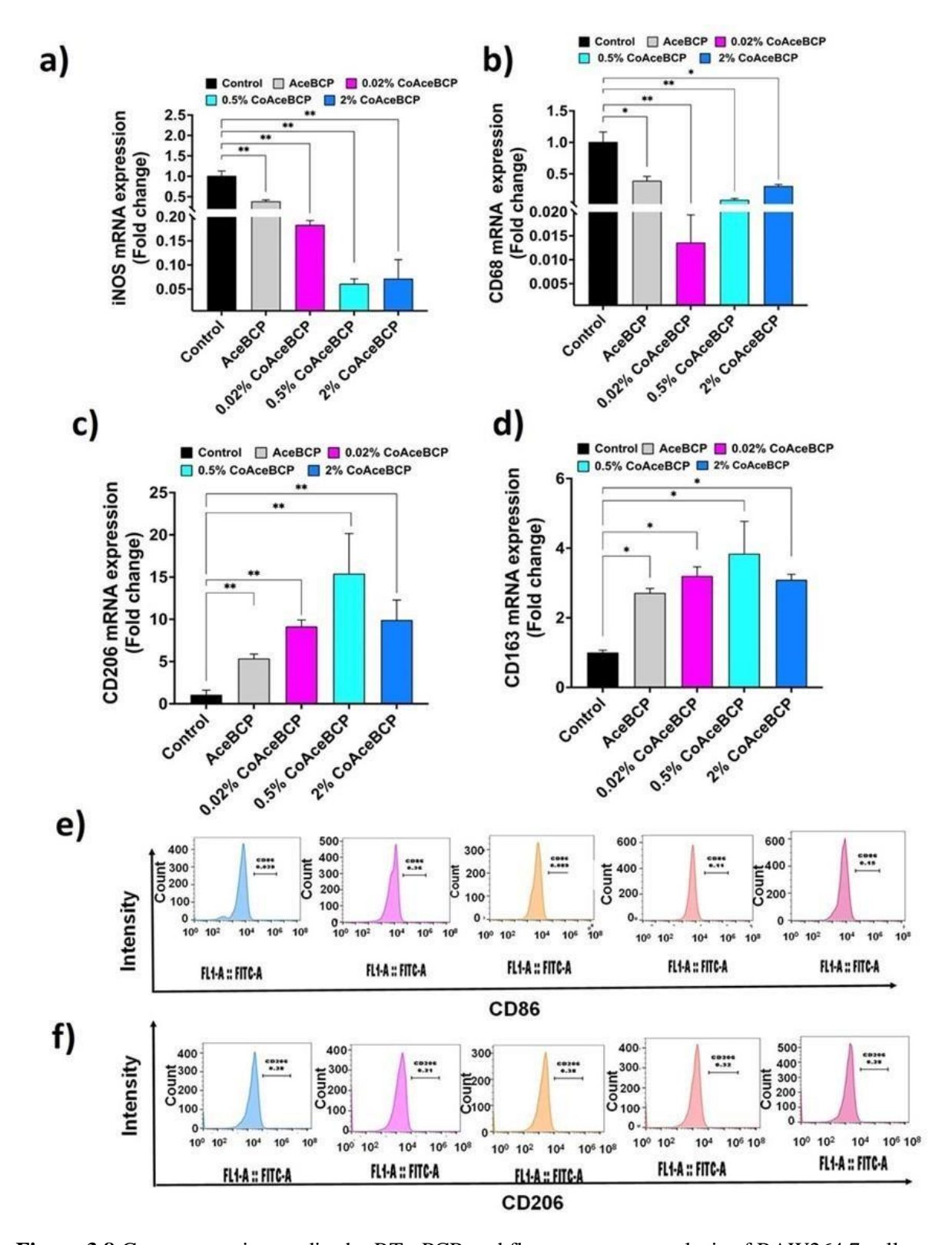


**Figure 3.7** Osteogenic potential of MC3T3-E1 cells in the presence of nanoparticles. (a) Alkaline phosphatase (ALP) activity assay; (b) Alizarin red staining assay for calcium deposition; and (c) Images of calcium nodules. \*\*p <0.005 and \*p <0.05 denotes significant difference and n.s. corresponds to non-significant difference (n = 3). Scale bar:  $50 \, \mu m$ .

#### 3.4.5. Immunomodulation studies

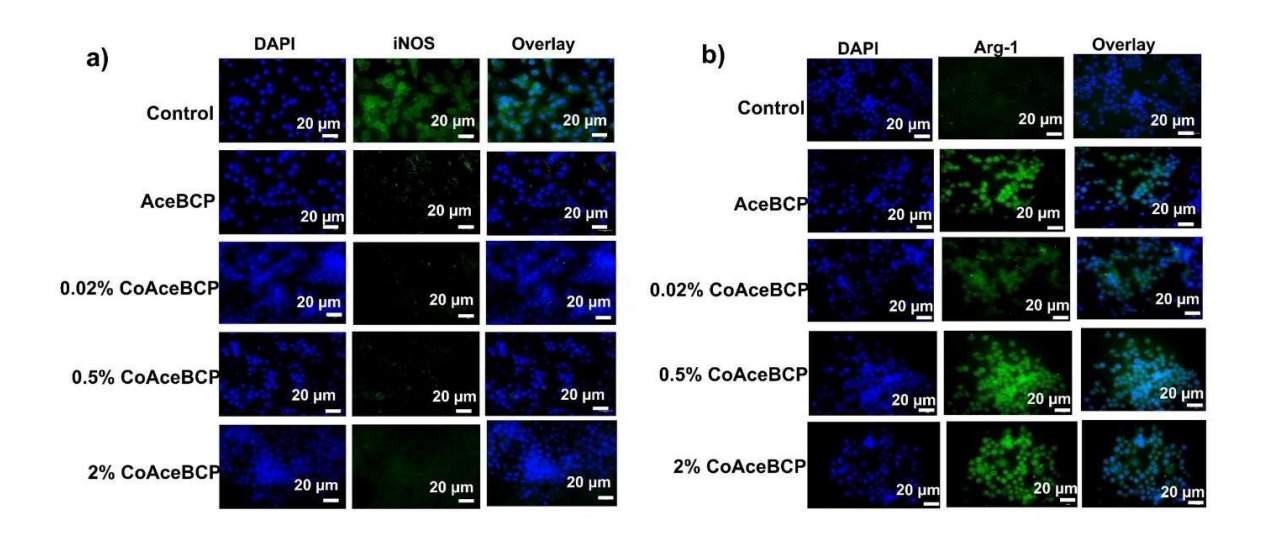
Tissue regeneration and repair are aided by macrophage polarization from the pro-inflammatory M1 phenotype, which is generally linked to inflammation, to the anti-inflammatory M2 phenotype<sup>53</sup>. An environment that is more favourable for bone regeneration can be created by promoting macrophage polarisation towards the M2 phenotype. To further verify macrophage polarization, quantitative real-time polymerase chain reaction (RT-qPCR), immunofluorescence, and flow cytometry analysis were conducted. To evaluate the inflammatory response of macrophages, RTqPCR was employed (Figure 3.8). CoAceBCP treatment resulted in a significant drop in the expression levels of proinflammatory cytokine iNOS and M1-macrophage associated marker gene CD68 after 14 days of treatment (Figure 3.8a, b). However, there was a significant increase in expression levels of CD206 and CD163, which are known to be markers for M2 macrophages, with cells treated with 0.5% CoAceBCP showing the highest fold change (Figure 3.8c, d). This might be because of the presence of low doses of cobalt, as cobalt affects the induction of the M2 phenotype and also possesses anti-inflammatory characteristics <sup>17,54</sup>. The results also indicated that there was an abrupt decrease in the expression of the anti-inflammatory marker when the cobalt doping concentration was raised from 0.5% to 2%. The results align with the study indicating that high concentrations of cobalt promote the expression of the M1 phenotype, characterized by reduced CD206 expression, and increased CD68 expression<sup>55</sup>. Additionally, the presence of acemannan might be helping in the downregulation of proinflammatory markers. The acemannan coating's ability to improve macrophage polarisation towards the M2 phenotype by influencing the PI3K/Akt/GSK-3β signalling pathway might have also contributed to immunomodulation as well.<sup>56</sup>

To further study the effect of nanoparticles on macrophage polarization, flow cytometry analysis was conducted. Macrophages were treated for 14 days with AceBCP, 0.02% CoAceBCP, 0.5% CoAceBCP, and 2% CoAceBCP nanoparticles, and the changes in these markers after coincubation were assessed. The group treated with AceBCP, 0.02% CoAceBCP, 0.5% CoAceBCP, and 2% CoAceBCP had increased levels of the M2 macrophage marker, CD206, by 0.28%, 0.38%, 0.32%, and 0.28% respectively, as per the flow cytometric analysis, in comparison with control with the value of 0.21% (**Figure 3.8e, f**). Additionally, cells treated with 0.02% CoAceBCP, 0.5% CoAceBCP, and 2% CoAceBCP showed downregulation in the levels of M1 macrophage marker, CD86, by 0.089%, 0.11%, and 0.15% respectively in comparison to AceBCP and control. These outcomes supported the results obtained from the RT-qPCR analysis. Immunocytochemistry (ICC) was also performed to study the immunomodulation potential of nanoparticles (**Figure 3.9**). Firstly, RAW264.7 cells were seeded and treated with AceBCP, 0.02% CoAceBCP, 0.5% CoAceBCP, and 2% CoAceBCP for 14 days.



**Figure 3.8** Gene expression studies by RT-qPCR and flow cytometry analysis of RAW264.7 cells treated with nanoparticles for 14 days. (a-d) RT-qPCR studies measuring the expression of: (a) iNOS (M1), (b) CD68 (M1), (c) CD206 (M2), and (d) CD163 (M2); and (e, f) flow cytometric assay

depicting the expression of CD86 and CD206. \*\*p < 0.005 and \*p < 0.05 denotes significant difference and n.s. corresponds to a non-significant difference (n = 3).



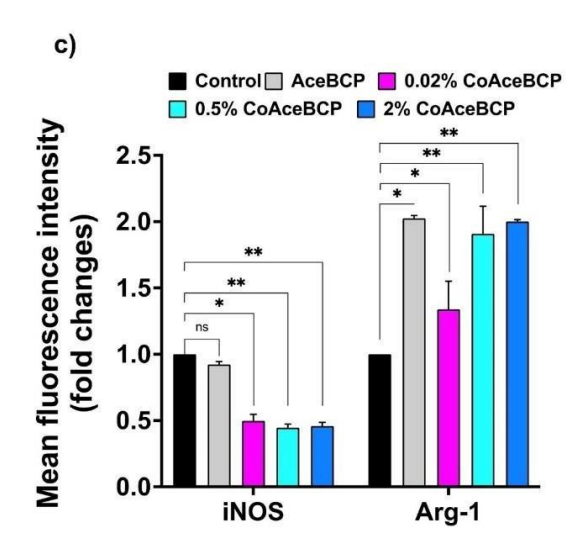


**Figure 3.9** Immunocytochemistry assay of RAW 264.7 cell lines treated with nanoparticles for 14 days. (a) Immunohistochemical staining of iNOS; (b) Arginase 1 expression; and (c) Quantification of mean fluorescent intensity. Scale bar: 20  $\mu$ m. \*\*p <0.005 and \*p <0.05 denotes significant difference and n.s. corresponds to non-significant difference (n = 3).

Treatment with AceBCP, 0.02% CoAceBCP, and 0.5% CoAceBCP decreased iNOS production in comparison to control, but a slight rise in iNOS was observed with 2%CoAceBCP (**Figure 3.9a**). The findings followed the results of RT-qPCR data. The expression of the M2 marker was also examined and the results indicated that Arg1 was elevated in cells treated with CoAceBCP nanoparticles for 14 days (**Figure 3.9b**). The increased Arg1 expression was validated by a fold change in mean fluorescence intensity (**Figure 3.9c**). The results further confirmed the

immunomodulatory characteristics of nanoparticles. The outcomes are consistent with a study that described the research on telmisartan-loaded PCL/PVP scaffolds to support immunomodulation for the production of endogenous bone<sup>57</sup> and the potential of peptide-modified chitosan scaffolds targeted at osteoblasts to enhance macrophage polarization in the treatment of bone deformities<sup>58</sup>.

The results obtained from the immunomodulation studies point to the possibility that acemannan-coated, cobalt-doped biphasic calcium phosphate nanoparticles cause macrophages to undergo a phenotypic shift. This shift is associated with the increased release of anti-inflammatory factors, which facilitates more effective bone tissue regeneration. These findings highlight the potential of these nanoparticles to modulate immune responses, paving the way for improved bone healing strategies in medical applications

#### 3.5 Conclusions

In this work, we aimed to develop a biomaterial with osteogenic and immunomodulatory properties to enhance bone tissue regeneration. To achieve it, we successfully developed biphasic calcium phosphate nanoparticles, doped them with different concentrations of cobalt, further coated them with acemannan, and evaluated their osteogenic and immunomodulatory properties. The nanoparticles demonstrated excellent cytocompatibility towards the pre-osteoblast cell line and promoted cell migration and scratch healing, alongside enhanced osteogenic properties, such as ALP activity and calcium deposition, which are prime indicators of cell differentiation. The immunomodulatory potential of nanoparticles was also estimated using RT-qPCR, immunofluorescence, and flow cytometry techniques. The results suggested that nanoparticles possess significant immunomodulatory properties, as they reduced the level of M1 markers, CD68 and iNOS, and increased the expression of M2 markers, CD206, CD163, and Arg-1. In particular, nanoparticles doped with 0.5% cobalt achieved a balance between immunomodulatory effects and cytotoxicity by showing minimal cytotoxic reactions and inducing a favorable shift in macrophage polarization towards an anti-inflammatory M2 phenotype. This effect decreased with higher cobalt concentrations, underscoring the importance of precise cobalt regulation. The ability to control cobalt doping levels in nanoparticles offers a potential method for influencing immune responses and creating more effective treatment plans for bone regeneration. Overall, the unique combination of biphasic calcium phosphate nanoparticles and cobalt, along with acemannan, developed in this work fosters an osteoimmune microenvironment conducive to bone regeneration. The results suggest that the fabricated nanoparticles can expedite bone regeneration by enhancing osteogenesis and macrophage polarization, ensuring timely and coordinated tissue regeneration, ultimately leading to improved patient outcomes. These findings align with the first chapter's focus on

developing polymer-based biomaterials to promote tissue regeneration in cases of bacteria-infected wounds. Both of these chapters collectively aim to advance treatment approaches and improve patient outcomes in regenerative medicine.

#### References

- (1) Zhou, Z.; Fan, Y.; Jiang, Y.; Shi, S.; Xue, C.; Zhao, X.; Tan, S.; Chen, X.; Feng, C.; Zhu, Y.; Yan, J.; Zhou, Z.; Zhao, Y.; Liu, J.; Chen, F.; He, S. Mineralized Enzyme-Based Biomaterials with Superior Bioactivities for Bone Regeneration. *ACS Appl. Mater. Interfaces* **2022**, *14* (32), 36315–36330.
- (2) Guo, L.; Liang, Z.; Yang, L.; Du, W.; Yu, T.; Tang, H.; Li, C.; Qiu, H. The Role of Natural Polymers in Bone Tissue Engineering. *Journal of Controlled Release* **2021**, *338*, 571–582.
- (3) Long, F. Building Strong Bones: Molecular Regulation of the Osteoblast Lineage. *Nature Reviews Molecular Cell Biology* **2012**, *13* (1), 27–38.
- (4) Tatsumi, S.; Ishii, K.; Amizuka, N.; Li, M.; Kobayashi, T.; Kohno, K.; Ito, M.; Takeshita, S.; Ikeda, K. Targeted Ablation of Osteocytes Induces Osteoporosis with Defective Mechanotransduction. *Cell Metabolism* **2007**, *5* (6), 464–475.
- (5) Salhotra, A.; Shah, H. N.; Levi, B.; Longaker, M. T. Mechanisms of Bone Development and Repair. *Nat Rev Mol Cell Biol* **2020**, *21* (11), 696–711.
- (6) Winkler, T.; Sass, F. A.; Duda, G. N.; Schmidt-Bleek, K. A Review of Biomaterials in Bone Defect Healing, Remaining Shortcomings and Future Opportunities for Bone Tissue Engineering: The Unsolved Challenge. *Bone & Joint Research* **2018**, *7* (3), 232–243.
- (7) Tsekoura, E. K.; K.C., R. B.; Uludag, H. Biomaterials to Facilitate Delivery of RNA Agents in Bone Regeneration and Repair. *ACS Biomater. Sci. Eng.* **2017**, *3* (7), 1195–1206.
- (8) Walmsley, G. G.; McArdle, A.; Tevlin, R.; Momeni, A.; Atashroo, D.; Hu, M. S.; Feroze, A. H.; Wong, V. W.; Lorenz, P. H.; Longaker, M. T.; Wan, D. C. Nanotechnology in Bone Tissue Engineering. *Nanomedicine: Nanotechnology, Biology and Medicine* **2015**, *11* (5), 1253–1263.
- (9) Wei, H.; Cui, J.; Lin, K.; Xie, J.; Wang, X. Recent Advances in Smart Stimuli-Responsive Biomaterials for Bone Therapeutics and Regeneration. *Bone Res* **2022**, *10* (1), 17.
- (10) Chen, Y.; Sheng, W.; Lin, J.; Fang, C.; Deng, J.; Zhang, P.; Zhou, M.; Liu, P.; Weng, J.; Yu, F.; Wang, D.; Kang, B.; Zeng, H. Magnesium Oxide Nanoparticle Coordinated Phosphate-Functionalized Chitosan Injectable Hydrogel for Osteogenesis and Angiogenesis in Bone Regeneration. *ACS Appl. Mater. Interfaces* **2022**, *14* (6), 7592–7608.
- (11) Qiao, Y.; Liu, X.; Zhou, X.; Zhang, H.; Zhang, W.; Xiao, W.; Pan, G.; Cui, W.; Santos, H. A.; Shi, Q. Gelatin Templated Polypeptide Co-Cross-Linked Hydrogel for Bone Regeneration. *Adv Healthcare Materials* **2020**, *9* (1), 1901239.
- (12) Shuai, C.; Yang, W.; Feng, P.; Peng, S.; Pan, H. Accelerated Degradation of HAP/PLLA Bone Scaffold by PGA Blending Facilitates Bioactivity and Osteoconductivity. *Bioactive Materials* **2021**, *6* (2), 490–502.
- (13) Feng, P.; Wu, P.; Gao, C.; Yang, Y.; Guo, W.; Yang, W.; Shuai, C. A Multimaterial Scaffold With Tunable Properties: Toward Bone Tissue Repair. *Advanced Science* **2018**, *5* (6), 1700817.
- (14) Qiu, Y.; Xu, X.; Guo, W.; Zhao, Y.; Su, J.; Chen, J. Mesoporous Hydroxyapatite Nanoparticles Mediate the Release and Bioactivity of BMP-2 for Enhanced Bone Regeneration. *ACS Biomater. Sci. Eng.* **2020**, *6* (4), 2323–2335.
- (15) Zhang, X.; Cheng, G.; Xing, X.; Liu, J.; Cheng, Y.; Ye, T.; Wang, Q.; Xiao, X.; Li, Z.; Deng, H. Near-Infrared Light-Triggered Porous AuPd Alloy Nanoparticles To Produce Mild Localized Heat To Accelerate Bone Regeneration. *J. Phys. Chem. Lett.* **2019**, *10* (15), 4185–4191.
- (16) Yang, X.; Zhang, C.; Zhang, T.; Xiao, J. Cobalt-Doped Ti Surface Promotes Immunomodulation. *Biomed. Mater.* **2022**, *17* (2), 025003.
- (17) Ignjatović, N.; Ajduković, Z.; Savić, V.; Najman, S.; Mihailović, D.; Vasiljević, P.; Stojanović, Z.; Uskoković, V.; Uskoković, D. Nanoparticles of Cobalt-Substituted Hydroxyapatite in Regeneration of Mandibular Osteoporotic Bones. *J Mater Sci: Mater Med* **2013**, *24* (2), 343–354.
- (18) Goonoo, N.; Bhaw-Luximon, A.; Passanha, P.; Esteves, S.; Schönherr, H.; Jhurry, D. Biomineralization Potential and Cellular Response of PHB and PHBV Blends with Natural Anionic Polysaccharides. *Materials Science and Engineering: C* **2017**, *76*, 13–24.
- (19) Sun, Y.; Liu, X.; Zhu, Y.; Han, Y.; Shen, J.; Bao, B.; Gao, T.; Lin, J.; Huang, T.; Xu, J.; Chai, Y.; Zheng, X. Tunable and Controlled Release of Cobalt Ions from Metal–Organic

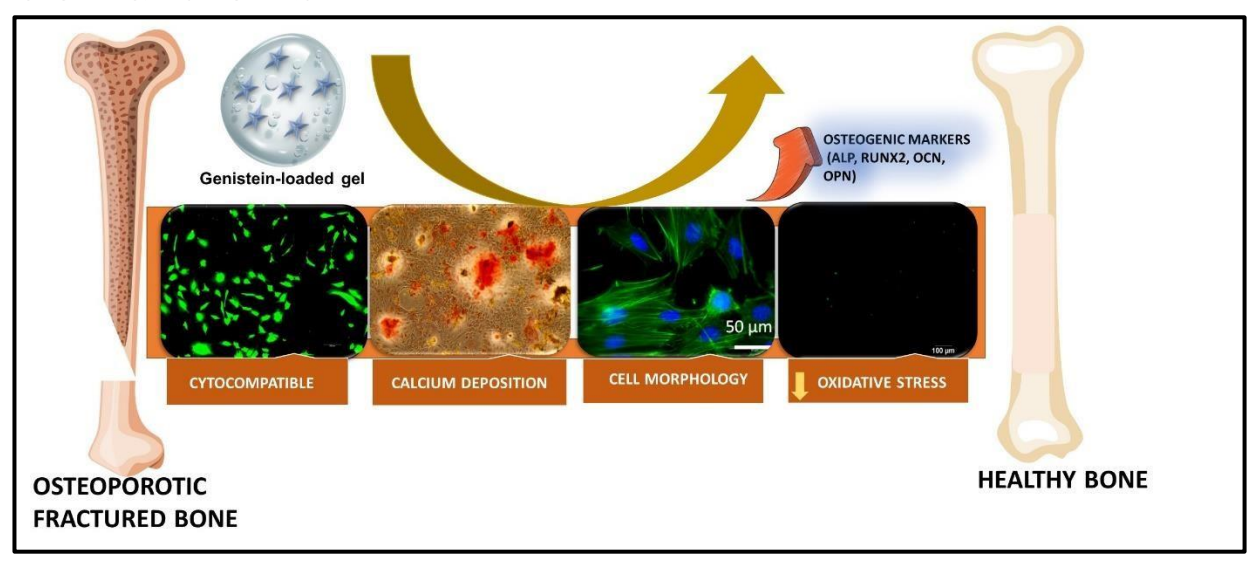
- Framework Hydrogel Nanocomposites Enhances Bone Regeneration. *ACS Appl. Mater. Interfaces* **2021**, *13* (49), 59051–59066.
- (20) Yu, F.; Lian, R.; Liu, L.; Liu, T.; Bi, C.; Hong, K.; Zhang, S.; Ren, J.; Wang, H.; Ouyang, N.; Du, L.-J.; Liu, Y.; Zhou, L.; Liu, Y.; Fang, B.; Li, Y.; Duan, S.-Z.; Xia, L. Biomimetic Hydroxyapatite Nanorods Promote Bone Regeneration via Accelerating Osteogenesis of BMSCs through T Cell-Derived IL-22. *ACS Nano* **2022**, *16* (1), 755–770.
- (21) Zhang, L.; Dong, Y.; Xue, Y.; Shi, J.; Zhang, X.; Liu, Y.; Midgley, A. C.; Wang, S. Multifunctional Triple-Layered Composite Scaffolds Combining Platelet-Rich Fibrin Promote Bone Regeneration. *ACS Biomater. Sci. Eng.* **2019**, *5* (12), 6691–6702.
- (22) Frasnelli, M.; Cristofaro, F.; Sglavo, V. M.; Dirè, S.; Callone, E.; Ceccato, R.; Bruni, G.; Cornaglia, A. I.; Visai, L. Synthesis and Characterization of Strontium-Substituted Hydroxyapatite Nanoparticles for Bone Regeneration. *Materials Science and Engineering: C* **2017**, *71*, 653–662.
- (23) Liang, H.; Jin, C.; Ma, L.; Feng, X.; Deng, X.; Wu, S.; Liu, X.; Yang, C. Accelerated Bone Regeneration by Gold-Nanoparticle-Loaded Mesoporous Silica through Stimulating Immunomodulation. *ACS Appl. Mater. Interfaces* **2019**, *11* (44), 41758–41769.
- (24) Watt, F. M.; Huck, W. T. S. Role of the Extracellular Matrix in Regulating Stem Cell Fate. *Nature Reviews Molecular Cell Biology* **2013**, *14* (8), 467–473.
- (25) Erickson, I. E.; Kestle, S. R.; Zellars, K. H.; Farrell, M. J.; Kim, M.; Burdick, J. A.; Mauck, R. L. High Mesenchymal Stem Cell Seeding Densities in Hyaluronic Acid Hydrogels Produce Engineered Cartilage with Native Tissue Properties. *Acta Biomaterialia* **2012**, *8* (8), 3027–3034.
- (26) Puppi, D.; Chiellini, F.; Piras, A. M.; Chiellini, E. Polymeric Materials for Bone and Cartilage Repair. *Progress in Polymer Science* **2010**, *35* (4), 403–440.
- (27) Guo, B.; Ma, P. X. Conducting Polymers for Tissue Engineering. *Biomacromolecules* **2018**, *19* (6), 1764–1782.
- (28) Boonyagul, S.; Banlunara, W.; Sangvanich, P.; Thunyakitpisal, P. Effect of Acemannan, an Extracted Polysaccharide from Aloe Vera, on BMSCs Proliferation, Differentiation, Extracellular Matrix Synthesis, Mineralization, and Bone Formation in a Tooth Extraction Model. *Odontology* **2014**, *102* (2), 310–317.
- (29) Sharma, A.; Mittal, P.; Yadav, A.; Mishra, A. K.; Hazari, P. P.; Sharma, R. K. Sustained Activity of Stimuli-Responsive Curcumin and Acemannan Based Hydrogel Patches in Wound Healing. *ACS Appl. Bio Mater.* **2022**, *5* (2), 598–609.
- (30) Ramírez Rodríguez, G.; Patrício, T.; Delgado López, J. 8 Natural Polymers for Bone Repair. In *Bone Repair Biomaterials (Second Edition)*; Pawelec, K. M., Planell, J. A., Eds.; Woodhead Publishing, 2019; pp 199–232.
- (31) Shim, K.-S.; Kim, S. E.; Yun, Y.-P.; Jeon, D. I.; Kim, H.-J.; Park, K.; Song, H.-R. Surface Immobilization of Biphasic Calcium Phosphate Nanoparticles on 3D Printed Poly(Caprolactone) Scaffolds Enhances Osteogenesis and Bone Tissue Regeneration. *Journal of Industrial and Engineering Chemistry* **2017**, *55*, 101–109.
- (32) Kim, E. S.; Ahn, E. H.; Dvir, T.; Kim, D.H. Emerging Nanotechnology Approaches in Tissue Engineering and Regenerative Medicine. *IJN* **2014**, 1.
- (33) Tautzenberger, A.; Kovtun; Ignatius. Nanoparticles and Their Potential for Application in Bone. *IJN* **2012**, 4545.
- (34) Faraji, A. H.; Wipf, P. Nanoparticles in Cellular Drug Delivery. *Bioorganic & Medicinal Chemistry* **2009**, *17* (8), 2950–2962.
- (35) Zhu, Y.; Zhang, K.; Zhao, R.; Ye, X.; Chen, X.; Xiao, Z.; Yang, X.; Zhu, X.; Zhang, K.; Fan, Y.; Zhang, X. Bone Regeneration with Micro/Nano Hybrid-Structured Biphasic Calcium Phosphate Bioceramics at Segmental Bone Defect and the Induced Immunoregulation of MSCs. *Biomaterials* **2017**, *147*, 133–144.
- (36) Deng, Z.; Lin, B.; Jiang, Z.; Huang, W.; Li, J.; Zeng, X.; Wang, H.; Wang, D.; Zhang, Y. Hypoxia-Mimicking Cobalt-Doped Borosilicate Bioactive Glass Scaffolds with Enhanced Angiogenic and Osteogenic Capacity for Bone Regeneration. *Int J Biol Sci* **2019**, *15* (6), 1113–1124.
- (37) Tahmasebi Birgani, Z.; Fennema, E.; Gijbels, M. J.; De Boer, J.; Van Blitterswijk, C. A.;

- Habibovic, P. Stimulatory Effect of Cobalt Ions Incorporated into Calcium Phosphate Coatings on Neovascularization in an in Vivo Intramuscular Model in Goats. *Acta Biomaterialia* **2016**, *36*, 267–276.
- (38) Chen, Y.; Kawazoe, N.; Chen, G. Preparation of Dexamethasone-Loaded Biphasic Calcium Phosphate Nanoparticles/Collagen Porous Composite Scaffolds for Bone Tissue Engineering. *Acta Biomaterialia* **2018**, *67*, 341–353.
- (39) Kato, R.; Uesugi, M.; Komatsu, Y.; Okamoto, F.; Tanaka, T.; Kitawaki, F.; Yano, T. Highly Stable Polymer Coating on Silver Nanoparticles for Efficient Plasmonic Enhancement of Fluorescence. *ACS Omega* **2022**, *7* (5), 4286–4292.
- (40) Rekha, S.; Anila, E. I. In Vitro Cytotoxicity Studies of Surface Modified CaS Nanoparticles on L929 Cell Lines Using MTT Assay. *Materials Letters* **2019**, *236*, 637–639.
- (41) Bhattacharyya, A.; Janarthanan, G.; Kim, T.; Taheri, S.; Shin, J.; Kim, J.; Bae, H. C.; Han, H.-S.; Noh, I. Modulation of Bioactive Calcium Phosphate Micro/Nanoparticle Size and Shape during in Situ Synthesis of Photo-Crosslinkable Gelatin Methacryloyl Based Nanocomposite Hydrogels for 3D Bioprinting and Tissue Engineering. *Biomater Res* **2022**, *26* (1), 54.
- (42) Rasool, N.; Negi, D.; Singh, Y. Thiol-Functionalized, Antioxidant, and Osteogenic Mesoporous Silica Nanoparticles for Osteoporosis. *ACS Biomater. Sci. Eng.* **2023**, *9* (6), 3535–3545.
- (43) Talukdar, Y.; Rashkow, J. T.; Lalwani, G.; Kanakia, S.; Sitharaman, B. The Effects of Graphene Nanostructures on Mesenchymal Stem Cells. *Biomaterials* **2014**, *35* (18), 4863–4877.
- (44) Dash, P.; Samal, S.; Prasad Panda, G.; Piras, A. M.; Dash, M. Polymeric Nanoformulation of Zoledronic Acid Rescues Osteoblasts from the Harmful Effect of Its Native Form: An In Vitro Investigation of Cytotoxic Potential on Osteoblasts and Osteosarcoma Cells. *Macromolecular Bioscience* **2023**, *23* (11), 2300211.
- (45) Wang, S.; Wang, X.; Draenert, F. G.; Albert, O.; Schröder, H. C.; Mailänder, V.; Mitov, G.; Müller, W. E. G. Bioactive and Biodegradable Silica Biomaterial for Bone Regeneration. *Bone* **2014**, *67*, 292–304.
- (46) Fleury, C.; Petit, A.; Mwale, F.; Antoniou, J.; Zukor, D. J.; Tabrizian, M.; Huk, O. L. Effect of Cobalt and Chromium Ions on Human MG-63 Osteoblasts in Vitro: Morphology, Cytotoxicity, and Oxidative Stress. *Biomaterials* **2006**, *27* (18), 3351–3360.
- (47) Alarifi, S.; Ali, D.; Ahamed, M.; Siddiqui, M.A.; Al-Khedairy, A.A. Oxidative Stress Contributes to Cobalt Oxide Nanoparticles-Induced Cytotoxicity and DNA Damage in Human Hepatocarcinoma Cells. *IJN* **2013**, 189.
- (48) Ding, Z.; Han, H.; Fan, Z.; Lu, H.; Sang, Y.; Yao, Y.; Cheng, Q.; Lu, Q.; Kaplan, D. L. Nanoscale Silk–Hydroxyapatite Hydrogels for Injectable Bone Biomaterials. *ACS Appl. Mater. Interfaces* **2017**, *9* (20), 16913–16921.
- (49) Khosrowshahi, A.K; Khoshfetrat, A. B.; Khosrowshahi, Y. B.; Maleki-Ghaleh, H. Cobalt Content Modulates Characteristics and Osteogenic Properties of Cobalt-Containing Hydroxyapatite in in-Vitro Milieu. *Materials Today Communications* **2021**, *27*, 102392.
- (50) Godoy, D. J. D.; Chokboribal, J.; Pauwels, R.; Banlunara, W.; Sangvanich, P.; Jaroenporn, S.; Thunyakitpisal, P. Acemannan Increased Bone Surface, Bone Volume, and Bone Density in a Calvarial Defect Model in Skeletally-Mature Rats. *Journal of Dental Sciences* **2018**, *13* (4), 334–341.
- (51) Kargozar, S.; Lotfibakhshaiesh, N.; Ai, J.; Samadikuchaksaraie, A.; Hill, R. G.; Shah, P. A.; Milan, P. B.; Mozafari, M.; Fathi, M.; Joghataei, M. T. Synthesis, Physico-Chemical and Biological Characterization of Strontium and Cobalt Substituted Bioactive Glasses for Bone Tissue Engineering. *Journal of Non-Crystalline Solids* **2016**, *449*, 133–140.
- (52) Zhao, Y.; Zou, B.; Shi, Z.; Wu, Q.; Chen, G.-Q. The Effect of 3-Hydroxybutyrate on the in Vitro Differentiation of Murine Osteoblast MC3T3-E1 and in Vivo Bone Formation in Ovariectomized Rats. *Biomaterials* **2007**, 28 (20), 3063–3073.
- (53) Dai, X.; Heng, B. C.; Bai, Y.; You, F.; Sun, X.; Li, Y.; Tang, Z.; Xu, M.; Zhang, X.; Deng, X. Restoration of Electrical Microenvironment Enhances Bone Regeneration under Diabetic Conditions by Modulating Macrophage Polarization. *Bioactive Materials* **2021**, *6* (7), 2029–2038.

- (54) Mandakhbayar, N.; Ji, Y.; El-Fiqi, A.; Patel, K. D.; Yoon, D. S.; Dashnyam, K.; Bayaraa, O.; Jin, G.; Tsogtbaatar, K.; Kim, T.-H.; Lee, J.-H.; Kim, H.-W. Double Hits with Bioactive Nanozyme Based on Cobalt-Doped Nanoglass for Acute and Diabetic Wound Therapies through Anti-Inflammatory and pro-Angiogenic Functions. *Bioactive Materials* **2024**, *31*, 298–311.
- (55) Díez-Tercero, L.; Delgado, L. M.; Bosch-Rué, E.; Perez, R. A. Evaluation of the Immunomodulatory Effects of Cobalt, Copper and Magnesium Ions in a pro Inflammatory Environment. *Sci Rep* **2021**, *11* (1), 11707.
- (56) Bai, Y.; Niu, Y.; Qin, S.; Ma, G. A New Biomaterial Derived from Aloe Vera—Acemannan from Basic Studies to Clinical Application. *Pharmaceutics* **2023**, *15* (7), 1913.
- (57) Wu, S.; Ma, J.; Liu, J.; Liu, C.; Ni, S.; Dai, T.; Wang, Y.; Weng, Y.; Zhao, H.; Zhou, D.; Zhao, X. Immunomodulation of Telmisartan-Loaded PCL/PVP Scaffolds on Macrophages Promotes Endogenous Bone Regeneration. *ACS Appl. Mater. Interfaces* **2022**, *14* (14), 15942–15955.
- (58) Tang, Y.; Chen, Y.; Huang, L.; Gao, F.; Sun, H.; Huang, C. Intramembranous Ossification Imitation Scaffold with the Function of Macrophage Polarization for Promoting Critical Bone Defect Repair. *ACS Appl. Bio Mater.* **2020**, *3* (6), 3569–3581.

# **CHAPTER – 4**

Genistein-loaded, quaternized dextran/ κ-carrageenan gels for bone regeneration in osteoporotic conditions



# 4.1. Introduction

# 4.1.1. Osteoporosis/post-menopausal osteoporosis

According to the World Health Organization, osteoporosis is a systemic bone metabolic disorder characterized by the chronic loss of bone resulting in increased fracture risk and fragility fractures<sup>1</sup>. These fragility fractures cause unfavourable conditions such as persistent pain, impairments, and reduced quality of life<sup>2</sup>. With a quick increase in the aging population worldwide, osteoporosis has emerged as a significant public health issue primarily affecting the older population and postmenopausal women. The main cause of postmenopausal osteoporosis in women is a dramatic drop in estrogen levels that occurs during menopause as estrogen is needed for maintaining the health of bones<sup>3</sup>. Globally, women over 50 face a 9.8–22.8% risk of fragility fractures. According to the Bone Health and Osteoporosis Foundation, it is projected that 3 million fractures and \$25.3 billion in direct healthcare expenses will occur annually by 2025. The overall cost of care related to osteoporotic fractures and non-union fractures is expected to reach \$95 billion by 2040<sup>4</sup>. Understanding the pathogenic molecular pathways, genetic factors, and alterations in the bone microenvironment of osteoporosis is crucial for achieving adequate treatment efficacy.

Bone comprises a dense outer layer known as cortical bone and an inner, porous structure called cancellous bone, each possessing unique characteristics that collaborate to ensure bone strength<sup>5</sup>. Bone consists of various cells, including osteoblasts, osteocytes, osteoclasts, and stem cells, along with the bone matrix, which is made up of calcium, phosphorus, inorganic salts, and collagen<sup>6</sup>. Osteoblasts help in new bone formation and osteoclasts help in bone resorption. The balance between these two types of cells preserves bone health and maintains the structural integrity of the skeleton. This process is referred to as bone remodelling or bone turnover<sup>7</sup>. One of the major reasons for osteoporosis is an imbalance between osteogenesis and osteoclastogenesis. Also, there is increasing evidence that oxidative stress caused by reactive oxygen species (ROS), which rises with aging or the onset of inflammation, can negatively impact bone homeostasis, promoting a proresorptive environment

### 4.1.2. Challenges

The traditional treatment modalities available for osteoporosis mostly involve the use of anabolic agents, which help in effectively growing bone mass and preventing the loss of bone and the use of anti-resorptive therapeutics that inhibit osteoclast function. However, these treatment strategies are

also associated with certain drawbacks including toxicity and poor absorption<sup>8</sup>. The use of antiresorptive drugs such as Denosumab, which works by targeting and inhibiting RANKL is associated
with reduced immunity<sup>9</sup>. Post-menopausal osteoporosis, which is linked with reduced levels of
estrogen is also associated with the production of reactive oxygen species (ROS). ROS production
further stimulates RANKL-mediated osteoclastogenesis accelerates osteoclastic bone resorption<sup>10</sup>.
For the treatment of bone regeneration in osteoporotic conditions, hormone replacement therapy is
the gold standard but it is associated with side effects and restrictions, which include an increased
risk of uterine bleeding, stroke, blood clots, breast cancer, and cardiovascular disease in
postmenopausal women<sup>11</sup>.

### 4.1.3. Research gap

Researchers have worked with various biomaterials for bone regeneration in osteoporotic conditions. Quan et al., fabricated multipurpose hydroxyapatite nanostructures for bone regeneration in osteoporotic conditions. The results showed enhanced implant osseointegration and accelerated bone remodelling<sup>12</sup>. Zhao et al., developed peptide coatings for titanium implants to enhance osseointegration in osteoporotic conditions<sup>13</sup>. Li et al., fabricated strontium ranelate-loaded silk fibroin aerogel for osteogenic properties. It showed stimulation of osteogenic differentiation of osteoblasts. Sandomierski et al., developed a chitosan-zeolite based scaffold for the controlled release of osteoporotic drugs. It has been demonstrated that these novel scaffolds retained drugs and released the drug gradually<sup>14</sup>. Li et al., fabricated injectable tetra-PEG hydrogel for the delivery of alendronate. Zhao et al., developed mineral-based hydrogels for bone regeneration in osteoporosis. The hydrogels demonstrated improved bone ingrowth with accelerated bone formation in osteoporotic conditions<sup>15</sup>. The hydrogels were able to release therapeutic payloads and successfully promote in situ bone repair, which is useful for clinical osteoporosis therapy<sup>16</sup>. Raimundo et al., fabricated mesoporous silica nanoparticles modified with alendronate functionalized PEG-coated with PEI to deliver osteostatin and SOST siRNA to achieve effective bone targeting. The codelivery of therapeutic agents enhanced the expression of osteogenic markers<sup>17</sup>. Kuang et al., fabricated near-infrared responsive parathyroid hormone to attain bone regeneration in ovariectomized (OVX) model<sup>18</sup>. Ray et al., developed iron foam scaffolds for osteoporosis fracture healing coated with strontium and bisphosphonates. The iron foams improved the bone defects as compared to plain foams. The coatings helped in enhanced bioactivity<sup>19</sup>. Ye et al., developed nitric oxide-based nanoparticles for the treatment of osteoporosis. The nanoparticles enhanced the differentiation of preosteoblasts<sup>20</sup>. Naito et al., developed a hyaluronic acid gel sheet assisted by phosphoric acid for effective transdermal alendronate administration in anti-osteoporotic therapy<sup>21</sup>. Most of the treatment strategies involve the use of therapeutic drugs or osteoprogenitor cells, which suffer from drawbacks such as high cost and instability. Also, the use of bisphosphonates like

zoledronate and pamidronate is associated with cases of osteonecrosis of the jaw and femur fracture<sup>22</sup>. The use of bioceramics for drug loading results in the denaturation of drugs as ceramic processes involve high temperature, which is the major drawback for their use as drug delivery agents. Therefore, there is a need for alternative drug delivery systems to promote effective bone tissue regeneration with minimal adverse effects.

# 4.1.4. Polymeric gels and phytoestrogens

Synthetic and natural polymers are widely employed in bone tissue engineering as they offer unique characteristics, including high biocompatibility, biodegradability, and their resemblance to extracellular matrix<sup>23</sup>. Also, these polymers can be modified for physiochemical, structural, and biological properties by using different techniques to meet the specific requirements of bone regeneration<sup>24</sup>. Several polymer-based materials have already reached clinical applications, for example BioMed®, mucograft, calcitek, Matriderm, and GC membrane<sup>25</sup>. The researchers have worked widely on different polymers such as collagen, chitosan, quaternized dextran, sodium alginate, silk fibroin, κ-carrageenan, and hyaluronic acid for bone regeneration applications<sup>26</sup>. Out of different polymers, k-carrageenan obtained from the red algae family is a sulfated polysaccharide consisting of  $\alpha$ -1,3-D-galactose and  $\beta$ -1,4-3,6-anhydro-galactose, which resemble naturally occurring glycosaminoglycans. Carrageenans have shown apatite layer formation activities along with the ability to enhance compressive strength, which makes it a material of choice for bone scaffold fabrication<sup>27</sup>. Also, the use of another polymer, dextran is widely studied as a drug carrier. It is a natural polysaccharide obtained from the bacteria. It is bioactive with the competency to enter the target site effectively without causing toxic reactions<sup>28</sup>. The dextran-based gels are widely used in drug-loading systems as they offer good drug loading ability and easy absorption<sup>29</sup>. Thus, these polymers, due to their versatile properties, can be effectively utilized in bone regeneration applications.

Phytoestrogens are obtained from the plants<sup>30</sup>. Phytoestrogen molecules such as curcumin, genistein, and quercetin are used in various biological functions, including anti-adipogenic, anti-osteoclastogenic, and osteogenic properties. The use of phytoestrogens to prevent osteoporosis by oral route was reported earlier<sup>31</sup>. They act by promoting osteoblast differentiation and bone formation while inhibiting osteoclast development. Their effects on osteoblast differentiation in MC3T3-E1 cells, a mouse calvaria osteoblast-like cell line, have been documented. However, their efficacy in promoting bone tissue regeneration from bone scaffolds remains unreported<sup>22</sup>. Therefore, phytoestrogen-loaded polymeric gels hold a strong potential for bone regeneration applications.

#### 4.2. Objectives

To address these problems, we have developed a genistein-loaded,  $\kappa$ -carrageenan/quaternized dextran-based polymeric gel system for accelerating bone regeneration in osteoporotic conditions.

Thus, we have combined the estrogen-mimicking and antioxidant properties of genistein along with extracellular matrix mimicking properties of  $\kappa$ -carrageenan and drug delivery properties of quaternized dextran. The ability of the polymeric gels to aid in bone regeneration was characterized and evaluated in cell culture. The genistein-loaded gel showed excellent ability to scavenge reactive oxygen species as suggested by ABTS assay. The osteogenic differentiation of MC3T3-E1 by genistein-loaded polymeric gel was evaluated by alkaline phosphatase assay and calcium deposition assay. Overall, this genistein-loaded polymeric gel showed significant potential in creating a favorable environment for bone regeneration and promoting bone healing.

# 4.3. Experimental section

#### 4.3.1. Materials

Genistein, κ-carrageenan, glycidyl trimethylammonium chloride, and dextran were obtained from TCI chemicals. Sodium hydroxide was purchased from Sigma. The 2'-azino-bis- (3-ethylbenzothiazoline-6-sulfonic acid (ABTS), 3-(4,5-dimethylthiazol)-2,5-diphenyltetrazolium bromide (MTT), DMSO, triton X, and ascorbic acid were purchased from HiMedia. The murine pre-osteoblast cells (MC3T3-E1) and mouse leukemic monocyte macrophage cell line (RAW 264.7) were obtained from ATCC. Dulbecco's Modified Eagle Medium (DMEM), Minimum Essential Medium alpha (MEM-α), Penstrep, 0.25% trypsin/EDTA, and Alexa Fluor phalloidin 488 were obtained from Thermo Fisher Scientific. The 4-nitrophenyl phosphate (pNPP) was also acquired from TCI chemicals, while 4',6-diamidino-2-phenylindole (DAPI), and Alizarin Red S were acquired from Sigma-Aldrich. Deionized water was obtained from a Milli-Q system and used in all experiments.

# 4.3.2. Preparation of k-carrageenan/quaternized dextran gels and genistein-loaded k-carrageenan/quaternized dextran gels

# 4.3.2.1. Preparation of quaternized dextran (QDex)

Dextran (0.6g) was dissolved in 30 mL of distilled water, followed by the addition of 120 mg of NaOH. The mixture was heated to 60 °C and agitated with a magnetic stirrer. The 2 mL of GTMAC was added to this solution and heated and stirred for 4 h at 60 °C. The reaction mixture was further allowed to cool and dialyzed using a dialysis tube for 48 h. The solution was finally lyophilized, and a white, fluffy solid was obtained<sup>32</sup>.

4.3.2.2. Fabrication of  $\kappa$ -carrageenan ( $\kappa$ -C)/quaternized dextran gels Different concentrations of  $\kappa$ -carrageenan (2%, 3%) and quaternized dextran (2%) were dissolved in distilled water to make different percentages of  $\kappa$ -carrageenan and quaternized dextran. The two solutions were mixed in various ratios (2% QD, 2% C (1:1), 2% QD, 2% C (1:2), 2% QD, 3% C

(1:2). The mixture was vortexed and then incubated at 37 °C. The formation of gels was determined by the cessation of flow in the solution, and the time required for gel formation was recorded.

# 4.3.2.3. Fabrication of genistein-loaded κ -carrageenan/ quaternized dextran gels

Genistein (1.25 mg) was dissolved in DMSO (250  $\mu$ L) and sonicated for 5 min. Different percentages of quaternized dextran and  $\kappa$ -carrageenan were made as discussed earlier. The 20  $\mu$ L of genistein solution was added to the quaternized dextran solution (90  $\mu$ L). To this solution,  $\kappa$ -carrageenan solution (90  $\mu$ L) was added. All these steps were performed while sonicating. The mixture was thoroughly mixed using a vortex shaker and the gels were allowed to stand. The time required for gel formation was found to be 1 h. The fabricated gels were characterized using FTIR, rheology, swelling degradation, and FESEM.

#### 4.3.3. Characterization of genistein-loaded, K-carrageenan/ quaternized dextran gels

The quaternization of dextran was confirmed by <sup>13</sup>C NMR and <sup>1</sup>H NMR analysis. The vial inversion method was used to confirm the gel formation and gels were characterized further by FT-IR, rheology, swelling and degradation, and FESEM. FT-IR was done in the ATR mode (Bruker Tensor). Field emission scanning electron microscopy (FESEM) was used to analyze the morphology of gels. The gels were freeze-dried and mounted on metal stubs. The surface was sputter-coated using platinum. The images were taken using a JEOL JSM-6610LV microscope with a tungsten filament at an accelerating voltage of 10 kV.

# 4.3.4. Viscoelastic analysis

The viscoelastic properties of gels were analyzed by performing rheology using an Anton Paar MCR 102 rheometer with a 25 mm parallel plate arrangement and a 0.3 mm shear gap. The 200 μL of gel was fabricated and subjected to amplitude sweep, frequency sweep, and self-healing measurements. For amplitude sweep, different strains ranging from 1% (low) to 1000% (severe) were applied to the gels. For the frequency sweep, a constant strain of 1% was applied at a varied frequency ranging from 1 to 100 rad/sec. To examine gels capacity for self-healing, six consecutive cycles of alternating intense (1000%) and low strains (1%) were applied to the gels. To check the injectable potential of gel, 500 μL was loaded in 1 mL of syringe and extruded<sup>33</sup>.

#### 4.3.5. Self-healing (dye diffusion method)

The genistein-loaded gel was fabricated in a mould to form a circular shape. Using a surgical blade, the gel was divided into two halves. Rhodamine dye was added to one of the halves, while the other one remained untreated. Both halves were kept in close contact with each other and visually inspected at different time intervals (0 h, 12 h, and 24 h) to study the diffusion of dye across the unloaded half<sup>34</sup>.

#### 4.3.6. Swelling and degradation

Phosphate buffer (7.4) at 37 °C was used to study the swelling and degradation of gels at different time intervals for 15 days<sup>35</sup>. Gels were immersed in phosphate buffer (1 mL) and incubated for around 24 h at 37 °C. After regular time intervals, the buffer was removed from the gel and weighed. The data was expressed in terms of swelling percentage and was calculated by the following equation:

Swelling ratio (%) = 
$$\left(\frac{W_S - W_0}{W_0}\right) \times 100$$
 Equation 4.1

where, Ws is the weight of swollen gel at time t and Wo is the initial weight.

## 4.3.7. Antioxidant properties

The ABTS assay was used to study the free radical scavenging activity of gels as discussed earlier. The 7 mM of ABTS solution was prepared in distilled water with an equal volume of 2.45 mM of potassium persulfate solution. This solution was kept at RT for 12 h in the dark to form ABTS radical. The absorbance was then adjusted to 0.8 at 734 nm using PBS (7.4), and 200  $\mu$ L of ABTS radical was added to 100  $\mu$ L of samples (gels) and further incubated for 1 h at 37 °C. After 1 h, 100  $\mu$ L of solution was withdrawn and absorbance was measured at 734 nm using a plate reader. The absorbance of the supernatant was measured at 734 nm<sup>36</sup>.

#### 4.3.8. *In vitro* drug release studies

The genistein-loaded polymeric gel was used to measure the *in vitro* drug release in phosphate buffer of pH 7.4. The 1 mL of release medium was then added to the gels and incubated with constant shaking of 100 rpm at 37 °C. The study was performed for 28 days. The 1 mL of release media was entirely removed at different time intervals and replaced with fresh buffer at various times. The amount of drug release was measured using a UV-visible spectrophotometer at  $\lambda$  max of 280 nm by measuring the absorbance using a glimepiride standard curve<sup>37</sup>.

#### 4.3.9. Cell culture studies

The murine pre-osteoblast cells (MC3T3-E1) and murine leukemic monocyte macrophage cell lines (RAW 264.7) were grown in MEM- $\alpha$  and DMEM media respectively, enriched with 10% FBS and 1% Penstrep antibiotic solution at 37 °C. For further cell culture experiments, cells were allowed to

grow till 70-80% confluency and harvested using a trypsin solution. The cells were then resuspended in a complete medium and seeded in tissue culture plates to conduct different cell culture assays. For osteogenic studies, osteogenic media was taken as a positive control containing MEM- $\alpha$  supplemented with 10% FBS, 1% antibiotic, 10 mM  $\beta$ -glycerophosphate disodium salt, 100 nM dexamethasone, hydrate, and 50  $\mu$ g/mL ascorbic acid<sup>38</sup>.

#### 4.3.8.1 MTT assay

The MTT assay was performed to check the percentage cell viability of MC3T3-E1 cells. Cells were seeded in 96-well plate. After 24 h, media was withdrawn from cells, and cells were treated with gel releasates and incubated at 37 °C for another 24 h. MTT solution (20  $\mu$ L) was added to each well and further incubated for another 3.5 h. Purple formazan crystals formed were dissolved using 100  $\mu$ L DMSO and absorbance was recorded at 570 nm. The absorbance of untreated cells was used to calculate the vitality of the cells.

% Cell viability 
$$\frac{\text{Absorbance of sample}}{\text{Absorbace of control}} \times 100$$

**Equation 4.2** 

#### 4.3.8.2 Live-dead assay

Live-dead assay was conducted on MC3T3-E1 cells using instructions (Invitrogen, LIVE/DEAD viability/cytotoxicity kit) to further confirm the cell viability. Followed by the treatment with samples for 24 h, samples were withdrawn and the cells were stained using a mixture (150  $\mu$ L) of calcein AM and ethidium bromide to stain live and dead cells. The cells were incubated for another 30 min avoiding any exposure to light. The images were acquired using a fluorescence microscope.

#### 4.3.8.3 Cytoskeletal staining

Cells were grown in a 6-well plate and incubated at 37 °C for 24 h. The media was then withdrawn and replaced with 1 mL of gel releasates and further incubated for another 24 h. This was followed by washing with phosphate buffer saline fixed with paraformaldehyde (4%) and incubated for another 30 min. After the incubation, the cells were washed with (PBS). Cells were permeabilized using triton X-100. For 30 min in the dark, the permeabilized cells were exposed to Alexa Fluor 488 phalloidin solution to stain F-actin. The cell nuclei were stained for 10 min with DAPI solution (1 µg/mL) and then rinsed with PBS. Cells were then examined under a fluorescence microscope.

#### 4.3.8.4 Reactive oxygen scavenging (ROS) scavenging activity

The effect of gels to scavenge the reactive oxygen species (ROS) generated in MC3T3-E1 cells was investigated using  $H_2$ -DCFDA. The 48 well black plate was used to grow the cells at a concentration of  $2 \times 10^4$  cells/ mL. The media was replaced after 24 h with 100  $\mu$ l gel releasates in incomplete media and incubated for another 24 h. For initiating the ROS production cells were exposed to 0.5

mM  $H_2O_2$  solution, followed by PBS washing and further exposure to DCFDA solution (25  $\mu$ M) for 1 h in the dark. The solution was removed and PBS was added, and cells were visualized for intracellular DCFDA using fluorescence microscope<sup>39</sup>.

### 4.3.8.5 *Scratch assay*

The six-well plate was used to seed MC3T3-E1 cells and was allowed to grow till 100% confluency. With the help of a sterile tip, a scratch was made on the cell monolayer. The cell debris was removed by rinsing the well plate with PBS followed by the addition of samples. After 12 and 24 h, the images of healing were taken using an Evos XL core and Invitrogen microscope. The results obtained were compared to the control and analyzed using Image J software.

#### 4.3.10. *In vitro* osteogenic studies

Alkaline phosphatase (ALP), calcium deposition assay, and gene expression studies were conducted to evaluate the osteogenic potential of gels. Cells were grown in a 48-well plate at a concentration of  $1\times10^5$ /mL. After 7 and 14 days, the media was removed and the cells were exposed to 200  $\mu$ L of gel extracts. After every 72 h, cells were replenished with fresh gel extracts. Osteogenic media (OM) was taken as positive control.

#### 4.3.9.1 ALP assay

To determine the ALP activity, cells were first rinsed with DPBS after 7 and 14 days. The cells were lysed using 200  $\mu$ L triton X (0.2%) for 30 min. The cell lysate was treated with 200  $\mu$ L p-nitrophenylphosphate (pNPP) solution and incubated at 37 °C for 90 min. Absorbance was measured at 405 nm using a plate reader.

#### 4.3.9.2 Calcium deposition

Calcium deposition on MC3T3-E1 cells was assessed using Alizarin Red S stain. When calcium binds to Alizarin Red S, it forms red-colored crystals. These crystals can be observed under a bright field microscope, providing a clear indication of calcium presence in the cells. On days 7 and 14 of cell culturing, the cells were rinsed with DPBS and fixed with a paraformaldehyde solution (4%). After a subsequent rinse with DI water, the fixed cells were stained with 500  $\mu$ L of alizarin red S solution for 1 h in the dark. Post-staining, the cells were washed with DI water to remove any excess dye and were then visualized under an inverted microscope to observe the red crystals. To further quantify the total calcium deposited in the mineralized cells, 200  $\mu$ L of 10% cetylpyridinium chloride solution was added to each well and incubated for 30 min in the dark. Approximately 100  $\mu$ L of the dissolved crystals were then transferred to a 96-well plate and the absorbance was measured at 562 nm.

#### 4.3.9.3 Gene expression analysis

The expression of markers linked to osteogenesis, such as alkaline phosphatase (ALP), runt-related transcription factor 2 (RUNX2), osteocalcin (OCN), and osteopontin (OPN) were measured to assess the impact of gels on osteogenic differentiation. Cells were seeded at a density of  $1 \times 10^4$  cells/mL on a 6-well plate and were allowed to grow. After 24 h, the media was withdrawn and 1 mL of gel extract was added. After 7 and 14 days, complete cellular RNA was extracted using TRIzol lysis followed by cDNA synthesis. Using the quantitative real-time polymerase chain reaction, the levels of particular genes were evaluated (qRT-PCR). GAPDH was used as a housekeeping gene. The gene primer sequences are displayed in **Appendix Table A3**.

#### 4.3.9.4 *Tartrate-resistant acid phosphatase (TRAP) assay*

TRAP activity is a key cytochemical marker of osteoclasts, with its serum concentration serving as a biochemical indicator of osteoclast function and bone resorption. TRAP expression is linked to the activation and differentiation of osteoclasts. RAW 264.7 cells were induced by treating RANKL (200 ng mL<sup>-1</sup>) for 14 days. Cells were collected from scaffolds at predefined intervals, lysed with a 1 RIPA buffer, and collected by centrifugation at 4 °C. The supernatants were incubated with p-nitrophenyl phosphate solution for 30 min at 37 °C and the reaction was stopped by adding 500 mL of 1 N NaOH. TRAP activity was determined by measuring the conversion of p-nitrophenyl phosphate to p-nitrophenol. Optical density was determined using a microplate reader at a wavelength of 405 nm.

# 4.3.11. Statistical analysis

The studies were conducted in triplicate, with results presented as mean values and standard deviations (n = 3). Data were analyzed using Student's t-test. \*p values  $\leq 0.05$  were considered significant and ns suggests a non-significant difference.

#### 4.4 Results and discussion

The aim of this work was to investigate the effect of genistein-loaded quaternized dextran and  $\kappa$ -carrageenan to treat bone regeneration in osteoporotic conditions. Genistein is a phytoestrogen that mimics the effects of estrogen, and helps in bone formation and reducing bone resorption. Quaternized dextran provides a biocompatible and biodegradable scaffold that enhances cellular adhesion and proliferation, needed for the formation of new bone.  $\kappa$ -carrageenan, a natural polysaccharide, offers excellent gel-forming ability and mechanical strength, which improves the structural integrity of the composite. Together, these components create a conducive microenvironment for osteoblast activity, facilitating the deposition of bone matrix, and restoring bone density in osteoporotic patients. Herein, we have developed genistein-loaded gels and evaluated their viscoelastic, antioxidant, and osteogenic properties (**Figure 4.1**).

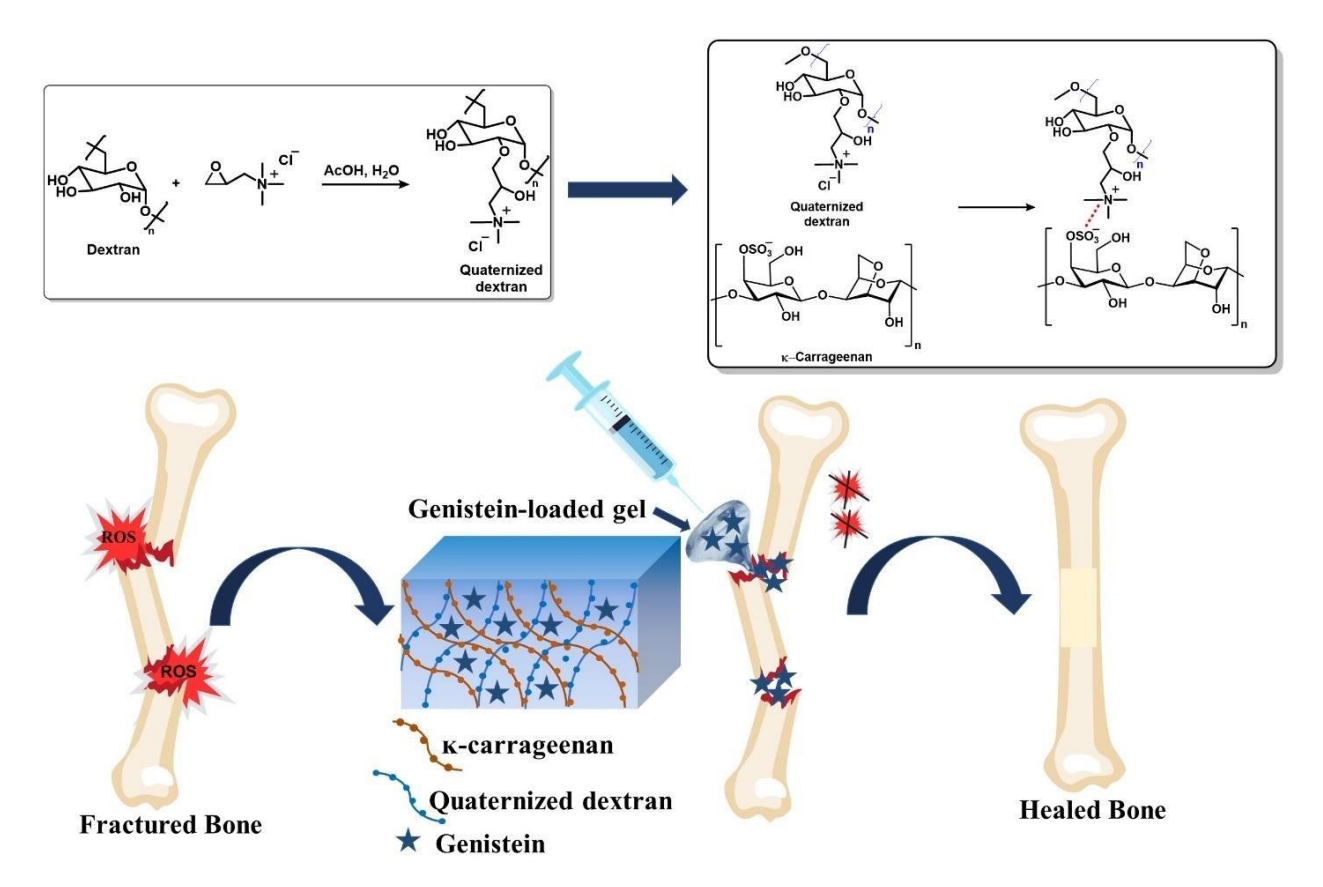


**Figure 4.1.** Genistein-loaded  $\kappa$ -carrageenan and quaternized dextran gels for effective bone regeneration in osteoporotic conditions.

# 4.4.1. Synthesis and characterization of quaternized dextran (QDex)

Quaternization of dextran was performed by grafting the GTMAC on dextran. The successful grafting was confirmed by FTIR analysis. A peak at 1480 cm<sup>-1</sup> in FTIR spectrum was assigned to the methyl group of ammonium<sup>40</sup>. In <sup>1</sup>H NMR spectra of quaternized dextran, a distinctive peak at 3.1 ppm was observed, while in <sup>13</sup>C NMR of quaternized dextran, peaks were obtained at 96.3 ppm and 80 ppm, both of which supported the quaternization of dextran (**Figure. 4.2**).

# 4.4.2. Fabrication and characterization of QDex-κ-C gel (UG) and genistein-loaded gel (LG)

Unloaded gels (UG) were fabricated by first dissolving QDex and  $\kappa$ -Carrageenan ( $\kappa$ -C) in distilled water separately, which were mixed in different ratios to develop unloaded gels. To develop a genistein-loaded gel, genistein solution was added to the quaternized dextran solution followed by the addition of  $\kappa$ -carrageenan solution, resulting in the formation of loaded gels. Sulphate groups in carrageenan (1212 cm<sup>-1</sup>) were shifted to 1237 cm<sup>-1</sup> and the broadening of a peak at 1709 cm<sup>-1</sup> was also observed indicating the formation of gel<sup>41,42</sup> (**Figure. 4.2**). The formation of gel was confirmed by the vial inversion method (**Figure 4.3 b**).

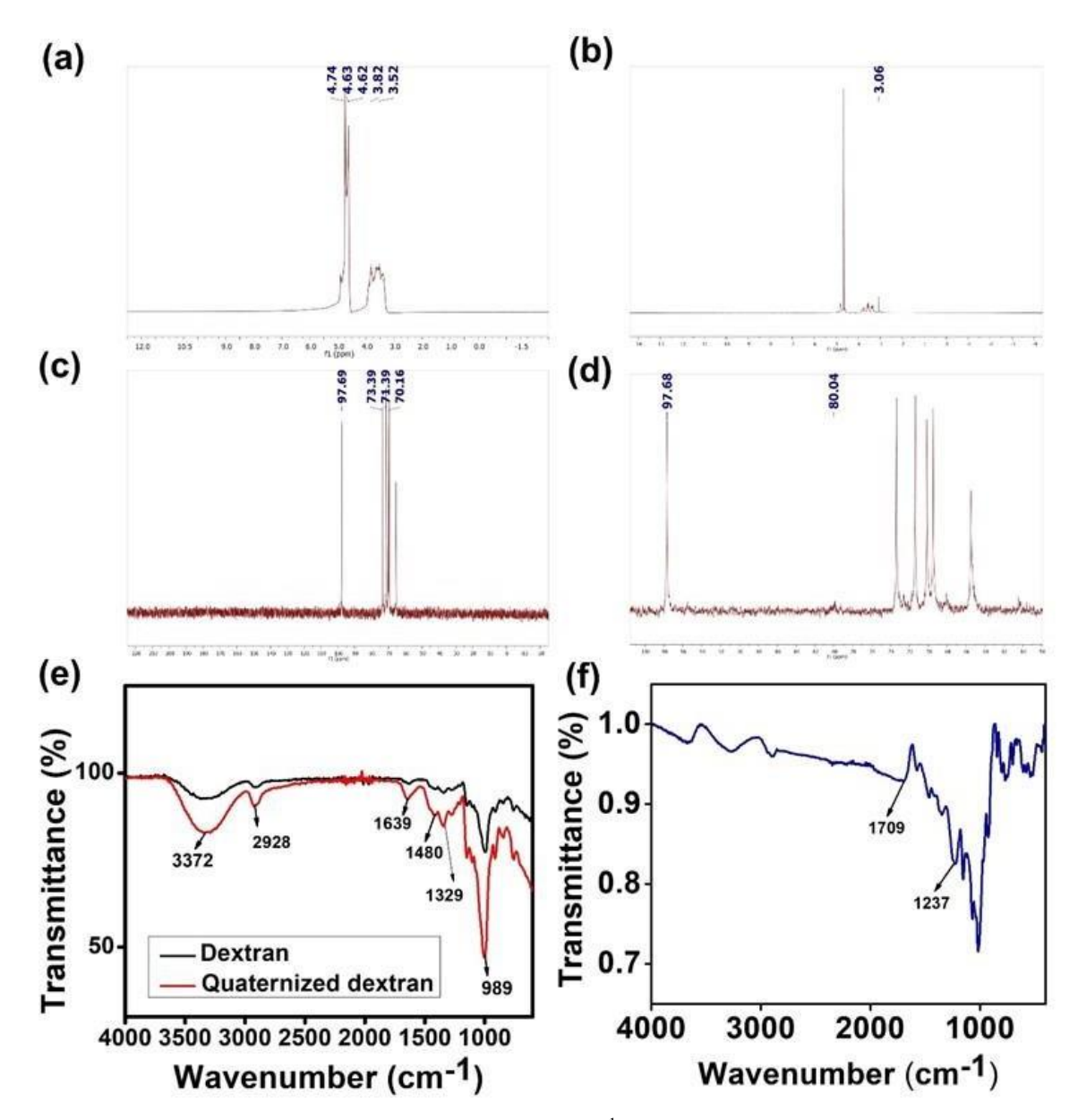


**Figure 4.2.** Characterization of polymers and gel. (a, b) <sup>1</sup>H NMR spectra of dextran and quaternized dextran. (c, d) <sup>13</sup>C NMR of dextran and quaternized dextran. (e) FTIR of dextran and quaternized dextran. (f) FTIR spectrum of gel.

The surface morphology of gels also plays a vital role in tissue regeneration applications, as porosity and pore size are critical parameters for scaffolds in biomedical applications, and porous and interconnected networks are essential for cell nourishment, proliferation, and tissue development<sup>43</sup>. The freeze-dried gel was cut and visualized under FESEM for morphological analysis, which confirmed the fibrous nature with porous morphology (**Figure 4.3 c**). The porous structure of the gels was similar to that of the cellulose nanocrystals-loaded polyacrylamide/sodium alginate/silica hydrogels, which were designed for bone tissue regeneration applications<sup>44</sup>. Self-healing gels have become attractive biomaterials due to their ability to repair their initial structure and properties in

response to damage, thus, showing potential in different biomedical applications including drug delivery, cell therapy, and tissue engineering<sup>45</sup>. The visual self-healing ability of gels was estimated by cutting a gel into equal halves. Half of the gel was loaded with rhodamine dye, kept in contact with the unloaded part, further incubated at 37 °C, and visualized after regular time intervals. The dye started migrating after 6 h and showed complete migration after 24 h, indicating the self-healing potential of the gel (**Figure 4.3 a**).

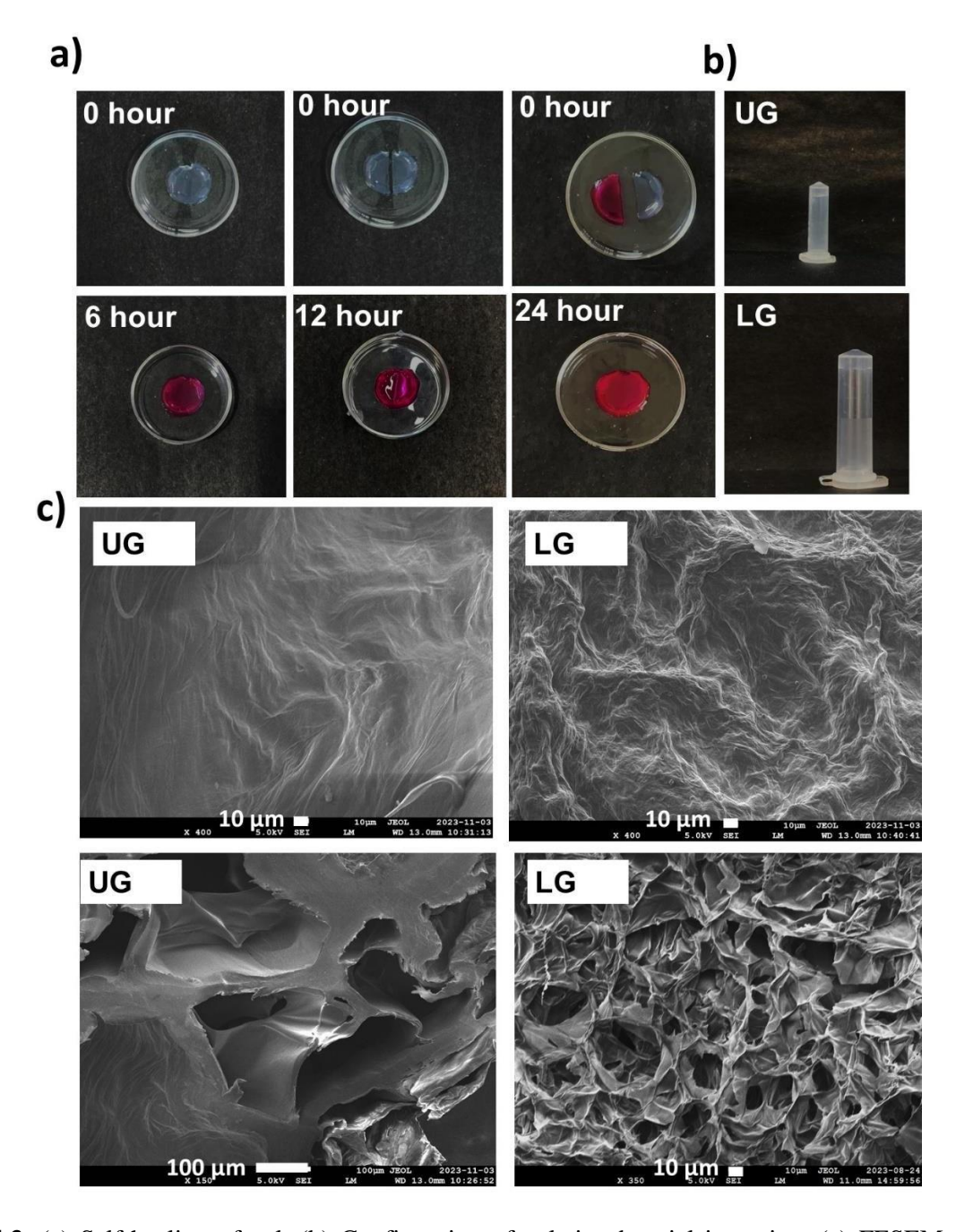


**Figure 4.3.** (a) Self-healing of gel. (b) Confirmation of gelation by vial inversion. (c) FESEM images showing surface morphology of loaded (LG) and unloaded gels (UG). Scale bar:  $10 \, \mu m$  and  $100 \, \mu m$ .

#### 4.4.3. Rheological analysis

The mechanical strength of gels is also an important parameter for biomedical applications. To study the viscoelastic properties of gel, a rheometer was used. The gels were developed in different ratios (2% QD, 2% C (1:1), 2% QD, 2% C (1:2), 2% QD, 3% C (1:2) and allowed to stand for 24 h and further subjected to different rheological studies. An amplitude sweep was first performed to assess the linear viscoelastic range (LVE) of the gel. Variable strain from 0.01% to 1000% was applied to UG and LG gels. The results indicated that the gels were able to retain their linear viscoelastic properties till 1% strain. The drug-loaded gels were relatively stiff with relatively higher storage modulus values (G':  $\sim$ 1.4 kPa for unloaded gels and  $\sim$ 3.1 kPa for loaded gels), which were higher as compared to G' of 619 Pa, reported for the hydrogel developed for bone regeneration applications<sup>46</sup> (**Figure 4.4 a**).

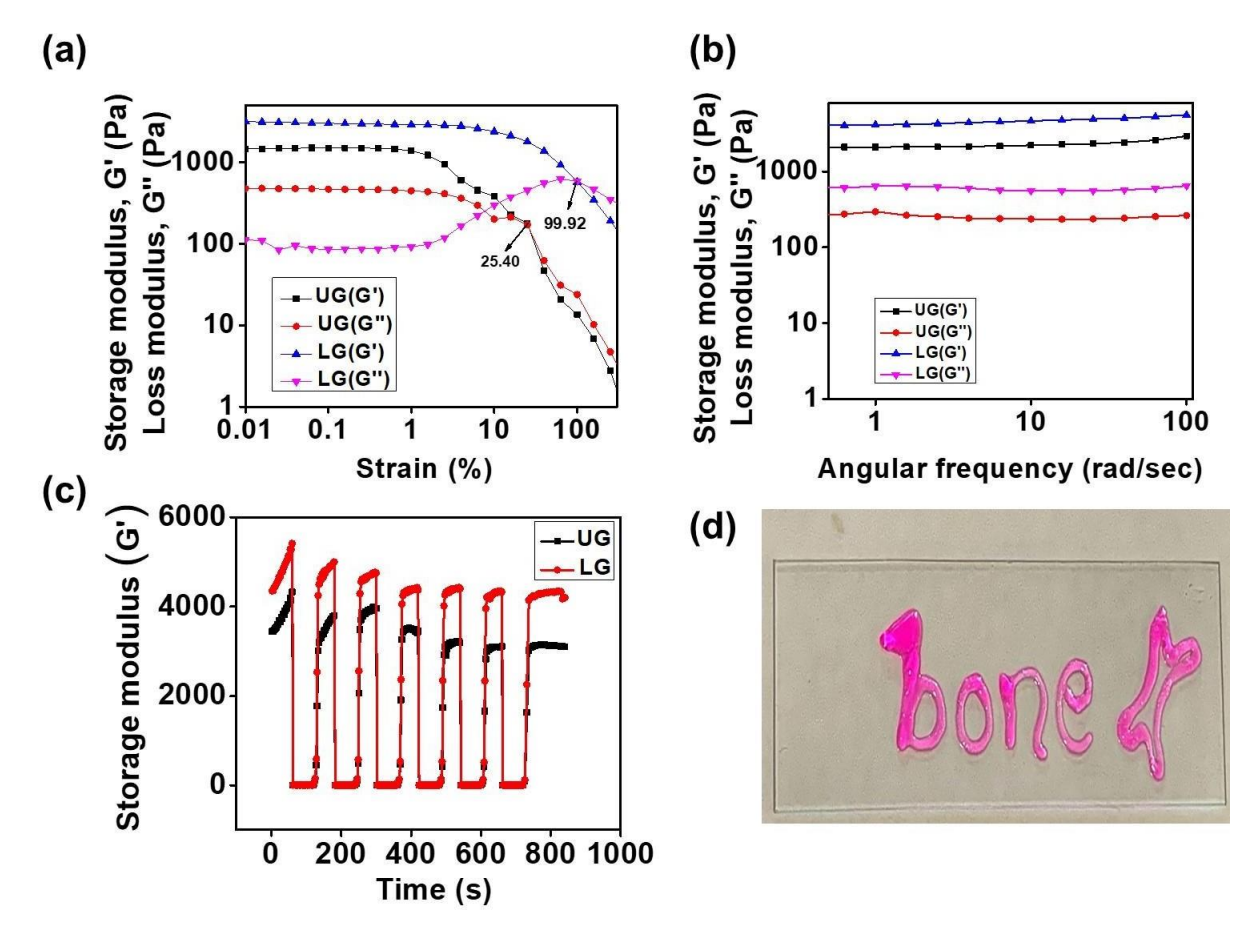


**Figure 4.4.** Rheological properties of gel. (a) Amplitude sweep studies showing G' and G" at different strains. (b) Frequency sweep studies showing G' and G" at different angular frequencies. (c) Self-healing characteristics of gel subjected to alternative high and low strains.

The storage modulus and crossover point of drug-loaded gel (LG) increased, which might be because of hydrogen and hydrophobic interaction between the drug and polymeric gel. Strain (1%) was taken as the constant amplitude for frequency sweep studies. The gels demonstrated mechanical

robustness across the angular frequency range of 0.01 to 100 rad/s (**Figure 4.4 b**). The self-healing property of gels is useful for its injectable potential, as it allows the loading of active moieties and their delivery. The self-healing properties of the gel were confirmed by subjecting the gels to alternating cycles of high (1000%) and low (1%) strain. The gels were able to regain their structure after high strain was removed, indicating their self-healing properties (**Figure 4.4 c**). The gel was also able to extrude easily from the syringe, indicating its thixotropic characteristics (**Figure 4.4 d**). The amplitude sweeps of 2% QD, 2% C (1:1) and 2% QD, 2% C (1:2) gels showed lower storage modulus when compared with gels made from 2% QD, 3% C (1:2) (**Figure A10, Appendix**). The frequency sweep of 2% QD, 2% C (1:1) and 2% QD, 2% C (1:2) gels also showed similar properties (**Figure A11, A12 Appendix**). The storage modulus and cross-over point of gels made from 2% quaternized dextran and 3% κ-carrageenan in a 1:2 ratio were higher, indicating greater strength. Therefore, this concentration was chosen for further studies, as strength is crucial for materials intended for bone regeneration.

# 4.4.4. Swelling and degradation

The swelling and degradation behavior of gels was also studied using phosphate buffer (pH 7.4) for 15 days. The genistein-loaded gel started to swell, for the initial 24 h and showed maximum swelling of 25.45%. After 24 h, the gels showed maximum degradation of 24% (**Figure 4.5a**). The initial swelling is because of the hydration of the gel matrix. The phosphate buffer might cause the sulfate groups in  $\kappa$ -carrageenan and the quaternized amine groups in QDex to interact with water molecules, leading to the swelling. The degradation was observed after 24 h, and it reached up to 24%, which can be attributed to hydrolytic cleavage of the polymer backbone or the breakdown of ionic cross-links<sup>47</sup>.

#### 4.4.5. Drug release studies

The gels were loaded with genistein and release studies were conducted in physiological conditions to understand the release kinetics of genistein at physiological pH (7.4). The 1 mL of release medium was sampled at designated intervals and replaced with fresh medium. The amount of genistein released was determined by measuring absorbance at 280 nm using a microplate reader. The experiment was performed in triplicates. The release data was fitted using KinetDs software. The release followed a zero-order kinetics indicating that the drug was released at a constant rate over time, independent of the concentration of the drug (**Figure 4.5b**). This can be compared to the zero-order controlled release of the BMP2-derived peptide P24 from a chemically grafted chitosan scaffold, which was designed to promote osteogenesis *in vitro* and enhance bone repair *in vivo*<sup>48</sup>.

#### 4.4.6. Antioxidant assay

Oxidative stress plays a notable role in bone regeneration, as an increased level of oxidative stress can impair the bone healing process by promoting the activity of osteoclasts, resulting in increased bone resorption and reduced osteoblast function<sup>49</sup>. Managing oxidative stress through antioxidants

can help support bone regeneration by protecting bone cells, enhancing osteogenesis, and improving the overall healing process. In this study, the antioxidant capacity of gels was measured by using ABTS assay. A solution with the presence of free radicals, which appears to be a colored solution, was reduced to a colorless state by antioxidants, demonstrating the antioxidant potential of materials. The antioxidant activity of genistein-loaded gel was found to be 87.45%, and it was comparable to positive control ascorbic acid (**Figure 4.5c**). The antioxidant activity of genistein-loaded gel was more than that of unloaded gel, which is because of the presence of genistein, which is proven to have antioxidant properties<sup>49</sup>. The antioxidant activity was greater than the 53.95% for hydrogel fabricated from carboxymethyl chitosan grafted with protocatechuic acid<sup>51</sup> and comparable to PCL/bioactive glass-based biomaterials developed to deliver polyphenolic compounds<sup>52</sup>.

### 4.4.7. Cell viability and cell migration studies

While developing biomaterials for bone regeneration, cell viability is crucial because it affects how well the material promotes tissue integration and repair. The cytocompatibility of gels was measured by MTT assay using MC3T3-E1 cells. Unloaded and loaded gel showed >85% cell viability (Figure **4.6 a**). The results were comparable to polyester-alginate-based biodegradable hydrogels<sup>52</sup> and gelatin and chitosan-based composite hydrogel fabricated for biomedical applications<sup>54</sup>. A Live/dead assay was also conducted to further confirm the cytocompatibility of gels. The images showed the predominance of green signal, further confirming the cytocompatible nature of unloaded and loaded gels (**Figure 4.6 b**). Also, the migration of mesenchymal stem cells is a critical process in bone fracture healing, as these cells must travel to the bone surface to contribute to new bone formation<sup>54</sup>. Therefore, the materials that promote cell migration are of prime importance in the bone regeneration process. The scratch healing abilities of gel were also measured. The genistein loaded gels showed maximum scratch closure where the scratch was reduced from 39% to 2.74%. This might be because of the presence of κ-carrageenan and genistein. Studies have shown that carrageenan helps in osteoblasts proliferation and differentiation<sup>55</sup>. Also, many research studies have further confirmed the effect of genistein on cell proliferation, osteogenic gene expression, and osteogenic differentiation in human and mouse bone mesenchymal stem cell cultures.<sup>57</sup>

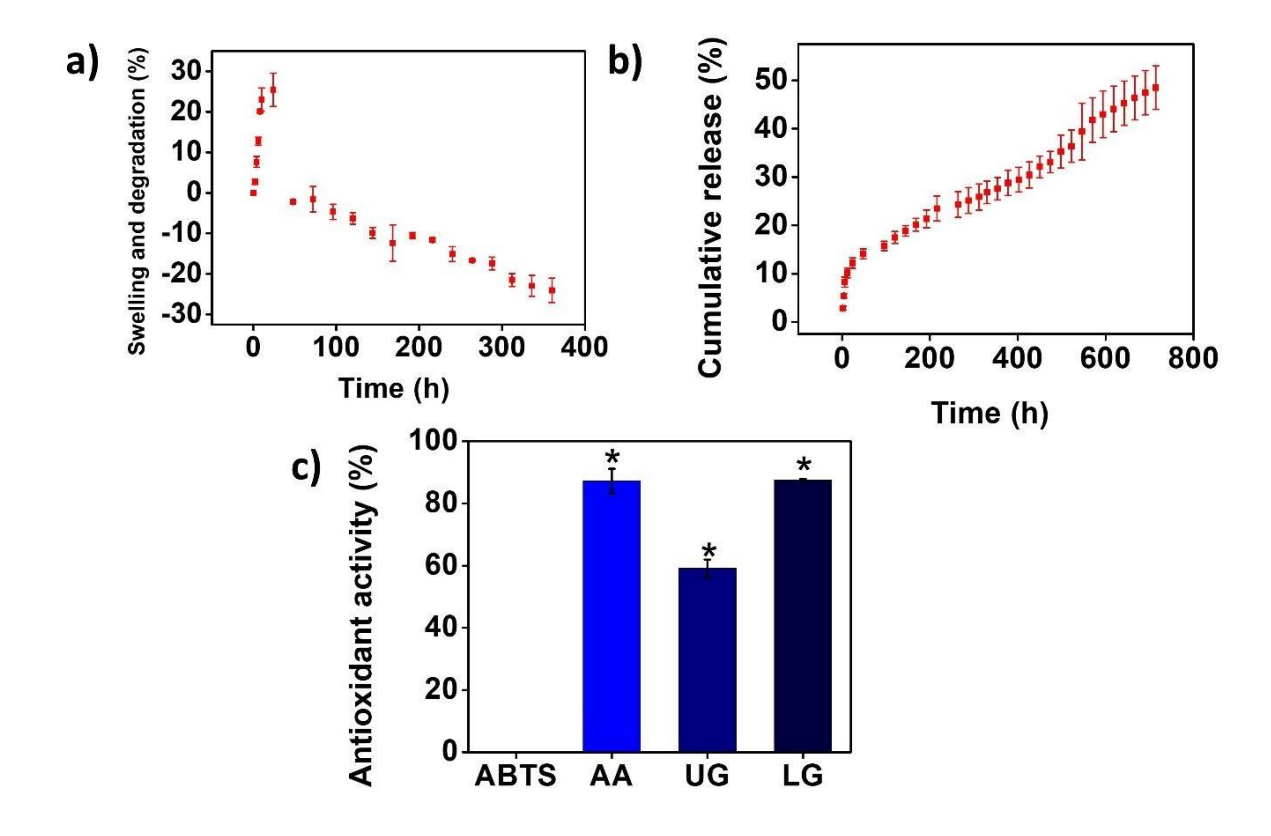


**Figure 4.5.** (a) Swelling and degradation of unloaded (UG) and loaded gels (LG). (b) Percentage cumulative release of genistein from loaded gels. (c) Antioxidant activity of gels by ABTS assay, where ABTS and ascorbic acid (AA) were used as negative and positive controls. Data is reported as mean  $\pm$  SD (n = 3). \*p < 0.05 indicates data is statistically significant.

#### 4.4.7. ROS scavenging assay

Reactive oxygen species (ROS) play a role in bone homeostasis and remodeling by promoting bone resorption<sup>57</sup>. Enhancing antioxidant defenses can help prevent estrogen deficiency-induced osteoporosis. Thus, the development of biomaterials with antioxidant potential can be beneficial in regulating osteoclast formation and function and could be a promising treatment for osteoporotic bone defects. H<sub>2</sub>O<sub>2</sub> was used to create oxidative stress in MC3T3-E1 cells and 2',7'-dichlorofluorescein diacetate (DCFDA) was used to estimate the ROS scavenging capacity of the genistein-loaded gels. The intracellular ROS formation was inhibited by genistein-loaded gels, resulting in decreased fluorescence intensity (**Figure 4.7a**). The incorporation of genistein enhanced the ROS scavenging ability as genistein is proven to have antioxidant activity<sup>58</sup>. The findings were consistent with those obtained using cerium incorporated mesoporous glass/alginate beads for bone regeneration<sup>59</sup>

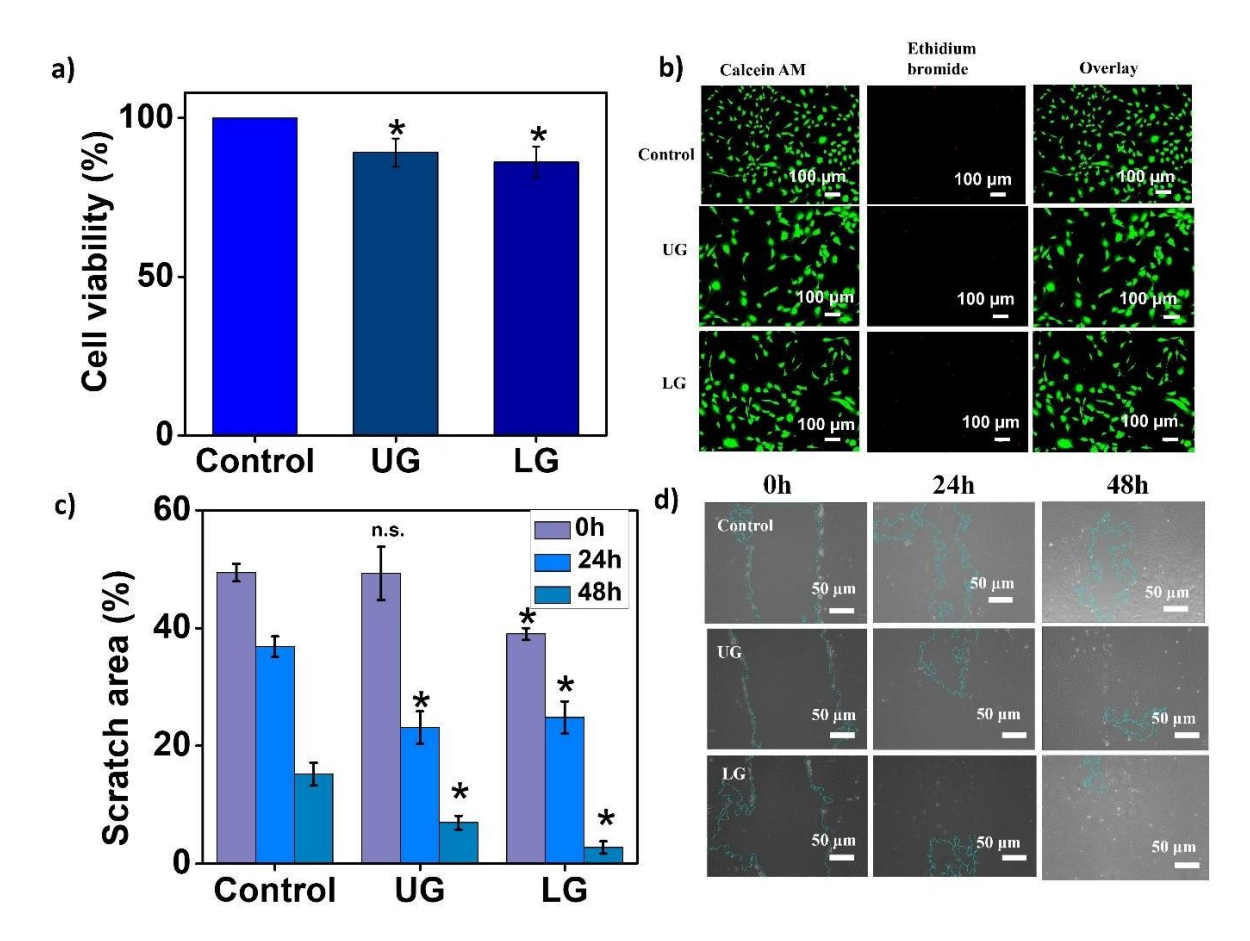


**Figure 4.6.** Cell viability and scratch healing of MC3T3-E1 cells in the presence of unloaded (UG) and genistein-loaded gels (LG). (a) MTT assay. (b) Live-dead assay. Scale bar: 100  $\mu$ m. (c-d) Scratch assay. Scale bar: 50  $\mu$ m. Data is reported as mean  $\pm$  SD (n = 3). \*p < 0.05 indicates data is statistically significant and n.s. indicates non-significant difference.

#### 4.4.8. Cytoskeletal staining

Maintenance of uniform shape and morphology in biomedical applications ensures improved biocompatibility, consistent functionality, and cellular interactions for reliable therapeutic outcomes. To study the effect of the gel on cell morphology, cytoskeletal staining was performed where Alexa Fluor 488 phalloidin was used to stain the cytoskeleton green and DAPI was used to stain the nucleus. The cells were able to maintain their fibroblast-like shape with extended cytoplasmic projection morphology, indicating that genistein-loaded gels were safe for cells (**Figure 4.7b**).

# 4.4.9. Osteogenic studies

Osteogenic studies are needed for bone regeneration applications to understand the ability of biomaterials to support stem cell differentiation into osteoblasts, bone formation promotion, and ensure successful integration with existing bone tissue. Alkaline phosphatase activity and alizarin red assay were performed to estimate the osteogenic potential of gels. Cells were grown in 48 well plates at a density of  $1 \times 10^5$ /mL. After 24 h, media was replaced with 200  $\mu$ L of gel releasates and

incubated for 7 and 14 days. MEM- $\alpha$  without sample was used as a negative control and osteogenic media (ascorbic acid, 50  $\mu$ g/mL, 10 mM  $\beta$ -glycerophosphate, and 100 nM dexamethasone) was taken as a positive control.

Alkaline phosphatase activity

Alkaline phosphatase (ALP) catalyzes the hydrolysis of phosphate esters and is essential for normal skeletal mineralization, making it the most widely recognized marker of osteoblast activity<sup>60</sup>. Therefore, ALP activity is an important marker. With an increase in incubation time, the expression of ALP increased. The ALP activity of loaded gels was comparable to the osteogenic media (**Figure 4.8a**). This might be because of the presence of genistein as studies have shown the stimulatory effect of genistein on protein synthesis and alkaline phosphatase<sup>61</sup>. Also, studies have shown that the incorporation of dextran in scaffolds enhances the osteogenic markers, including ALP<sup>62</sup>.

# Alizarin red assay

A calcium deposition assay is crucial in bone regeneration studies because it quantifies the mineralization process, indicating the effectiveness of materials or treatments in promoting new bone formation, which is essential for assessing the potential of biomaterials or therapies to support bone repair and growth. The Alizarin red assay is widely performed to analyze the calcium deposition properties of biomaterials. Briefly, Alizarin red S binds with calcium salts specifically and stains mineralized areas in cells. The intensity of the red color indicates the extent of calcium deposition, which can be quantified to evaluate the mineralization capacity of biomaterials in promoting bone regeneration. The unloaded and genistein-loaded gels showed enhanced calcium deposits when compared with untreated cells. The more value was seen in the case of genistein-loaded gels comparable to osteogenic media (**Figure 4.8 b,c**). The results were comparable to those observed in the study examining the biological responses and mechanisms of human bone marrow mesenchymal stem cells to Zn and Mg biomaterials<sup>63</sup> and better than phytoestrogen, quercetin-loaded scaffold for osteoporotic bone regeneration<sup>22</sup>.

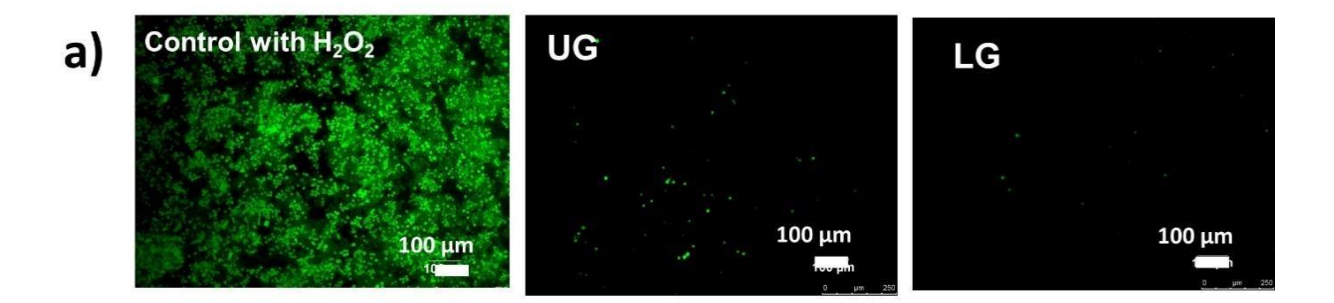


**Figure 4.7.** (a) Fluorescence microscopy images of MC3T3-E1 cells treated with gel and DCFDA. Scale bar: 100 μm.

This might be due to the presence of genistein, which has been proven to enhance calcium deposition<sup>64</sup>. Also, some studies have shown that dextran can bind to bone morphogenic protein 2 and increase its activity, thus facilitating the osteogenesis process<sup>65</sup>. So, the enhanced calcium deposits might be because of a combination of quaternized dextran and genistein.

#### **4.4.10. TRAP assay**

The effect of unloaded and loaded gels on the osteoclast differentiation was performed to analyze TRAP activity (**Figure 4.8c**). TRAP activity is a key cytochemical marker for osteoclasts, and its serum concentration serves as a biochemical indicator of osteoclast function and bone resorption levels. RAW 264.7 cells were treated with RANKL (200 ng/mL) for 14 days. The cells treated with loaded gels (LG) showed decreased activity of TRAP. The results further confirm that genistein-loaded gels are beneficial in suppressing osteoclast differentiation while simultaneously promoting osteoblast differentiation. The results were comparable to phytoestrogen-loaded calcium phosphate scaffold<sup>22</sup>.

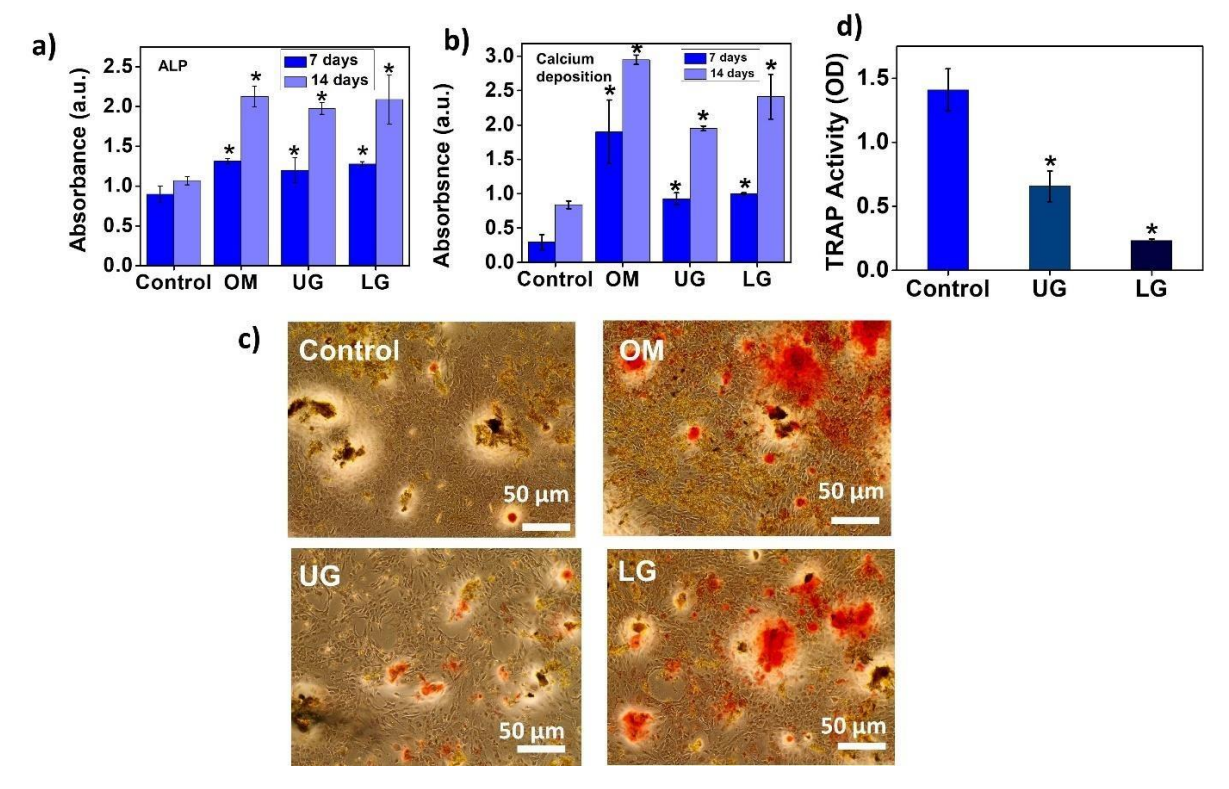


**Figure 4.8.** (a) Alkaline phosphatase (ALP) activity of MC3T3-E1 cells after 7 and 14 days. (b) Quantitative analysis of calcium deposits on MC3T3-E1 cells after 7 and 14 days. Data are presented as mean  $\pm$  SD, n = 3, and \*p < 0.05 indicates the statistical significance and ns indicates a non-significant difference. (c) Microscopic images of MC3T3-E1 cells after 14 days of treatment. Scale bar: 50  $\mu$ m. (d) TRAP activity of RAW 264.7 cells with RANKL after 14 days of treatment.

#### Gene Expression Studies

Gene expression studies were performed to assess the impact of samples on the expression of osteogenic markers, including alkaline phosphatase (ALP), an early indicator of osteoblast differentiation, RUNX2, a critical transcription factor for bone formation, Osteocalcin (OCN), a bone matrix protein, and Osteopontin (OPN), a multifunctional protein involved in bone remodeling and mineralization were analyzed. Expression of the genes was more in cells treated with genistein-loaded gels when compared with control and unloaded gels (**Figure 4.9**). The increased expression in the case of loaded gels might be because of the presence of phytoestrogen, genistein as many studies have demonstrated its activity in the promotion of osteogenic gene expression in human and mouse bone marrow mesenchymal stem cell cultures<sup>57</sup>. The enhanced expression shows that materials developed in this study have the potential to promote mesenchymal stem cell differentiation and can be utilized as scaffolds for the treatment of bone-related disorders.

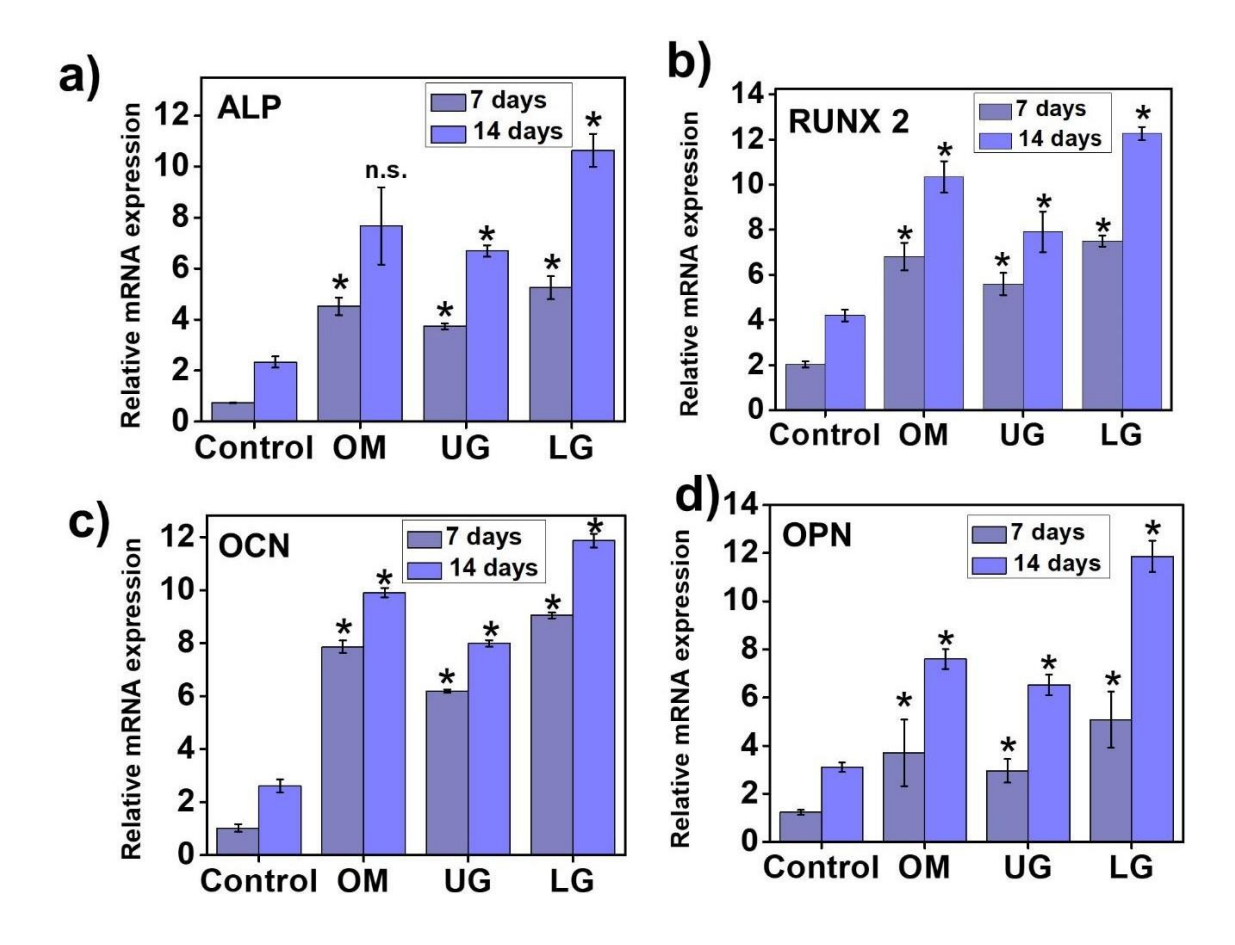


**Figure 4.9.** Gene expression studies. (a–d) Expression of ALP, RUNX 2, OCN, and OPN in MC3T3-E1 cells after culturing with OM and gels for 7 and 14 days. The data are presented as mean  $\pm$  SD (n = 3), and \*p < 0.05 values indicate significant difference from the control, whereas n.s. indicating non-significant differences.

#### 4.5. Conclusions

In conclusion, we have successfully developed a novel drug-loaded polymeric gel system tailored for bone regeneration in osteoporotic conditions. This gel, composed of quaternized dextran and  $\kappa$ -carrageenan, was loaded with the phytoestrogen genistein, known for its estrogen-mimicking properties. The fabricated gel exhibited excellent cytocompatibility, supported cell viability, and promoted cell migration, essential factors for effective tissue regeneration. In addition to cytocompatibility, the gel was also able to show notable reactive oxygen species (ROS) scavenging capabilities, as confirmed by the  $H_2$  DCFDA assay, which is crucial in mitigating oxidative stress associated with osteoporotic bone loss. The osteogenic potential of the gel was further validated through alkaline phosphatase, alizarin red assay, and gene expression studies, which demonstrated enhanced alkaline phosphatase activity, increased calcium deposition, and upregulated gene

expression of osteogenic markers, all of which are crucial indicators of bone formation. Moreover, the TRAP assay revealed a decrease in osteoclast resorption activity, indicating the gel's efficacy in suppressing osteoclast differentiation, which is vital for preventing bone degradation in osteoporotic conditions. This dual functionality of gel works by promoting osteogenesis while inhibiting osteoclast activity, thus positioning the developed gel as a promising biomaterial for tissue regeneration applications. Building on the earlier work in this thesis, which centered on developing polymer-coated nanoparticles for bone regeneration, the polymeric gel introduced here demonstrates its potential to not only regenerate bone but also create a protective environment by mitigating the oxidative stress that supports long-term bone health in osteoporotic patients. While the results are promising, future studies can include investigating the long-term stability of the gel by assessing its physical, chemical, and biological stability over time. Additionally, optimizing the drug-loaded polymeric gel system will enhance its clinical applicability, focusing on key steps such as investigating drug release kinetics under physiological conditions to achieve sustained release and conducting long-term biodegradation assessments. Improving biocompatibility through surface modifications or the incorporation of bioactive compounds is also essential. Preclinical animal studies will be crucial for evaluating the gel's performance in osteoporotic models, alongside optimizing formulation parameters like polymer and phytoestrogen concentration. Finally, preparing for regulatory compliance by compiling comprehensive safety and efficacy data will facilitate the transition from laboratory studies to clinical applications.

#### References

- (1) Lei, C.; Song, J.; Li, S.; Zhu, Y.; Liu, M.; Wan, M.; Mu, Z.; Tay, F. R.; Niu, L. Advances in Materials-Based Therapeutic Strategies against Osteoporosis. *Biomaterials* **2023**, *296*, 122066.
- (2) Xie, Y.; Zhang, L.; Xiong, Q.; Gao, Y.; Ge, W.; Tang, P. Bench-to-Bedside Strategies for Osteoporotic Fracture: From Osteoimmunology to Mechanosensation. *Bone Res* **2019**, *7* (1), 25.
- (3) Rogers, A.; Saleh, G.; Hannon, R. A.; Greenfield, D.; Eastell, R. Circulating Estradiol and Osteoprotegerin as Determinants of Bone Turnover and Bone Density in Postmenopausal Women. *The Journal of Clinical Endocrinology & Metabolism* **2002**, *87* (10), 4470–4475.
- (4) Szwed-Georgiou, A.; Płociński, P.; Kupikowska-Stobba, B.; Urbaniak, M. M.; Rusek-Wala, P.; Szustakiewicz, K.; Piszko, P.; Krupa, A.; Biernat, M.; Gazińska, M.; Kasprzak, M.; Nawrotek, K.; Mira, N. P.; Rudnicka, K. Bioactive Materials for Bone Regeneration: Biomolecules and Delivery Systems. *ACS Biomater. Sci. Eng.* **2023**, *9* (9), 5222–5254.
- (5) Putra, N. E.; Zhou, J.; Zadpoor, A. A. Sustainable Sources of Raw Materials for Additive Manufacturing of Bone-Substituting Biomaterials. *Advanced Healthcare Materials* **2024**, *13* (1), 2301837.
- (6) Liang, B.; Burley, G.; Lin, S.; Shi, Y.-C. Osteoporosis Pathogenesis and Treatment: Existing and Emerging Avenues. *Cell Mol Biol Lett* **2022**, 27 (1), 72.
- (7) Kenkre, J.; Bassett, J. The Bone Remodelling Cycle. *Ann Clin Biochem* **2018**, *55* (3), 308–327.
- (8) Russell, R. G. G. Bisphosphonates: The First 40years. *Bone* **2011**, *49* (1), 2–19.
- (9) Mackey, P. A.; Whitaker, M. D. Osteoporosis: A Therapeutic Update. *The Journal for Nurse Practitioners* **2015**, *11* (10), 1011–1017.
- (10) Li, J.; Deng, C.; Liang, W.; Kang, F.; Bai, Y.; Ma, B.; Wu, C.; Dong, S. Mn-Containing Bioceramics Inhibit Osteoclastogenesis and Promote Osteoporotic Bone Regeneration via Scavenging ROS. *Bioactive Materials* **2021**, *6* (11), 3839–3850.
- (11) Liu, J.; Burdette, J. E.; Xu, H.; Gu, C.; Van Breemen, R. B.; Bhat, K. P. L.; Booth, N.; Constantinou, A. I.; Pezzuto, J. M.; Fong, H. H. S.; Farnsworth, N. R.; Bolton, J. L. Evaluation of Estrogenic Activity of Plant Extracts for the Potential Treatment of Menopausal Symptoms. *J. Agric. Food Chem.* **2001**, *49* (5), 2472–2479.
- (12) Quan, H.; He, Y.; Sun, J.; Yang, W.; Luo, W.; Dou, C.; Kang, F.; Zhao, C.; He, J.; Yang, X.; Dong, S.; Jiang, H. Chemical Self-Assembly of Multifunctional Hydroxyapatite with a Corallike Nanostructure for Osteoporotic Bone Reconstruction. *ACS Appl. Mater. Interfaces* **2018**, *10* (30), 25547–25560.
- (13) Zhao, H.; Huang, Y.; Zhang, W.; Guo, Q.; Cui, W.; Sun, Z.; Eglin, D.; Liu, L.; Pan, G.; Shi, Q. Mussel-Inspired Peptide Coatings on Titanium Implant to Improve Osseointegration in Osteoporotic Condition. *ACS Biomater. Sci. Eng.* **2018**, *4* (7), 2505–2515.
- (14) Sandomierski, M.; Adamska, K.; Ratajczak, M.; Voelkel, A. Chitosan Zeolite Scaffold as a Potential Biomaterial in the Controlled Release of Drugs for Osteoporosis. *International Journal of Biological Macromolecules* **2022**, 223, 812–820.
- (15) Zhao, Y.; Li, Z.; Jiang, Y.; Liu, H.; Feng, Y.; Wang, Z.; Liu, H.; Wang, J.; Yang, B.; Lin, Q. Bioinspired Mineral Hydrogels as Nanocomposite Scaffolds for the Promotion of Osteogenic Marker Expression and the Induction of Bone Regeneration in Osteoporosis. *Acta Biomaterialia* **2020**, *113*, 614–626.
- (16) Li, D.; Zhou, J.; Zhang, M.; Ma, Y.; Yang, Y.; Han, X.; Wang, X. Long-Term Delivery of Alendronate through an Injectable Tetra-PEG Hydrogel to Promote Osteoporosis Therapy. *Biomater. Sci.* **2020**, 8 (11), 3138–3146.
- (17) Mora-Raimundo, P.; Lozano, D.; Benito, M.; Mulero, F.; Manzano, M.; Vallet-Regí, M. Osteoporosis Remission and New Bone Formation with Mesoporous Silica Nanoparticles. *Advanced Science* **2021**, *8* (16), 2101107.
- (18) Kuang, L.; Huang, J.; Liu, Y.; Li, X.; Yuan, Y.; Liu, C. Injectable Hydrogel with NIR Light-Responsive, Dual-Mode PTH Release for Osteoregeneration in Osteoporosis. *Adv Funct Materials* **2021**, *31* (47), 2105383.
- (19) Ray, S.; Thormann, U.; Eichelroth, M.; Budak, M.; Biehl, C.; Rupp, M.; Sommer, U.; El

- Khassawna, T.; Alagboso, F. I.; Kampschulte, M.; Rohnke, M.; Henß, A.; Peppler, K.; Linke, V.; Quadbeck, P.; Voigt, A.; Stenger, F.; Karl, D.; Schnettler, R.; Heiss, C.; Lips, K. S.; Alt, V. Strontium and Bisphosphonate Coated Iron Foam Scaffolds for Osteoporotic Fracture Defect Healing. *Biomaterials* **2018**, *157*, 1–16.
- (20) Ye, J.; Jiang, J.; Zhou, Z.; Weng, Z.; Xu, Y.; Liu, L.; Zhang, W.; Yang, Y.; Luo, J.; Wang, X. Near-Infrared Light and Upconversion Nanoparticle Defined Nitric Oxide-Based Osteoporosis Targeting Therapy. *ACS Nano* **2021**, *15* (8), 13692–13702.
- (21) Naito, C.; Katsumi, H.; Yoneto, K.; Omura, M.; Nishidono, M.; Kamei, S.; Mizoguchi, A.; Tamba, A.; Tanaka, A.; Morishita, M.; Yamamoto, A. Development of a Phosphoric Acid-Mediated Hyaluronic Acid Gel Sheet for Efficient Transdermal Delivery of Alendronate for Anti-Osteoporotic Therapy. *Pharmaceutics* **2019**, *11* (12), 643.
- (22) Tripathi, G.; Raja, N.; Yun, H. S. Effect of Direct Loading of Phytoestrogens into the Calcium Phosphate Scaffold on Osteoporotic Bone Tissue Regeneration. *J. Mater. Chem. B* **2015**, *3* (44), 8694–8703.
- (23) A. Al-allaq, A.; Kashan, J. S.; Abdul-Kareem, F. M. In Vivo Investigations of Polymers in Bone Tissue Engineering: A Review Study. *International Journal of Polymeric Materials and Polymeric Biomaterials* **2024**, 1–16.
- (24) Shi, C.; Yuan, Z.; Han, F.; Zhu, C.; Li, B. Polymeric Biomaterials for Bone Regeneration. *Ann Joint* **2016**, *1*, 27–27.
- (25) Chocholata, P.; Kulda, V.; Babuska, V. Fabrication of Scaffolds for Bone-Tissue Regeneration. *Materials* **2019**, *12* (4), 568.
- (26) Puppi, D.; Chiellini, F.; Piras, A. M.; Chiellini, E. Polymeric Materials for Bone and Cartilage Repair. *Progress in Polymer Science* **2010**, *35* (4), 403–440.
- (27) Yegappan, R.; Selvaprithiviraj, V.; Amirthalingam, S.; Jayakumar, R. Carrageenan Based Hydrogels for Drug Delivery, Tissue Engineering and Wound Healing. *Carbohydrate Polymers* **2018**, *198*, 385–400.
- (28) Fang, J.; Li, P.; Lu, X.; Fang, L.; Lü, X.; Ren, F. A Strong, Tough, and Osteoconductive Hydroxyapatite Mineralized Polyacrylamide/Dextran Hydrogel for Bone Tissue Regeneration. *Acta Biomaterialia* **2019**, 88, 503–513.
- (29) Huang, S.; Huang, G. Preparation and Drug Delivery of Dextran-Drug Complex. *Drug Delivery* **2019**, *26* (1), 252–261.
- (30) Huang, L.; Wang, X.; Cao, H.; Li, L.; Chow, D. H.-K.; Tian, L.; Wu, H.; Zhang, J.; Wang, N.; Zheng, L.; Yao, X.; Yang, Z.; Qin, L. A Bone-Targeting Delivery System Carrying Osteogenic Phytomolecule Icaritin Prevents Osteoporosis in Mice. *Biomaterials* **2018**, *182*, 58–71.
- (31) Moutsatsou, P. The Spectrum of Phytoestrogens in Nature: Our Knowledge Is Expanding.
- (32) Kamiński, K.; Płonka, M.; Ciejka, J.; Szczubiałka, K.; Nowakowska, M.; Lorkowska, B.; Korbut, R.; Lach, R. Cationic Derivatives of Dextran and Hydroxypropylcellulose as Novel Potential Heparin Antagonists. *J. Med. Chem.* **2011**, *54* (19), 6586–6596.
- (33) Halder, M.; Singh, A.; Negi, D.; Singh, Y. Investigating the Role of Amino Acids in Short Peptides for Hydroxyapatite Binding and Osteogenic Differentiation of Mesenchymal Stem Cells to Aid Bone Regeneration. *Biomacromolecules* **2024**, *25* (4), 2286–2301.
- (34) Karan, C. K.; Bhattacharjee, M. Self-Healing and Moldable Metallogels as the Recyclable Materials for Selective Dye Adsorption and Separation. *ACS Appl. Mater. Interfaces* **2016**, 8 (8), 5526–5535.
- (35) Meyvis, T. K. L.; De Smedt, S. C.; Demeester, J.; Hennink, W. E. Influence of the Degradation Mechanism of Hydrogels on Their Elastic and Swelling Properties during Degradation. *Macromolecules* **2000**, *33* (13), 4717–4725.
- (36) Kim, B.; Kang, B.; Vales, T. P.; Yang, S. K.; Lee, J.; Kim, H.-J. Polyphenol-Functionalized Hydrogels Using an Interpenetrating Chitosan Network and Investigation of Their Antioxidant Activity. *Macromol. Res.* **2018**, *26* (1), 35–39.
- (37) Ibrahim, S.; Sayed, H. M.; EL-Rafei, A. M.; El Amir, A.; Ismail, M.; Allam, N. K. Improved Genistein Loading and Release on Electrospun Chitosan Nanofiber Blends. *Journal of Molecular Liquids* **2016**, 223, 1056–1061.

- (38) Rasool, N.; Negi, D.; Singh, Y. Thiol-Functionalized, Antioxidant, and Osteogenic Mesoporous Silica Nanoparticles for Osteoporosis. *ACS Biomater. Sci. Eng.* **2023**, *9* (6), 3535–3545.
- (39) Poole, K. M.; Nelson, C. E.; Joshi, R. V.; Martin, J. R.; Gupta, M. K.; Haws, S. C.; Kavanaugh, T. E.; Skala, M. C.; Duvall, C. L. ROS-Responsive Microspheres for on Demand Antioxidant Therapy in a Model of Diabetic Peripheral Arterial Disease. *Biomaterials* **2015**, *41*, 166–175.
- (40) Pei, A.; Butchosa, N.; Berglund, L. A.; Zhou, Q. Surface Quaternized Cellulose Nanofibrils with High Water Absorbency and Adsorption Capacity for Anionic Dyes. *Soft Matter* **2013**, *9* (6), 2047.
- (41) Ismillayli, N.; Hadi, S.; Andayani, I. G. A. S.; Honiar, R.; Mariana, B.; Sanjaya, R. K.; Hermanto, D. Synthesize of Self-Electrostatic Interaction Chitosan-Carrageenan Membrane and Its Properties. *J. Phys.: Conf. Ser.* **2021**, *1943* (1), 012177.
- (42) Ru, J.; Wang, Z.; Tong, C.; Liu, H.; Wang, G.; Peng, Z. Nonleachable Antibacterial Nanocellulose with Excellent Cytocompatible and UV-Shielding Properties Achieved by Counterion Exchange with Nature-Based Phenolic Acids. *ACS Sustainable Chem. Eng.* **2021**, 9 (47), 15755–15767.
- (43) Gaharwar, A. K.; Peppas, N. A.; Khademhosseini, A. Nanocomposite Hydrogels for Biomedical Applications. *Biotechnology and Bioengineering* **2014**, *111* (3), 441–453.
- (44) Kumar, A.; Rao, K. M.; Han, S. S. Synthesis of Mechanically Stiff and Bioactive Hybrid Hydrogels for Bone Tissue Engineering Applications. *Chemical Engineering Journal* **2017**, *317*, 119–131.
- (45) Karvinen, J.; Kellomäki, M. Characterization of Self-Healing Hydrogels for Biomedical Applications. *European Polymer Journal* **2022**, *181*, 111641.
- (46) Kocak, F. Z.; Talari, A. C. S.; Yar, M.; Rehman, I. U. In-Situ Forming pH and Thermosensitive Injectable Hydrogels to Stimulate Angiogenesis: Potential Candidates for Fast Bone Regeneration Applications. *International Journal of Molecular Sciences* **2020**, *21* (5).
- (47) Davison, N. L.; Barrère-de Groot, F.; Grijpma, D. W. Chapter 6 Degradation of Biomaterials. In *Tissue Engineering (Second Edition)*; Blitterswijk, C. A. V., De Boer, J., Eds.; Academic Press: Oxford, 2014; pp 177–215.
- (48) Chen, Y.; Liu, X.; Liu, R.; Gong, Y.; Wang, M.; Huang, Q.; Feng, Q.; Yu, B. Zero-Order Controlled Release of BMP2-Derived Peptide P24 from the Chitosan Scaffold by Chemical Grafting Modification Technique for Promotion of Osteogenesis *in* Vitro and Enhancement of Bone Repair *in Vivo. Theranostics* **2017**, *7* (5), 1072–1087.
- (49) Huang, L.; Wang, J.; Yu, J.; Bian, M.; Xiang, X.; Han, G.; Chen, W.; Wang, N.; Ge, J.; Lu, S.; Zhang, J. Picein Alleviates Oxidative Stress and Promotes Bone Regeneration in Osteoporotic Bone Defect by Inhibiting Ferroptosis via Nrf2/HO-1/GPX4 Pathway. *Environmental Toxicology* **2024**, *39* (7), 4066–4085.
- (50) Bhattarai, G.; Poudel, S. B.; Kook, S.-H.; Lee, J.-C. Anti-Inflammatory, Anti-Osteoclastic, and Antioxidant Activities of Genistein Protect against Alveolar Bone Loss and Periodontal Tissue Degradation in a Mouse Model of Periodontitis. *Journal of Biomedical Materials Research Part A* **2017**, *105* (9), 2510–2521.
- (51) Xu, C.; Guan, S.; Xu, J.; Gong, W.; Liu, T.; Ma, X.; Sun, C. Preparation, Characterization and Antioxidant Activity of Protocatechuic Acid Grafted Carboxymethyl Chitosan and Its Hydrogel. *Carbohydrate Polymers* **2021**, *252*, 117210.
- (52) Dziadek, M.; Dziadek, K.; Checinska, K.; Zagrajczuk, B.; Golda-Cepa, M.; Brzychczy-Wloch, M.; Menaszek, E.; Kopec, A.; Cholewa-Kowalska, K. PCL and PCL/Bioactive Glass Biomaterials as Carriers for Biologically Active Polyphenolic Compounds: Comprehensive Physicochemical and Biological Evaluation. *Bioactive Materials* **2021**, *6* (6), 1811–1826.
- (53) Thankam, F. G.; Muthu, J. Influence of Physical and Mechanical Properties of Amphiphilic Biosynthetic Hydrogels on Long-Term Cell Viability. *Journal of the Mechanical Behavior of Biomedical Materials* **2014**, *35*, 111–122.
- (54) Peng, Z.; Peng, Z.; Shen, Y. Fabrication and Properties of Gelatin/Chitosan Composite

- Hydrogel. *Polymer-Plastics Technology and Engineering* **2011**, *50* (11), 1160–1164.
- (55) Qu, F.; Guilak, F.; Mauck, R. L. Cell Migration: Implications for Repair and Regeneration in Joint Disease. *Nature Reviews Rheumatology* **2019**, *15* (3), 167–179.
- (56) Cao, W.; Jin, J.; Wu, G.; Bravenboer, N.; Helder, M. N.; Pathak, J. L.; Zandieh-Doulabi, B.; Hogervorst, J. M. A.; Matsukawa, S.; Geonzon, L. C.; Bacabac, R. G.; Schulten, E. A. J. M.; Klein-Nulend, J. K-Carrageenan Stimulates Pre-Osteoblast Proliferation and Osteogenic Differentiation: A Potential Factor for the Promotion of Bone Regeneration? *Molecules* **2021**, *26* (20), 6131.
- (57) Dai, J.; Li, Y.; Zhou, H.; Chen, J.; Chen, M.; Xiao, Z. Genistein Promotion of Osteogenic Differentiation through BMP2/SMAD5/RUNX2 Signaling. *Int. J. Biol. Sci.* **2013**, *9* (10), 1089–1098.
- (58) Wang, R.; He, X.; Su, S.; Bai, J.; Liu, H.; Zhou, F. Multifunctional Tannic Acid-Based Nanocomposite Methacrylated Silk Fibroin Hydrogel with the Ability to Scavenge Reactive Oxygen Species and Reduce Inflammation for Bone Regeneration. *International Journal of Biological Macromolecules* **2024**, 266, 131357.
- (59) Spanou, K.; Barbosa, A. I.; Detsi, A.; Costa Lima, S. A.; Reis, S. Development and Characterization of Gel-like Matrix Containing Genistein for Skin Application. *Journal of Drug Delivery Science and Technology* **2023**, *90*, 105119.
- (60) Varini, E.; Sánchez-Salcedo, S.; Malavasi, G.; Lusvardi, G.; Vallet-Regí, M.; Salinas, A. J. Cerium (III) and (IV) Containing Mesoporous Glasses/Alginate Beads for Bone Regeneration: Bioactivity, Biocompatibility and Reactive Oxygen Species Activity. *Materials Science and Engineering: C* 2019, 105, 109971.
- (61) Stucki, U.; Schmid, J.; Hämmerle, C. F.; Lang, N. P. Temporal and Local Appearance of Alkaline Phosphatase Activity in Early Stages of Guided Bone Regeneration: A Descriptive Histochemical Study in Humans. *Clinical Oral Implants Res* **2001**, *12* (2), 121–127.
- (62) Strong, A. L.; Jiang, Q.; Zhang, Q.; Zheng, S.; Boue, S. M.; Elliott, S.; Burow, M. E.; Bunnell, B. A.; Wang, G. Design, Synthesis, and Osteogenic Activity of Daidzein Analogs on Human Mesenchymal Stem Cells. *ACS Med. Chem. Lett.* **2014**, *5* (2), 143–148.
- (63) Şeker, Ş.; Aral, D.; Elçin, A. E.; Yaşar Murat, E. Biomimetic Mineralization of Platelet Lysate/Oxidized Dextran Cryogel as a Macroporous 3D Composite Scaffold for Bone Repair. *Biomedical Materials* **2024**, *19* (2), 025006.
- (64) Zhu, D.; Su, Y.; Young, M. L.; Ma, J.; Zheng, Y.; Tang, L. Biological Responses and Mechanisms of Human Bone Marrow Mesenchymal Stem Cells to Zn and Mg Biomaterials. *ACS Appl. Mater. Interfaces* **2017**, *9* (33), 27453–27461.
- (65) Liao, Q.; Xiao, Z.; Qin, Y.; Zhou, H. Genistein Stimulates Osteoblastic Differentiation via P38 MAPK-Cbfa1 Pathway in Bone Marrow Culture. *Acta Pharmacologica Sinica* **2007**, 28 (10), 1597–1602.
- (66) Wan, H.-Y.; Shin, R. L. Y.; Chen, J. C. H.; Assunção, M.; Wang, D.; Nilsson, S. K.; Tuan, R. S.; Blocki, A. Dextran Sulfate-Amplified Extracellular Matrix Deposition Promotes Osteogenic Differentiation of Mesenchymal Stem Cells. *Acta Biomaterialia* **2022**, *140*, 163–177.

# CHAPTER - 5

# Conclusions and Future Perspectives

# **5.1. Summary of thesis**

The aim of this thesis was to develop polymer-based biomaterials for tissue regeneration applications, including skin tissue regeneration and bone tissue regeneration. These materials offer various properties, including excellent biocompatibility and tunable mechanical properties. They can also be engineered to meet specific tissue requirements, including porosity, surface chemistry, and degradation rates, while minimizing the immune responses, thus, making them versatile for various biomedical applications. Polymer-based biomaterials have been explored for tissue regeneration, but they often fall short of providing multifunctional treatment approaches that can address the complexities of the wound healing process. They also often overlook the critical role of the immune system and the need to create an environment conducive to successful tissue regeneration. Therefore, we have rationally designed multifunctional polymeric biomaterials by customizing various biopolymers to incorporate antibacterial, antibiofilm, cell-proliferating, hemostatic, immunomodulatory, and ROS-scavenging properties, which are required for efficient tissue regeneration. In particular, we have developed metallic nanoparticles-based imine crosslinked polymeric gel for bacteria-infected wounds, calcium phosphate nanoparticles coated with polymer for immunomodulation-regulated bone regeneration, and drug-loaded polymeric gel for bone regeneration in osteoporotic conditions.

This thesis is organized into 5 chapters. **Chapter 1** is the introductory chapter of the thesis, which provides a comprehensive overview of tissue regeneration, with emphasis on wound healing and bone regeneration. It also provides an exhaustive literature survey on the use of polymeric biomaterials for tissue regeneration applications, in particular, wound healing and bone regeneration. The literature review is followed by highlighting crucial research gaps and areas that require further exploration. It further outlines the objectives of this research to address these research gaps.

Chapter 2 deals with the development of an imine crosslinked hydrogel fabricated using oxidized sodium alginate and quaternized chitosan for the management of bacteria-infected wounds. Additionally, we have enhanced its properties by incorporating  $\beta$ -Ga<sub>2</sub>O<sub>3</sub> nanoparticles synthesized using the sol-gel method. The combination of quaternized chitosan and  $\beta$ -Ga<sub>2</sub>O<sub>3</sub> nanoparticles significantly enhances the antibacterial activity of the hydrogel system and provides a promising solution for managing bacteria-infected wounds over the long term. This antibiotic-free approach effectively addresses the growing issue of antibiotic resistance, and offer a sustainable and effective therapeutic option for patients with bacterial infections. Furthermore, the hydrogel system was able

to provide antioxidant and hemostatic abilities, thus, making it a promising candidate for tissue regeneration in bacteria-infected wounds.

Chapter 3 deals with the development of cobalt-doped biphasic calcium phosphate nanoparticles coated with acemannan for immunomodulation regulated bone tissue regeneration. Different concentrations (0.02%, 0.5%, and 2%) of cobalt were doped in biphasic calcium phosphate nanoparticles and coated with acemannan, which were further evaluated for their osteogenic and immunomodulatory properties for effective bone regeneration. These nanoparticles demonstrated excellent cytocompatibility, enhanced cell migration, and osteogenic properties, including ALP activity and calcium deposition and increased expression of M2 markers. This combination promotes both osteogenesis and immune modulation as suggested by improved expression of osteogenic and anti-inflammatory markers, thus, creating a supportive microenvironment that enhances tissue regeneration.

**Chapter 4** involves the development of a phytoestrogen genistein-loaded, ionic cross-linked cationic quaternized dextran and anionic κ-carrageenan gels to address oxidative stress and estrogen deficiency impeding bone regeneration in osteoporotic conditions. The gels demonstrated excellent ROS scavenging activity and the potential to enhance osteogenic markers, such as alkaline phosphatase (ALP) and calcium deposition, while reducing TRAP activity, a marker of osteoclast differentiation. The fabricated polymeric system thus holds a strong potential to be used as a therapeutic strategy for bone regeneration in osteoporosis cases.

**Chapter 5**, the final chapter of this thesis, provides a summary of the work completed, outlines its contributions to existing knowledge, and offers future perspectives.

#### 5.2. Contribution to the existing knowledge

The main aim of this thesis was to develop different polymer-based biomaterials with a variety of characteristics to meet challenges associated with skin and bone regeneration.

Wound healing is a multifactorial process, requiring effective management of inflammation, cell proliferation, and tissue remodeling. Different material-based strategies, including nanoparticles, peptide-based materials, composites, and polymer-based scaffolds, have been developed by various researchers to address the challenges associated with wound healing. However, there is still a lack of multifunctional materials capable of addressing the multiple factors that contribute to delayed wound healing. Additionally, relying on antibiotics in material-based strategies is contributing to the growing threat of antibiotic-resistant bacterial strains. To address these challenges, we have developed an antibiotic-free multifunctional nanoparticle hydrogel system. Our system, besides being drug-free also provided antibacterial, antibiofilm, antioxidant, and cell migration activities, which potentially makes it a treatment of choice for efficient wound healing.

Next, we have developed a polymer-coated nanoparticle systems for immunomodulation-regulated bone tissue regeneration. Current biomaterial-based approaches for bone regeneration primarily focus on enhancing osteogenesis, with limited attention given to the immune system. However, the immune system plays a crucial role in bone regeneration by modulating inflammation, promoting tissue repair, and facilitating the remodeling of bone tissue. Therefore, a well-regulated immune response is essential for optimizing healing and achieving successful bone regeneration. To address these challenges, we have developed cobalt-doped, biphasic calcium phosphate nanoparticles and coated them with biopolymer acemannan. The low doses of cobalt and acemannan coating induced immunomodulatory properties and the presence of biphasic calcium phosphate nanoparticles induced osteogenic properties. The proposed system can be potentially used for effective bone regeneration.

Bone regeneration in osteoporotic conditions is hampered due to impaired bone remodeling, weakened osteoblast activity, and increased oxidative stress, all of which disrupt the balance between bone formation and resorption. Additionally, the loss of estrogen in postmenopausal further hinders the healing process. Current treatment approaches primarily focus on the use of traditional strategies including the use of anabolic drugs and hormone replacement therapy, which are associated with drawbacks including poor absorption, toxicity, and chances of breast and uterine cancer. To overcome these limitations, we have developed a phytoestrogen, genistein-loaded quaternized dextran/κ-carrageenan loaded polymeric gel. The gel was able to scavenge reactive oxygen species and also enhanced the expression of osteogenic markers. The gel system was able to provide zero-order release of the drug for up to 28 days, resulting in consistent therapeutic levels with decreased side effects. The gels were also able to reduce the expression of TRAP, an osteoclast marker, further highlighting their potential for promoting bone regeneration.

#### **5.3. Future perspectives**

This thesis focuses on the development of polymer-based biomaterials to overcome the challenges associated with tissue regeneration applications. The  $\beta$ -Ga<sub>2</sub>O<sub>3</sub> nanoparticles loaded gel showed hemostatic, antibacterial, antibiofilm, and antioxidant properties needed for the bacteria-associated wound healing. To further assess its potential, the efficacy of this biomaterial can be evaluated against resistant bacterial strains that are responsible for antibiotic resistance. Additionally, the effectiveness of this material can be investigated in simulated chronic wound environments, where it can be tested for its ability to combat infection and promote healing under conditions that mimic the complexities of chronic wounds.

We have also explored the use of polymer-coated nanoparticles for immunomodulation-regulated bone tissue regeneration, with the system demonstrating enhanced osteogenesis and immunomodulation, as evidenced by increased ALP activity, calcium deposition, and upregulation of M2 markers. However, further evaluation is needed to study the material's effect on the expression of osteogenesis-related markers, such as alkaline phosphatase (ALP), collagen type 1 (Col 1), osteocalcin (OCN), and osteopontin (OPN), using RT-PCR analysis. Additionally, *in vivo* 

studies in mouse models can be conducted further to validate the biomaterial's potential for bone regeneration.

Lastly, we have developed genistein-loaded quaternized dextran/κ-carrageenan gels to promote bone regeneration in osteoporotic conditions. However, the use of DMSO to dissolve genistein may hinder clinical translation. Alternatively, drug solubility could be improved by encapsulating the drug in a suitable carrier instead of using DMSO. Future enhancements could involve modifying the polymers to incorporate covalent interactions, thereby improving the mechanical properties of the gel for more effective bone regeneration.

The biomaterials and technologies developed in this thesis have shown promising results, indicating their potential for further investigation. To advance their application, these innovations should be evaluated in animal models to assess their efficacy and safety, followed by clinical trials to determine their suitability for widespread medical use.

# **APPENDIX**

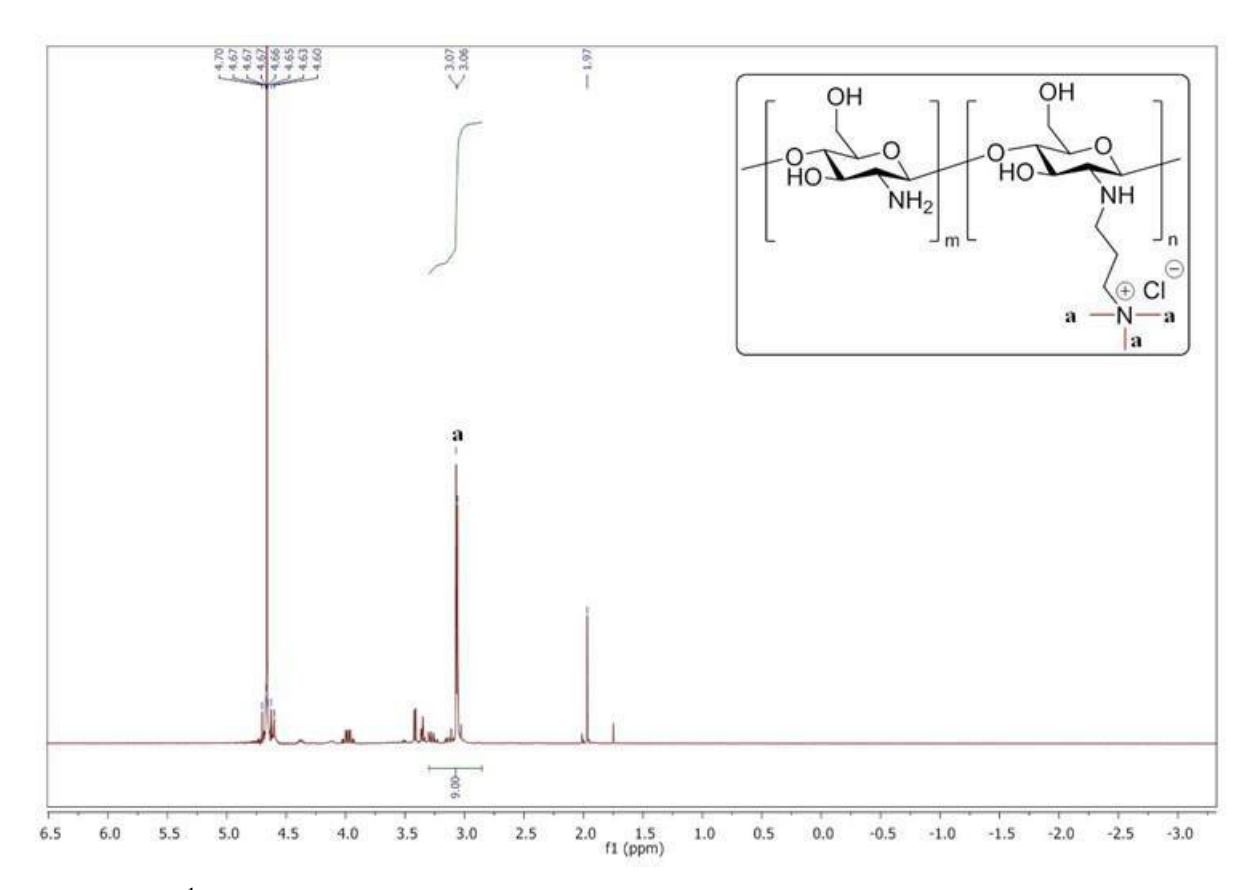


**Figure A1.** <sup>1</sup>H NMR spectrum of quaternized chitosan. The peak at 3.06 ppm was assigned to the protons of the methyl groups of the quaternary ammonium salt.

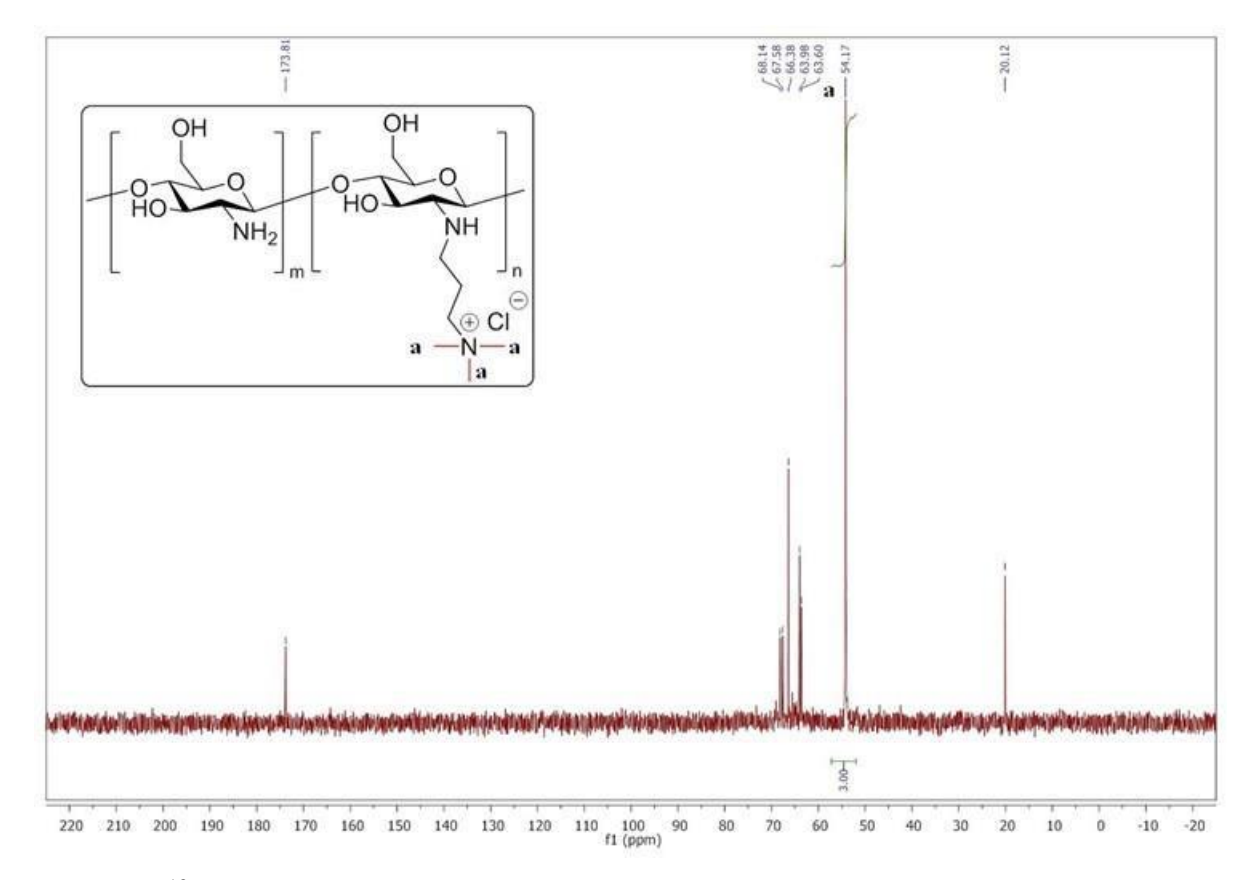


**Figure A2.**  $^{13}$ C NMR spectrum of quaternized chitosan. The typical signal at 54.17 ppm was attributed to the carbons ( $C_{10}$ ) of the trimethylammonium group.

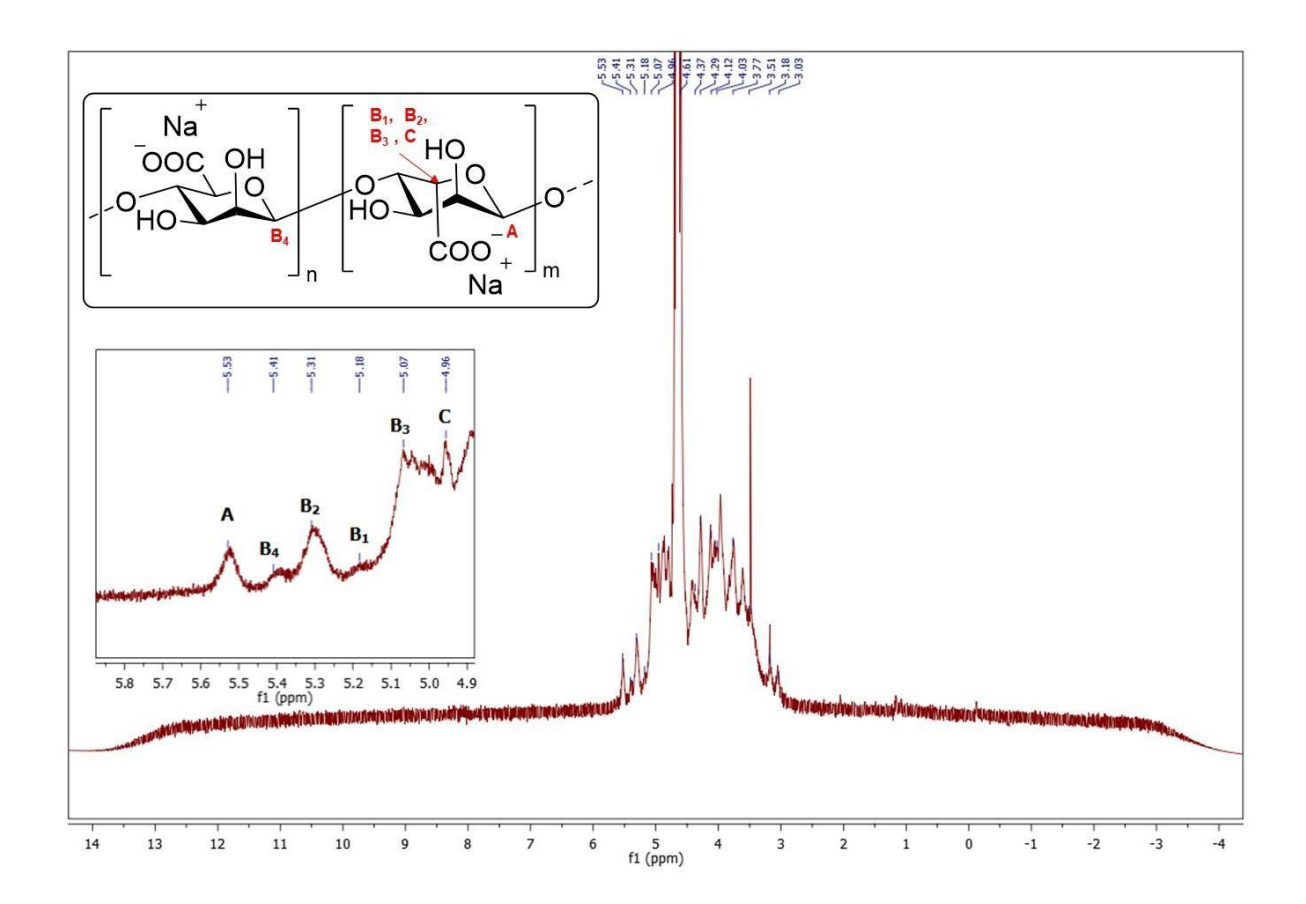


**Figure A3.** <sup>1</sup>H NMR spectrum of sodium alginate. The estimation of mannuronate/guluronate ratio is shown in the inset.

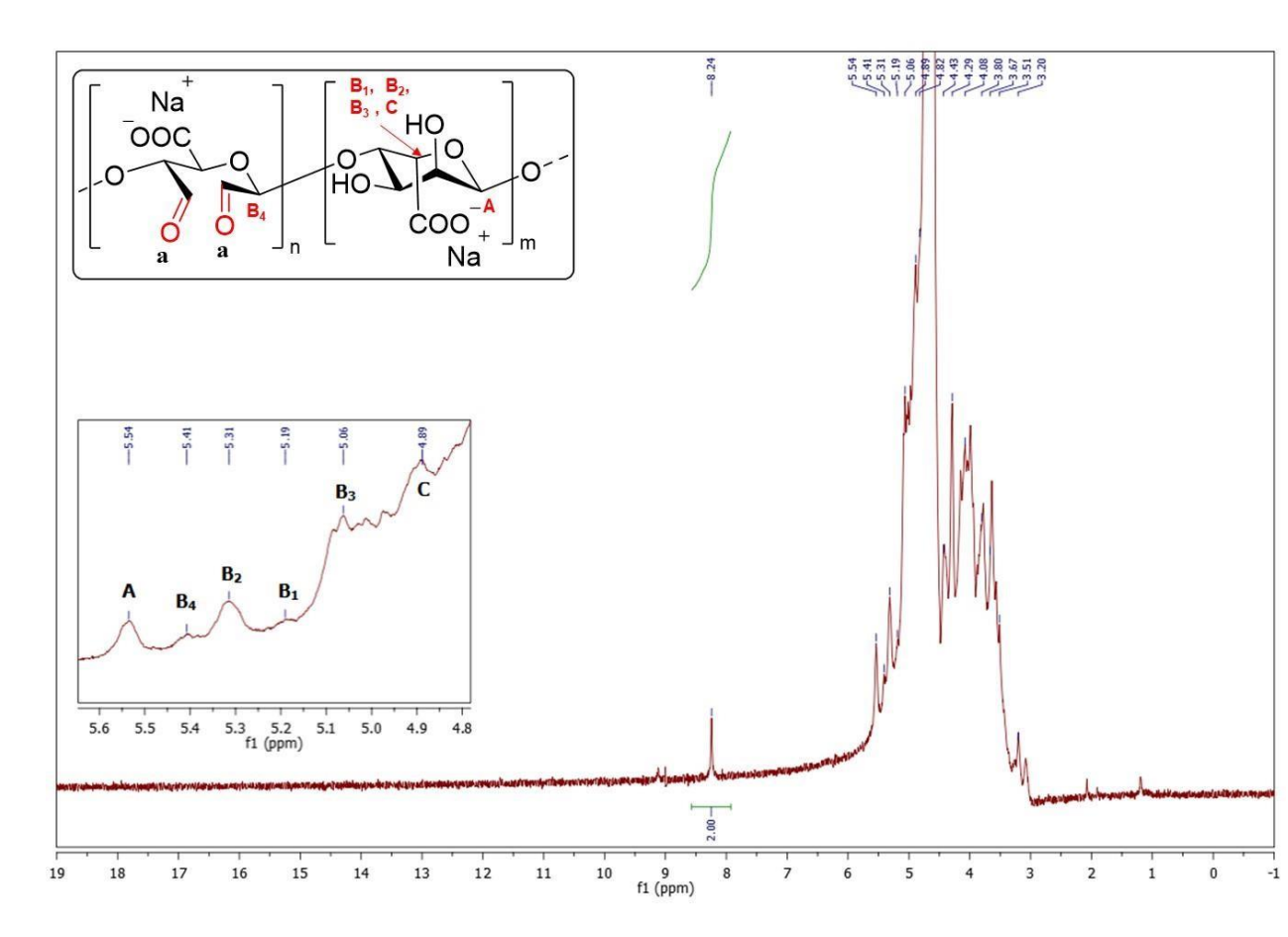


**Figure A4.** <sup>1</sup>H NMR spectrum of oxidized sodium alginate. The peak at 8.31 in the spectrum corresponds to aldehyde group, indicating the formation of aldehyde groups. The estimation of mannuronate/guluronate ratio is shown in the inset.

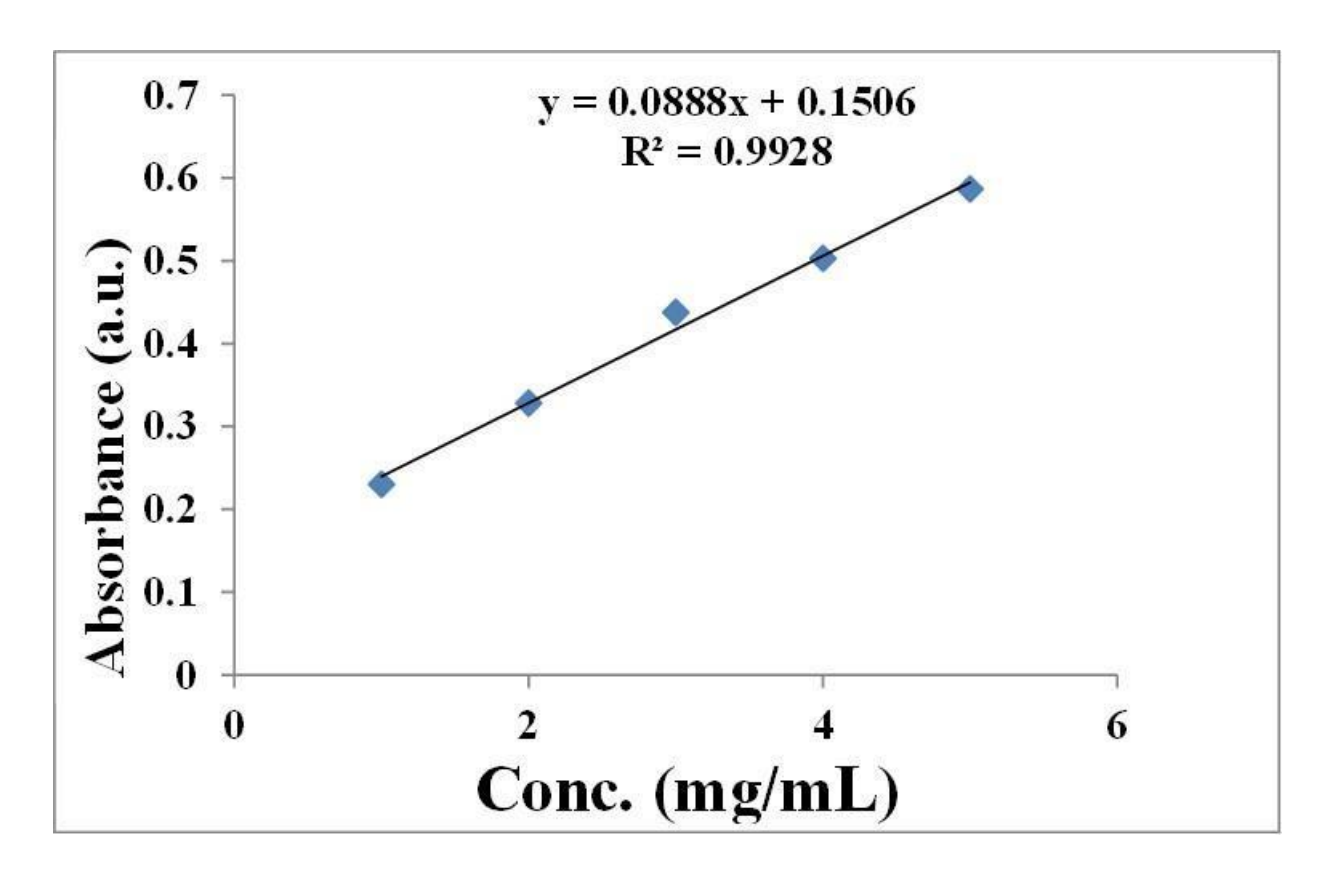


Figure A5. Standard curve for TNBS assay

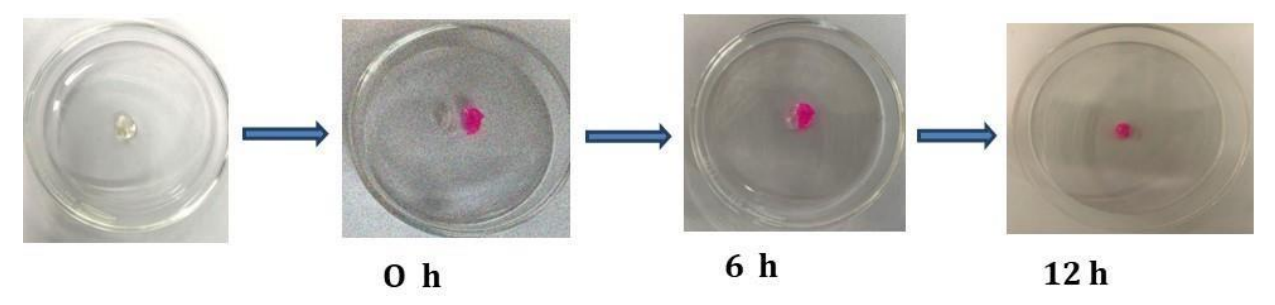


Figure A6. Self-healing of QC-OA hydrogels.

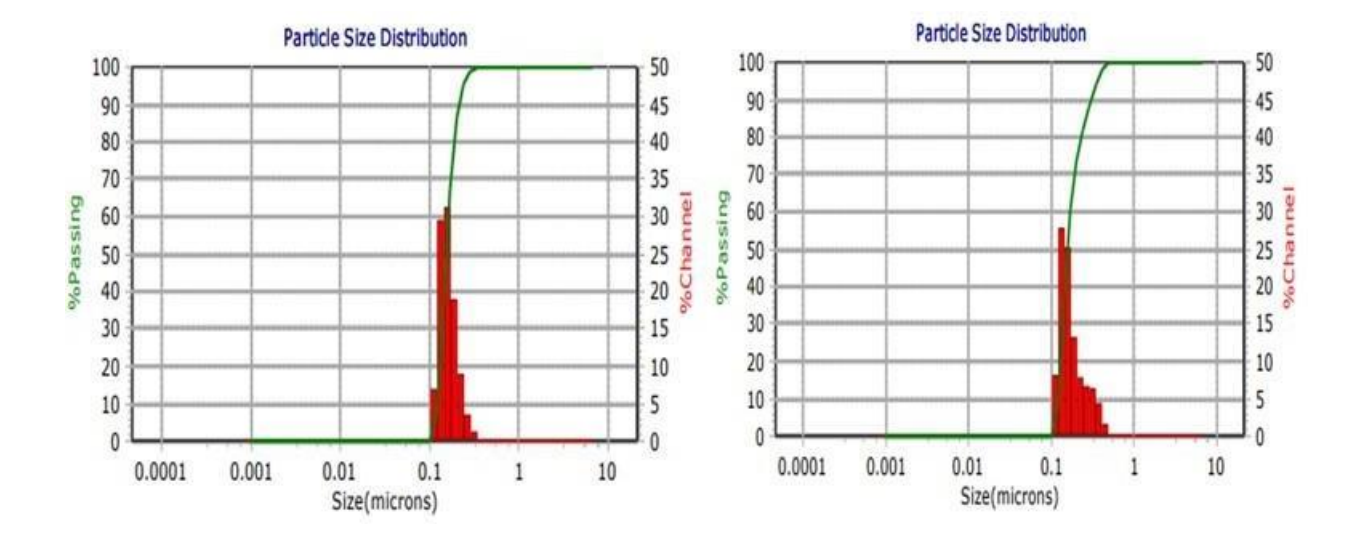
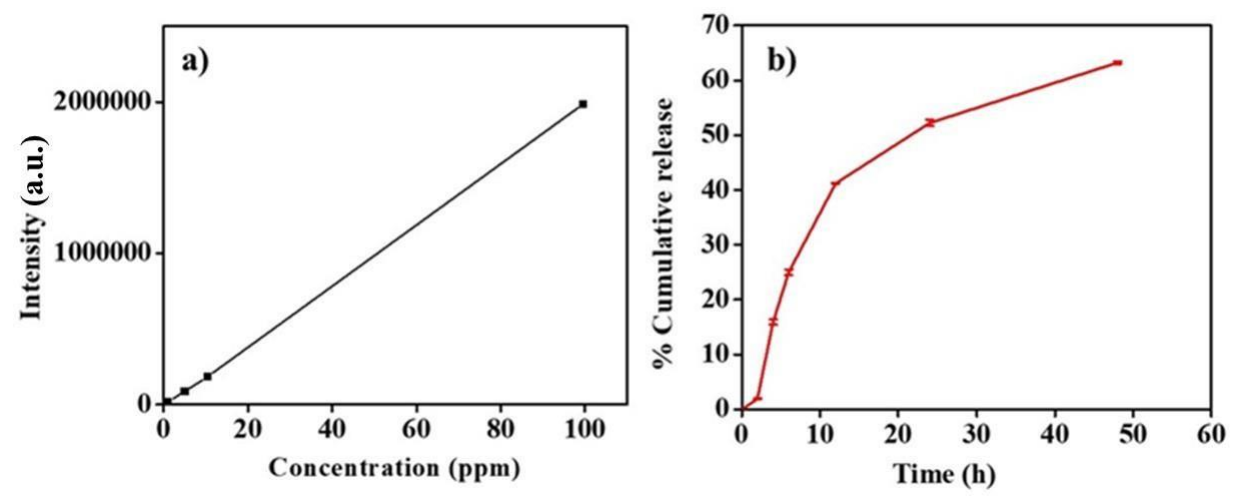
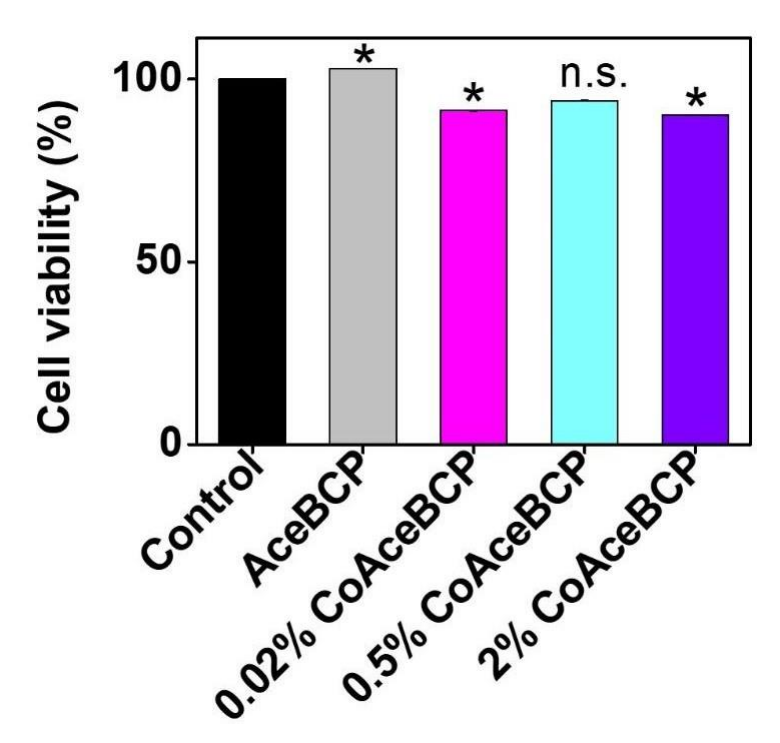


Figure A7. Particle size distribution of gallium nanoparticles.



**Figure A8.** Gallium ion release from NP-loaded hydrogel (GL Hyd) using MPAES: (a) calibration curve of gallium; and (b) gallium release from the hydrogel. Release studies were carried out at 37  $^{\circ}$ C, 100 rpm for 48 h. After different time intervals, samples were filtered and analyzed using MPAES. The data obtained was fitted in different kinetic models and the best fit was found to be Weibull model with a R<sup>2</sup> value of 0.9969, indicating the Fickian diffusion release (n = 3).



**Figure A9.** Viability of RAW264.7 cells in presence of nanoparticles using MTT assay. \*\*p < 0.005 and \*p < 0.05 denotes significant difference and n.s. corresponds to non-significant data (n = 3).

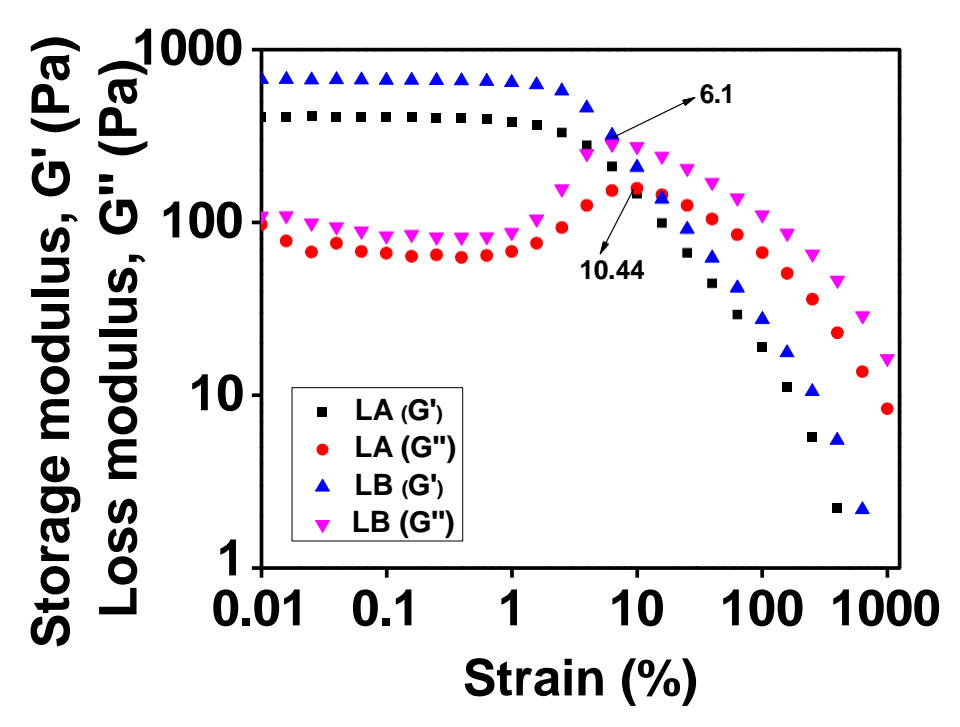


**Figure A10.** Amplitude sweep studies showing G' and G" of LA (2% QD, 2% C (1:2) and LB (2% QD, 2% C (1:1) at different strains.

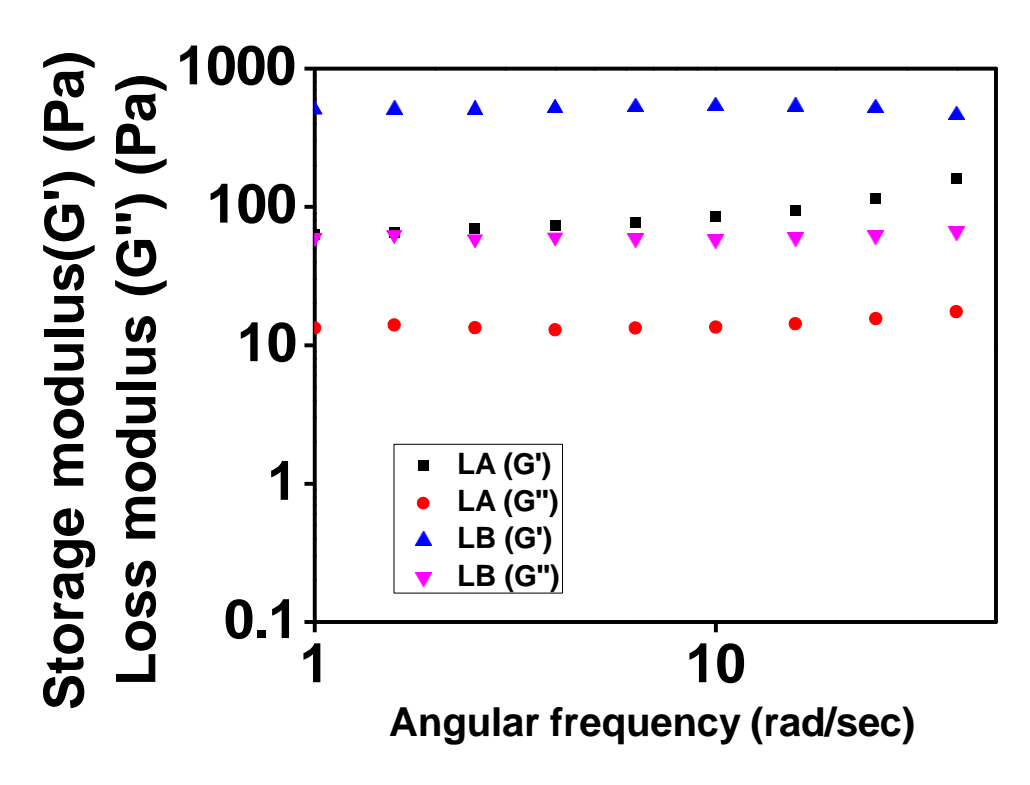


**Figure A11.** Frequency sweep studies showing G' and G" of LA (2% QD, 2% C (1:2) and LB (2% QD, 2% C (1:1) at different strains.

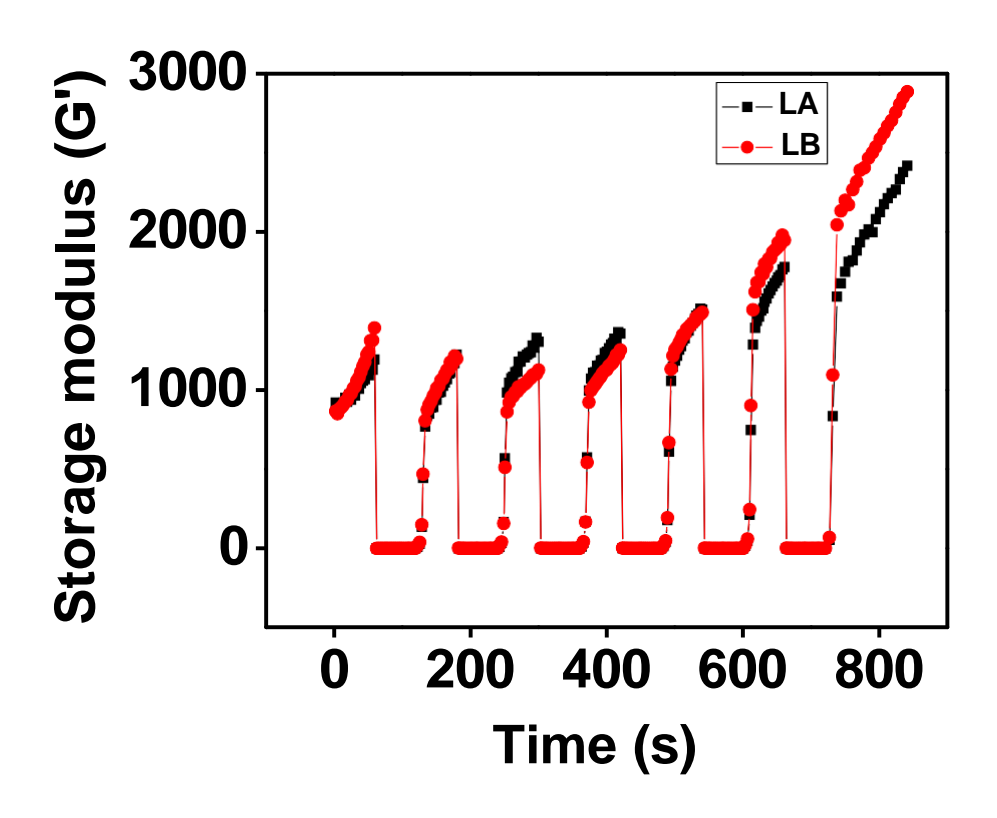


**Figure A12.** Self-healing characteristics of LA (2% QD, 2% C (1:2) and LB (2% QD, 2% C (1:1) gel subjected to alternative high and low strains.

**Table A1.** List of antibodies used along with their details.

No.	Antibody	Dilution	Company	Catalog No.
1	iNOS	1:400 for IF	CST	13120
2	Arginase-1	1:50 for IF	CST	AM4302
3	Anti-rabbit IgG (Alexa Fluor 488 conjugated)	5 μg/ml for ICC	Invitrogen	A-11034
4	TruStainFcX <sup>TM</sup> (antimouse CD16/32	0.1 μg/million cells for FC	BioLegend	101319
5	FITC anti-mouse CD86	5 μl/million cells for FC	BioLegend	105005
6	APC anti-mouse CD206	5 μl/million cells for FC	BioLegend	141707
7	Anti-rabbit IgG (Alexa Fluor 568 conjugated)	2 μg/ml for ICC	Invitrogen	A-1101
8	HRP-conjugated anti- mouse IgG antibody	1:20000 for WB	Sigma- Aldrich	A9044
9	HRP-conjugated anti- rabbit IgG antibody	1:20000 for WB	Sigma- Aldrich	A9169

Table A2. List of primers and their sequences.

Mous	Mouse Primers						
No.	Gene	F.P. (5'-3')	R.P. (5'-3')				
1	β-Actin	GTACTCTGTGTGGATCGGTGG	AGGGTGTAAAACGCAGCTCAG				
2	CD163	TGCTCAGGAAACCAATCCCA	ACCTCCACTCTTCCAGCG				
3	CD206	TTCAGCTATTGGACGCGAGG	GAATCTGACACCCAGCGGAA				
4	CD68	GGACTACATGGCGGTGGAAT	TGGTCACGGTTGCAAGAGAA				
5	iNOS	CTTGGTGAAGGGACTGAGCTG	CGTTCTCCGTTCTCTTGCAGT				

 Table A3. Primer sequences used in real-time PCR.

GAPDH FP	5'-AGGTCGGTGGAACGGATTTG-3'
GAPDH RP	5'-GGGGTCGTTGATGGCAACA-3'
ALP FP	5'-CCAACTCTTTTGTGCCAGAGA-3'
ALP RP	5'-GGCTACATTGGTGTTGAGCTTTT-3'
RUNX2 FP	5'-TCCACCACGCCGCTGTCT-3'
RUNX2_RP	5'-TCAGTGAGGGATGAAATGCT-3'
OCN FP	5'-CTGACCTCACAGATCCCAAGC-3'
OCN RP	5'-TGGTCTGATAGCTCGTCACAAG-3'
OPN FP	5'-CTTGCTTGGGTTTGCAGTCTT-3'
OPN RP	5'-GGTCGTAGTTAGTCCCTCAGA-3'